# DESIGN RATIONALE OF EXPANDABLE PEDICLE SCREWS FOR LUMBAR SPINE

*A Thesis submitted to the*
*Indian Institute of Technology Guwahati*
*for the award of the degree*
*of*

**Doctor of Philosophy**

*by*

**Devismita Sanjay**

**(Roll Number: 186106114)**

*Under the supervision of*

**Dr. Souptick Chanda**


**Department of Biosciences and Bioengineering,**
**Indian Institute of Technology Guwahati**
**Guwahati 781039, Assam, India**

**February 2025**

*Dedicated to*

*Dr. Sanjay Kumar Talukdar, Father*

*And*

*Dr. Ranjita Tamuli Talukdar, Mother*

# DECLARATION

I declare that

a. the work contained in this thesis is original and has been done by me under the guidance of my supervisor.

b. the work has not been submitted to any other Institute for any degree or diploma.

c. I have followed the guidelines provided by the Institute in preparing the thesis.

d. I have conformed to the norms and guidelines given in the Ethical Code of Conduct of the Institute.

e. whenever I have used materials (data, theoretical analysis, figures, and text) from other sources, I have given the credit to them by citing them in the text of the thesis and giving their details in the references. Further, I have taken permission from the copyright owners of the sources, whenever necessary.

**February 2025** **Devismita Sanjay**

Department of Biosciences and Bioengineering

Indian Institute of Technology Guwahati

Guwahati-781039, Assam, India

# CERTIFICATE OF APPROVAL

It is certified that the work described in this thesis entitled **"Design Rationale of Expandable Pedicle Screws For Lumbar Spine"** submitted by Devismita Sanjay for the award of Doctor of Philosophy is an authentic record of the results obtained from the research work carried out under my supervision in the Department of Biosciences and Bioengineering, Indian Institute of Technology Guwahati, Guwahati, Assam, India. The findings embodied in this thesis have not been submitted to any other University or Institute for the award of any degree or diploma.

Dr. Souptick Chanda

Assistant Professor

Department of Biosciences and Bioengineering

Indian Institute of Technology Guwahati

Guwahati-781039, Assam

# Acknowledgements

First, I would like to express my heartfelt thankfulness to God for giving me the blessings to go through this journey. I am indebted to all those individuals involved in nurturing my life from childhood and beyond and further to those who have helped and encouraged me in so many different ways during my tenure of doctoral study at Indian Institute of Technology Guwahati

I deeply express my heartiest gratitude to my thesis supervisor, Dr. Souptick Chanda, Department of Biosciences and Bioengineering, IIT Guwahati, for providing me the opportunity to be a part of the Biomechanics lab and pursue this research work. I must acknowledge valuable advice, critical comments, continuous support, encouragement and motivation given by him in every step of my research work, while keeping faith and confidence in my capabilities. His valued lessons and experience will prove to be helpful in my future endeavours as well. It was truly a great pleasure and privilege to work under his supervision.

I am very thankful to my Doctoral Committee members, Dr. Cota Navin Gupta, Dr. Rajkumar P. Thummer, and Prof. Vimal Katiyar for their valuable suggestions, constructive criticism and insightful comments at different stages of my doctoral work. I would also like to acknowledge my former Doctoral Committee member Prof. Debabrata Chakraborty for his valuable suggestions during the initial annual evaluations.

I would like to thank the present and former Heads of the Department, Prof. Utpal Bora, Dr. Rakhi Chaturvedi, Dr. Latha Rangan and other faculty members of the Department of Biosciences and Bioengineering for their support. I would like to thank Central Instrumentation Facility (CIF) and Mechanical Workshop, IIT Guwahati for providing high-end instruments to perform some of the experiments. I am indebted to Dr. Chandralekha Baruah, Consultant Radiologist, Dr. Prem Superspeciality and Cancer Centre, Panipat, Haryana for providing me the CT scan dataset. Further, I would like to acknowledge Dr. Utpal Kumar Tamuli, Orthopaedic surgeon, Down Town Hospital, Guwahati for his valuable input from time to time. I would further like to acknowledge Tool Room and Training Centre MSME, Guwahati for helping with the expandable pedicle screws manufacturing. I sincerely acknowledge the financial

support provided by the institute during the entire period of the doctoral research study. The help of the office and laboratory staff members of the department is thankfully acknowledged.

My special thanks to Dr Rajdeep Ghosh, Dr. Rahul Gautam Talukdar, Neeraj Kumar for their continuous support and various help related to the research work. I would like to express my sincere thanks to my friend in the Biomechanics lab, Rahul, Jaideep, Soumyadeep, Swetank Shree, Adeline, Ankan, Tirtharaj, Sushantika for their moral support, continuous encouragement and for maintaining a friendly working environment in the laboratory. I would especially like to mention the contributions of Jaideep and Soumyadeep for their critical insights into the work. I also wish to acknowledge all my friends, Mridusmita, Doli, Konika, Sinchini, Krishna, Rumela, Anjali, Richa, Sangeeta, Hirok, Dhanjita, Sneha who helped me in different ways during the critical phase and great company during my PhD journey. I would like to acknowledge Dr. Binita Sarma Das for her help and support during my miserable days. I sincerely appreciate Haren Dada for his consistent support in ensuring my timely and safe travels to campus on numerous occasions.

I express my sincere gratitude to my relatives, sister-in-law, and brother-in-law for their love and affection. My biggest support system, my father and my mother, stood like pillars of enormous strength, inspiring, and encouraging all my decisions. I am indebted to my parents for their blessings, understanding and unconditional love throughout my life. I would like to acknowledge my mother-in-law, Mrs. Akan Talukdar Barman and sister-in-law, Miss. Chandasmita Barman for encouraging and supporting me during my Ph.D. tenure. Finally, I would like to dedicate special thanks to my best friend and my husband, Mr. Nabankur Barman, for his numerous personal sacrifices that have enabled me to reach this juncture in life. He provided unwavering care, love, patience, and empathy and comforted me during my tough moments. It would never have been possible to accomplish my goal without their moral support and constant encouragement.

Indian Institute of Technology Guwahati **Devismita Sanjay**

Date:

# ABSTRACT

Lumbar spine complications rank among the most prominent reasons for medical attention, especially for elderly subjects. Spinal fusion surgery is a common procedure to address some operative cases. Pedicle screw fixation is popular amongst the extensive range of spinal fusion developed. However, issues such as aseptic loosening, screw pullout, screw breakage, disposition of screws and pedicle fracture often lead to revision surgery. To reduce these problems, the concept of expandable pedicle screws came by with improved anchorage owing primarily to greater screw-bone interface. Clinically, they showed improved biomechanical fixation by facilitating bone growth around the fins, reducing strain shielding and promoting favourable bone remodelling. In this study, anatomically viable finite element (FE) models of a functional spinal unit (FSU) of intact L4-L5 vertebra were used to estimate stress-strain fields and the same were compared with FSUs instrumented with normal and expandable pedicle screws under different physiological loading conditions. The expandable pedicle screws predicted marginally improved anchorage with more contact area with the bone indicating improved stability. Greater area with peak stresses at the bone-screw interface indicated lesser stress shielding. Further, a strain energy density-based bone remodelling algorithm was employed on patient-specific lumbar FSU to investigate the bone density changes around the screws. Bone apposition was predicted near screw insertion region in L4 and L5 vertebra (for normal pedicle screws) and central anterior screw insertion region for both vertebra (for expandable pedicle screws). Bone resorption was predicted in posterior region, near screw length in L4, central anterior right side and posteriorly in L5 vertebra for normal pedicle screws. In context to bone remodelling, overall result favoured expandable pedicle screws over normal pedicle ones. Further, pullout tests were performed on three novel designs of expandable pedicle screws and thereafter, validated numerically. Next, two FE mechanoregulation based tissue differentiation algorithms were implemented to assess osseointegration for the three types of expandable pedicle screws. Six weeks post-surgery bone growth of 12-29% (load case 2) and 11-21% (load case 1), respectively, was predicted for the three types of screws. Type 3 (proximally coarse pitch screw) was estimated to have highest maximum pullout force (POF) and greater ossification among expandable pedicle screws with dual-threads.



***Keywords***: lumbar spine; finite element analysis; pedicle screw; expandable pedicle screw; bone remodelling; pullout force; mechanoregulation.

# Contents


Declaration iii
Certificate of approval v
Acknowledgements vii
Abstract ix
Contents xi
List of symbols and abbreviations xv
List of figures xix
List of tables xxiii

**Chapter 1: Introduction and Review of Literature 1**

1.1 Introduction 1
1.2 Anatomy and biomechanics of the spine 3
1.2.1 Anatomical planes and directions 3
1.2.2 Spine anatomy 4
1.2.3 Functional Spinal Unit 5
1.2.3.1 Vertebrae 5
1.2.3.2 Intervertebral disc 6
1.2.3.3 Facet joint 7
1.2.3.4 Ligaments 7
1.2.4 Spinal muscles 7
1.2.5 Spine Coordinate and Movement 7
1.2.6 Loads on spine 8
1.3 Degenerative disc disease 10
1.3.1 Surgical Treatment 11
1.3.1.1 Vertebral Screw Fixation 11
1.3.1.2 Failure Scenario of Pedicle Screw Fixation 13
1.4 Bone 14
1.4.1 Bone Structure 14
1.4.2 Mechanical properties of bone 14
1.4.2.1 Cortical bone 14
1.4.2.2 Cancellous bone 15
1.4.3 Bone cells 15
1.5 Literature Review: Lumbar Spine Biomechanics 16
1.5.1 Finite element models of lumbar spine 16
1.5.2 Modelling of different elements 17
1.5.3 Geometry Discretization 18
1.5.4 Material Properties of Vertebral Components 19

1.5.5 Boundary and loading Conditions 21
1.5.6 Adaptive bone remodelling 22
1.5.6.1 Mathematical formulation of bone remodelling process 25
1.5.7 Bone Ingrowth 28
1.5.7.1 Mathematical formulation of evolutionary bone ingrowth 30
1.5.7.2 Cell migration implemented through diffusion model 34
1.6 Clinical Investigation 35
1.7 Motivation of the present work: Research gap observed in the state-of-art 37
1.8 Objectives and scope of the study 39
1.9 Structure of the thesis 40

**Chapter 2: Development of 3D FE models of lumbar spine instrumented with expandable pedicle screws: intact versus implanted cases (Comparison between intact and implanted models) 43**

2.1 Introduction 43
2.2 Materials and methods 46
2.2.1 Development of the intact model 46
2.2.2 Development of the implanted models 47
2.2.3 FE model generation and analysis 48
2.2.4 Material properties 51
2.2.5 Loading and boundary conditions 52
2.3 Results 53
2.3.1. L4-L5 FSU: model validation based on ROM 53
2.3.2. ROM of the implanted models 54
2.3.3. Stress (von Mises) for cortical and cancellous bone 55
2.3.4. Strain (von Mises) for cortical and cancellous bone 59
2.3.5 Stress-strain within the intervertebral disc 63
2.4. Discussion 63
2.5 Summary of the findings 67

**Chapter 3: Bone Remodelling comparison between normal pedicle screw and expandable pedicle screw instrumented L4-L5 vertebrae 69**

3.1 Introduction 69
3.2 Materials and Methods 71
3.2.1 Development of 3D FE model of the intact model and implanted models 72
3.2.2 FE model generation and analysis 74
3.2.3 Material properties 75
3.2.4 Applied Loading and Boundary Conditions 76
3.2.5 Contact simulation 76

3.2.7 Bone remodelling algorithm 77
3.3 Results 78
3.3.1 Verification and Validation of FE model 78
3.3.2 Strain (von Mises) for cancellous bone 79
3.3.3 Strain energy density (SED) distribution for cancellous bone 81
3.3.4 Bone remodelling for cancellous bone 82
3.4 Discussion 84
3.5 Summary of the findings 91

**Chapter 4: Pullout strength comparison among three novel expandable pedicle screws 93**

4.1 Introduction 93
4.2 Materials and methods 95
4.2.1 Expanded Pedicle screw designs 95
4.2.2 Synthetic Bone 96
4.2.3 Pullout Test 97
4.2.4 Statistical analysis 98
4.2.5 FE modelling and geometry 98
4.3 Results 100
4.3.1 Experimental Validation of Pullout Test 100
4.3.2 Pullout FE simulation of foam 101
4.4 Discussion 102
4.5 Summary of the findings 104

**Chapter 5: Influence of three novel expandable pedicle screws on osseointegration: An FE study based on mechanoregulation algorithms 105**

5.1 Introduction 105
5.2 Materials and Methods 107
5.2.1 Development of expandable pedicle screw implanted 3D FE model 107
5.2.2 Applied loading and boundary conditions 109
5.2.3 Mechanobiological Tissue Differentiation Algorithm 110
5.3 Results 113
5.3.1. Spatial distribution of tissue phenotype according to mechanoregulation based algorithm 113
5.3.2. Temporal Distribution Around Tissue Phenotype 115
5.3.3. Average Young's modulus of tissue phenotype 118
5.4. Discussion 119
5.5 Summary of the findings 123

**Chapter 6: Conclusions and Future Scope of Work** **125**

6.1 Introduction 125
6.2 Significance and major contribution of the thesis 126
6.3. Limitations of the study 128
6.4 Scope for Future Research 128

**References** **131**

# NOMENCLATURE

## Symbols

| | |
|---|---|
| F | Force (N) |
| E | Young's Modulus (MPa or GPa) |
| ρ | Apparent density (g.cm-3) |
| S | Elastic strain energy per unit bone mass for implanted bone (J.g-1) |
| Sref | Elastic strain energy per unit bone mass for intact bone (J.g-1) |
| s | Dead zone |
| A(ρ) | Internal free surface area |
| a(ρ) | Internal free surface area per unit volume |
| Δt | Change in time |
| τ | Adaptive rate (g.mm-2(j/g)month) |
| U | Strain energy density |
| $U_a$ | Average strain energy density |
| k | Diffusion constant |
| c | Cell concentration |
| Z | Combined stimulus |
| γ | Shear strain |
| ʊ | Thermal conductivity |
| Ψ | Specific heat of the material |

# ABBREVIATIONS

| | |
|---|---|
| LBP | Lower Back Pain |
| LSS | Lumbar Spinal Stenosis |
| TDA | Total Disc Arthroplasty |
| FSU | Functional Spinal Unit |
| Fig | Figure |
| IVD | Intervertebral Disc |
| IAR | Instant Axis of Rotation |
| NZ | Neutral Zone |
| EZ | Elastic Zone |
| ROM | Range Of Motion |
| DDD | Degenerative Disc Disease |
| MSC | Mesenchymal Stem Cell |
| ECM | Extracellular Matrix |
| PEEK | Polyetherethrtketone |
| CBT | Cortical Bone Trajectory |
| TT | Traditional Trajectory |
| AT | Anatomic Trajectory |
| PMMA | Polymethylmethylacrylate |
| HA | Hydroxyapatite |
| PDSS | Posterior Dynamic Stabilization system |
| ISD | Interspinous Space Disease |
| ASD | Adjacent Segment Disease |
| SED | Strain Energy Density |
| FE | Finite Element |
| Eq. | Equation |
| BMD | Bone Mineral Density |
| TDR | Total Disc Replacement |
| 3D | Three Dimensional |
| 2D | Two Dimensional |
| CT | Computer Tomography |
| MRI | Magnetic Resonance Imaging |
| TLIF | Transforaminal Lumbar Interbody Fusion |

| | |
|---|---|
| Ti | Titanium |
| HU | Hounsfield Unit |
| POF | Pullout Force |
| PU | Polyurethane |
| ASTM | Americal Society of Testing and Materials |
| SS | Stainless Steel |
| FEA | Finite Element Analysis |
| HPDST | Hydrostatic pressure-deviatoric strain theory |
| DST | Deviatoric strain theory |
| ML | Machine Learning |

# List of Figures


| | | |
|---|---|---|
| **Fig. 1.1:** | Sketch showing the anatomical planes of reference and directions (Relly et al. 2018) | 4 |
| **Fig. 1.2:** | Regions of spine (Gharei 2018). | 5 |
| **Fig. 1.3:** | (a) Functional spinal unit (b) Vertebrae (c) Intervertebral disc (d) Ligaments (Somovilla-Gomez et al. 2020). | 6 |
| **Fig. 1.4:** | A coordinate system of FSU and different movements (Somovilla-Gomez et al. 2020). | 8 |
| **Fig. 1.5:** | Maximum compressive force at L4-L5 during different physical activities under training conditions in the laboratory (Schefer et al. 2023). | 9 |
| **Fig. 1.6:** | Degenerative disc disease (https://nielasher.com). | 10 |
| **Fig. 1.7:** | Radiographs after lumbar interbody fusion surgery (Kwon et al. 2020). | 11 |
| **Fig. 1.8:** | Types of screws (a)Cylindrical pedicle screw (b) Conical pedicle screw (c) Fenestrated pedicle screw (d) Expandable pedicle screw € Polyaxial pedicle screw (Tandon et al. 2020) | 12 |
| **Fig. 1.9:** | Computational Scheme of adaptive bone remodelling. | 26 |
| **Fig. 1.10:** | The relationship between stimulus and rates of bone adaptation in bone remodelling (Ghosh et al. 2013). | 27 |
| **Fig. 1.11:** | Martin's equation of relationship between free surface area per unit volume and apparent density (Scandell and Prendergast 2009). | 28 |
| **Fig. 1.12:** | Tissue differentiation from Mesenchymal stem cells (Merimi et al. 2021) | 29 |
| **Fig. 1.13:** | Mechanoregulatory hypotheses of Carter et al. (1988). | 31 |
| **Fig. 1.14:** | Mechanoregulatory principles of Claes and Heigele (1999). | 31 |
| **Fig. 1.15:** | Mechanoregulatory algorithm by Prendergast et al. 1997 | 32 |
| **Fig. 1.16:** | Influence of combined stimulus on tissue differentiation. | 32 |
| **Fig. 1.17:** | Computational scheme for mechanoregulatory tissue differentiation simulation. | 34 |
| **Fig. 2.1:** | 3D CAD models of the L4-L5 FSU: (a) intact, (b) implanted with normal pedicle screw, (c)implanted with expandable pedicle screw. | 46 |
| **Fig. 2.2:** | The curated models of different parts of an intact L4-L5 FSU. | 49 |
| **Fig. 2.3:** | The curated models representing different parts of the two implanted L4-L5 FSUs. | 50 |
| **Fig. 2.4:** | The various physiological loading and boundary conditions for (a) intact FE model, (b) implanted FE model for normal pedicle screw and (c) implanted FE model for expandable pedicle screw. 'RBE3' denotes the rigid body element surrounding the L4 | 52 |

vertebra, whereas 'CGAP' elements were defined to simulate ligament properties.

**Fig. 2.5:** Comparison of ROM values of the current intact FE model with those obtained from the literature: (a) Flexion, (b) Extension, (c) Torsion, (d) Lateral bending and € Axial compression. 53

**Fig. 2.6:** Von Mises stress contours (in MPa) in cortical bone for (a) intact FSU and FSUs corresponding to (b) normal and (c) expandable pedicle screws, respectively. 56

**Fig. 2.7:** Von Mises stress contours (in MPa) in cancellous bone for (a) intact FSU and FSUs corresponding to (b) normal and (c) expandable pedicle screws, respectively. 57

**Fig. 2.8:** Von Mises stress contours (in MPa) in cancellous bone (sectional view) (a) intact FSU and FSUs corresponding to (b) normal and (c) expandable pedicle screws, respectively. 58

**Fig. 2.9:** Von Mises strain contours in cortical bone for (a) intact FSU and FSUs corresponding to (b) normal and (c) expandable pedicle screws, respectively. 60

**Fig. 2.10:** Von Mises strain contours in coancellous bone for (a) intact FSU and FSUs corresponding to (b) normal and (c) expandable pedicle screws, respectively. 61

**Fig. 2.11:** Von Mises strain contours in coancellous bone (sectional view) for (a) intact FSU and FSUs corresponding to (b) normal and (c) expandable pedicle screws, respectively. 62

**Fig. 2.12:** Stress-strain diagram for intervertebral disc (IVD) for intact FSU under compression. 63

**Fig. 3.1:** The curated models of different parts of an intact L4-L5 FSU - (a) with ligament ALL, ITL (b) with ligament PLL, FCL, LF, ISL, SSL (c) Intervertebral disc (d) Loading and Boundary Condition. 73

**Fig. 3.2:** The curated models of different parts of an implanted L4-L5 FSU-(a) with ligament ALL, ITL, ISL, SSL (b) normal pedicle screw-rod system (c) expandable pedicle screw-rod system (d) cage (e) Intervertebral disc (f) Loading and boundary condition. 74

**Fig. 3.3:** Comparison of ROM values of the current intact FE model with those obtained from earlier literature: Flexion, Extension, Torsion, and Lateral bending. 79

**Fig. 3.4:** Von Misses strain contours in cancellous bone for (a) intact FSU and FSUs corresponding to (b) normal and (c) expandable pedicle screw, respectively. 80

**Fig. 3.5:** Strain Energy Density distribution (J/g) for cancellous bone in (a) intact FSU and FSUs corresponding to (b) normal and (c) expandable pedicle screw, respectively. 81

**Fig. 3.6:** Bone density distribution ($g/cm^3$) for cancellous bone (L4-L5 vertebra separately) in implanted FSUs corresponding to (a) normal pedicle screw and (b) expandable pedicle screw, respectively. 82

| | | |
|---|---|---|
| **Fig. 3.7:** | Bone density distribution ($g/cm^3$) for cancellous bone (sectional view) in sectional view in AA plane in implanted FSUs corresponding to normal pedicle screw and expandable pedicle screw, respectively. | 83 |
| **Fig. 3.8:** | Average bone density variation with time increments for cancellous bone ROI of (a) L4 vertebra, (b) L5 vertebra after implantation. | 88 |
| **Fig. 3.9:** | Average bone density variation with time increments for cancellous bone for L4-L5 vertebra in (a)ROI1, (b)ROI2, (c)ROI3, (d)ROI4, (e)ROI5, (f)ROI6, (g)ROI7, (h)ROI8. | 89 |
| **Fig. 4.1:** | Non-expanded (2D and 3D) and expanded pedicle screws (L-R) of (a) type 1 (b) type 2 (c) type 3. | 95 |
| **Fig. 4.2:** | Pre-pullout set up: (a) screw inserted on foam (b) Loading and boundary condition of the meshed model (c) Schematic diagram of test set up (d) test set up. | 97 |
| **Fig. 4.3:** | Axial pullout test validated with FE studies for (a) type 1 (b) type 2 (c) type 3 screws. | 101 |
| **Fig. 4.4:** | Axial pullout simulation results for type 1, type 2, and type 3 screws (a) starting of the simulation, (b) Foam fracture started (c) pullout completed. | 102 |
| **Fig. 5.1:** | (a) Implanted vertebra equivalence to screw-foam system (b) Representative CAD model of the bone-implant system with (top to bottom) foam, tissue, and implant (Type 1, Type 2, Type 3) (c) Loading and boundary condition. | 108 |
| **Fig. 5.2:** | Schematic overview of mechanoregulation based tissue differentiation algorithm. | 111 |
| **Fig. 5.3:** | Spatial distribution of tissue on-growth for three types of expandable pedicle screws for loading cases considering hydrostatic pressure and deviatoric strain after 6 weeks of healing. | 114 |
| **Fig. 5.4:** | Spatial distribution of tissue on-growth for three types of expandable pedicle screws for loading cases considering deviatoric strain after 6 weeks of healing. | 115 |
| **Fig. 5.5:** | Influence of mechanical stimulus (HPDST) on tissue growth for loading-10Nm,150N (a) Type 1 (b) Type 2 (c) Type 3, 5Nm,150N (d) Type 1 (e) Type 2 (f) Type 3. | 116 |
| **Fig. 5.6:** | Influence of mechanical stimulus (DST) on tissue growth for loading-10Nm,150N (a) Type 1 (b) Type 2 (c) Type 3, 5Nm,150N (d) Type 1 (e) Type 2 (f) Type 3. | 117 |
| **Fig. 5.7:** | Influence of tissue stiffness based on mechanical stimulus at the bone-implant interface for loading-(a)10Nm,150N (b)5Nm,150N | 118 |
| **Fig. 5.8:** | Spatial distribution (cross-sectional view) of tissue on-growth for three types of expandable pedicle screws for loading cases considering deviatoric strain+hydrostatic pressure (HPDST) and deviatoric strain (DST) after 6 weeks. | 119 |

# List of Tables


| | | |
|---|---|---|
| **Table 1.1:** | Material properties of vertebral body used in earlier studies. | 20 |
| **Table 1.2:** | Mechanical properties of the ligaments used in earlier studies. | 21 |
| **Table 2.1:** | Material properties corresponding to various components of the FSU. | 51 |
| **Table 2.2:** | Ligament properties. | 52 |
| **Table 2.3:** | ROM (in degrees) of the intact model during different physiological movements. | 54 |
| **Table 3.1:** | Material properties corresponding to various components of the FSU. | 75 |
| **Table 3.2:** | Ligament properties taken from Talukdar et al. 2021. | 76 |
| **Table 3.3:** | Average Bone Density in $g/cm^3$ of L4 and L5 vertebra: Immediate post-operative and after equilibrium condition. | 84 |
| **Table 3.4:** | Average Bone Density in $g/cm^3$ of L4 and L5 vertebra in ROI 1-8: Immediate post-operative and after equilibrium condition. | 85 |
| **Table 4.1:** | Design specifications of expandable pedicle screw. | 96 |
| **Table 4.2:** | Material properties of foam and screws. | 99 |
| **Table 4.3:** | Johnson-Cook plasticity model constants for cancellous bone adapted from Demirbas et al. 2022. | 100 |
| **Table 4.4:** | Comparison of pullout results for three types of expandable pedicle screws. | 100 |
| **Table 5.1:** | Material properties of bone, tissue and screw. | 109 |
| **Table 5.2:** | Predicted tissue phenotype material properties and the mechanical stimulus based on different mechanoregulation algorithm (Carter *et al*. 1988, Claes and Heigele 1999, Lacroix and Prendergrast 2002a, Isaksson *et al.* 2006, Mehboob *et al*. 2017, Mehboob *et al*. 2020, Ghosh *et al.* 2020, Mohendas *et al.* 2021). | 112 |

# Chapter 1

## Introduction and Review of Literature

### 1.1 Introduction

The lumbar spine, a crucial component of the human body, comprises five vertebrae (L1-L5) along with their posterior elements articular facet joints, intervertebral discs, ligaments and associated muscles. The upper ends of the posterior surfaces are strengthen by pedicles, offering protection as well as serving as a bridge, connecting anterior-posterior aspects of the vertebra. The fracture of the pedicles results in extreme pain and caused degradation of life (Keramat *et al.* 2012). The vertebral compression failure causes potentially acute and chronic pain and finally life quality deterioration (Elin *et al.* 2015, La Barbera *et al.* 2019). According to resources, around 1.5 million vertebral compressions occur in elderly persons in the USA annually (Alexandru and William 2012). A significant percentage of the world population experiences lower back pain (LBP), ranging from chronic to post-operative conditions. Degenerative lumbar diseases such as lumbar spinal stenosis (LSS), degenerative spondylolistheses, lumbar instability, and ligament strain might induce lower back pain (Nikkhoo *et al.* 2021, Serhan *et al.* 2011). LSS is a condition commonly associated with elderly persons, especially those over the age of 65. However, owing to a sedentary lifestyle, younger populations are also being affected (Fan *et al.* 2019). With ageing people experiencing degeneration, the process eventually results in lower back pain, significantly contributing to global disability (Godinho *et al.* 2021, Hartvisgen *et al.* 2018). In 2015, around 7.3% of the global population i.e. around 540 million people were suffering from lower back pain at any given time (Hartvisgen *et al.* 2018). Post-diagnosis, the treatment could be based on a conservative or surgical approach. In the case of a conservative approach, medication and physical therapies are used. If pain even after that, a surgical approach may be necessary. For treating lower back pain, the surgical approach involves fusion surgery, total disc arthroplasty (TDA) and dynamic stabilizer. Spinal fusion is the most commonly used method for spine surgery for degenerated discs. The life expectancy of the global population is increasing and proper spinal fusion would be beneficial in overcoming geriatric challenges (Bereczki *et al.* 2021, Fuster 2017, Shamji *et al.* 2015). Approximately 25% of postmenopausal women experience spinal fractures, which cost an enormous amount of money for healthcare.

Based on patient-specific data, it was estimated that for women over 70 years, one-third of them suffered from vertebral fractures following posterior fusion (Nakahashi *et al.* 2019). Pedicle screw fixation has slowly garnered popularity through an extensive range of spinal fusions developed in the past 50 years.

Osteoporosis is often associated with reduced spinal stability, decreased bone strength and deformity most commonly in elderly patients (Burval *et al.* 2007, Li *et al.* 2013, Ponnusamy *et al*. 2011). Elderly patients with osteoporosis often experience postoperative complications, e.g. loosening of pedicle screws, rod breakage, and pedicle fracture (Huang *et al*. 2022b, Park *et al*. 2004). In Europe, over 27.6 million people are affected by osteoporosis and in the US more than 20 million people suffer from this condition (Burval *et al*. 2007, Girardo *et al.* 2017). In Europe, approximately 6% of men and around 21% of female patients between the age of 50-84 years were diagnosed with osteoporosis (Girardo *et al*. 2017, Rahyussalim *et al*. 2019). In the US, 17-20% of women over 50 years, 26% of women over 65 years and around 50% over 80 years suffer from osteoporosis (Li *et al.* 2013). Around 14.5% of male and 51.3% of female patients over the age of 50 years in the US were reported to have undergone spinal surgery (Li *et al.* 2013). From 1990-2001, an increase of around 220% in lumbar fusion surgery was reported (Martin *et al*. 2007). Data collected in 2018 revealed that more than 3,50,000 interbody fusion procedures were found to be the most commonly performed spinal procedures in the USA alone (de Kater *et al*. 2022). The annual report by "the New Zealand Joint Registry 2020" showed 195 registered lumbar disc replacements and 3 revision surgeries performed from January 2002 to December 2020. A total number of 348 primary and 6 revision lumbar disc replacement was performed from the year 2002 to 2020, as stated by the Norwegian Arthroplasty Register (2021). The British Spine Registry 2021 recorded a total number of 73,787 primary decompression. The Australian Spine Registry 2022 reported that 53% of male and 47% of female patients suffer from discectomy and among them, 72% of male and 75% of female patients were above age 50.

Spine fusion is considered to be stabilizing treatment that might reduce the necessity of additional surgery. For clear reasons, it is quite undesirable to proceed with repeated lumbar surgery because of reasons such as persistent symptoms, degenerative changes, and treatment complications (Martin *et al.* 2007). Pedicle screws are quite effective for the treatment of spinal problems but they sometimes fail due to aseptic

loosening, pullout and fatigue fractures (Kwon *et al.* 2020). A significant amount of surgery failure could be seen for spinal surgeries conducted to restore the normal disc height and to relieve lower back pain (Hsieh *et al.* 2007, Zhou *et al.* 2019). Around 15% of the patients with degenerative cases end up having revision surgery of the lumbar spine (Alanay *et al.* 2007). The failure rate of lumbar surgery was estimated to reach up to 50% in the US (Rajaee *et al.* 2014, Daniell *et al*. 2018). Around 14-27% of patients underwent revision surgery due to complications, e.g. the improper placement of the implant, fixation loss, fatigue-bending failure, nerve root injury, and aseptic loosening (Pearson *et al*. 2017). A study based on broken pedicle screws suggested that breakage was influenced by symptomatic indication of the patient, implant material and load sharing of the screws (Chen *et al*. 2005). Clinical studies also explained the various reasons for failure and the need for pertinent improvements (Gautschi *et al.* 2011).

The pedicle screws are intrusively implanted to the vertebra such that osseointegration can be achieved with the host bone. The success rate of osseointegration plays a crucial role in the success of the implant in the long run. However, the success of the implant is reliant on the quality of the bone. Diminished bone quality would result in screw loosening and eventually failure. It is already mentioned how the elderly population is severely affected by reduced bone quality due to osteoporosis. Considering these factors, some new alternative designs have been proposed in recent years. The expandable screws are one of those alternative designs that are expected to have better holding capacity minimizing the influence of loosening and screw pullout. A few studies present the potential viability of expandable pedicle screws in clinical and experimental aspects. However, there is a scarcity of preclinical studies considering the success of expandable pedicle screws over traditional pedicle screws, and post-surgery host bone adaptation. Before delving deeper into these implants, it is important to understand the anatomy and biomechanics of the spine.

## 1.2 Anatomy and biomechanics of the spine

### 1.2.1 Anatomical planes and directions

The concept of anatomical planes is essential for understanding the basic human anatomy. The three anatomical planes are assumed based on various orientations of the human body in standing erect position as shown in Fig. 1.1 (Relly *et al.* 2018). The plane parallel to the ground dividing the superior (top) and inferior (bottom) halves of the human body is termed the transverse (axial) plane. A plane perpendicular to the

ground and dividing the anterior (front) and posterior (back) parts of the body is known as the coronal (frontal) plane. The sagittal (median) plane is a vertical plane perpendicular to both the transverse and coronal planes, dividing the human body's left and right half.

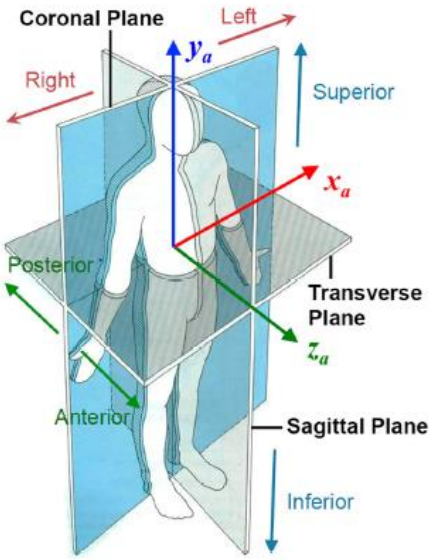


**Fig. 1.1:** Sketch showing the anatomical planes of reference and directions (Relly *et al.* 2018).

### 1.2.2 Spine anatomy

The human spine is comprised of seven cervical vertebrae (C1-C7), twelve thoracic vertebrae (T1-T12), five lumbar vertebrae (L1-L5), and one sacrum along with the coccyx. The primary functions of the spine are motion, flexibility, support of upper body weight and protection of the spinal cord. An adult healthy spine is double S-shaped with two convex curvatures and one concave curvature. The S-curves help provide resistance to the axial loads applied on the spine and maintain elasticity. The cervical spine is situated at the superior region of the spine. The primary function of the cervical spine is to provide stability, and mobility to the head and the most flexible part of the spine. The size of the thoracic spine increases from T1 to T12 and has limited movement. It holds the rib cage and protects internal organs such as the heart, and lungs. The lumbar vertebrae are larger and have more flexibility than the thoracic spine. It bears the weight of the upper body and transfers the load to the sacrum and thus becomes the most vulnerable zone of the spine to injury. The spine is connected to the hip bones via the sacrum. The sacrum is situated between the pelvic bones and is large,

flat, triangular-shaped. The connection of the sacrum with the hip bones (iliac) on both sides form the sacroiliac joints. The last segment of the vertebra is known as the coccyx (tailbone). The pelvic girdle is comprised of a sacrum, coccyx and two sacroiliac joints.

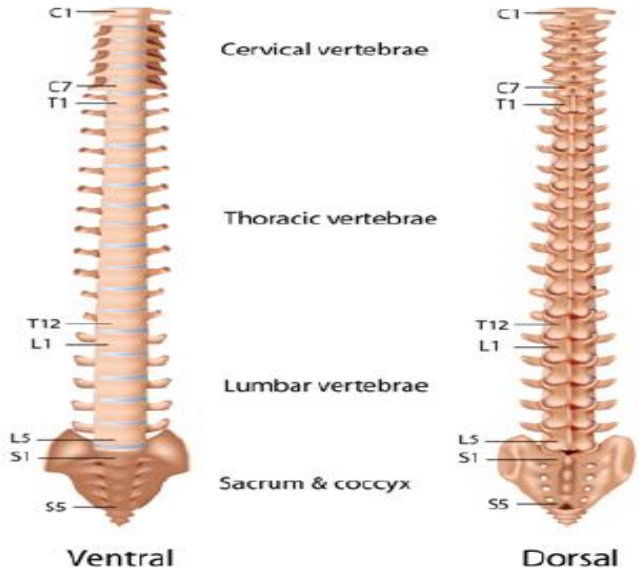


**Fig. 1.2:** Regions of the spine (Gharei 2018).

### 1.2.3 Functional Spinal Unit

The functional spinal unit (FSU) is the smallest unit of the spine and represents all its major biomechanical and characteristic features (Kurtz 2010) (Fig. 1.3a). It is essentially composed of two vertebrae, an intervertebral disc, two facet joints, and seven ligaments surrounding them except the muscles. Its various components are described below.

#### 1.2.3.1 Vertebrae

The vertebra has roughly a cylindrical shape and consists of vertebral body, vertebral arch, two transverse processes, one spinous process and four articulating facets (Fig.1.3b). The vertebral body (anterior part of vertebra) is composed of outer cortical bone and inner cancellous (trabecular) bone. The vertebral arch is the posterior part of the vertebra and is comprised of two pedicles and a lamina. The laminae and the pedicles combined form the neural arch. The shape, size and physical properties of the vertebra vary with age.

### 1.2.3.2 Intervertebral Disc

The intervertebral discs (IVD) are fibro-cartilages of roughly cylindrical shapes (Fig. 1.3c). They act as shock absorbers separating two vertebrae. Usually, during daily life activities, under the influence of compressive loads, the water gets squeezed out reducing the height and during bedtime, the water gets back restoring disc height. The intervertebral disc is composed of the annulus fibrosus, nucleus pulposus and endplates.

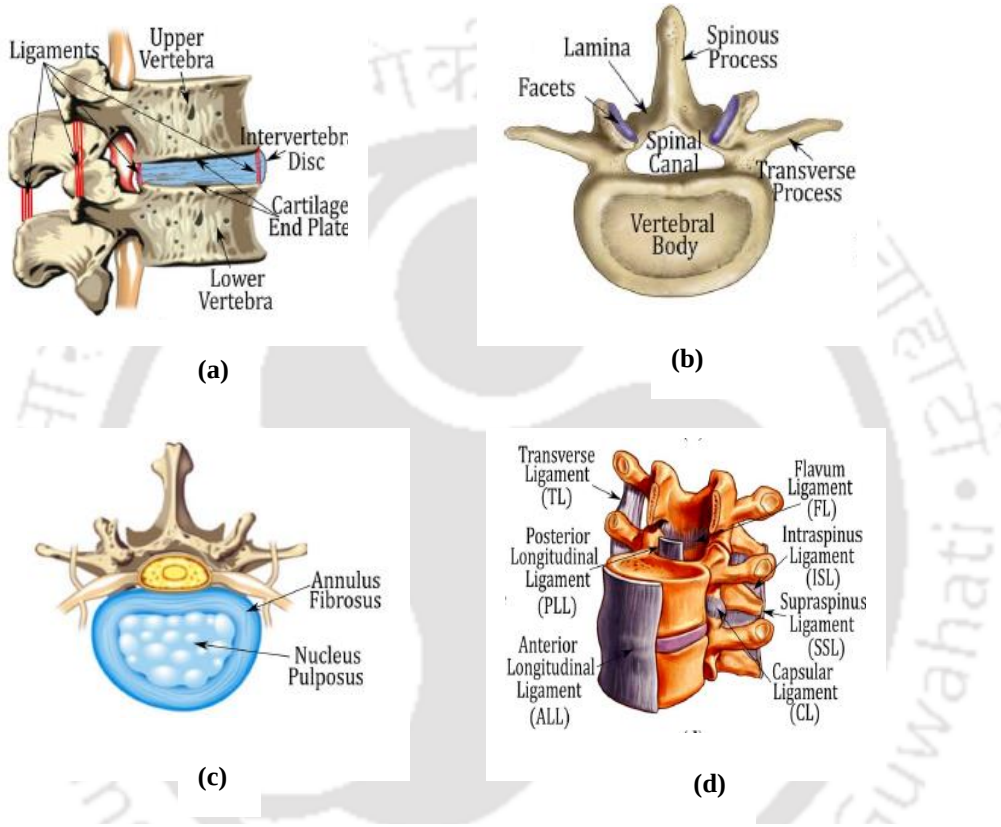


**Fig. 1.3:** (a) Functional spinal unit (b) Vertebrae (c) Intervertebral disc (d) Ligaments (Somovilla-Gomez *et al.* 2020).

The nucleus pulposus is the innermost part comprised of loose fibres in a hydrating gel that exerts pressure in different directions. The annulus fibrous surrounds the nucleus pulposus and is composed of concentric layers of collagen fibres and ground substance. The endplates separate the nucleus and annulus from the vertebral bodies. The cartilaginous endplates occupy the adjacent surface of the vertebral body and the bony endplates act as a narrow rim covering the area of the cartilaginous endplates.

#### 1.2.3.3 Facet Joint

The facet joints are synovial joints that are situated between the superior articular facet of one vertebra and the inferior articular facet of the adjacent vertebra on both sides of the vertebra (Fig. 1.3b). The facet joints are composed of fibrous capsules, articular cartilage and synovial fluids. They help the spine to bend and twist and can transmit load to the discs.

#### 1.2.3.4 Ligaments

The ligaments are strong fibrous bands of tissues that hold the bone, joints, and organs together. They are composed of collagen fibres, fibrocytes and ground substance. Ligaments provide stability to the spine within its physiological ranges of motion and constrain excess movements, like hyperextension and hyperflexion. There are seven ligaments in the lumbar spine namely: (i) Anterior longitudinal ligament (ALL), (ii) Posterior longitudinal ligament (PLL), (iii) Ligamentum flavum (LF), (iv) Intertransverse ligament (ITL), (v) Capsular ligament (CL), (vi) Interspinous ligament (ISL), (vii) Supraspinous ligament (SSL) (Fig. 1.3d).

### 1.2.4 Spinal Muscles

Spinal muscles are known as back muscles and provide stability, support and dynamic movement for the spine. Based on location, the muscles are distinguished as postvertebral and prevertebral muscles. The prevertebral muscles are the abdominal muscles. The postvertebral muscles consist of short muscles that connect adjacent spinous and transverse processes and laminae. The erector spine group helps in spinal extension, lateral flexion, and rotation; the multifidus muscles offer segmental stability; and intrinsic back muscles provide spinal alignment and posture.

### 1.2.5 Spine Coordinate and Movement

The FSU's coordinate system is fixed upon centre of the upper vertebral body known as the instant axis of rotation (IAR)(Fig.1.4). Based on the coordinate system the following movements are defined, flexion-extension on the transverse axis (Sagittal plane); lateral bending, left and right rotation to the sagittal axis (Frontal plane); torsional movement, rotation about the longitudinal axis (Transverse plane). The spine provides motion to the trunk.

Spine instability is defined as the reduction of stiffness in a segment resulting in abnormal and excess deformation of motion. The spinal movement is characterized in

the following segments-(1) the initial part known as the neutral zone (NZ) with no resistance, (2) the elastic zone (EZ) producing internal resistance, (3) the range of motion (ROM) is the sum of the neutral zone and elastic zone. Considering the erect standing position as the reference position, the ROM varies for different vertebrae. Usually, the ROM for flexion-extension is $12^0$-$16^0$, lateral bending is $6^0$ and $3^0$ for torsion.

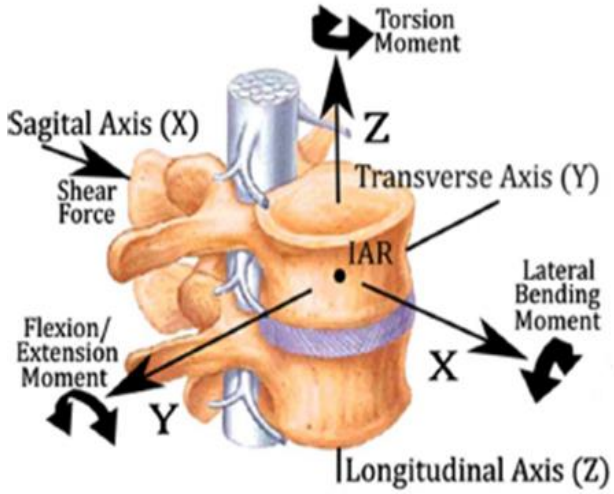


**Fig. 1.4:** A coordinate system of FSU and different movements (Somovilla-Gomez *et al*. 2020).

The spinal mobility depends on factors like the states of intervertebral discs like geometry, stiffness, fluid content, viscoelastic properties, degeneration, and ageing. The ROM might be influenced by the ligament condition, articular facet joint and even posterior bony endplates.

### 1.2.6 Loads on Spine

The spine serves as the primary load-bearing component of the human musculoskeletal system. The force on the spine is a combination of upper body weight, ligamentous tension, muscle force, and applied external loads. The forces applied are characterized as physiological loads and traumatic loads. The physiological loads include everyday action on the spine like short-term load (flexion, extension), long-term load (sitting, standing), cyclic load (walking) and dynamic load (running). Traumatic loads are sudden and accidental forces with great amplitude. Though direct assessment of spinal loading is not feasible, indirect calculation is done via in-vivo measurements and mathematical modelling. Authors used indirect measurements like internal disc

pressure (Nachemson 1966, Wilke *et al.* 1999), daily life activities (Granhead *et al.* 1987), force on the internal spinal fixator (Rohlmann *et al*. 2007), and daily life sports activity (Schafer *et al*. 2023). The high mechanical loads combined with higher mobility on the lumbar spine make it vulnerable to injury and low back pain. As the lumbar spine bears the highest amount of load in the spine, it has become a major region of interest for researchers and clinicians. Previous studies (Atlas *et al.* 2001) suggested the peak incidence of back pain was for 30-55-year-old people in the L4-L5 or L5-S1 region.

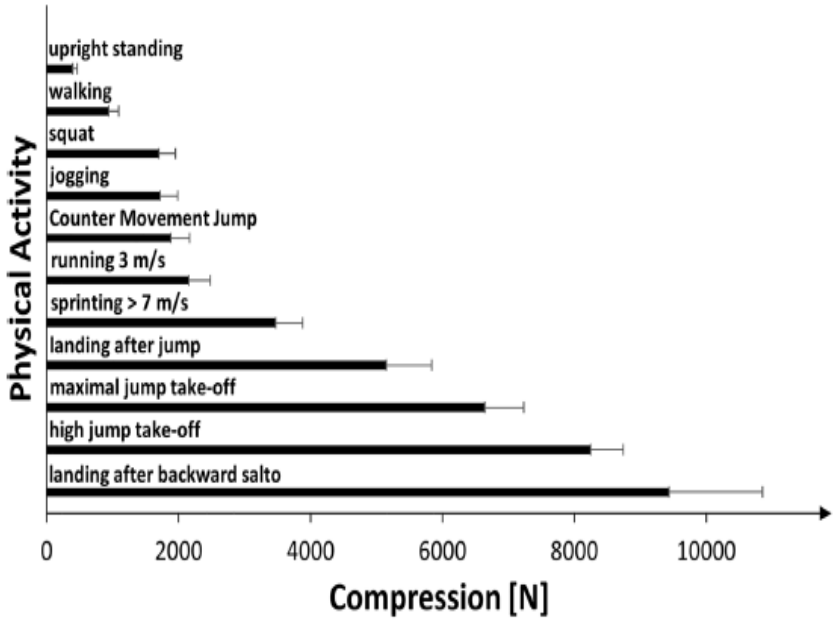


**Fig. 1.5:** Maximum compressive force at L4-L5 during different physical activities under training conditions in the laboratory (Schafer *et al*. 2023).

The posture of the body has a direct influence on the compressive force acting on the lumbar spine. The minimum loading on the spine occurs when lying in a supine position. Sitting in an upright position, with or without support and, sitting in a bending position with or without a load increase the compressive force. It is expected that external loading increases the load to the highest extent. Generally, the vertical load reaches around 50-60% of the body weight while standing upright. The line of action passes ahead of the lumbar spine creating a forward bending moment. The ligaments and erector muscles balance the forward bending moment. The muscles due to their short moment arm from the spinal segment increase the compressive load on the osseoligamentous spine.

In their study, Schafer *et al*. (2023) estimated compressive load on L4-L5 in terms of body weight (BW). Some of these estimated loads are as follows:- standing upright equals 0.93 times BW, lifting a barbell of 10 kg equals 4 times BW, walking equals 1.4 times BW, jogging and jumping are 3.6 times and around 4.7 times of the BW, respectively.

### 1.3 Degenerative Disc Disease

Degeneration refers to specific injuries resulting in variations in the composition, structure and function of the spine. One of the primary causes of spinal instability and lower back pain can be addressed as intervertebral disc degeneration. Degeneration can be a long-term (age-related) or a short-term (environmental-related) condition. Numerous factors like trauma, ageing, obesity and genetics might influence degeneration.

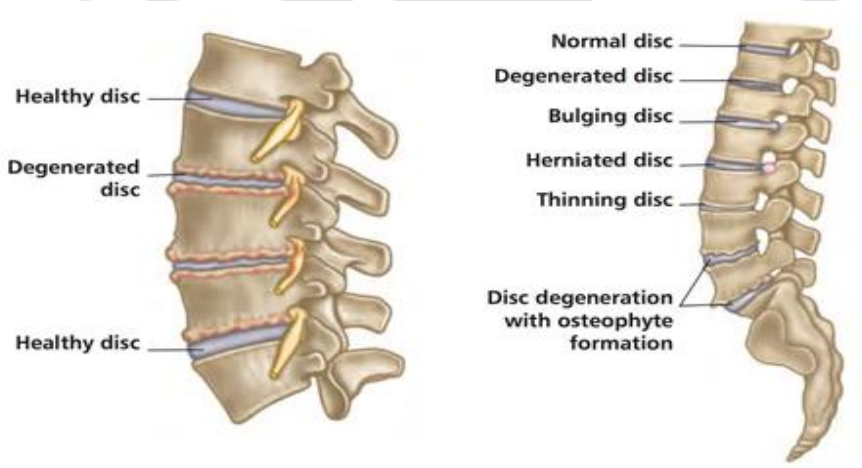


**Fig. 1.6:** Degenerative disc disease (https://nielasher.com).

In case of age-related degeneration, annulus tear or disc prolapse and herniation or osteoporotic failure of trabecular bone might take place. With ageing, disc loses water absorbing components and results in reduced disc height and disc dehydration. The short-term degeneration is caused by sudden or unexpected movements, overloads, accidents, trauma and finally mechanical damage of the spine. The loss of biomechanical function with pain is called degenerated disc disease (DDD). Disc degeneration along with bulging is termed as herniation causing nerve root compression. Anatomic narrowing of the spine is known as lumbar spinal stenosis (LSS). Spondylolysis is commonly observed in the lower lumbar vertebra and is an influential reason behind lower back pain.

### 1.3.1 Surgical Treatment

Surgical treatment for spinal disorders has two major interventions namely fusion and non-fusion. The spinal fusion technique is used to join two or more vertebrae together to restrict motion in the non-stabilized segments of the spine. The biomechanical goals of fusion are to restore intervertebral disc height and promote fusion by providing immediate stability. Interbody cages or spacers preserve the disk height, lead to bone growth and finally enhance stability. Pedicle screws add extra support and strength during the healing process.

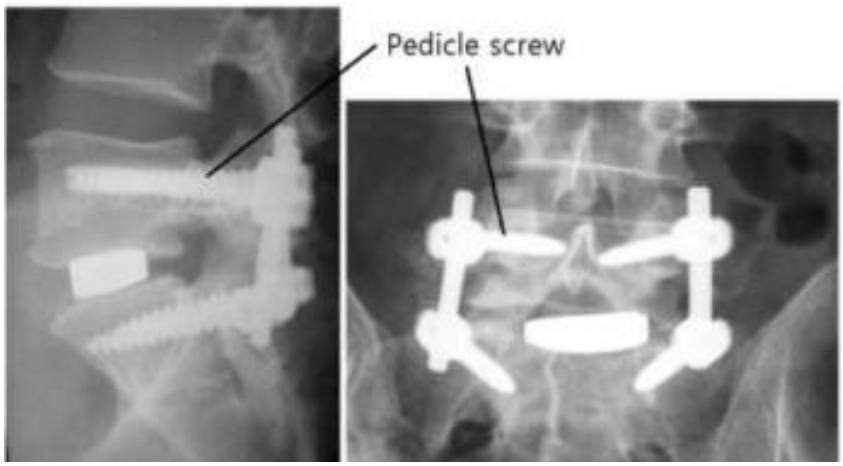


**Fig. 1.7:** Radiographs after lumbar interbody fusion surgery (Kwon *et al*. 2020).

During some of the spinal complications, such as scoliosis, spinal stenosis and discogenic low back pain, some non-fusion techniques are proposed to preserve the motion as an alternative to fusion. They try to resolve the anatomic surgical defects with the use of a non-fusion approach by replacing pro-inflammatory tissues, restoring spinal alignment and decompressing neural elements. They do not use bone grafts. Examples of non-fusion are growth-sparing devices and artificial discs.

#### 1.3.1.1 Vertebral Screw Fixation

The first vertebral screw fixation was performed in 1944 by placing screws to avoid postoperative external immobilization. Pedicle screws were first described by Boucher in 1959 using stainless steel for internal fixation. The proper documentation of pedicle screw fixation was started by Roy-Camille in the 1970s. For treating spinal instability, deformity correction, trauma, degenerative diseases, and osteoporosis-related issues like spondylolisthesis, vertebral compression fracture pedicle screws are widely used. Pedicle screw fixation is considered as the gold standard for fixation surgery.

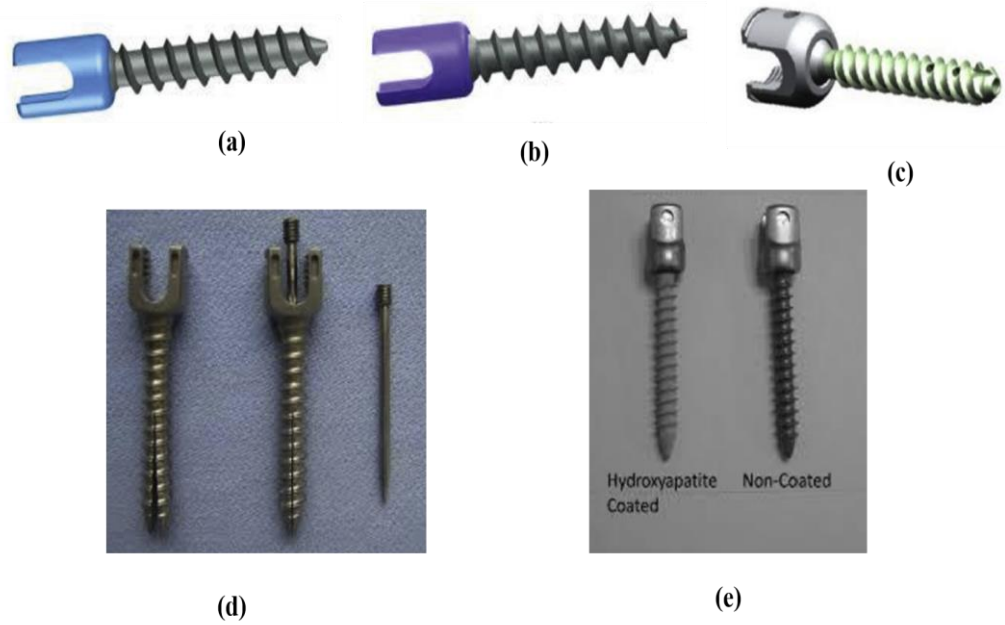


**Fig. 1.8:** Types of screws(a)Cylindrical pedicle screw (b)Conical pedicle screw (c)Fenestrated pedicle screw (d) Expandable pedicle screw (e) Polyaxial head pedicle screw (Tandon *et al*. 2020)

The biomechanics of screws is characterized by mainly three aspects-(a) screw characteristics (b) insertion technique of screw and (c) cement augmentation (Rahyussalim *et al.* 2019). The screw is composed of three parts, e.g.-head, neck and the body. The screws exhibit cylindrical or conical shapes characterized by outer diameter, inner diameter and pitch. The designs of screws are modified by altering their shapes and forms. Some examples of modified screws are fenestrated pedicle screws that have cannulated core with a hole in the distal part, cannulated pedicle screws with cement augmentation, expandable pedicle screws and anchor-type pedicle screws with an anchor made of polyetheretherketone (PEEK). To achieve ideal bone fixation with osteoporotic patients is a challenge for surgeons. It was noticed that screw track modification involving pilot holes became a method to enhance the screw-bone interface. Cortical bone trajectory (CBT) provides enhanced fixation strength as it increases the thread contact area with the cortical bone surface and better screw grip (Matsukawa *et al*. 2015). CBT is less invasive, and thus requires smaller incisions and less lateral tissue dissection (Wang *et al.* 2020). The traditional trajectory (TT) requires extensive tissue dissection and has been used from earlier days. Some new trajectory techniques like anatomic trajectory (AT), and straightforward trajectory (ST) were also

introduced (Guvenc *et al.* 2019). Some surgical instruments like spinal hooks, sublaminar bands, sacral alar iliac (S2AI) screws, and modified screwing techniques are introduced for the augmented pedicle screw fixation (Kanno *et al*. 2022). To augment the pedicle screws for better fixation, materials like polymethylmethacrylate (PMMA) and hydroxyapatite (HA) are used.

#### 1.3.1.2 Failure Scenario of Pedicle Screw Fixation

The vulnerability of osteoporotic bone to fracture increases to a high extent due to low bone mineral density. The low bone density weakens the screw fixation strength causing the loosening of screws and ultimately fixation strength loss. The screw loosening rate for non-osteoporotic patients varies from 0.6-15% and around 60% for osteoporotic patients (Galbusera *et al.* 2015, Kanno *et al*. 2022). The primary goal of the surgeons is to diminish fractures, achieve bony union to reestablish spinal anatomy and provide posterior spinal stability (Li *et al*. 2014). Though the pedicle screws are associated with the long-term stability of the human lumbar spine, however, complications arise like screw loosening, screw breakage, fracture, fatigue and bending failure, improper instrumentation placement, fixation loss, screw pullout, nerve root injury, infections leading to failure and adjacent disc degeneration (Alanay *et al.* 2007, Pearson *et al*. 2017, Zhou *et al.* 2018, Xu *et al.* 2019). Improper selection, orientation and positioning of the screw would lead to reduced fatigue life of the screws (Chu *et al.* 2019, Giacaglia and Lamas 2015, la Barbera *et al.* 2014). To abolish lower back pain, degenerated discs are often replaced with a cage (Godinho *et al*. 2021, Postacchini *et al*. 2016).

Some devices known as posterior dynamic stabilization system (PDSS) are attached to the back of the vertebra to have control over abnormal motion due to spinal diseases and to ease the disease (Heo *et al.* 2020). To diminish problems like lumbar tissue damage associated with PDSS, Interspinous space devices (ISD) are developed (Heo *et al.* 2020). Implant placement comes with an excessive amount of dissection leading to muscle weakness and eventually failed back surgery (Fu *et al.* 2020, Huang *et al.* 2022b). Spinal fusion might increase stress on the non-operated adjacent lumbar segment and create complications related to adjacent segment degeneration like endplate fracture, cage fracture and fracture and finally reoperation (Park *et al*. 2004, Inoue *et al.* 2021). Reduction of adjacent segment disease (ASD) was associated with the introduction of artificial discs and dynamic stabilization implants (Beatty 2018,

Nikkhoo *et al.* 2021). A hybrid stabilization system was introduced later to resolve disc degenerated diseases (Demir *et al*. 2020, Más *et al.* 2017).

## 1.4 Bone

Bone is a connective tissue that forms the primary structural element of the body, providing support to maintain posture. It also protects vital internal organs such as the heart, lungs, brain etc. The bones interact with the muscles to enable various movements.

### 1.4.1 Bone Structure

From an engineer's viewpoint, bone is anisotropic, non-homogenous and viscoelastic by nature. Bone is a composite structure consisting of macrostructure (cortical, cancellous bone), microstructure (osteons), sub-microstructure (lamellae), nanostructure (collagen fibrils, embedded minerals), sub-nanostructure (mineral, collagen). Bone contains around 40% inorganic component (hydroxyapatite), 35% organic component and 25% water. Macroscopically, bone is classified as cortical bone and cancellous bone based on their relative densities (Gibson 1985). The outer shell of the bone is a dense solid lamellar structure having a volume fraction of more than 70%. The inner spongy core is cancellous/ trabecular bone having a volume fraction of less than 70%. On a microscopic scale, bone can be classified into woven and lamellar bone. Woven bone is premature, temporary and later replaced by stronger lamellar bone. The collagen fibres of woven bone are loose and randomly oriented compared to lamellar bone. However, the growth rate of woven bone is higher than that of lamellar bone.

### 1.4.2 Mechanical properties of bone

#### 1.4.2.1 Cortical bone

Cortical bone makes up 80% of the body's total bone mass but accounts for just 20% of the overall bone volume in human skeleton. In general, cortical bone is considered transversely isotropic and inhomogeneous. These properties depend on the rate of loading and beyond the yield point, exhibit plastic behaviour. Cortical bone is stronger and stiffer in the longitudinal direction than in the transverse direction. The Young's modulus variation in the longitudinal direction and transverse direction are 10-22 GPa (Ashman *et al.* 1984) and 6-14 GPa (Ashman *et al.* 1984, Dong and Guo 2004) respectively. Cortical bone demonstrates relatively more brittleness in tension under transverse loading and opposite behaviour when subjected to tensile stress. Subjected

to normal uniaxial test, cortical bone exhibits linear elastic behaviour upto yield point and fails at a relatively low strain rate.

#### 1.4.2.2 Cancellous bone

The mechanical characteristic of cancellous bone is influenced by mechanical loading. Under compressive load, the stress-strain diagram is initially linear elastic up to 5% strain and flat till fracture point. The material yields with the initiation of fracture and thus indicates a ductile nature. However, under tensile loading, cancellous bone is brittle. Due to the heterogeneous nature of cancellous bone, its material property variation is wider in range. Mostly, the biomechanical properties of cancellous bone are defined in terms of apparent density depending on the anatomic site. Apparent density can be defined as the ratio of bone tissue mass to the bulk supplement volume (Morgan *et al.* 2003).

### 1.4.3 Bone cells

Bone cells can broadly be categorized into the following types

***Osteogenic Cells:*** Osteogenic cells are undifferentiated bone stem cells derived from mesenchymal tissues. As they originate from mesenchymal, they are known as Mesenchymal Stem Cells (MSCs). These cells are the lone pluripotent bone cells that can undergo cellular differentiation in response to various mechanical signals through mechano-transduction. These are found in the inner lining of the periosteum, within the endosteum and in the vascular regions of bone cells (Snell 2011).

***Osteoblasts:*** These are rounded or oval in appearance, organelle-rich differentiated MSCs responsible for bone formation. They synthesize and produce collagen fibers and other organic materials essential for extracellular matrix (ECM) creation (Puthumanapully PK 2010). Osteoblasts are found as neighbouring cells with varying diameters ranging from 20-50µm (Snell 2011).

***Osteocytes:*** When osteoblasts get trapped in the ECM during secretion, they undergo differentiation and transform into mature, stellate-shaped bone cells known as osteocytes. They constitute most of the bone tissue (approximately 90-95%) which is long-lived and plays a crucial role in maintaining the daily activities of the bone. They release specific proteins to signal in response to environmental changes and thus coordinate other bone cell actions. They play a pivotal role in mineral homeostasis regulation, and morphogenic and restructuring processes (Snell 2011). Osteocyte size

varies from 5-20 µm. The premature death of osteocytes might lead to osteoporosis, osteoarthritis, and osteonecrosis (Andreev *et al*. 2020, Aguirre *et al.* 2021).

***Osteoclasts:*** Osteoclasts are large, multi-nucleated cells responsible for bone resorption, and they are formed through the fusion of precursor cells in the myeloid or monocyte lineage (Snell 2011). They are concentrated in the region 'Howship's Lacunae' within the endosteum and look like foam due to the abundance of cellular organelles on their surface (Jee 2008). Their average size ranges from 150 to 200 µm. They secrete lysosomal enzymes and acids to break the protein and mineral components of the surrounding extracellular matrix (ECM).

## 1.5 Literature Review: Lumbar Spine Biomechanics

Initially, a brief introduction of the Finite element (FE) model of the lumbar spine is given. Finite element models are very powerful tools for solving complex biomechanical problems. Further sections include topics like modelling of different elements, geometry discretization, material properties, boundary and loading conditions. Thereafter, in the final section, the mathematical formulation of adaptive bone remodelling and bone ingrowth are described.

### 1.5.1 Finite element models of lumbar spine

The FE analysis of the lumbar spine is broadly used to study the load transfer in intact and implanted models to estimate the influence of various parameters. Nachemson (1966) took the initiative by investigating load transfer of the spine in different positions of the body and the mechanism of stress distribution in the lumbar discs. The development of FE analysis of the lumbar spine began with the introduction of the biomechanical model (Belytchko *et al.* 1974). With the development of computational power, imaging, and material modelling, the accuracy and application of the models significantly enhanced. Initially, the lumbar spine models were simplistic mostly representing the spine as a 2D beam or plate focused on linear elastic material properties and load distribution (Spilker 1978). In 1980s 3D models with more anatomically accurate geometries were developed (Shiraji Adl *et al*. 1984). Facet joints and ligaments are introduced, IVD is modelled using linear elastic materials, and earlier studies on spinal motion and load sharing are initiated. Computed Tomography (CT)/ Magnetic Resonance Images (MRI) enabled detailed geometry, introduced nonlinear and anisotropic properties, and improved IVD and bone modelling in the 1990s (Panjabi *et al.* 1991). The application of FE analysis expanded to degenerative disc diseases as well

as implant studies like pedicle screws and implant cages. In the 2000's the patient-specific FE models were refined and degenerated discs, and dynamic stabilization were studied (Rohlmann *et al.* 2006, Vena *et al.* 2005, Rohlmann *et al.* 2007). Post-2010 era, the advancement was driven by improvements in imaging, computational power, and software algorithms, enabling accurate and clinically relevant articles (Xu *et al.* 2017, Zhao *et al*. 2018, Liu *et al.* 2022). The evolution of FE analysis has helped in understanding of lumbar biomechanics, enhancing the spinal implant design and treatment planning.

The developed FE models are validated either by comparing the numerically predicted results with the experimental results or with peer-reviewed models. The theoretically developed numerical models by the geometrical data adaptation were validated by comparing the range of motion (ROM), and stresses with experimental data from the literature. The FE models developed were used to study biomechanical formalities, the influence of implantation, the development of new implants and finally customized treatment according to subject-specific geometry. The presently available FE models are either subject-specific, derived from CT scan datasets, or commercially available models based on the average morphometric geometry of individual components.

### 1.5.2 Modelling of different elements

To create the 3D models of vertebra accurately, 2D images generated from subject-specific Computer Tomography (CT) data are used. The CT scan data used for different studies use various combinations of lumbar vertebra. Some of the combinations found in the literature are L1-L5 vertebra (Chen *et al.* 2005, Rohlmann *et al*. 2007, Ayturk and Puttlilz 2011, Heo *et al.* 2022), L1-S1 vertebra (Zander et al. 2009, Chen et al. 2012, Fan and Guo 2019), L2-L5 vertebra (Kim *et al*. 2015, Biswas *et al.* 2022, Huang *et al.* 2022a), L3-S1vertebra (Zhou *et al*. 2019, Liu *et al*. 2022), L3-L5 vertebra (Ambati et al. 2014), L2-L4 vertebra ( Bereczki et al. 2021), L3-L4 vertebra (Heo *et al.* 2020, Talukdar *et al*. 2021), L4-L5 vertebra (Boccaccio *et al.* 2008, Lv *et al*. 2018, Han *et al*. 2002).

Different modelling techniques have been considered by various authors to model the parts of the vertebra. Mostly, the ligaments were denoted by tension-only spring elements having nonlinear properties (Rohlmann *et al.* 2007, Bowden *et al.* 2008, Zander *et al.* 2009, Kim *et al.* 2010). The authors modelled the ligaments and annulus

fibres by cable elements that were active in tension only (Chen *et al.* 2005). The nucleus pulposus was around 44% of the intervertebral disc (Talukdar *et al.* 2021). Nucleolus pulposus was modelled as incompressible fluid-filled cavities (Lu *et al.* 1996, Rohlmann *et al.* 2007, Kim *et al*. 2010). The facet cartilage joints were modelled as frictionless contact (Zander *et al.* 2009, Xu *et al.* 2016) or with a friction coefficient of 0.1 (Kim *et al.* 2010, Chen *et al*. 2012) with an initial gap of 0.5 mm. Talukdar *et al.* (2021) modelled facet cartilage joint with a friction coefficient of 0.1 with a gap of 0.1 mm and a thickness of 0.5 mm. Some studies considered facet cartilage to have sliding contact using target and contact elements (Liu *et al.* 2011, Chen *et al.* 2012).

### 1.5.3 Geometry Discretization

The discretization of a solid model of the bony structures along with the implants is a necessary step in FE analysis. Some studies used 10-noded solid elements for modelling cortical bone, cancellous bone, endplate, posterior bony element and disc (Chen e*t al.* 2012); some used 10-noded tetrahedral elements (Biswas *et al.* 2019, Heo *et al.* 2020, Kang *et al*. 2022), 20-node hexahedral elements (Jain and Khan 2022). Some investigators modelled cortical bone, cancellous bone, endplate, posterior bone, annulus (ground) as hexahedral (C3H8) and ligaments as tension-only 3D truss elements (T3D2) (Ambati *et al.* 2015). Some studies considered different material properties as tetrahedral and ligaments as spring elements (Guo *et al.* 2020, Su *et al.* 2021). The vertebrae and intervertebral discs were modelled as 8-node brick elements and ligaments as 4-node shell elements (Xu *et al*. 2016). The study by Kumaran *et al*. (2021) used hexahedral elements to represent bone, implants and tension-only truss elements for the ligaments. Some studies generated cortical bone, cancellous bone, endplates as 8-noded hexahedral elements (C3D8) and posterior elements as 4-noded tetrahedral elements (C3D4) (Heo *et al.* 2022, Liu *et al.* 2022). The bones, endplates, and cartilages were meshed as 4-noded tetrahedral elements (Sanjay *et al.* 2022, Talukdar *et al.* 2021). Some studies used 8-node solid elements to model cortical bone, cancellous bone, posterior bony elements, endplates, annulus ground substance and 8-node fluid elements for nucleus pulposus (Haddas *et al.* 2019, Liu *et al*. 2011). Some authors meshed cortical bone, cancellous bone, posterior elements, normal bony endplates bone graft, cage, rod, screw as tetrahedron (C3D4) elements; osteoporotic bony endplates, cartilaginous endplates, facet cartilage, nucleus pulposus,

AF ground substance as hexahedron (C3D8) and ligaments as spring elements (Liu *et al.* 2022, Bereckzi *et al.* 2021).

### 1.5.4 Material Properties of Vertebral Components

The mesh generation is followed by assigning material properties to bones, ligaments, cartilage, pedicle screws, cage and rods. Segmenting the cortical and cancellous bones is advised to diminish the effects of partial volume.

The empirical relation between CT number and bone for simulating inhomogeneity of bone distribution was given as $\rho = 47 + 1.22CT$ number. Then, the density value was converted into the corresponding elastic modulus as

$$\text{Cancellous bone: } E = 0.63\rho^{1.35}$$

$$\text{Cortical bone: } E = 1.89\rho^{1.35}.$$

For segmenting cortical bone and cancellous bone, the CT number used was 1800 (Chen *et al*. 2003). Talukdar *et al*. (2021) calculated cancellous bone material properties based on the pixel grey value dataset as $\rho = 0.022 + 0.00124CT$ number (in HU). The elastic modulus was obtained by following the equation $E = 4730\rho^{1.56}$.

At lower density, cancellous bone exhibits an open cell rod-like structure and at higher density a plate-like structure. The elastic modulus of cancellous bone varies with apparent density and follows a power law, $E = C\rho^{D}$ (Carter *et al*. 1989, Morgan *et al.* 2003). The exponential constant D varies from 1.14 to 3.2 and constant C for various sites varies from 1000 to 34000. The elastic modulus varies from 10 to 5000 MPa (Saghei *et al*. 2023).

In their study authors considered models as homogenous, isotropic and linear elastic (Huang *et al*. 2022a, Ling *et al*. 2019, Liu *et al.* 2022, Sanjay *et al.* 2022, Talukdar *et al.* 2021). The study considered cortical and cancellous bone as poroelastic (Cegoñino *et al.* 2015). Nikkhoo *et al.* (2021) considered cortical bone, cancellous bone, and endplates as linear poroelastic. Some studies considered cortical bone, and cancellous bone as linearly elastic and transversely isotropic (Ayturk and Puttlitz 2011). Xu *et al*. (2022) considered cortical, cancellous bone as anisotropic; cartilage, and endplates as isotropic.

The intervertebral disc is a complex structure with inhomogeneous and anisotropic properties, making its functional simulation challenging and prompting the development of various approaches to represent its mechanical behaviour. Annulus

fibrous ground substance was considered to have hyperelastic properties (Rohlmann *et al.* 2007, Rohlmann *et al.* 2010, Xu *et al.* 2022). In some studies annulus fibrosus ground substance was considered incompressible poro-hyperelastic (Nikkhoo *et al.* 2021), and anisotropic material (Cegoñino *et al.* 2015). The nucleus pulposus and annular ground substance were modelled as isotropic, hyper-elastic material using Mooney-Rivilin material model (Xu *et al.* 2016). In their study, Rohlmann *et al.* (2007) considered both healthy and degenerated type of nucleus pulposus and their properties as incompressible and compressible respectively. In some studies, authors modelled the nucleus pulposus as linearly elastic and almost incompressible solids (Ayturk and Puttlitz 2011, Xu *et al*. 2022). Sanjay *et al.* (2022) considered nucleus pulposus as incompressible fluids with low elastic modulus. The properties of vertebral bodies are provided in Table 1.1.

**Table 1.1:** Material properties of vertebral body used in earlier studies.

| | **Young's modulus (MPa)** | **Poisson's ratio** | **Reference** |
|---|---|---|---|
| Cortical bone | 12000 | 0.3 | Xu *et al.* 2016 |
| | 10000 | 0.3 | Rohlmann *et al*. 2007 |
| | $E_{11}$=8000, $E_{22}$=800, $E_{33}$=12000 | $\nu_{11}$=0.4, $\nu_{22}$=0.35, $\nu_{11}$=0.3 | Ayturk and Puttlitz 2011 |
| Cancellous bone | 100 | 0.2 | Xu *et al*. 2016 |
| | 200/140 | 0.315 | Zander *et al*. 2009 |
| | Based on CT scan | 0.2 | Ayturk and Puttlitz 2011 |
| Nucleus pulposus | 1 | 0.499 | Ayturk and Puttlitz 2011 |
| | $C_1$=0.12, $C_2$=0.9 | | Xu *et al.* 2016 |
| Annulus Fibrosus | 4.2 | 0.45 | Goel *et al*. 2007 |
| | $C_1$=0.56, $C_2$=0.56 | | Xu *et al.* 2016 |
| Bony endplates | 1000 | 0.4 | Ayturk and Puttlitz 2011 |
| Cartilage | 10 | 0.4 | Kim *et al*. 2009 |
| Posterior element | 3500 | 0.3 | Ayturk and Puttlitz 2011 |

The ligaments are described by stress-strain curves (Xu *et al.* 2016). Some studies established ligaments as calibrated deflection-force curves (Liu *et al.* 2022). Some index models used each ligament's tension-only linear elastic material properties (Bowden *et al*. 2008). Kim *et al*. (2015) modelled ligaments as tension-only truss elements. Li *et al.* (2022) modelled the ligaments as tension-only spring elements.

The majority of the pedicle screws were made up of Titanium alloy with Young's modulus of 110000 MPa and Poisson's ratio of 0.3. Stainless steel was used as screw and rod material and placed bone grafts between two nearby transverse processes (Chen

*et al.* 2005). A model was considered (Alizadeh *et al*. 2013) with Young's modulus of 110000 MPa and Poisson's ratio of 0.3 and the Titanium cage with the same material properties. The authors considered Ti6Al4V alloy for screws and endplates of artificial discs (Biswas *et al.* 2022).

**Table 1.2:** Material properties of the ligaments used in earlier studies.

| Ligament | Mechanical properties | Young's modulus (MPa) | Poisson's ratio | Reference |
|---|---|---|---|---|
| All ligament type | Non-linear stress-strain curve<br>Exponential force-displacement curve<br>Progressive non-linear string | | | Xu *et al.* 2016<br><br>Ayturk and Puttlitz 2011<br>Zander *et al*. 2009 |
| Anterior longitudinal | Linear elastic | 7.8<br>20 | 0.3 | Kim *et al.* 2010<br>Guo *et al.* 2020 |
| Posterior longitudinal | Linear elastic | 10<br>20 | 0.3 | Kim *et al*. 2010<br>Guo *et al.* 2020 |
| Intertransverse | Linear elastic | 10<br>59 | 0.3 | Kim *et al.* 2010<br>Guo *et al*. 2020 |
| Capsular | Linear elastic | 7.5 | 0.3 | Kim *et al*. 2010<br>Guo *et al*. 2020 |
| Flavum | Linear elastic | 15<br>19.5 | 0.3 | Kim *et al.* 2010<br>Guo *et al.* 2020 |
| Interspinous | Linear elastic | 10<br>12 | 0.3 | Kim *et al.* 2010<br>Guo *et al*. 2020 |
| Supraspinous | Linear elastic | 8<br>15 | 0.3 | Kim *et al.* 2010<br>Guo *et al.* 2020 |

### 1.5.5 Boundary and Loading Conditions

The boundary and loading conditions directly influence the model's accuracy. Depending upon the vertebra model, the loading and boundary condition varies. 300 N axial load and 7.5 Nm moment for various movements were applied on the upper surface node of L4 and the bottom nodes of L5 were fixed for the study (Huang *et al.* 2022b). 500 N load and 10 Nm moment in different directions were applied on L4 vertebra and bottom nodes of L5 were constrained (Sanjay *et al*. 2022, Han *et al*. 2022, Xiao *et al.* 2011). Bashkuev *et al*. (2018) used pure compressive force of 1600 N; flexion (7.5Nm), and extension (5Nm) alone and with a compressive load of 1600 N on L4 and lower nodes of L5 were constrained to conduct probabilistic FE analysis. In their study, Lv *et al.* (2018) applied 7.5 Nm moment on the superior node of L4 for different movements and fixed the inner nodes of L5. To assess fracture prediction of

cancellous bone of both healthy and osteoporotic sections, a combination of loads and moments were applied on the L4 vertebra for various daily activities and the inferior node of L5 was fixed (Boccaccio *et al.* 2008).

To illustrate the effects of screw position during load transfer (Newcomb *et al.* 2017) applied around 500 N (mass of trunk above L4 for 80kg person) to the screw head in four different directions up (flexion), down (extension), right and left rotation (axial rotation). Similarly, 280 N compressive load and 7.5 Nm moment were used for various movements on the upper surface of L2 and the bottom nodes of L5 were fixed in all directions (Zhang *et al*. 2018). Biswas *et al.* (2022) simulated FE models with the application of 6,8,10 Nm on L2 for lateral bending, flexion, extension and the bottom surface of L5 were constrained. 10 Nm moment and 1 and 2 kN load were applied on the upper surface of L3 and the lower surface of L4 was fixed (Heo *et al.* 2020). Compressive load of 400 N and 10 Nm bending moments were applied on the uppermost L3 nodes for simulating flexion, extension, lateral bending, and axial rotation and the bottom layer of S1 was kept fixed (Goel *et al.* 2007, Li *et al.* 2015). The study used 150 N preload and 10Nm moment for basic movements on the superior surface of L3 and completely constrained L5 (Guo *et al*. 2020, Zhao *et al.* 2018). Shen *et al*. (2021) used a follower load of 280 N representing partial body weight applied through the curvature of the spine and applied 7.5 Nm moment on L1 for various movements and fixed inferior nodes of L5. Similarly, 7.5 Nm moments were applied at the superior endplate of L1 in flexion, extension, unilateral bending and uniaxial rotation with the inferior part of L5 constrained for parametric convergence study (Ayturk and Puttlitz 2011). Talukdar *et al.* (2021) used a pre-load of 150 N on the slave node and then 10 Nm moment was applied for flexion, extension, torsion, and lateral bending on L3 vertebra. The bottom nodes of the L4 vertebra were fixed for all degrees of freedom. Bereczki *et al.* (2021) conducted the simulation using a 150N follower load along with 10Nm torque on the L2 vertebra for various movements and fixed lower endplate of L4.

### 1.5.6 Adaptive Bone Remodelling

Bone is a composite structure consisting of macrostructure (cortical, cancellous bone), microstructure (osteons), sub-microstructure (lamellae), nanostructure (collagen fibrils, embedded minerals), sub-nanostructure (mineral, collagen). The outer shell of the

bone is a dense solid lamellar structure having a volume fraction of more than 70%. The inner spongy core is cancellous/ trabecular bone having a volume fraction of less than 70%. Bone can undergo substantial changes both in internal structure and shape (external geometry) in response to variations in mechanical and physiological environment by bone apposition (increase in bone density) and bone resorption (decrease in bone density). This process is regulated through the activities of osteoblast and osteoclast with the accumulation of minerals and collagen fibres in the bone. This adaptive process of bone structure variation is known as adaptive bone remodelling. Internal bone remodelling is the change in bone density of cancellous bone (Carter *et al*. 1989, Huiskes *et al.* 1987), whereas external bone remodelling is the geometric or shape variation of the cortical bone (Hart *et al*. 1984). In a natural state, an equilibrium is achieved between bone apposition and resorption, resulting in minimum noticeable variation in bone morphology (Weinans 1991). However, mechanical environment alterations due to the insertion of a prosthesis would potentially disrupt the equilibrium and induce adaptive bone remodelling. Though both the remodelling (internal and external) occurs simultaneously, the changes in internal remodelling are higher compared to external remodelling. This can be explained by the fact that for an adult, bone density is changed more rapidly in cancellous bone owing to its higher rate of metabolic activity than the cortical bone (Garcia *et al.* 2002). While the majority of the studies on bone remodelling were based on internal remodelling, there is a scarcity of existing studies investigating the combined influence of both internal and external remodelling (Huiskes *et al.* 1987, Beaupre *et al*. 1990a, Weinans e*t al.*1993, Garcia *et al.* 2002). The implantation induces alterations in the mechanical environment of the bone and disrupts the natural equilibrium state. Immediately after post-operative condition, the implant must carry the majority of the load that was previously carried by the natural bone. Post-implantation, the bone aspires to attain a new equilibrium by internal and external adaptation.

A considerable amount of studies have been conducted to understand the relationship between bone structure and its functions. The first observation of the relation between mechanical forces (body weight) and bone morphology was observed by Galileo Galili in the 17$^{th}$ century (Carter 1984). The functional adaptation theory by Roux concluded bone apposition and resorption are biological processes that are governed by the local state of stress (Roux 1981). Julius Wolff hypothesized that the alterations in the form and function of the bone cause variations in the internal

architecture and external geometry of the bone. The mathematical law of bone transformation is postulated as "Wolff's law". Over the past few decades, numerous researchers attempted to mathematically established the law for quantifying the bone remodelling process (Cowin and Hegedus 1976, Hart *et al*. 1984, Fyhrie and Carter 1986, Huiskes *et al.* 1987, Hart and Davy 1989, Beaupre *et al.* 1990a, García *et al.* 2002).

The bone remodelling process is influenced by factors like genetics, age, metabolism and hormones. The adaptive bone remodelling theory assumes that bone can sense the internal variations in the mechanical conditions through mechanical stimulus within it and respond to the change (in combination with other biological factors) by osteoblasts and osteoclasts. Most of the earlier literature used bone apparent density ($\rho$) as the variable to represent the remodelling state. Some of the other mechanical stimuli are defined as a function of stress, strain, strain energy density (SED), the elastic strain energy density per unit bone mass (Cowin and Hegedus 1976, Cowin 1986, Hart and Davy 1984, Fyhrie and Carter 1986, Huiskes *et al.* 1987, Carter *et al.* 1989, Weinans *et al*. 1993). Cowin and Hegedus (1976) proposed a theory based on a 'site-specific' (site-dependent) bone remodelling technique and normalized active local strain values (remodelling stimulus) to the strain values occurring under normal physiological conditions at the same locations. Cowin (1986) proposed another theory suggesting strain to be the function of the mechanical stimulus rather than stress since strain is a chief measurable physical quantity to represent deformation. Further, Huiskes *et al*. (1987) predicted local SED as the remodelling signal in place of strain to estimate bone adaptation.

Flyhie and Carter (1986) introduced a 'non-site specific' (site-independent) method considering that the tissue strives to optimize its state of stress and strain to a uniform stimulus level calculated over the entire volume. This theory was dependent on external loading conditions and did not consider 'intact' or 'normal' conditions. In their theory, the mechanical stimulus was considered as the elastic strain energy per unit of bone mass (SED).

Bone does not respond to minute deviations in the mechanical stimulus (Frost 1964). To initiate the bone remodelling process, a minimum threshold value of the inhibitory signal i.e., the difference in mechanical stimulus for the implanted and intact condition is needed. The region that remains non-reactive to small mechanical stimuli

is known as the 'dead zone' or 'lazy zone'. This mathematical formulation of adaptive bone remodelling was forwarded by Huiskes *et al.* (1987). For all these theories of bone remodelling, the bone was assumed to be isotropic.

The orientation of cancellous bone is regulated by heterogeneity of bone density distribution and thus induces anisotropic continuum material properties (Garcia *et al.* 2002). Carter (1978) supplied anisotropic strain data, and a daily stress stimulus at the tissue level was considered into account within the time-dependent bone remodelling theory. Beaupré *et al.* (1990a,1990b), and Jacobs *et al.* (1995a, 1997) introduced an anisotropic model that incorporated density adaptation and anisotropy reorientation by considering principal stress as the mechanical stimulus. Further, some aspects of bone remodelling were predicted correctly using a damage-based theoretical model (Prendergast and Taylor 1994, Prendergast and Huiskes 1995). Doblaré and García (2002) proposed an anisotropic bone remodelling theory based on damage repair theory and considered microdamage as the remodelling stimulus. In a study by McNamara and Prendergast (2007), the remodelling stimulus was assumed to be a combination of strain and microdamage. In recent times, bone remodelling simulations have been conducted based on structural topology optimization (Hollister *et al.* 1994, Fernandes *et al.* 1999, Bagge 2000, Jang and Kim 2008, Jang *et al.* 2009). However, research on bone remodelling in lumbar vertebrae remains relatively scarce.

#### 1.5.6.1 Mathematical formulation of bone remodelling process

The change in apparent density (ρ) was used to represent the bone remodelling state for different proposed mathematical formulations and was based on Wolff's law (Wolff 1982). The adaptive bone remodelling simulation employed a site-specific formulation and elastic strain energy per unit bone mass was considered to be a mechanical stimulus (Cowin and Hegedus 1976, Huiskes *et al.* 1987, Carter *et al.* 1989). The schematic diagram of iterative bone remodelling process is presented in Fig.1.9. The reference stimulus for intact bone is represented by '*Sref*' and for implanted bone denoted by '*S*', and they are compared for each bone element. The extent of the bone remodelling amount depends on the difference between '*Sref*', '*S*' and dead zone '*s*'. After each iteration, a new model is attained having updated material properties and a new stimulus '*S*' is determined. This process of iteration is continued till a new equilibrium with no more bone density variation occurs. In this process, the elements that have mechanical stimulus within the dead zone having restrictive density values of no bone condition

(0.1g/cm$^3$) and cortical bone (1.73 g/cm$^3$) were not considered. The reference stimulus for intact bone ($S_{ref}$) and for implanted bone ($S$) was the local (per element) elastic strain energy ($U$) per unit bone mass averaged over a loading history (n) (Ghosh *et al.* 2013). The mechanical stimulus for each element was derived using the finite element (FE) model outputs. Owing to variations of loading conditions of the lumbar vertebra, for various movements during daily physiological work, the loads, strain energy density, and elastic strain energy per unit bone mass vary for each bone element. The mechanical remodelling stimuli ($S$) across multiple loading cases were calculated by considering some of these variations, by an average strain energy density, $U_a$, overloading condition (Carter *et al.* 1989, van Rietbergan et al. 1993) and expressed as

$$S = \frac{1}{n}\sum_{i=1}^{n}\frac{U_i}{\rho} = \frac{U_a}{\rho} \qquad (1.1)$$

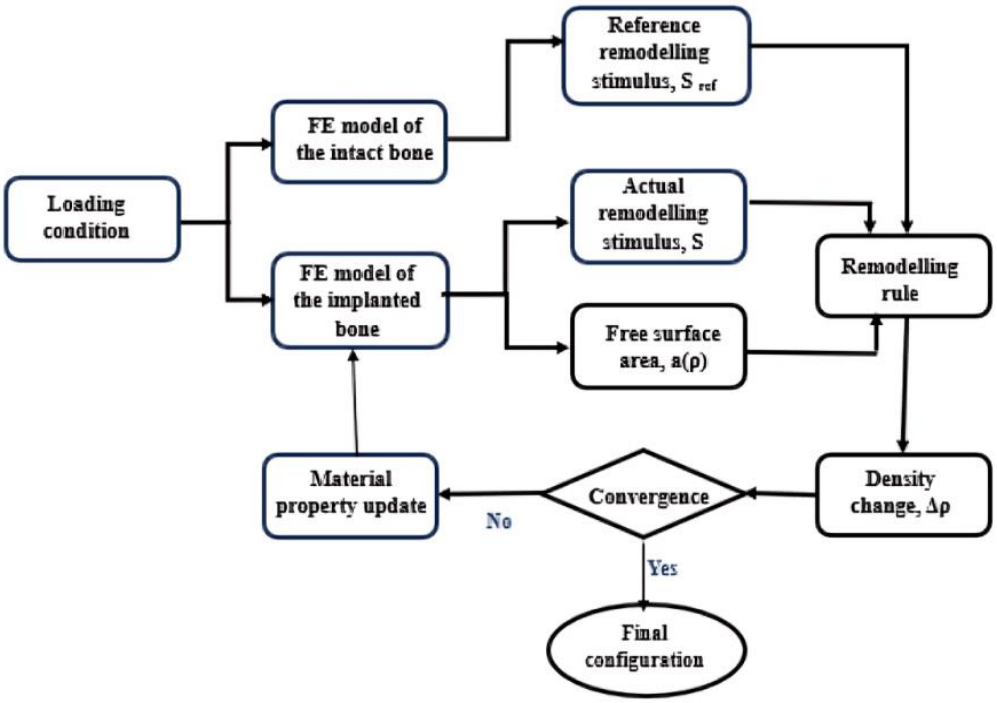


**Fig.1.9:** Computational Scheme of adaptive bone remodelling.

As discussed earlier, the bone remains non-responsive to mechanical stimulus in the 'dead zone' (s) (Huiskes *et al.*1987, Beaupré *et al.* 1990a, van Rietbergen *et al.* 1993) shown in fig.1.10. To overcome this, a minimum threshold of the restraint signal *'S-Sref'* is needed. The dead zone for human cancellous bone is chosen as ±0.75 of the reference stimulus *Sref* for humans (Huiskes *et al.* 1992). Martin (1972) introduced a way to estimate the free surface area available based on apparent density ($A = A(\rho)$). Based on Martin's assumption (1972), the internal surface area per unit volume of the

entire bone was calculated as $a(\rho) = A(\rho)/V$. Martin (1972) assumed $a((\rho) = 0.0$ for $\rho = \rho max = 1.73$ g/cm$^3$ for cortical bone with an apparent density of 1.73 g/cm$^3$ where no remodelling occurs.

The rate of change of bone mass for the adaptive bone remodelling process in the operated bone is given by the following expression

$$\frac{dM}{dt} = \tau A(\rho)[S - (1-s)S_{ref}] \quad \text{if } S \leq (1-s)S_{ref} \tag{1.2a}$$

$$\frac{dM}{dt} = 0, \quad \text{if } (1-s)S_{ref} < s < (1+s)S_{ref} \tag{1.2b}$$

$$\frac{dM}{dt} = \tau A(\rho)[S - (1+s)S_{ref}], \quad \text{if } S \geq (1+s)S_{ref} \tag{1.2c}$$

$$0.01 \leq \rho \leq 1.73 \text{ g.cm}^{-3}$$

Here $\tau$ represents the time constant given by 129.6 g/ (mm$^2$ (J/gm) month). The time t is expressed in units of one month. Further, the rate of change of bone mass is given by the amount of variation of internal mass as a result of porosity variation

$$\frac{dM}{dt} = V\frac{d\rho}{dt} \tag{1.3}$$

Where *V* is the volume of the element in which bone mass variation is taking place and *dρ*/*dt* is the rate of change of apparent density.

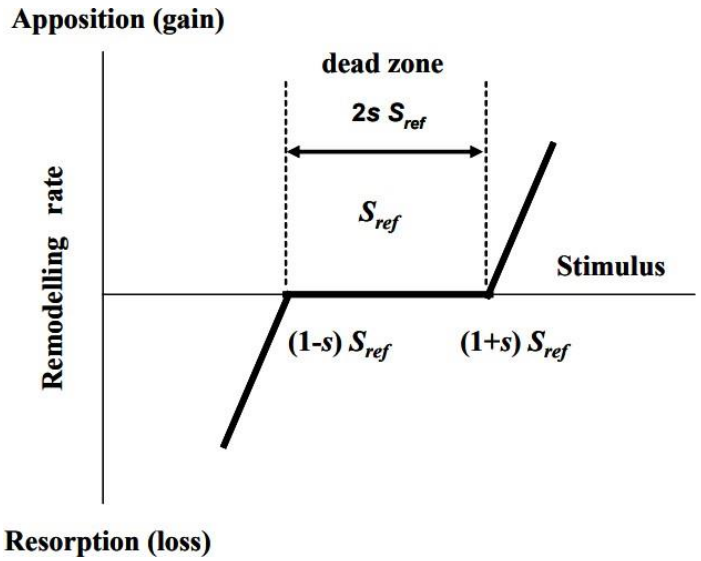


**Fig. 1.10:** The relationship between stimulus and rates bone adaptation in bone remodelling (Ghosh *et al.* 2013).

The change in apparent density is mathematically expressed as follows:

$$\Delta\rho = \tau A(\rho)[S - (1 \pm s)S_{ref}]\Delta t, \quad \text{if } S \leq (1-s)S_{ref} \text{ or } S \geq (1+s)S_{ref} \tag{1.4}$$

Euler's forward integration was used to solve the above equation (1.4) to yield a new apparent density value for all bone elements after each iteration. Thus, the apparent density of each element and chosen time step Δt can be determined by using the following equation:

$$\Delta\rho_i = \tau A(\rho)[S - (1 \pm s)S_{ref}] \text{ if } S \leq (1-s)S_{ref} \text{ or } S \geq (1+s)S_{ref} \quad (1.5a)$$

$$\rho_{i+1} = \rho_i + \Delta\rho_i \text{ if } S \leq (1-s)S_{ref} \text{ or } S \geq (1+s)S_{ref} \quad (1.5b)$$

The integration was carried out in steps of 'simulation time scale' $\tau\Delta t$ (Weinans et al. 1993). The time step ($\Delta t$) was variable and was determined in each iteration using the following equation, where the maximum bone density change in the most highly stimulated element was assumed to be equal to the half of maximum bone density ($\frac{1}{2}\rho_{max} = 0.865$ g.cm$^{-3}$) (Weinans *et al.* 1993):

$$\tau\Delta t = \frac{0.865}{\{a(\rho)(S-(1\pm s)S_{ref}\}_{max}} \quad (1.6)$$

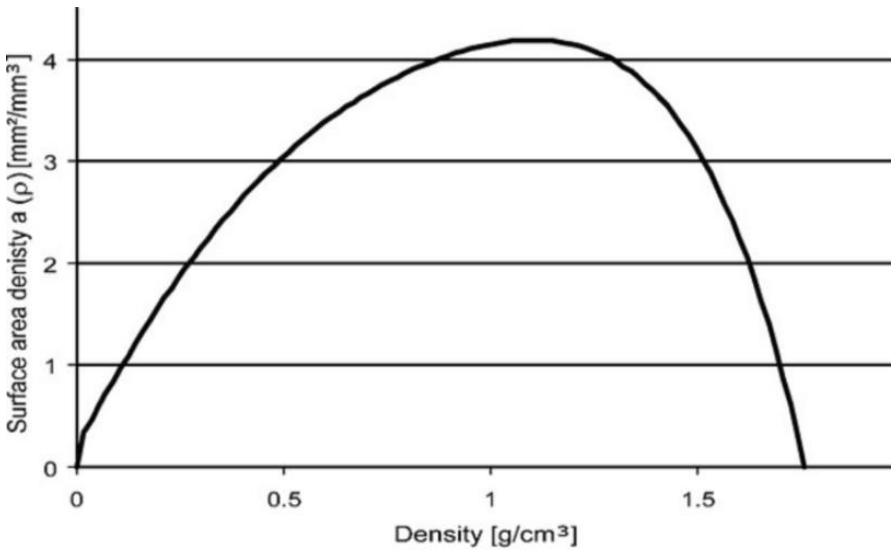


**Fig1.11:** Martin's equation of relation between free surface area per unit volume and apparent density (Scandell and Prendergast. 2009).

### 1.5.7 Bone ingrowth

Bone ingrowth is a complex biological process that follows various cellular activities and tissue differentiation, and it resembles primary bone fracture healing (Davies 1996,2003). In primary bone fracture repair, the MSCs play an essential role. The phenomenon is termed mechanotransduction where undifferentiated progenitor MSCs respond by converting mechanical stimulus to corresponding biochemical response and

differentiate to a variety of connective tissue cells leading to the development of new tissue (Barry 2003). Bone marrow contains concentrated MSCs and moves towards a bone defect zone to heal and differentiate into fibroblast (tendon/ligament cells), osteoblasts (bone cells), chondrocytes (cartilaginous cells), myoblasts (muscle cells), adipocytes (fat cells for the formation of bone marrow fat) and other cell types through the mechanism of cellular differentiation (Fig. 1.12). It has been noticed that connective tissue differentiation is influenced by a range of stimuli, including growth hormones, fluctuations in oxygen tension (hypoxia) and mechanical strain. Thus, to promote differentiation and growth of a particular type of connective tissue, it is essential to achieve equilibrium between various kinds of stimuli (Matsuda *et al*. 1998).

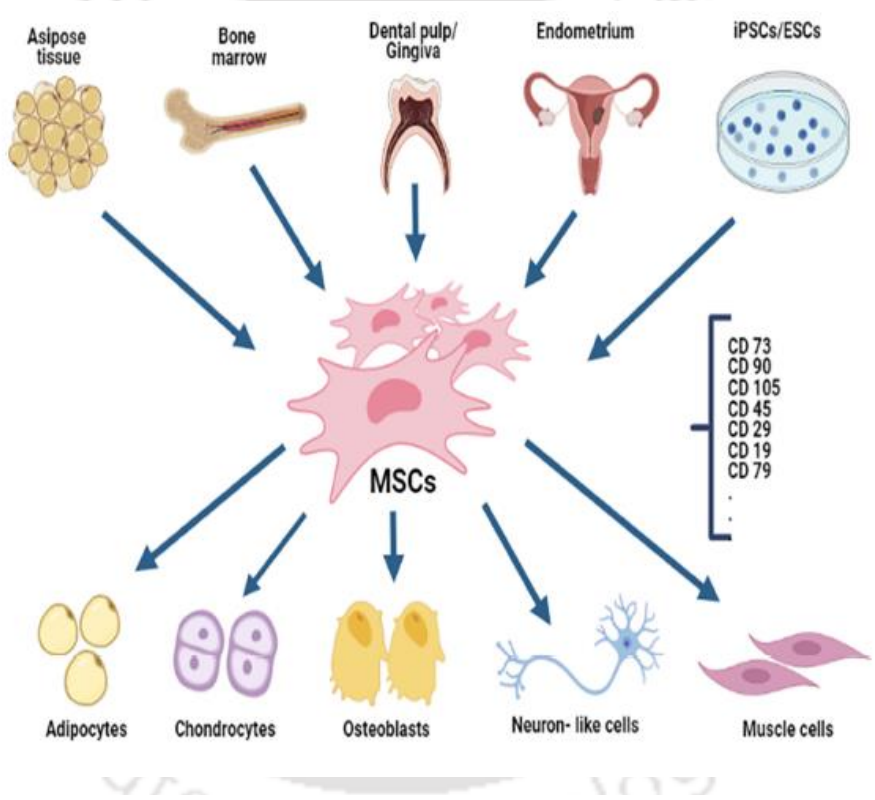


**Fig. 1.12:** Tissue differentiation from Mesenchymal stem cells (Merimi *et al*. 2021).

In terms of implant design, the impact of mechanical stimuli on tissue differentiation is of prime importance. Bone adaptation is characterized by sequence of events (Weinbaum *et al.* 1994, Stolz *et al.* 2018) as follows: Mechanocoupling (mechanical stimuli converted to biological inputs to act on the cell), Mechanotransduction (biological input signal converted to electrical, chemical or biochemical signals), Transduction (intracellular conversion of the mechanotransduced signals into final signals for the cells to act upon) and Cell response (cell differentiation, proliferation etc.).

Frost (1987) proposed a model named 'mechanostat of bone adaptation' to get the optimum level of bone strain for the physiological growth of bone. According to this model, a lower strain level promotes bone resorption by osteoclast formation and a moderate level is considered physiological. Earlier studies suggested that static loading prohibits bone formation, promotes bone resorption, and decreases RNA, and protein synthesis; whereas cyclic loading promotes osteogenesis (Stolz *et al.* 2018). Mechanical stimuli can regulate cellular differentiation in the chondrogenic medium even in the absence of growth factors (Angele *et al.* 2003, Altman *et al.* 2002). It is classically assumed that an adequate supply of growth factors is necessary for osteoblast proliferation in cases of a well-vascularised orthopaedic procedure. Local mechanical stimuli such as deviatoric and hydrostatic stresses influence the differentiation process of MSC (Pauwel 1960, Carter *et al*. 1988). Both these stimuli meaningfully rely on the relative interfragmentary micromotion of two fractured fragments (Speirs *et al*. 2000). Numerous studies were conducted to evaluate the influence of mechanical simulations on tissue differentiation (Carter *et al*. 1988, Prendergast et al. 1997, Huiskes *et al.* 1997, Claes and Heigele 1999). Most of these models estimated fibrous tissue formation in response to substantial shear or tensile stresses. Mature bone formation was considered for models having profound vascularity and a smaller magnitude of stress.

#### 1.5.7.1 Mathematical formulation of evolutionary bone ingrowth

To quantify tissue differentiation, numerous mechanoregulatory algorithms have been proposed (Claes and Heigele 1999, Carter et al. 1988, Prendergest *et al*. 1997, Huiskes e*t al*. 1997, Prendergast and Huiskes 1996). The majority of these studies executed a two-simulation approach that incorporated octahedral shear (S) and dilatational hydrostatic (D) stresses as

$$S = \frac{1}{3}\sqrt{[(\sigma_1 - \sigma_2)^2 + (\sigma_2 - \sigma_3)^2 + (\sigma_3 - \sigma_1)^2]} \quad (1.7)$$

$$D = \frac{1}{3}[\sigma_1 + \sigma_2 + \sigma_3] \quad (1.8)$$

where $\sigma_1$, $\sigma_2$, $\sigma_3$ are the cyclic principal stresses.

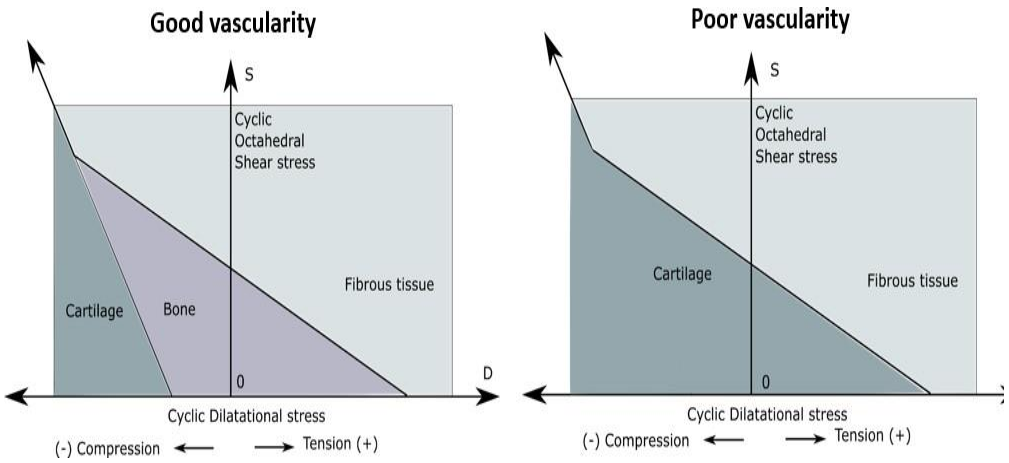


**Fig. 1.13:** Mechanoregulatory hypotheses of Carter *et al.* (1988).

Based on Pauwel's theory (Pauwel 1960) of mechanoregulation, Carter *et al.* (1988) combined these two stimuli into a single parameter known as the Osteogenic Index (Fig. 1.13). This osteogenic index approach successfully predicted the early trends of tissue differentiation in initial fracture fixation (Carter *et al.* 1988), embryonic morphogenesis (Carter and Wong 1988) and around implant-bone interfaces (Giori *et al.* 1995). However, with the advancement of research based on quantitative tissue differentiation established that osteogenic index-based technique failed with progressive tissue differentiation (Gardener *et al.* 2004).

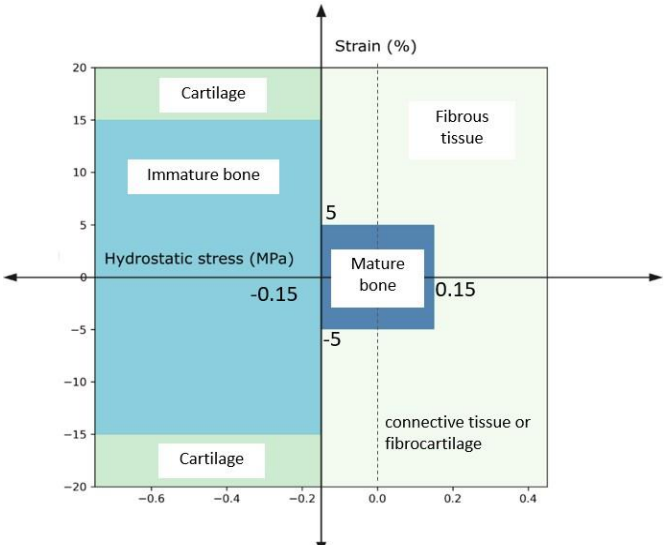


**Fig. 1.14:** Mechanoregulatory principles of Claes and Heigele (1999).

Thereafter, Claes and Heigele (1999) developed a new mechanoregulatory model considering deviatoric strains and hydrostatic stresses as two mechanical stimuli

governing a tissue differentiation process for a fracture healing study on an ovine model (Fig. 1.14). For strain less than 5% and hydrostatic pressure in the range of ±0.15 MPa, the theory projected threshold limits for intramembranous bone formation. Further, endochondral ossification is linked to compressive hydrostatic pressures greater than 0.15 MPa and strains less than ±0.15%.

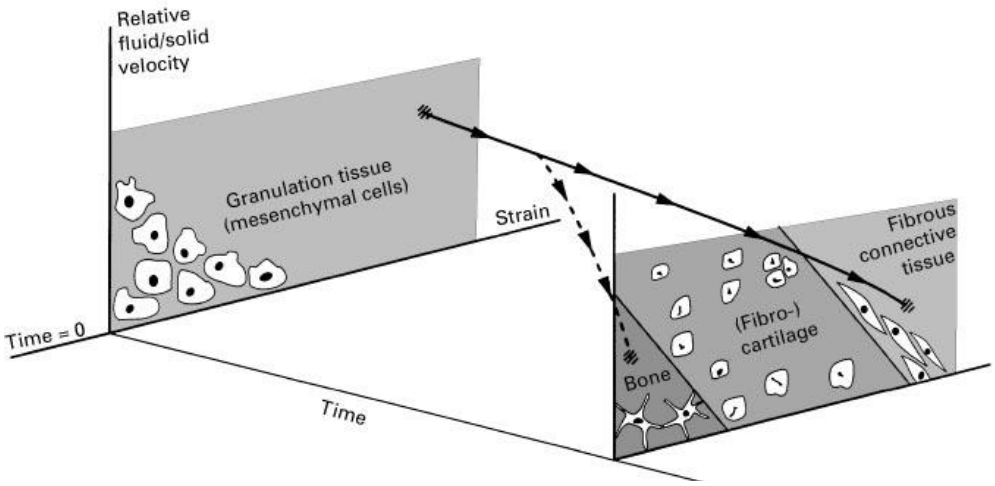


**Fig.1.15:** Mechanoregulatory algorithm by Predergast et al. 1997.

A novel mechanoregulaory model was proposed considering bone as a biphasic material and combined effects of strain and interstitial fluid velocity (Fig. 1.15) (Prendergast and Huiskes 1996, Prendergast et al. 1997). The biphasic model is attributed to soft tissues at the bone-implant interface comprised of a collagenous solid phase and a fluid media. Further, the quantitative confines on the mechanical stimuli in the biphasic mechanoregulatory algorithm were attained through an empirical fit to a canine model (Huiskes et al. 1997).

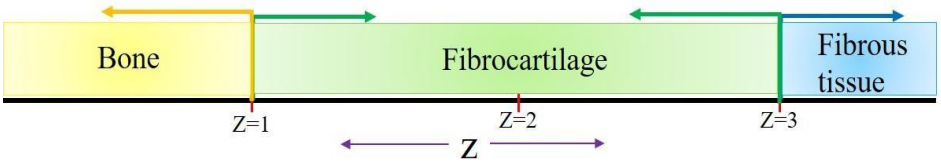


**Fig. 1.16:** Influence of combined stimulus on tissue differentiation.

A combined stimulus (Z) (Fig.1.16) was developed by combining the magnitude of shear strain (γ) and relative velocity (ν) regulating tissue differentiation as:

$$Z = \frac{\gamma}{a} + \frac{\nu}{b} \tag{1.9}$$

Where a (=0.0375) and b(=3μms$^{-1}$) are constants (Huiskes *et al.* 1997). Woven

bone is found to develop for Z<1 and Z>3 fibrous tissue is formed.

A diffusion-based poroelastic model (Eq 1.10) was developed to study cell migration (Lacroix *et al.* 2002, Lacroix and Prendergast 2002a). This biphasic model was executed to simulate fracture healing in a computational framework.

$$k\nabla^2 c = \frac{dc}{dt} \tag{1.10}$$

where *k* is the diffusion constant, and *c* is the cell concentration at each finite element at the fracture callus. The biological phenomenon of cellular migration is simplified by assuming the diffusion model would simulate cellular dispersion. The cells at the interface helped in achieving homogeneity of cellular migration. The study did not consider the migration of intermediate regenerating cellular phenotypes that might influence the healing process, cellular mitosis and necrosis/apoptosis. Yet the adaptive model reasonably mimics the periosteal bone formation, endochondral ossification, and bone bridging at the callus followed by bone formation.

In a physically feasible geometric domain, granulation tissue and expected tissue phenotype coexist within a single finite element. This realistic representation within a finite element is not implemented in the mechanoregulation-based tissue differentiation scheme. To resolve this discrepancy, a rule of mixture is introduced to calculate the effective material property $(E_{n+1})$ of newly formed tissue by combining element-specific cell concentration obtained during diffusion analysis with the predicted material properties in a mathematical equation (Lacroix and Prendergast 2002a, Isaksson *et al.* 2006a, Boccaccio *et al*. 2007).

$$E_{n+1} = \left(\frac{c_{max}-c_{min}}{c_{max}}\right) E_{granulation} + \left(\frac{c_{tissue}}{c_{max}}\right) E_{tissue} \tag{1.11}$$

Where, $c_{max}$ and $c_{tissue}$ are the maximum cell concentration, considered to be unity and actual concentration of cells. $E_{tissue}$ and $E_{granulation}$ are the material properties of newly formed tissue and granulation tissue, respectively. To avoid numerical instabilities caused by sudden variations of material properties at each finite element at the granulation tissue, a temporal smoothing procedure (Lacroix and Prendergast 2002a, Isaksson *et al.* 2006a, Boccaccio *et al*. 2007) was used iteratively in each of the inter- bead spacing elements while updating the material properties.

$$E_{n+1,smoothened} = \frac{1}{10} \sum_{i=n}^{n-9} E_i \tag{1.12}$$

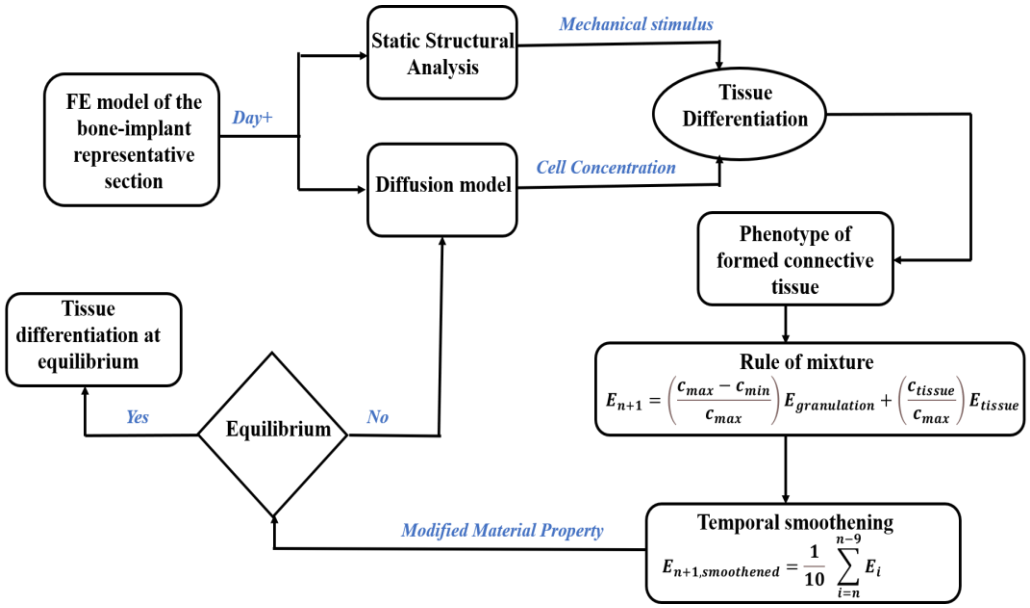


**Fig. 1.17:** Computational scheme for mechanoregulatory tissue differentiation simulation.

The conceptual framework of this approach is portrayed in Fig. 1.17. Many researchers utilised the technique to examine fracture healing (Isaksson *et al.* 2006a, 2008a, 2008b, 2009), repair of osteochondral defect (Kelly and Prendergast. 2005), and implant-bone interfacial tissue differentiation (Scannell 2006, Chou and Müftü 2013, Dickinson *et al.* 2012). Subsequently, the effectiveness of numerous mechanoregulatory algorithms was assessed and it was evident that all algorithms could estimate similar tissue adaption trends (Isaksson *et al.* 2006a). Further, some cell-phenotype-specific algorithms were developed, detailing the individual biological activities of each cell and their explicit influence on tissue differentiation (Isaksson *et al.* 2008a, Andreykiv *et al.* 2008a). However, it was established that cell-phenotype-specific algorithms are more computationally complex than diffusion-based phenomenological algorithms.

### 1.5.7.2 Cell migration implemented through diffusion model

Mathematically though heat flow and diffusion are the same phenomenon, but to depict the dispersal of MSC across granulation tissue region a detailed discussion in change of notation is discussed. Mass diffusion (MSC) across a region in a particular direction is based on Fick's law:

$$k\nabla^2 c = \frac{dc}{dt} \tag{1.10}$$

$$\Pi_c = -k\frac{\partial c}{\partial \Omega} \tag{1.13}$$

where, where k = diffusion coefficient, c = concentration of undifferentiated MSCs, $\Pi_c$ = rate of transfer of cells in direction Ω.

Its corresponding heat flow equation based on Fourier's law of heat conduction is given as

$$\left(\frac{\mho}{\rho\Psi}\right)\nabla^2\theta = \frac{d\theta}{dt} \tag{1.14}$$

$$\Pi_\theta = -\mho\frac{\partial\theta}{\partial\Omega} \tag{1.15}$$

where ℧ = thermal conductivity, ρ = density of the material through which heat flows, Ψ = specific heat of the material, ρΨ = heat capacity of the material, θ = temperature, $\Pi_\theta$ = rate of transfer of heat in direction Ω.

The correlation between concentration, c and temperature θ in above equations and comparing equations 1.10 and 1.14,

$$k = \frac{\mho}{\rho\Psi} \tag{1.16}$$

Similarly, comparing equation 1.13 and 1.15,

$$\Pi c = \Pi\theta \tag{1.17}$$

From equation 1.15

$$k \equiv \mho \tag{1.18}$$

Comparing equations 1.16 with 1.18

$$\rho\Psi = 1 \tag{1.19}$$

In thermal diffusion, heat conduction takes place and not temperature. In physical significance, $\rho\Psi$ being the heat capacity of the material is an important factor in the heat equation responsible for converting temperature, $\theta$ into the amount of heat per unit volume. However, this factor has no significance in mass diffusion since in mass diffusion, the term "concentration, *c*" represents diffusion of mass unit volume is unity.

### 1.6 Clinical Investigation

Clinical investigations into lumbar fusion surgery aim to understand patient outcomes, particularly the complications that arise during the postoperative period or later in life. Mechanical weakening is frequently observed due to daily physiological loading, with the primary cause of fixation failure being the loosening of the bone-implant interface. Various studies have explored these complications, offering insights into their causes and potential solutions.

In a pivotal study by R. Louis (1984), 440 of 455 patients who underwent lumbar fusion surgery were followed for an average of 31.6 months. Complications such as screw loosening, anatomical variations, osteoporosis, and neural or vascular injuries were identified (Weinstein *et al.* 1992). Studies by Castro *et al.* (1996) and Girardi *et al.* (1999) revealed that accurate pedicle screw placement remains challenging, with CT scans showing cases of medial and inferior pedicle wall penetration. Computer-guided techniques were found to improve placement accuracy. Subsequent studies have expanded on these findings. Halm *et al.* (2000) examined 12 patients with thoracolumbar and lumbar scoliosis over a 4-year follow-up period, reporting that among 85 screws, 10 exhibited lateral penetration, 5 bilateral penetration, and 4 medial penetrations. Okuyama *et al.* (2001) studied 52 patients undergoing posterior lumbar interbody fusion and found that lumbar spine bone mineral density (BMD) was a crucial factor influencing pedicle screw stability, with follow-up conducted over an average of 2.8 years. Another study by Ghiseli *et al.* (2004) focused on adjacent segment degeneration following posterior lumbar arthrodesis. Their results indicated symptomatic degeneration in 16.5% of cases after 5 years and 36.1% after 10 years. Chen *et al.* (2005) analysed pedicle screw fixation in 16 patients with spine instability and found that 75% of screw failures occurred on the caudal side due to larger axial stress, with 23 screws breaking within a 2-year follow-up period.

Innovative techniques have shown promise. Schaeren *et al*. (2008) demonstrated that the Dynesys system effectively reduced donor site morbidity in elderly patients, achieving a 95% satisfaction rate over 52 months. Mohi Eldin and Ali (2014) observed that implant failure, often involving screw or rod fractures, occurred primarily within six months post-surgery. Similarly, Laugesen *et al.* (2017) found that 33% of lumbar total disc replacement patients required revision surgery after 10 years, often with poorer outcomes.

Studies also focused on specialized solutions for at-risk populations. Expandable pedicle screws were deemed safe and effective for elderly patients with osteoporosis (Gazzeri *et al.* 2016). Robot-assisted minimally invasive surgeries achieved a 97.4% accuracy rate for screw placement (Vardiman *et al.* 2020). A meta-analysis by Yagi *et al*. (2021) confirmed lower revision rates for cannulated pedicle screws, particularly in osteoporotic patients.

Overall, advancements in techniques and materials have improved outcomes for lumbar fusion surgeries, but challenges like screw loosening and adjacent segment degeneration persist, especially in elderly and osteoporotic patients.

### 1.7 Motivation of the present work: Research gap observed in the state-of-art

The stability of the posterior spinal devices is dependent largely on the pedicle screws. When pedicle screws are inserted into an osteoporotic spine, their fixation strength is substantially reduced due to low bone mineral density (BMD), increasing the risk of screw loosening and subsequent pullout. Thus, it becomes very challenging for surgeons to enhance the strength of pedicle screw fixation, especially with osteoporotic patients (Rahyussalim *et al.* 2019). The primary causes of pedicle screw loosening are increased load sharing, high-stress concentration due to bending, repeated loading-unloading and delay in bone fusion (Biswas *et al*. 2019, Chen *et al*. 2003, Pearson *et al.* 2017). In many clinical cases, persistent pain caused by instrumentation loosening often demanded revision surgery for certain patients.

In some cases, removal of pedicle screws is necessary, but these procedures can be costly (Pearson *et al*. 2017, Xu *et al.* 2019). Spinal fusion surgery, for example, incurs an average hospital charge of US$ 40,000, with patients typically staying over 4 days (Martin *et al*. 2007). To address these challenges, alternative pedicle screw designs, such as expandable pedicle screws (Cook *et al.* 2001), dual-threaded screws, and magnetic resonance-compatible screws, show promise in improving fixation strength. Expandable pedicle screws, in particular, enhance the connection between the bone and screw by increasing the contact area without increasing the pedicle insertion diameter or screw length (Cook *et al.* 2001). These innovative designs offer the potential for more reliable outcomes and cost-effective solutions by improving the overall stability of the spine while reducing the need for costly revision surgeries.

FE analysis is a useful tool for preclinical investigation considering various physiological loading conditions. Several studies were conducted to see the influence of physiological loading conditions, and ligament stiffness on the intact model (Kang *et al.* 2022, Talukdar *et al*. 2021). Most of the previous studies calculated stress for the intact model under different loading conditions and ultimately compared it with the implanted models. Earlier studies estimated the influence of material properties, and anchoring arrangement of pedicle screws for long-segment lumbar vertebra (Natarajan *et al.* 2018). The screw positioning also plays a vital role in load transfer (Newcomb *et*

*al.* 2017). Studies were conducted to see the variation of pitch length under bending load (Biswas *et al*. 2019). However, no studies were conducted to develop an appropriate 3D model of the FSU and estimate the influence of physiological loading for the novel expandable pedicle screws.

There have been numerous studies based on adaptive bone remodelling using FE analysis on implanted bones to predict the bone density change due to physiological loads (Huiskes *et al.* 1987, Ghosh *et al.* 2014, Mathai *et al*. 2021a, Mondal and Ghosh 2021). However, the studies on bone remodelling in lumbar vertebrae remain quite limited. Some researchers applied adaptive bone remodelling to observe variation in vertebral end plate shape due to disc injury (Goel *et al*. 1994). In another study, the authors studied internal and external remodelling and predicted Young's modulus distribution within the vertebra (Goel *et al.* 1995). The influence of fixation screws on the trabecular structure was studied for long-term stability (Tsubota *et al.* 2003). Moreover, bone remodelling post-cervical spine surgery (Espinha *et al*. 2010) and due to disc degeneration (van Rijsbergen *et al.* 2018) were also investigated. The impact of the porosity variation of the interbody cage on bone density variation was further studied (Talukdar *et al.* 2022). Nonetheless, a comparison of conventional pedicle screws with novel expandable pedicle screws for long-term performance would be beneficial.

One of the major concerns of spinal fixation is that osteoporosis leads the bone to be fragile and ultimately fail. The fixation issue becomes severe for low BMD and that lower the pullout strength (Demir *et al.* 2012). The pullout strength depends on BMD, screw design, insertion technique, pedicle screw shape etc. (Demir *et al.* 2012, Hsu *et al.* 2005, Bianco *et al.* 2017). Many experimental studies used different polyurethane (PU) foams of different densities to evaluate pullout strength (Varghese *et al.* 2016a, Lee *et al*. 2019, Cetin *et al*. 2021a). Previous studies showed improved pullout strength using dual-thread pedicle screws compared to cylindrical screws (Kubaik *et al.* 2019, Wu *et al*. 2023). The pullout force of expandable pedicle screws increased with an increase in number of fins (Kiyak *et al.* 2018). Design variations of expandable pedicle screws to enhance axial pullout performance would be beneficial for future applications, particularly with thorough evaluation through computational methods.

To evaluate the impact of mechanical stimuli on bone growth, various mechanoregulation models were implemented along with FE analysis during fracture

healing and bone-implant fixation (Isaksson *et al.* 2006a, Lacroix and Prendergast 2002a, Mukherjee and Gupta 2015, Ghosh *et al*. 2020, Mohendas *et al.* 2021, Mathai and Gupta 2021b). Most of these studies were conducted on long bones (Mohendas *et al.* 2021). Few studies considered bone ingrowth in vertebral body and cage design (Boccaccio *et al.* 2011, Postigo *et al.* 2014). Some studies combined bone growth with adaptive bone remodelling to assess tissue differentiation post-nucleotomy and disc degeneration (van Rijsbergen *et al.* 2018, Calvo Echenique *et al*. 2019). However, the incorporation of bone adaptation phenomenon in the evaluation of pedicle screws has to be considered.

### 1.8 Objectives and Scope of the Study

The current study aimed to address the limitations discussed in the previous section by integrating advanced biomechanical assessment techniques. The primary goal was to design and develop expandable pedicle screws to reduce the failure rates commonly associated with conventional pedicle screws. To achieve this, the study focused on investigating detailed models of intact and implanted lumbar spine units, comparing the performance of conventional and expandable pedicle screws under physiological loading conditions.

Following the modelling phase, a preclinical assessment was conducted to examine bone remodelling around the expandable pedicle screws, with a direct comparison to conventional screws under similar conditions. This was essential to understand how the bone interacts with the screws, which is crucial for long-term stability. Additionally, three distinct designs of expandable pedicle screws were developed to estimate their pullout strength. This step was vital for evaluating the mechanical performance of these new designs.

Finally, the study aimed to investigate the extent of bone growth around the newly designed expandable pedicle screws using a mechanoregulation-based algorithm. This allowed an understanding of the bone response to these screws and helped assess their potential for improved fixation and stability. Through these investigations, the study aimed to enhance spinal fixation by improving screw design and reducing the failure rates observed with conventional pedicle screws.

**Objective 1:** Development of 3D FE models of lumbar spine with and without expandable pedicle screws to get baseline of preliminary data (comparison between intact and implanted models).

**Objective 2:** Numerical comparison and assessment of bone remodelling of normal and expandable pedicle screws based on patient-specific FE model.

**Objective 3:** Comparison of pullout strength for expandable pedicle screws with various thread designs and validation with FE analysis.

**Objective 4:** Influence of various thread designs of expandable pedicle screws on bone growth using mechanoregulation algorithm.

### 1.9 Structure of the thesis

This research was conducted to advance the understanding of computational biomechanics in spinal implants. The primary objective was to numerically evaluate the innovative expandable pedicle screws, to benefit the public healthcare sector. Integrating modern technology into traditional healthcare practices offers several advantages, including cost- effectiveness, improved diagnosis, and faster, more optimized patient-specific solutions. This thesis is structured into six distinct chapters, each contributing to the achievement of the study's primary objective, as outlined in the following order.

Chapter 1: This chapter deals with the general introduction of the lumbar spine, spine biomechanics, failure scenario of the pedicle screws, literature review, clinical investigation, motivation behind the study, the available research gap and the specific objective of the study.

Chapter 2: This chapter presents the development of the FE model of intact as well as implanted FE models instrumented with normal and expandable pedicle screws acquired from the manufacturer-supplied CAD model. The development of the FE model was elaborately explained with needful data about the geometry, meshing, ligament, material properties, loading and boundary conditions. The results were validated based on range of motion (ROM) to quantify the anticipated results. This study is helpful to understand the load transfer due to physiological conditions through the pedicle screws based on stress-strain results.

Chapter 3: This chapter deals with the development of the intact and implanted FE models of the lumbar vertebra using CT scan dataset. Firstly, strain and strain energy density (SED) distribution under physiological loads is presented. The variation of bone density around normal pedicle screws and expandable pedicle screws owing to bone remodelling is shown in the chapter. The bone remodelling algorithm was combined

with FE analysis for this purpose.

Chapter 4: This chapter investigates the pullout strength of three newly designed expandable pedicle screws by varying the thread pitch. The pullout tests were conducted on synthetic polyurethane (PU) foam having properties of low osteoporotic bone. Further, the validation of the study was performed using FE analysis.

Chapter 5: This chapter presents the bone growth around the three types of expandable pedicle screws. Two mechanoregulation algorithms based on (a) deviatoric strain with hydrostatic pressure and (b) deviatoric strain alone were utilized for two load cases around the expandable pedicle screws. This study helped assess the spatial distribution of the tissue phenotype for the two mechanoregulation models. This study emphasized the formation of new tissue for bone growth given the potential osseointegration capacity of the screws.

Chapter 6: This is the ultimate chapter of the thesis providing the conclusion, major contribution, limitation and significance of the present study. Here, the overall findings of the thesis are presented based on the studies presented in the earlier chapters. The future scope of the study is also included in the final chapter.

# Chapter 2

## Development of 3D FE models of lumbar spine instrumented with expandable pedicle screws: intact versus implanted cases (Comparison between intact and implanted models)

### 2.1 Introduction

A great number of people across the globe suffer from mild to severe lower back pain, the onset of which can sometimes be post-operative. The lower back pain was reported as the second most symptomatic reason and overall, the fifth most common reason for all physician visits (Atlas and Deyo 2001). The most common complaint of spine and hip for elderly people is osteoporosis with mortality rates ranging from 10 to 20 percent (Keramat *et al.* 2012). These osteoporotic fractures also cause extensive pain and, in certain cases, disability, depression and increased dependency leading to diminished quality of life (Keramat *et al*. 2012). Each year nearly 700,000 patients suffer from spinal fractures known as vertebral compression fractures. Lumbar surgeries are predominantly performed 3 times more for patients older than 60 years than younger ones (Zou *et al.* 2020, Sivasubramaniam *et al*. 2015). It may be noted here that the lumbar spine helps in transferring weight to the pelvis and allows different bodily movements during day-to-day activities (Yoganandan *et al.* 2000, White and Panjabi 1978).

During the pre-renaissance era and the two world wars, physicians tried different surgical techniques to treat lumbar spine fractures. Vertebral and pedicle screw fixations were introduced in the 1940s and have become popular ever since among spine surgeons (Kabins and Weinstein 1991). The first case of vertebral screw fixation started way back in 1944. However, the use of pedicle screws was well documented since the 1970s by Roy-Camille (Kabins and Weinstein 1991). The primary aim of the surgeons was to reduce fracture by achieving bony union, such that the spinal anatomy is restored while delivering stability to the posterior spinal devices (Li *et al*. 2014).

Pedicle screws offer stability to the posterior side with rigid bony fixation by connecting the fractured bones (Wang *et al.* 2020). The primary advantage of pedicle screws over conventional bone screws is that they provide 3-column fixation, assist in

the instrumentation of short segments, and also maintain desired alignment (Moore *et al.* 1997, Wu *et al.* 2010). The success rate of pedicle screw fixation was found to be more than 80% in a 10-year follow-up study (Glaser *et al*. 2003). In the case of posterior fixation, however, it was estimated that the pedicle screw was the weakest link (Moran *et al*. 1989, Alizadeh *et al.* 2013). The primary failure of pedicle screw was found to occur either due to screw loosening or pedicle root breakage (Wang *et al*. 2020, Moran *et al*. 1989, Liao *et al.* 2017, Alanay *et al*. 2007, Qi *et al.* 2011, Viezens *et al*. 2021, Otsuki *et al.* 2021). Loosening of pedicle screw can be ascribed to increased load sharing, high-stress concentration caused by bending, frequent loading-unloading and prolonged bone fusion (Biswas *et al.* 2019, Chen *et al*. 2003, Pearson *et al.* 2017). Earlier studies suggested that bone mineral density, insertion technique and screw dimensions act as necessary factors for screw stability (Viezens *et al.* 2021, Cho *et al.* 2010). Patients with osteoporosis have low bone mineral density and thus have lower pullout strength at the fixation points (Zou *et al.* 2020, Halvorson *et al*. 1994, Paxinos *et al.* 2010, Fu *et al.* 2017). The inferior bone quality in the osteoporotic spine may pose a challenge for surgeons to operate on as it may lead to complications in the neural structures owing to failure at the bone-screw interface (Gazzeri *et al*. 2016, Rahyussalim *et al.* 2019, Su *et al*. 2021). Earlier studies suggested that sagittal imbalance was the primary pathogenic cause of lower back pain and its correction was essential for degenerative spinal deformity.

Expandable pedicle screws, on the other hand, have many advantages over traditional pedicle screws because of their capacity for better anchorage. Earlier studies indicated that expandable pedicle screws provide better fixation due to greater bone contact without any increase in diameter or screw length (Cook *et al.* 2001). The use of expandable pedicle screws increased by around 30% and 50% in pullout strength in the case of healthy and osteoporotic bone, respectively, as compared to conventional pedicle screws (Cook *et al*. 2000). This suggests that expandable pedicle screws tend to provide superior fixation strength in case of compromised bone. For osteoporotic patients, an expandable pedicle screw provides fewer complications, quick and surgically satisfactory postoperative effect, short operation time and less intraoperative bleeding (Weng *et al*.2018). Breakage of expandable pedicle screws occurred for around 2.8% of patients and 2.6% in total number of screws that were placed (Cook *et al*. 2001). Another study on expandable pedicle screws with different designs showed 7% related complications (Bokov *et al.* 2018). Despite the availability of clinical

studies, there remains a paucity of preclinical investigations on expandable pedicle screws used on lumbar vertebrae. Therefore, more rigorous investigations are warranted to evaluate its performance and to further ascertain its competitive edge over other techniques, if any.

Over the last few decades, FEA (Finite Element Analysis) has attained much popularity as a preclinical tool in orthopaedics and courtesy of its non-invasive nature, novel designs of implants have been studied *in silico* (Chanda *et al*. 2016, Sahu and Kaviti 2016, Sanjay *et al.* 2018, Mondal and Ghosh 2019a, Talukdar *et al*. 2021, Biswas et al. 2022). It has been used extensively to solve many biomechanical problems owing primarily to low financial and computational cost, as well as high precision simulation (Sanjay *et al.* 2018, Dreischarf *et al*. 2014). It further reduces the complexity of clinical or *in vitro* tests. In studies involving lumbar spine biomechanics, FE helped gain insights at crucial sites, e.g. bone-screw interfaces under different physiological conditions of spinal loads (Ayturk and Puttlitz 2011, Kiapour *et al.* 2012, Rohlmann *et al.* 2013, Xu *et al.* 2019). Thus, evaluation of different spinal implants and development of subject-specific implants have been attempted using FE (Talukdar *et al.* 2021, Dreischarf *et al.* 2014, Ayturk and Puttlitz 2011, Kiapour *et al*. 2012, Xu *et al.* 2016, Goel *et al.* 2007). Nonetheless, a realistic FE model of spinal osteotomies is paramount in this regard, which may successfully allude to more detailed preclinical insights and thereby help clinicians choose the right implant (Talukdar *et al*. 2021, Zander *et al.* 2006, Rohlmann *et al*. 2007).

It was estimated that failure was greatest (33% for single-level fusion) at the L4-L5 level among all vertebral screw fixation (Kabins and Weinstein 1991). By employing anatomically viable FE models, the present study intended to estimate stress-strain fields of a functional spinal unit (FSU) of intact L4-L5 vertebra and to further compare the same with FSUs instrumented with normal and expandable pedicle screws under various physiological loading conditions. Stress and strain results for intact and implanted models, corresponding to various physiological movements, were derived and subsequently used to compare the normal and expandable pedicle screws. It is hypothesized here that an expandable pedicle screw may result in improved stability and more anatomic load transfer as opposed to a normal pedicle screw.

## 2.2 Materials and Methods

An elaborate description of materials and methods, starting from the development of virtual osteotomies to the *in silico* biomechanical investigations has been systematically presented under the following subcategories.

### 2.2.1 Development of the intact model

The Fig.2.1a shows the CAD model of intact L4-L5 vertebrae. All different parts of the FSU, i.e. the intact L4-L5 vertebrae, are illustrated in Fig. 2.2. The virtual FSU was generated using the CAD models of L4 (model #3902) and L5 (model #3901) vertebrae, procured from the manufacturer (Sawbones, Europe AB, Malmo, Sweden). The FSU was anatomically positioned by aligning it with standardized anatomical reference planes (sagittal, coronal and transverse) and key anatomical landmarks using Rhinoceros CAD software (Rhinoceros v7.0, Robert McNeel & Associates Seattle, USA) and the modifications such as the boolean operations were carried out for the digital separation of cortical and cancellous bone. The average thickness of the cortical bone was considered to be 1.0 mm (Boccaccio *et al.* 2008, Zhang e*t al*. 2018). Thereafter, annulus fibrosus and nucleus pulposus comprising the IVD were curated. Around 43% of the whole disc volume was occupied by the nucleus pulposus (Kim *et al.* 2010). The bony endplates and cartilaginous endplates were given a thickness of 0.5 mm (Talukdar *et al.* 2021). Further, the facet cartilage was developed based on an initial gap of 0.1 mm (Talukdar *et al.* 2021).

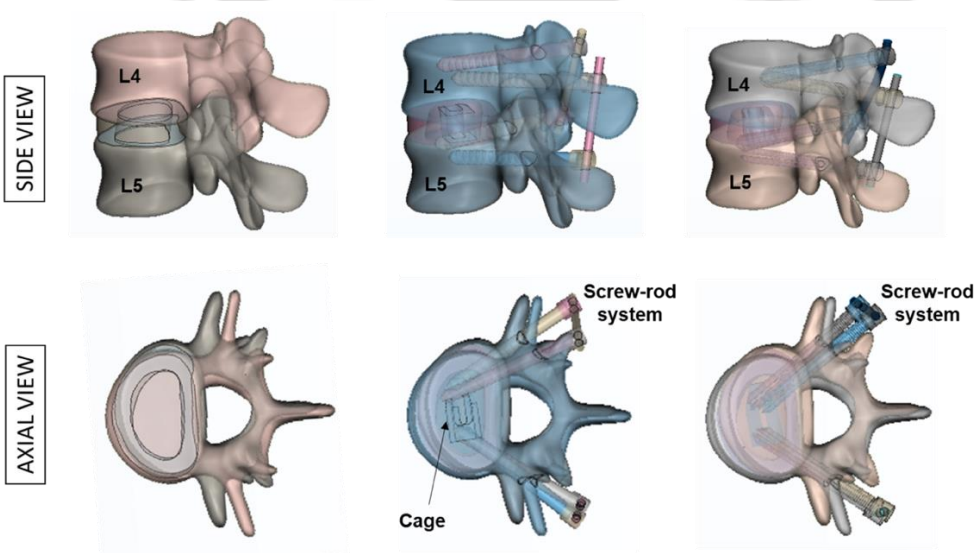


**Fig. 2.1:** 3D CAD models of the L4-L5 FSU: (a) intact, (b) implanted with normal pedicle screw, (c) implanted with expandable pedicle screw**.**

### 2.2.2 Development of the implanted models

Fig. 2.1b and Fig. 2.1c presented the CAD models of implanted L4-L5 vertebrae with normal pedicle screws and expandable pedicle screws respectively. Lumbar loading reconstruction is generally performed using posterior pedicle screw-rod fixation due to the high loading condition in that region (Song *et al.* 2021). Various parts of implanted L4-L5 vertebrae are displayed in Fig. 2.3. Transforaminal lumbar interbody fusion (TLIF) has been reported to be a popular choice for the treatment of degenerated lumbar spine and against premature pedicle screw loosening (Ambati *et al.* 2014, Kim *et al.* 2010). As such, a one-sided total facetectomy was performed to virtually place the TLIF cage (Ardis$^{TM}$, Zimmer Biomet, Warsaw, IN, USA, 26 x 11 x 12 mm) inside the FSU (Fig. 2.3). The TLIF was virtually implanted by simulating the surgical steps in a computational environment. For all the implanted models, the removal of nucleus pulposus, cartilaginous endplates and left facet cartilage was performed as per the surgical guidelines. A TLIF cage was inserted into the L4-L5 disc space through a postero-lateral annular window and secured with pedicle screws. It was estimated that the enlarged screw diameter that optimally fits the pedicle leads to a better screw stability (Viezens *et al.* 2021, Otsuki *et al.* 2021). Cylindrical screws of 60.0 mm length (body length: 26.5 mm; thread length: 33.5 mm), 6.0 mm shaft diameter and 3.0 mm pitch having triangular threads (angles: $90^0$, $36.7^0$ and $53.3^0$) were considered for both normal and expandable pedicle models (Fig. 2.3). The normal pedicle screw design was based on EXPEDIUM 5.5 system (Depuy Synthes Spine, Inc, Raynham, MA) and expandable pedicle screw design was adopted from Tai *et al.* (2015). The expandable pedicle screw had an extension of around 2.0 mm in diameter after the expansion (Wu *et al*. 2010). Two rods each 50.0 mm long having a diameter of 4.0 mm were inserted through the screw head for securing the implants properly. Surgeons need to place the pedicle screws properly to have correct placement as well as to minimize the risk of revision surgery (Fisher *et al.* 2022). The screws were guided by anatomical landmarks and aligned parallel or slightly convergent to the midline axially and angle cephalad in the sagittal plane. The screws were inserted with traditional trajectory, with entry points at the intersection of the transverse process and superior articular facet after consulting with an experienced orthopaedic registrar (Max Hospital, Mohali, India).

### 2.2.3 FE model generation and analysis

The FE models of both intact and implanted L4-L5 vertebrae were generated using HyperMesh 2021.1 (Altair Engineering Inc., Troy, Michigan, United States) (Figs. 2.2, 2.3). The solid models of bones and the implants were discretized into 4-noded unstructured tetrahedral mesh. However, the six ligaments, namely anterior longitudinal ligament (ALL), posterior longitudinal ligament (PLL), ligamentum flavum (LF), intertransverse ligament (ITL), interspinous ligament (ISL) and supraspinous ligament (ISL), were modelled using 1D tension-only spring elements, termed as CGAP elements (Figs. 2.2, 2.4a). The ligaments are placed at anatomically precise positions, connecting the specific bony landmarks to replicate the physiological roles to provide stability as well as restricted motion. These elements can mimic the soft tissue properties since they impart stiffness only under tension (Biswas *et al.* 2022), whereas in compression the stiffness becomes zero. Both LF and PLL were removed for all implanted models as per surgical guidelines (Figs. 2.3, 2.4b, 2.4c).

A mesh convergence study of the intact L4-L5 FE model was performed to optimize the element size for a trade-off between accuracy and solution speed. Three FE models of different element sizes were generated to estimate the dependency on mesh density. Equivalent (von Mises) stress of cortical and cancellous bone under pure compression was chosen for the mesh convergence study. The first model used an element size of 1.0 mm to 3.0 mm, the second model used 0.5 mm to 2.5 mm and the third model used 0.25 mm to 2.0 mm. The von Mises stress varied between 4-6% for the first two FE models whereas ~1-2% deviation was observed for the second and third models (Biswas *et al.* 2022). Thus, the second model which consisted of 647,837 elements with element sizes 0.5 mm to 2.5 mm was selected for further analyses. The average edge length was considered to be ~1.0 mm (Fig.2.2 and Fig.2.3).

All analyses were performed using the ‘OptiStruct’ solver of HyperMesh 2021.1. To account for stiffness as a function of displacement, a nonlinear analysis was performed using a piecewise linear approach, dividing the load into small incremental steps for accurate computation. Thus, the stiffness matrix was restructured after each increment of applied load. Newton-Raphson method was used to solve the equations iteratively (Gokhale *et al.* 2008).

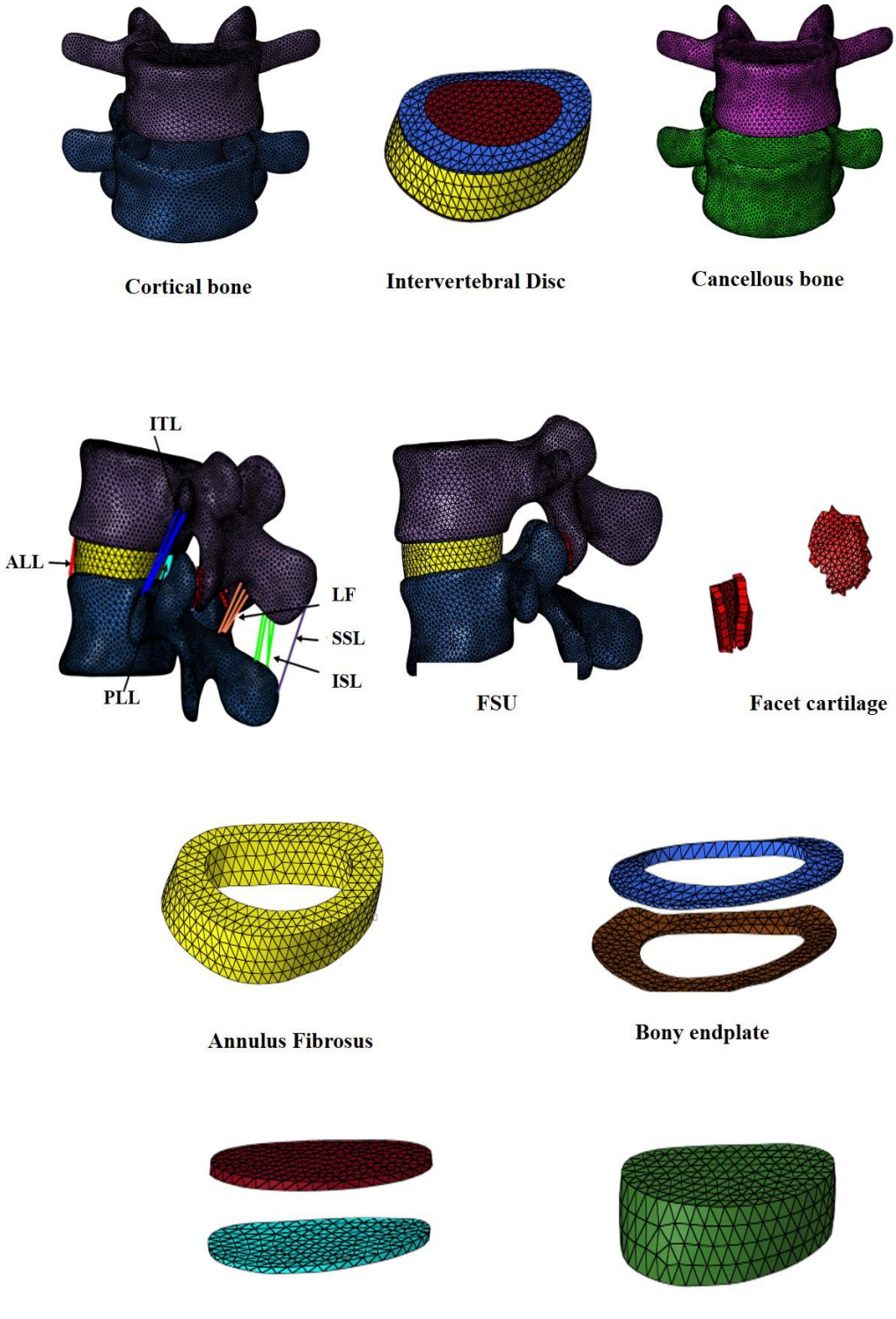


**Fig. 2.2:** The curated models of different parts of an intact L4-L5 FSU.

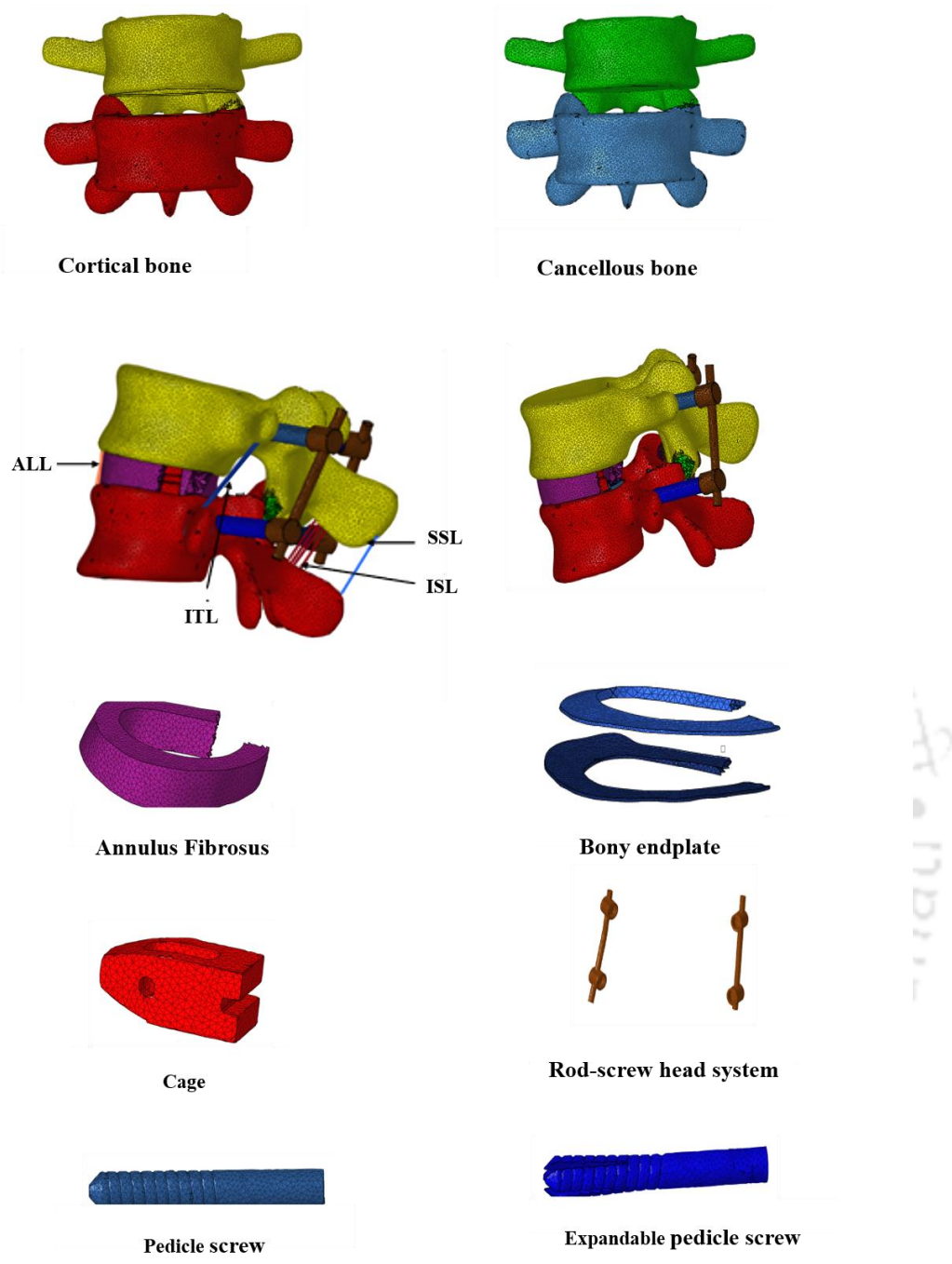


**Fig. 2.3:** The curated models representing different parts of the two implanted L4-L5 FSUs.

The contact analysis was solved using the Augmented Lagrangian method, where L4 cartilage was considered as the slave (contact) and L5 cartilage as the master body (target) in the contact pair (Sanjay *et al.* 2021). The reason behind the use of the Augmented Lagrangian Method for contact formulation is its balanced accuracy and computational efficiency. It is important to note that surface-to-surface contact

elements were used (coefficient of friction, μ = 0.2) (Zhou *et al*. 2020) on both the left and right side of the facet cartilage interface of L4-L5 vertebrae.

### 2.2.4 Material properties

**Table 2.1**: Material properties corresponding to various components of the FSU.

| Components | Young's modulus (MPa) | Poisson's ratio | Reference |
|---|---|---|---|
| Cortical bone | 12000 | 0.3 | Li *et al.* 2014, Goel *et al.* 2007 |
| Cancellous bone | 100 | 0.3 | Li *et al.* 2014, Goel *et al.* 2007 |
| Bony endplates | 12000 | 0.29 | Li *et al*. 2014 |
| Cartilaginous endplates | 23.8 | 0.4 | Xu *et al.* 2016 |
| Nucleus pulposus | 0.1 | 0.49 | Li *et al*. 2014 |
| Annulus fibrosus | 9 | 0.4 | Li *et al*. 2014 |
| Cage | 110000 | 0.3 | Su *et al*. 2021 |
| Pedicle screw | 110000 | 0.3 | Wong *et al*. 2022 |
| Ti Rod | 110000 | 0.3 | Wong *et al*. 2022 |

The material properties of cortical bone, cancellous bone and end plates were assumed to be linear, elastic and isotropic (Alanay *et al.* 2007, Wong *et al.* 2022). For nucleus pulposus, low elastic modulus (E=0.1 MPa) was applied with the aim of simulating incompressible fluid-like behaviour (Li *et al*. 2015). The implant material was considered to be titanium alloy (Ti-alloy) having Young's modulus of 110 GPa and Poisson's ratio of 0.3. All material properties are tabulated in Table 2.1.

The lengths of the ligaments were obtained from data available in the literature (Yoganandan *et al.* 2000). The stiffness values of the ligaments, as shown in Table 2.2, were estimated based on the length, anatomical cross-section and Young's moduli (Boccaccio *et al*. 2008, Li *et al.* 2015, Vena *et al*. 2005). For calculating the ligament stiffness, the axial stiffness formula, i.e. $K = AE/L$ was used, where $K$ is the geometric stiffness, $A$ is the cross-sectional area, $E$ is Young's modulus and $L$ is the length of the ligament. The calculated values were found to corroborate well with the literature (Yoganandan *et al*. 2000).

**Table 2.2:** Ligament properties

| Ligaments | Stiffness (N/mm) |
|---|---|
| Anterior longitudinal | 45.20 |
| Posterior longitudinal | 26.49 |
| Flavum | 43.71 |
| Intertransverse | 2.77 |
| Interspinous | 35.50 |
| Supraspinous | 12.72 |

### 2.2.5 Loading and boundary conditions

The analyses were performed for five loading conditions, i.e. compression, flexion, extension, lateral bending and torsion, and all load values loosely correspond to the body weight of an adult person (Sanjay *et al.* 2021, Xiao *et al*. 2011). A rigid body element (RBE3) was created for the application of load (Figs. 2.4a, b, c). Roughly at the centre of the top surface of L4 cortical bone, a 'dependent' node was selected whereas all surface nodes of L4 cortical bone were selected as 'independent' nodes. The loads were applied at the central node of RBE3 and calculated based on the

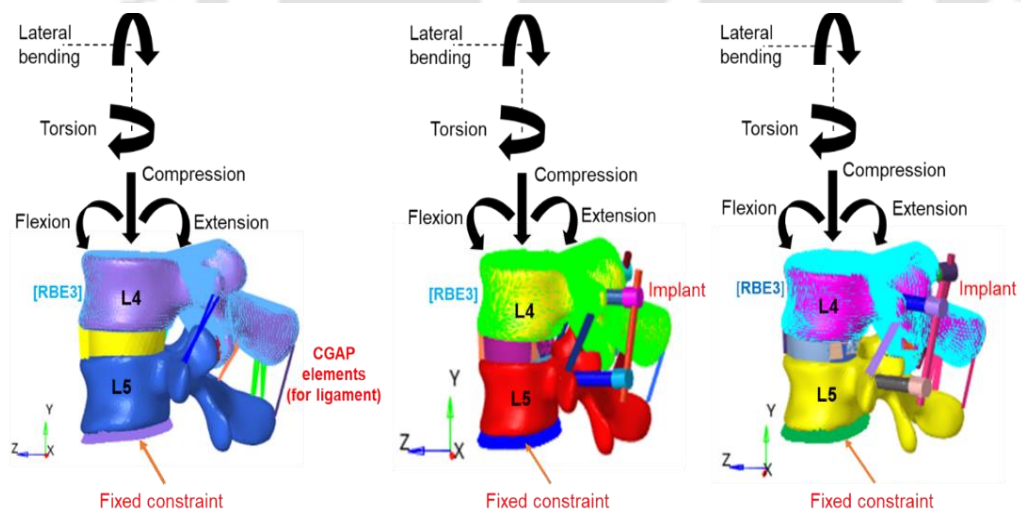


**Fig. 2.4:** The various physiological loading and boundary conditions for (a) intact FE model, (b) implanted FE model for normal pedicle screw and (c) implanted FE model for expandable pedicle screw. 'RBE3' denotes the rigid body element surrounding the L4 vertebra, whereas 'CGAP' elements were defined to simulate ligament properties.

weighted average of motions for all the surface nodes of L4 cortical (Fig. 2.4) (Sanjay *et al.* 2021). Thus, the loads were assumed to be acting through the centre of gravity of L4. For axial compression loading conditions, a load of 500N was applied vertically downward. However, for flexion, extension, lateral bending and torsion, a 10 Nm moment plus an axial load of 500N acted upon simultaneously on the FSU (Sanjay *et al.* 2021, Xiao *et al.* 2011, Markolf 1972). For FE analysis, all interfaces in the FSU – intact and implanted models were assumed to be bonded under all conditions (Sanjay *et al.* 2021). The bonded approach using a non-manifold assembly allows seamless load transfer between components, with bonded contacts used for bone-implant and internal interfaces to ensure proper integration without gap or overlap. All the bottom surface nodes of the L5 cortical of the FSU were constrained for all six degrees of freedom (Sanjay *et al*. 2021).

## 2.3 Result

### 2.3.1 L4-L5 FSU: model validation based on ROM

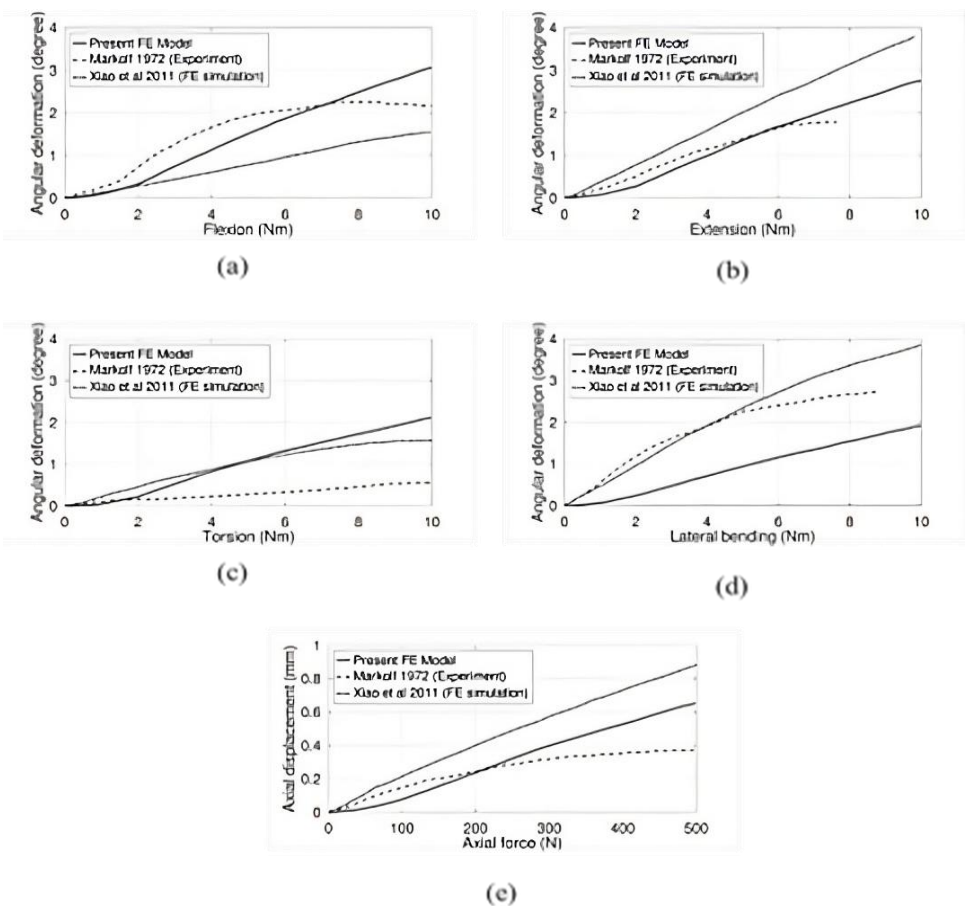


**Fig. 2.5:** Comparison of ROM values of the current intact FE model with those obtained from the literature: (a) Flexion, (b) Extension, (c) Torsion, (d) Lateral bending and (e) Axial compression.

The validation of the L4-L5 FSU (intact model) was performed by comparing results of range of motion (ROM) vis-à-vis various loading regimes, both based on experimental data (Markolf 1972) as well as FE analysis reported erstwhile (Xiao *et al.* 2011) (Fig. 2.5). Under axial compression, the experimental study by Markolf (1972) reported a maximum relative displacement of 0.38 mm, while the FE study by Xiao et al. (2011) predicted a displacement of 0.88 mm. In our study, the predicted linear displacement (in mm) under axial compression (Fig. 2.5e) was found to lie midway between the earlier two findings (~0.65 mm). In the case of flexion, extension, torsion and lateral bending, the ROM (calculated as angular displacements having unit in degrees) versus load graphs were found to follow similar trends and to agree reasonably with the literature (Fig. 2.5a-d). All ROM values (in degrees) are shown in Table 2.3 for direct comparison with data from the literature.

**Table 2.3:** ROM (in degrees) of the intact model during different physiological movements.

| | **Flexion** | **Extension** | **Torsion** | **Lateral Bending** |
|---|---|---|---|---|
| Present study | 3.0 | 2.7 | 2.1 | 1.9 |
| Talukdar *et al*. 2021 | 3.2 | 3.1 | 2.3 | 3.1 |
| Xiao *et al.* 2011 | 1.6 | 3.7 | 3.8 | 1.6 |
| Zhong *et al*. 2006 | 2.4 | 2.3 | 3.2 | 3.7 |
| Chen *et al.* 2001 | 4.5 | 3.9 | 2.0 | 2.0 |
| Yamamoto *et al*. 1989 | 7.1 | 4.0 | 2.4 | 3.8 |

### 2.3.2 ROM of the implanted models

ROM was reported to be the highest in the intact spine (Jain and Khan 2022) and hence, for all ROM deviations in the implanted models, the intact spine was considered as the reference (i.e. 100%). Considerable reductions in ROM were predicted for the implanted models while subjected to different loading regimes (Zhong *et al.* 2006, Coombs *et al.* 2013, Talukdar *et al.* 2021). For normal pedicle screw models, the reductions were 74%, 75%, 63% and 50% under flexion, extension, torsion and lateral bending, respectively. In the case of expandable pedicle screws, the respective reductions were predicted in the order of 75%, 62%, 48% and 39%.

### 2.3.3 Stress (von Mises) for cortical and cancellous bone

The equivalent (von Mises) stress contours for the cortical and cancellous bone of L4-L5 vertebrae, subjected to the five physiological loading regimes, are presented in Fig. 2.6 and Fig. 2.7, respectively. Fig. 2.8 depicts the stress contour for cancellous bone in a sectional view. While subjected to torsion, high-stress magnitudes in the order of ~50 MPa (Fig. 2.6a) and ~1.6 MPa (Fig. 2.7a) were predicted in cortical and cancellous bone, respectively, in the case of intact FSU. Under extension, peak stress was close to 50 MPa for cortical bone albeit at a localized region, whereas for cancellous bone, the peak stress was ~0.9 MPa. Under compression loading, however, the peak stresses were predicted to be the least, i.e. ~15 MPa (Fig. 2.6a) for cortical bone and ~0.7 MPa (Fig. 2.7a) for cancellous bone. The peak stresses were found towards the posterior side of the FSU in all loading conditions except for the lateral bending condition where the peak stress was observed towards the anterior side (Figs. 2.6a, 2.7a).

For the implanted vertebrae with normal pedicle screw, peak stresses of ~10 MPa for cortical and ~1.6 MPa for cancellous bone were predicted under compression, whereas the same were found to be ~50 MPa and 1.6 MPa, respectively, under extension (Fig. 2.6b and Fig. 2.7b). These higher stress magnitudes were found at the site of screw insertion for cortical bone and near the cage insertion area for cancellous bone. Under lateral bending, the peak stress area was found to be shifted towards the anterior side, more predominantly on the L5 vertebra compared to the L4 vertebra (Figs. 2.6b, 2.7b).

In the case of the expandable pedicle screw model, the highest stress of ~1.6 MPa (Fig. 2.7c) for cancellous bone was predicted under all the loading scenarios near the cage insertion area. However, scattered regions of comparable stress concentration were also observed at the posterior side of the L4 vertebra. In cortical bone, peak stresses (~50 MPa) (Fig. 2.6c) were found near the posterior top side of the L5 vertebra and also near the screw insertion area under extension. Relatively moderate peak stress values (~45 MPa) were found under torsion and lateral bending for cortical bone towards the anterior side of the L5 vertebra. The least amount of peak stress values for both cortical (~30 MPa) and cancellous bone (~1.4 MPa) were found under compression (Figs. 2.6c, 2.7c).

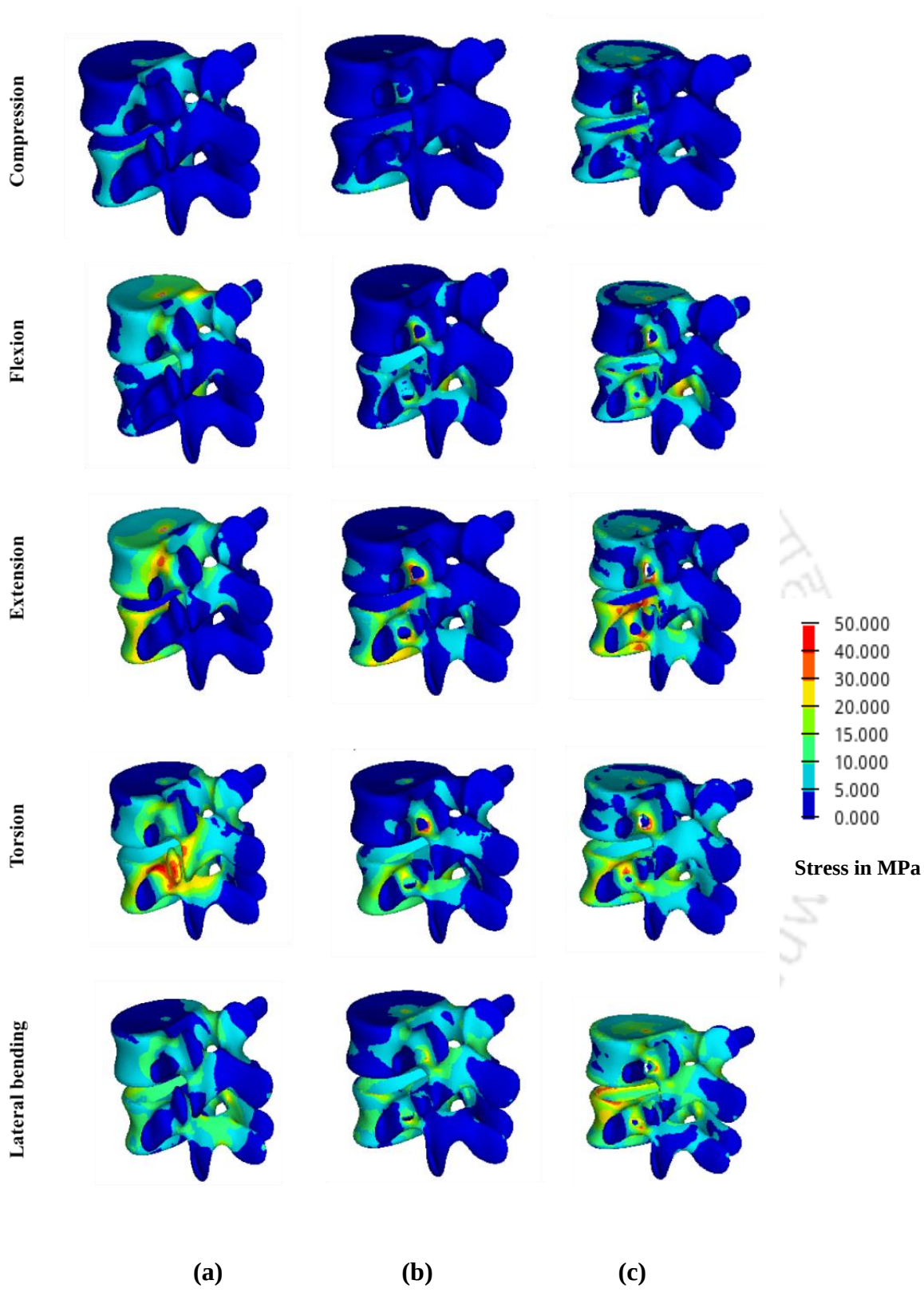


**Fig. 2.6:** Von Mises stress contours (in MPa) in cortical bone for (a) intact FSU and FSUs corresponding to (b) normal and (c) expandable pedicle screw, respectively.

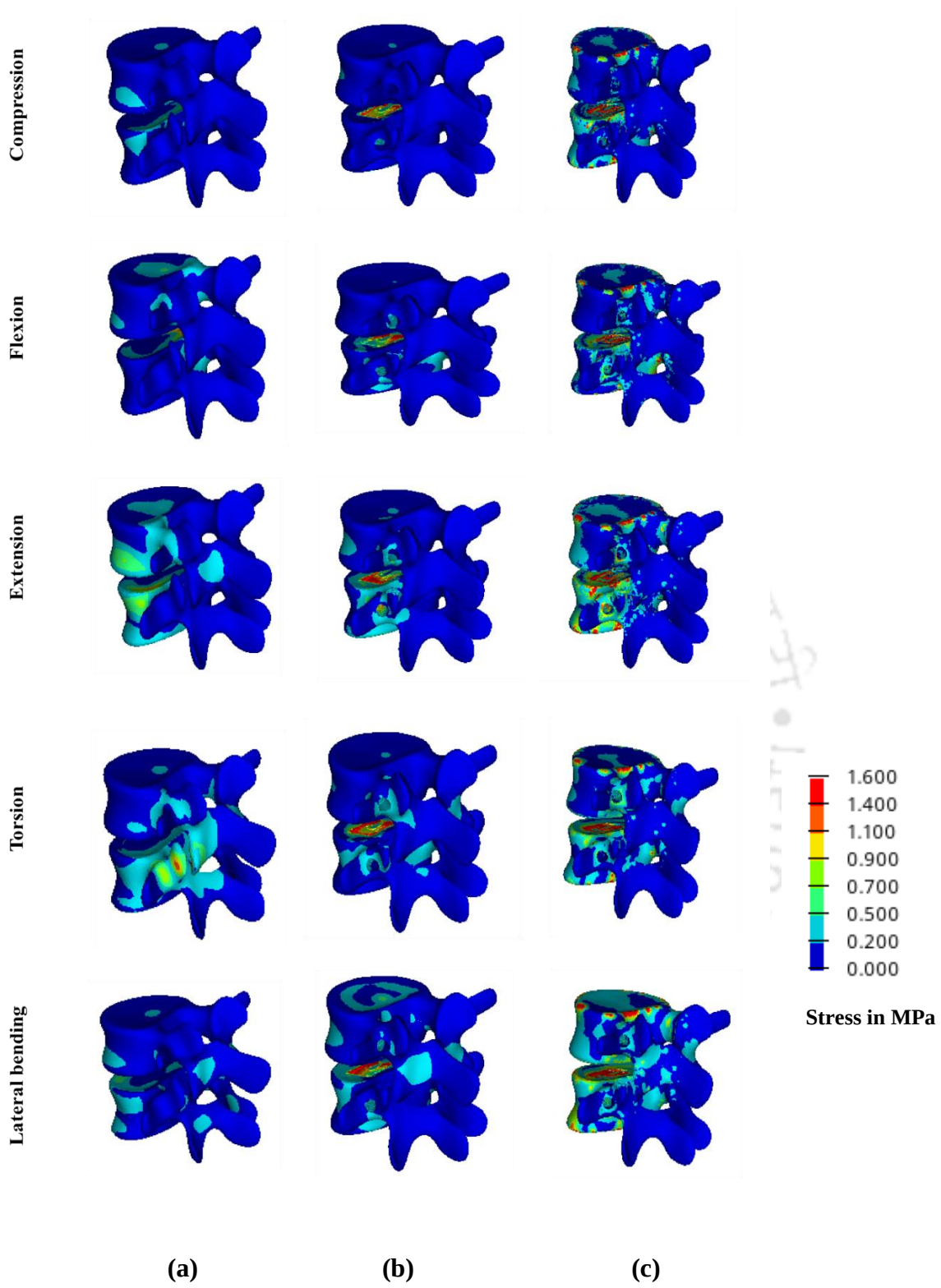


**Fig. 2.7:** Von Mises stress contours (in MPa) in cancellous bone for (a) intact FSU and FSUs corresponding to (b) normal and (c) expandable pedicle screw, respectively.

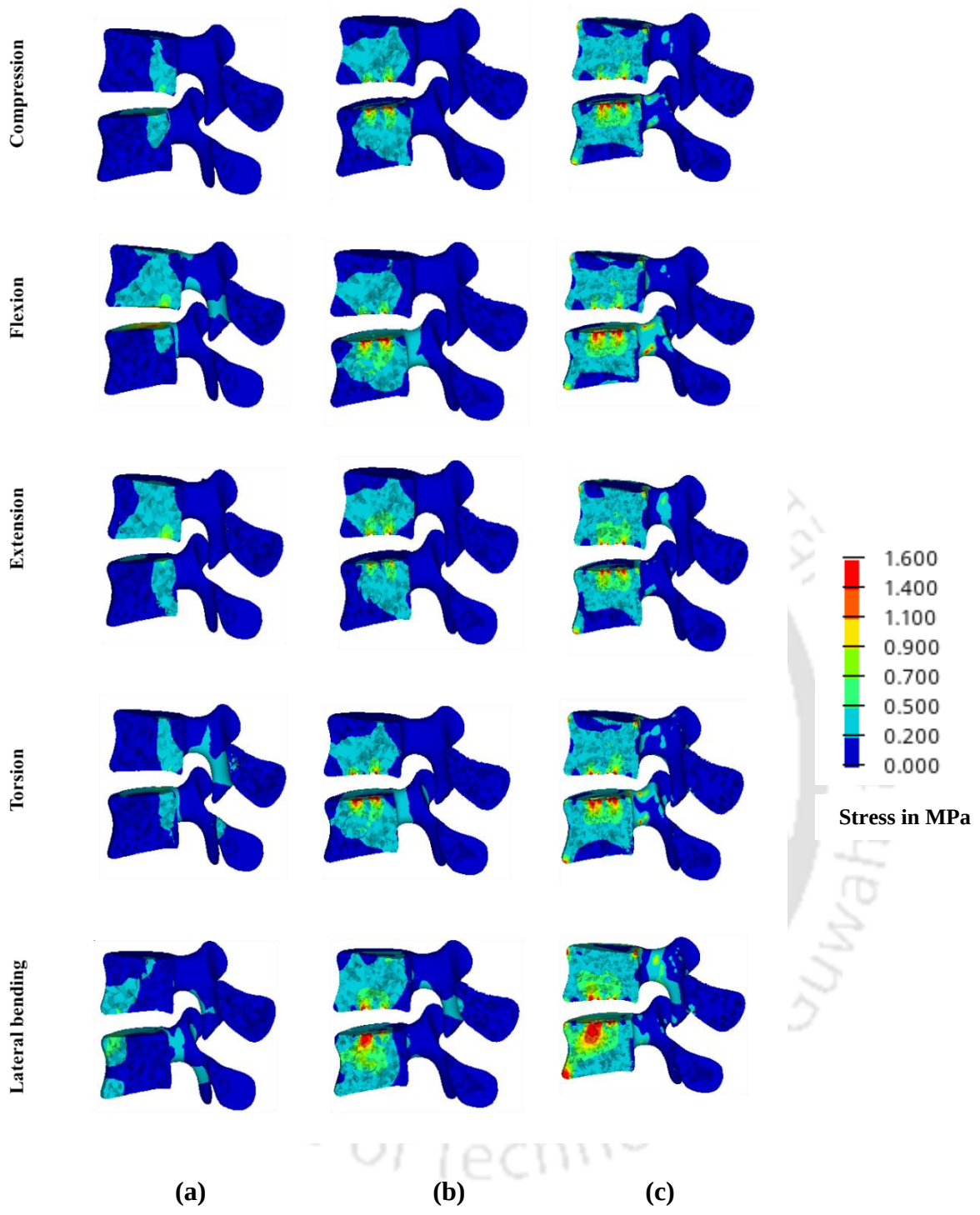


**Fig. 2.8:** Von Mises stress contours (in MPa) in cancellous bone (sectional view) (a) intact FSU and FSUs corresponding to (b) normal and (c) expandable pedicle screws, respectively.

### 2.3.4 Strain (von Mises) for cortical and cancellous bone

The equivalent (von Mises) strain contour for the L4-L5 vertebra for both cortical bone (Fig. 2.9) and cancellous bone (Fig. 2.10) under five physiological loading conditions are presented. Fig 2.11 portrays the strain contour for cancellous bone in a sectional view. In the case of intact FSU, peak strains of ~0.0015 (Fig. 2.9a) for cortical bone and ~0.005 (Fig. 2.10a) for cancellous bone were observed under torsion. Under compression loading, peak strain was below 0.0005 for cortical bone (Fig. 2.9a) and under 0.003 (Fig. 2.10a) for cancellous bone in the case of intact FSU. The peak strain for cortical bone (Fig.2. 9a) and cancellous bone (Fig. 2.10a) was found near the posterior side of the FSU under all loading conditions except for lateral bending.

For implanted L4-L5 vertebra with normal pedicle screw, peak strains of ~0.002 for cortical bone (Fig. 2.9b) and ~0.007 for cancellous bone (Fig. 2.10b) were observed. However, peak strains were predicted to prevail over relatively greater areas while subjected to extension load (Figs. 2.9b, 2.10b). High strain area was predominantly found near screw insertion in the case of cortical bone and near cage area for cancellous bone. For various loading cases, the peak strain was estimated to be higher in the L5 than in the L4 vertebra (Figs. 2.9b, 2.10b). Following trends from stress results, the peak strain area corresponding to expandable pedicle screws was found to be greater than that in normal pedicle screws (Figs. 2.9c, 2.10c).

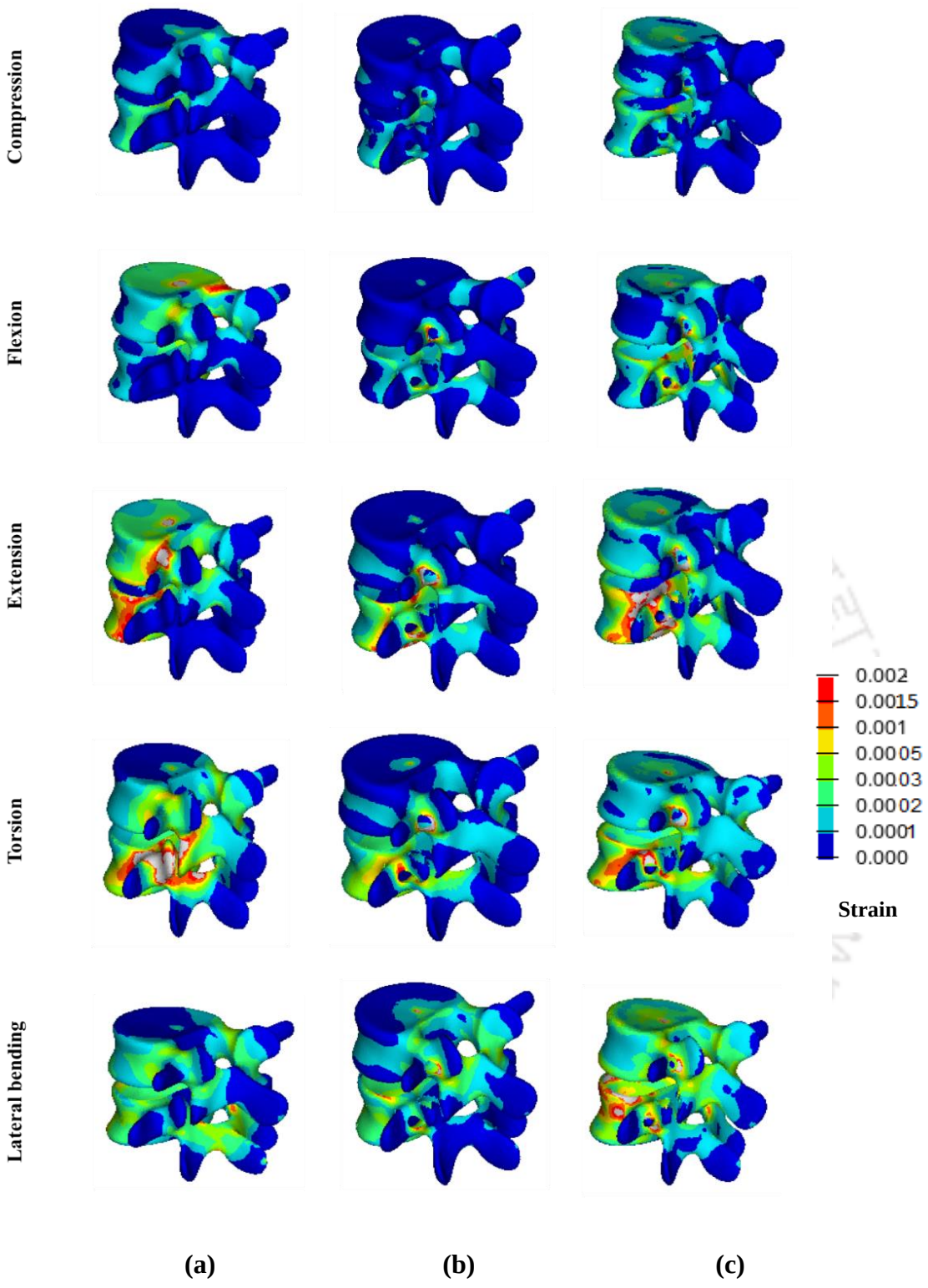


**Fig. 2.9:** Von Mises strain contours in cortical bone for (a) intact FSU and FSUs corresponding to (b) normal and (c) expandable pedicle screw, respectively.

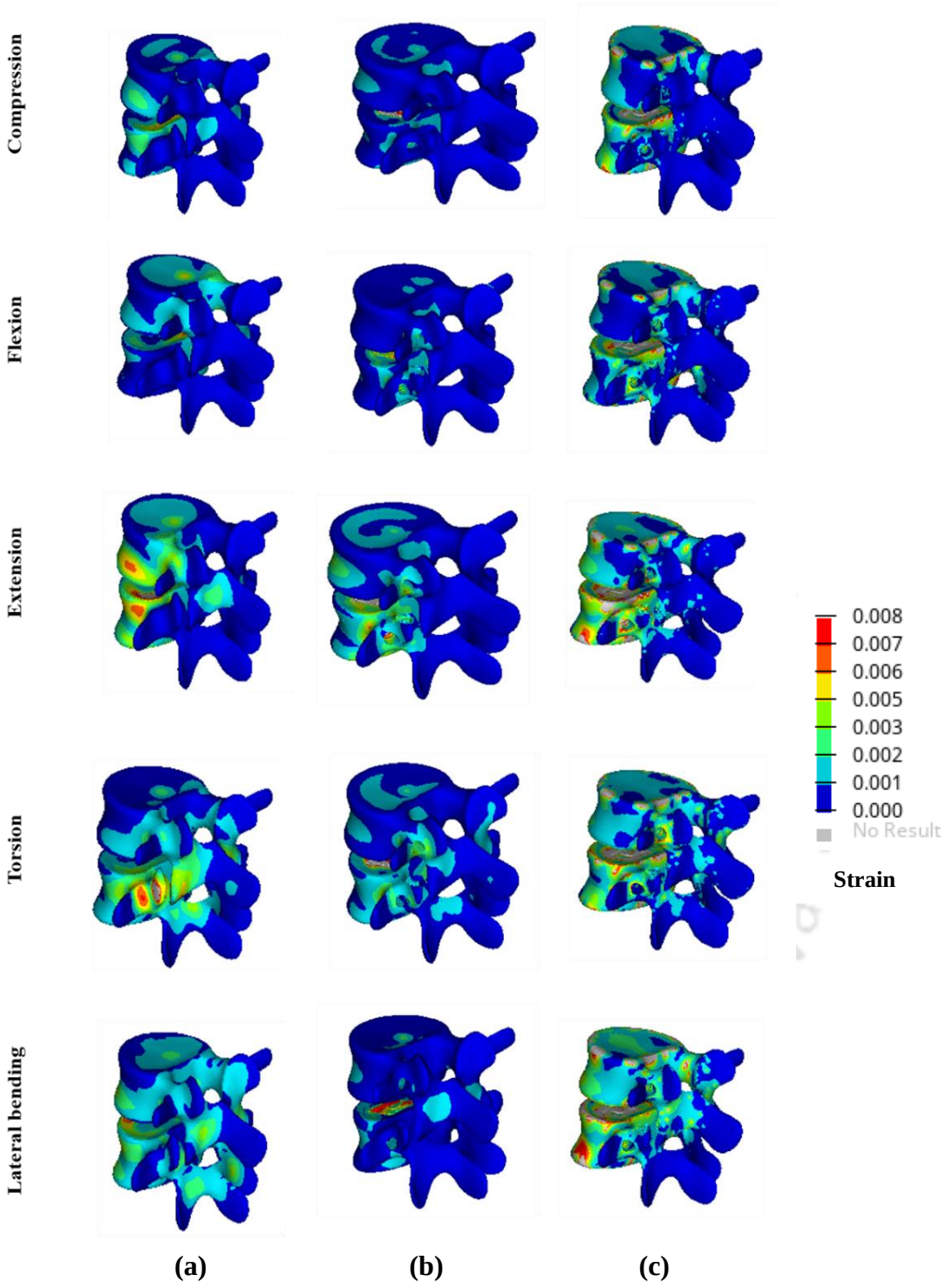


**Fig. 2.10:** Von Mises strain contours in cancellous bne for (a) intact FSU and FSUs corresponding to (b) normal and (c) expandable pedicle screw, respectively.

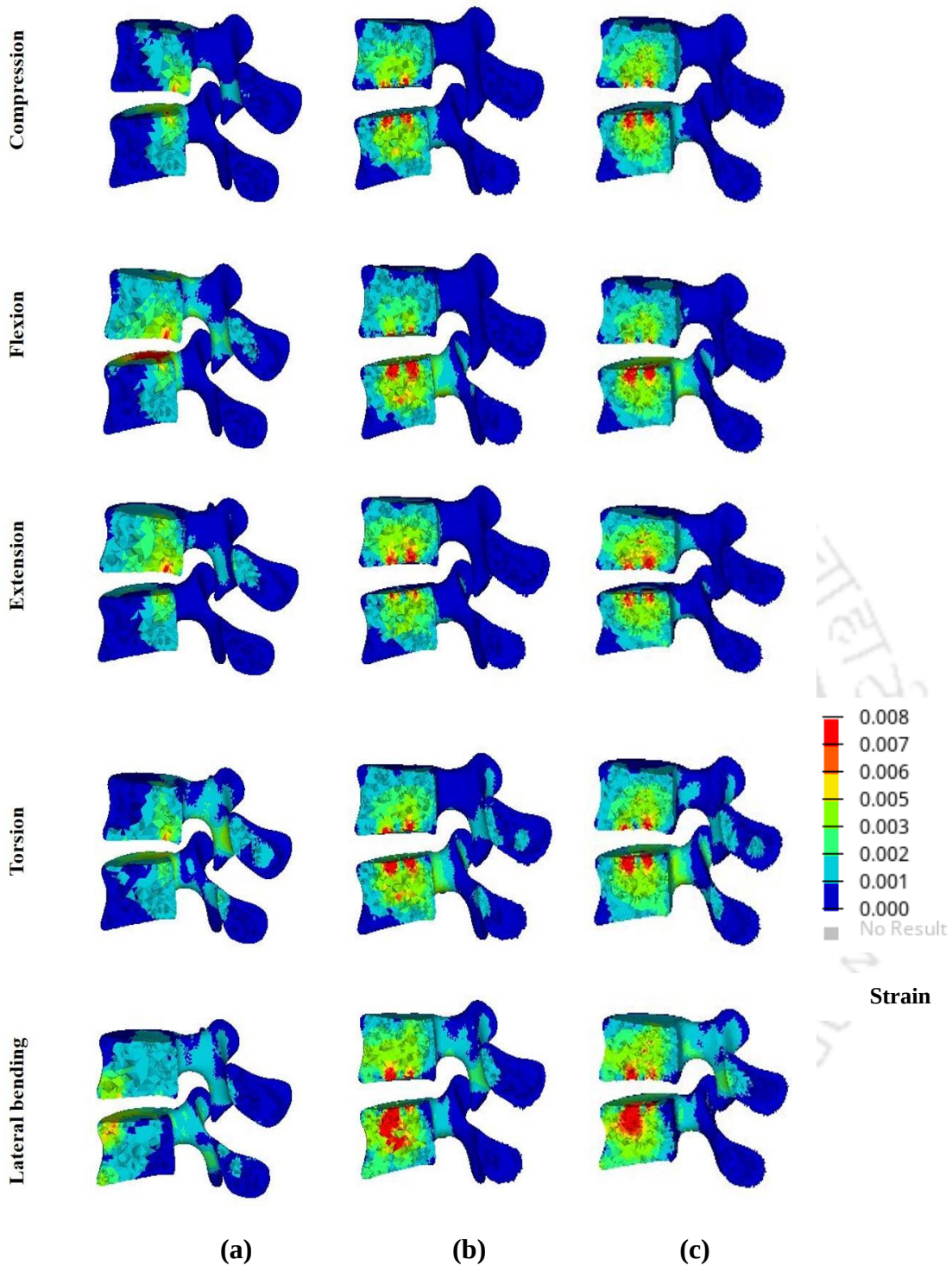


**Fig. 2.11:** Von Mises strain contours in cancellous bone (sectional view) for (a) intact FSU and FSUs corresponding to (b) normal and (c) expandable pedicle screws, respectively.

### 2.3.5 Stress-strain within the intervertebral disc

Fig. 2.12 highlights the impact of implantation on IVD stress-strain behaviour. As shown in Fig. 2.12, the stress-strain response remained similar across models, closely aligning with an earlier study by Biswas *et al.* (2018). However, Biswas *et al.* (2018) reported a maximum stress of 1.86 MPa, compared to 1.53 MPa in our study. This alteration was likely due to differences in loading conditions and material property assumptions. In implanted models, the stress in the IVD decreased (0.9 MPa for normal screws, 0.5 MPa for expandable screws) due to greater load transfer through the cage. Clinically, the reduced stress in the expandable screw model suggests increased stress shielding on the IVD, potentially influencing long-term disc health and adjacent segment degeneration.

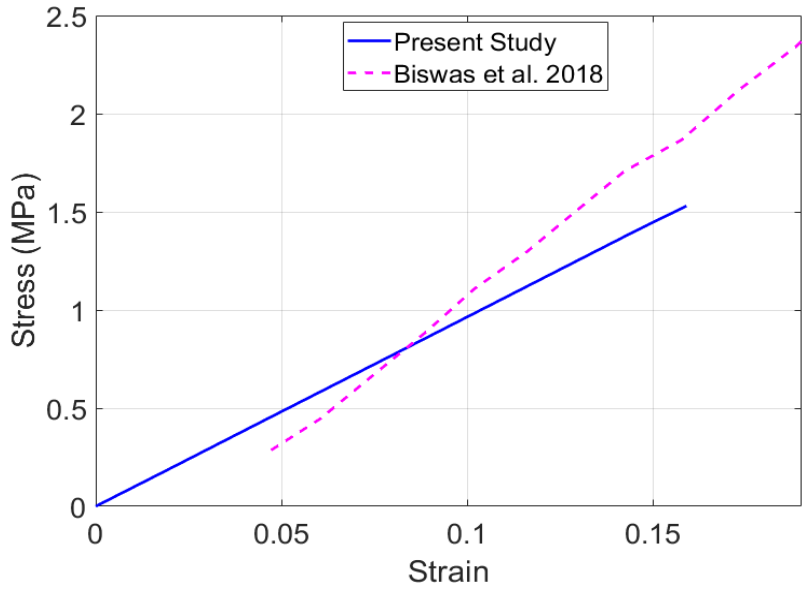


**Fig. 2.12:** Stress-strain diagram for intervertebral disc (IVD) for intact FSU under compression.

## 2.4 Discussion

The present study aimed at carrying out a comparative analysis between normal pedicle screws and expandable pedicle screws about their post-operative performance in lumber vertebrae fixation. The implanted models were preclinically assessed vis-à-vis intact L4-L5 FSU under different physiological movements to gain insights into their biomechanical behaviour. This study is specifically helpful in understanding any deviation in load transfer and stability occurring in the implanted bones regarding the intact condition.

Previous studies suggested that proper loading and boundary conditions play a significant role in biomechanical analysis in lumbar FSU (Talukdar *et al.* 2021). The model was validated considering the ROM under various loading conditions (Xiao *et al*. 2011, Markolf 1972). The loading conditions were obtained from the available literature (Boccaccio *et al*. 2008, Xiao *et al.* 2011, Markolf 1972). Axial compression loading of 500 N was applied vertically downward at the top surface of cortical L4. This type of loading may arise while standing. In all the other four loading conditions, the axial force of 500 N was considered together with the moment of 10 Nm. The magnitude of the moment was kept the same in all four cases of physiological movements though it differed in direction depending on the load case (Fig. 2.4).

The ROM of the intact L4-L5 model was validated with previous studies and found to be in good agreement with earlier reported literature (Talukdar *et al.* 2021, Xiao *et al.* 2011, Yamamoto *et al.* 1989, Zhong *et al.* 2006, Chen *et al*. 2001). Implantation led to a discernible reduction in ROM in most cases (Talukdar *et al*. 2021). The ROM reduction was found to be the highest in the case of flexion extension, and the least in the case of lateral bending. The reductions in ROM were lesser in the case of the expandable pedicle screw model as compared to those for normal pedicle screws. The lesser ROM reduction with expandable pedicle screws suggests greater flexibility, potentially aiding primary stability and reducing stress on surrounding bones, especially in osteoporosis (Gazzeri *et al*. 2020). Balancing stability with controlled motion may lower the risk of screw loosening and improve clinical outcomes (Witek *et al.* 2023). Furthermore, the ROM values for the former were found to be relatively identical to the intact case, suggesting a more anatomic functioning of the implanted FSU.

Different loading and boundary conditions used in FE models were found to have a notable influence on stress variations in lumber vertebrae. Earlier studies with implants (pedicle screw) (Gokhale *et al.* 2008) reported stress concentration in the neck region of the screw for loading conditions, e.g. flexion, extension, lateral bending and torsion. The stress distribution pattern in the case of intact FSU corroborated well with the predictions from Talukdar *et al.* (2021). In contrast, the value of the highest maximum stress in cancellous bone was quite in agreement with Xu *et al.* (2019). However, the peak stress was predicted across different locations, depending on the type of load.

While subjected to torsion, the peak stress was predicted on the posterior side of the L5 vertebra though under lateral bending, it was found on the anterior side (Fig. 2.6a). It can, therefore, be inferred that under lateral bending, stress might be concentrated towards the anterior side of the vertebrae. Under torsion, regions with high-stress concentration were found to be less pronounced in L4 when compared to those under flexion or extension (Figs. 2.6a, 2.7a). This could be because the loading was more concentrated on L5 during torsion. Moreover, the stress concentration was more towards the right side of L4 under flexion but on the left side under extension (Figs. 2.6a, 2.7a). This can be attributed to the direction of loading (moment).

The implantation of normal pedicle screws, expandable pedicle screws and cage resulted in a significant change of stress contours (around 30-100%) for different loading conditions. Marginally greater stress shielding was predicted in the case of the normal pedicle screw as opposed to the expandable pedicle screw under all loading scenarios (Figs. 2.6b,c, 2.7b,c). The peak stress was found to be near the base of the pedicle screw in cortical bone for all load cases. The reason was supposed to be due to high-stress concentration near the pedicle area. Apart from the peak stress region, the overall stress values were below 30 MPa for cases other than compression. It could also be noted that for cancellous bone the stress was higher near the cage insertion area for both normal and expandable pedicle screws (Figs. 2.7b,c, 2.8b,c).

Like stress, the strain distribution patterns for both cortical and cancellous bone were found to be influenced by the application of various loading conditions. The equivalent (von Mises) strain under compression corroborated well with previous literature (Talukdar *et al.* 2021, Morgan *et al.* 2003). The peak strain was the least under compression and the highest under torsion for the intact L4-L5 vertebra (Fig. 2.9a). For the intact model, the peak strain area was predicted towards the posterior side of the L5 vertebra under torsion (Fig. 2.9a). However, the peak strain was found more towards the anterior side under lateral bending (Fig. 2.9a, 2.10a). The peak strain area in the L4 vertebra was more in flexion and extension than torsion (Fig. 2.9a, 2.10a). Following the stress concentration pattern, the strain was high towards the right side under flexion but on the left side of L4 under extension (Figs. 2.9a, 2.10a) due to loading direction.

Under various physiological loading conditions, the instrumentation of both normal and expandable pedicle screws resulted in around 40-100% increase in peak strain field. The peak strain was found near the screw insertion area in cortical bone

(Figs. 2.9b,c) and near the cage insertion area in cancellous bone (Fig. 2.10b,c, 2.11b.c). The peak strain was predicted to be the least under compression and the highest under lateral bending in the implanted bones (Figs. 2.9b,c, 2.10b,c). Nonetheless, the peak strain values in the bone were found to be considerably higher in the case of expandable pedicle screws.

It was estimated that fixation with an expandable pedicle screw provided greater fixation strength in case of compromised bone. The compromised situation arises during osteoporosis or revision surgery, and it was found that during those situations expandable pedicle screws showed improved results in clinical studies (Cook *et al.* 2001). Wu *et al*. (2010) reported no failure/breakage of expandable pedicle screws. It was further concluded that an expandable pedicle screw might have acted as a valued tool for growth in the armamentarium for spinal fixation (Gokhale *et al.* 2008). Vertebra instrumented with expandable pedicle screws for patients with degenerative spinal deformity showed improved results in clinical as well as radiological outcomes with only 2.1% cases of screw pullout on larger stress sites (Qi *et al.* 2011). The authors attributed this to the design of the expandable pedicle screw (Qi *et al.* 2011). Marginally greater area (15-80%) with peak stresses at the bone-screw interfaces, as predicted in our present study, may elevate the risk of such pullout instances in expandable screws. It appears from the stress-strain contours that the expandable pedicle screw may result in a lower loosening rate as compared to a normal pedicle screw. The pullout force of expandable screws is enhanced by increased surface area and better mechanical interlock with the bone due to expansion, distributing stress over a larger volume and improving frictional resistance. However, greater stress concentration predicted at the screw insertion area may also increase the risk of pullout due to interfacial debonding. Studies link pullout force to thread engagement, insertion depth, and stress distribution, all of which influence implant stability (Qi *et al*. 2011, Jendoubi *et al.* 2018).

The stress-strain curve of IVD of the intact model for the present study was closely associated with the values reported in the literature (Biswas *et al.* 2018) (Fig. 2.12). However, the maximum stress in the IVD was reported to be 1.86 MPa by Biswas *et al.* (2018), as opposed to 1.53 MPa in our study. This deviation may be attributed to the difference in loading conditions. Further, Biswas *et al.* (2018) used a stress-strain curve as an input criterion for material properties. The reduced stress in the IVD in the case of implanted models could be due to more load transfer in the cage. The maximum

stress in IVD was found to be the lowest in the case of FSU instrumented with an expandable pedicle screw. This suggests that the expandable pedicle screw exerted more stress shielding on IVD than the normal pedicle screws.

There were, however, certain limitations and assumptions made in the current study. Firstly, cancellous bone was considered as linear, elastic and isotropic though cancellous bone is typically anisotropic (Wolfram *et al*. 2010). Moreover, muscles were not included in this study though muscle plays a significant role in lumbar spine stability (Biswas *et al.* 2019, Zhang *et al.* 2018, Chiang *et al*. 2006). The ligaments were considered to be tension-only elements for static load transfer (Talukdar *et al.* 2021, Zhang *et al.* 2018, Zhong *et al*. 2009). The capsular ligament was not included (Talukdar *et al.* 2021). It may further be noted that the load values may vary significantly depending on the body weight. Though the study provided useful insight into stress-strain comparison among the three models, experimental validation would have provided the accuracy of the prediction. The study did not consider potential cancellous bone damage after expandable pedicle screw insertion and thus over-estimate the bone strength and implant stability.

Although the study has limitations, e.g. simplified bone-implant interactions, it still provides key insights into the performance of expandable screws vis-à-vis normal pedicles thus helping clinicians choose one over another. The model helps compare stress, and strain, with results aligning with existing literature. Future studies with detailed bone properties and experimental validation can further improve on these findings.

### 2.5 Summary of the findings

The study highlighted the biomechanical advantages of the expandable pedicle screws and predicted marginally improved anchorage due to greater contact area with the bones as compared to the normal pedicle screws. The greater contact area with the bone resulted in higher stresses at the bone-screw interface, indicative of better stability and load transfer. Nevertheless, the increased stress might lead to a marginally greater risk of screw pullout. A greater area (15-80 %) with peak stresses at the bone-screw interfaces also indicated reduced stress shielding, which could lower the likelihood of screw loosening over time. The analysis revealed various physiological loading conditions influenced overall load distribution in the L4-L5 vertebrae. However, peak

stresses in cortical and cancellous bone remained within clinically admissible limits, supporting the feasibility of expandable pedicle screws for enhanced spinal fixation.

# Chapter 3

## Bone remodelling comparison between normal pedicle screw and expandable pedicle screw instrumented L4-L5 vertebrae

### 3.1 Introduction

The contemporary medical system has made remarkable advancements, enabling the treatment of diseases like cancer through surgery, radiotherapy, and chemotherapy (Xiong *et al.* 2022). Despite these successes in medical science, effective management of spinal diseases remains a significant challenge. The seriousness of the situation can be inferred from the fact that lower back pain is recognized as the second most indicative reason for individuals to seek medical attention (Atlas and Deyo 2001). Even in the context of significant technical advancements, enhancements in perioperative optimization and medical care, it remains a sobering fact that spinal complications are predominantly linked to functional deterioration, loss of independence, severe pain and even mortality (Xiong *et al.* 2022, Farshad *et al*. 2020, Lange *et al.* 2022). Osteoporosis is the most common skeletal complaint for the ageing population, affecting roughly around 200 million people worldwide. The condition is typically characterised by decreased bone strength, low bone mass, microstructure deterioration of bone mass and increased skeletal fragility (Aghajanloo *et al*. 2023, Gazzeri *et al.* 2020, Homminga *et al.* 2012). Zou *et al.* (2020) estimated ~200 million osteoporotic patients in China alone by the year 2050 while the majority of them are expected to be elderly females.

Clinical decisions are taken by considering the problems associated with the spine treatment, to get maximum benefit from surgery or non-operative care by minimizing potential complications and reducing functional disability. The pedicle screw system fixes the spinal fusion and offers adequate stability (Miyanshita *et al.* 2019). In the clinical and radiographic 10-year follow-up, the pedicle screw fixation showed pain and functional improvement, lesser complication and relatively high patient satisfaction (Glaser *et al.* 2003). However, in the case of osteoporotic patients, maintaining lumbar spine stability with pedicle screws is quite challenging. The chief reason for pedicle screw failure is known to be screw loosening or screw root breakage (Viezens *et al.* 2021, Otsuki *et al*. 2021, Alanay *et al.* 2007). The scenario becomes more serious for

osteoporotic patients as the risk becomes twice that of non-osteoporotic patients and that ultimately might lead to revision surgery (Zou *et al.* 2020). The Norwegian Arthroplasty Register reported that 2% of revision surgeries for lumbar disc replacement were conducted between 2000 and 2020. The primary reason for revision lumbar surgery is pedicle screw loosening, and osteoporosis is the most frequent risk factor associated with the loosening of screws and greater surgical complications (Zou *et al.* 2020, Goldstein *et al.* 2015). To minimise the problems and improve fixation, several techniques like bigger/longer screws, screw fit optimisation and optimal trajectory are used. Alternative methods such as expandable pedicle screws were introduced to provide better anchorage capacity through an increase in screw diameter/length and an improved screw-bone interface (Gazzeri *et al*. 2020).

Wolff's law suggested that loading condition alterations resulted in bone density and architecture change (van Rijsbergen *et al.* 2018). The process of bone apposition (i.e. bone density increase) and resorption (i.e. bone density reduction) is influenced directly by the amount of stress exerted on the bone. To predict implant-based bone remodelling and evaluate implant design, the FEA is combined with an adaptive bone remodelling algorithm (Ghosh *et al*. 2013, Huiskes *et al.* 1987, Weinans *et al*. 1993). According to adaptive bone remodelling theory, bone can adapt to mechanical stimulus where external remodelling alters the outer shape of the body and internal remodelling alters bone density. For internal remodelling, strain energy density (SED) serves as a feedback control variable that governs bone density adaptations to alternate functional requirements. Additionally, SED is assumed to be the initial indication of bone density change owing to bone remodelling. In recent times, the integration of strain-based adaptive bone remodelling theory with FE analysis has attained immense traction to accurately predict peri-prosthetic bone remodelling (Ghosh *et al.* 2013, Huiskes *et al*. 1987, Talukdar *et al.* 2022, Mathai *et al.* 2021a, Chanda *et al*. 2020, Mondal and Ghosh 2021).

The majority of the FE studies concerning clinical issues related to the lumbar vertebra were predominantly focused on immediate post-operative conditions. This gap was addressed using a SED-based bone remodelling algorithm and eventually estimated that change in vertebral structure and alteration in Young's modulus occurred in cancellous bone post-surgery attributed to applied load (Goel *et al.* 1994, Goel *et al*. 1995). The study investigated the influence of fixation screw on cancellous bone, based

on voxel-based FE models of trabecular surface remodelling for long-term fixation (Tsubota *et al.* 2003). In a detailed study on anterior cervical fusion, intact and implanted models having bone graft with or without cages were investigated based on bone remodelling (Espinha *et al.* 2010). A study conducted by Homminga *et al.* (2012) aimed to estimate the influence of disc degeneration based on bone density variation. A large-scale microstructural load adaptive bone remodelling study was conducted for the whole vertebra by rotating the loading directions adapting to new loading conditions (Badilatti *et al.* 2016). Calvo-Echenique *et al.* (2019) conducted a tissue-based bone remodelling study following nucleotomy. An FE study comparing healthy and having lower back pain (LBP) models showed that for LBP models an increase in stress indicates potential stress allocation bias in areas and finally leads to stress shielding (Newell and Driscoll 2021). Favier *et al*. (2021) used a bone remodelling study to check the amount of physical activity to maintain bone health in the lumbar spine. The study by Talukdar *et al.* (2022) focused on bone density variation study owing to the alteration of the porosity of the interbody cage.

It was numerically estimated in Chapter 2 that the use of expandable pedicle screws would be beneficial over normal pedicle screws in terms of reduced loosening, and greater anchorage capacity. In the clinical follow-up study of patients with osteoporosis, it was found that multiaxial expandable pedicle screws would be a safer tool (Gazzeri *et al.* 2016). However, to the author's knowledge, no bone remodelling study was conducted based on expandable pedicle screws. Therefore, the primary objective of the current study was to comprehensively compare and analyse the influence of SED-based bone remodelling between normal and expandable pedicle screw instrumented L4-L5 vertebrae, utilizing a patient-specific dataset.

### 3.2 Materials and Methods

Three-dimensional (3D) FE models of intact and implanted lumbar spine to be precise L4-L5 vertebrae with both normal as well as expandable pedicle screws were developed using computed tomography (CT) data sets. The process of creating intact and implanted vertebrae, FE model generation, assignment of material properties, loading and boundary conditions, contact simulation, and bone remodelling algorithm are described in the following subsections. The intact and implanted L4-L5 vertebras are shown in Figures 3.1a and 3.2a, respectively.

### 3.2.1 Development of 3D FE model of the intact model and implanted models

The CT scan images of a 27-year-old female patient were stored in DICOM format in a resolution of 512×512 pixels. Each pixel had a size of 0.582 mm and each slice thickness was 1.0 mm. To obtain the 3D solid model of the lumbar vertebra, the stored dataset was imported to MIMICS software version 19.1 (Materialise, Leuven, Belgium). The FE models of the L4-L5 vertebra were generated by segmenting the cortical and cancellous bone based on thresholding of the CT grey value ranging from 0 to 1526 Hounsfield Units (HU). A manual threshold CT grey value of 1140 HU corresponding to 1.3 g/cm$^3$ density was applied to separate cancellous and cortical bone. This threshold was considered to address and minimize the partial volume effect (Sanjay *et al.* 2018, Ghosh *et al.* 2014). The cortical bone was modelled by selecting the region starting from the external contour of the segmented vertebra, with an average thickness of 1.0 mm (Zhang *et al.* 2018). Subsequently, IVD consisting of the annulus fibrous and nucleus pulposus were carefully curated. It was estimated that around 43% of the total volume of the intervertebral disc was accounted for by the nucleus pulposus (Kim *et al.* 2010). Further, bony and cartilaginous endplates of 0.5 mm thickness were generated (Talukdar *et al.* 2021). The bony and cartilaginous endplates were generated above and below the annulus fibrosus and nucleus pulposus respectively. The facet cartilage thickness was taken to be 0.5 mm and an initial gap of 0.1 mm between facet cartilage was developed (Talukdar *et al.* 2021).

To investigate bone remodelling, CAD models of the L4-L5 vertebra were generated with normal pedicle screws and expandable pedicle screws respectively. It was achieved by posterior pedicle screw-rod fixation system (Song *et al*. 2021) as shown in Figures 3.2a, 3.2b, and 3.2c. Appropriate insertion of the pedicle screws was essential for the surgeons to minimise the risk of revision surgery (Fisher *et al.* 2022). The pedicle screws were inserted following traditional trajectory by identifying the entry point at the intersection of the transverse process and superior articular facet, guided by anatomical landmarks and imaging. The screws were aligned parallel or slightly convergent to the midline to the axial plane and angled slightly cephalad in the sagittal plane. It was to be taken care that the screw remains within the pedicle without breaching the cortical wall. The IVD and the endplates were virtually reamed performing one-sided facetectomy. The discectomy with unilateral total facetectomy

was performed for cage insertion as shown in figure 3.2e to insert the TLIF cage (ArdisTM, Zimmer Biomet, Warsaw, IN, USA,22x13x 9 mm) (figure 3.2d) in FSU.

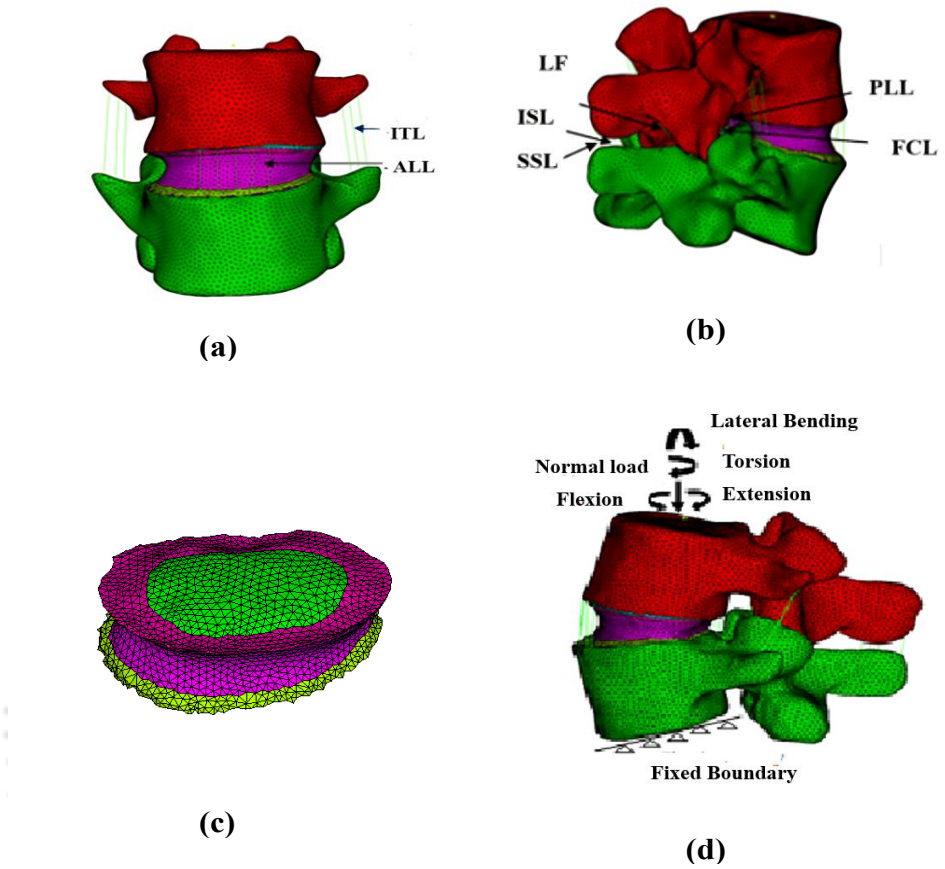


**Fig. 3.1:** The curated models of different parts of an intact L4-L5 FSU -(a) with ligament ALL, ITL (b) with ligament PLL, FCL, LF, ISL, SSL (c) Intervertebral disc (d) Loading and Boundary Condition.

The disc, endplates, left facets, and ligamentum flavum were removed. The TLIF cage was placed at the L4-L5 disc space through a postero-lateral window of the annulus fibrosus and augmented with pedicle screws. The selection of the TLIF cage was based on its advantages over other cages in preventing premature pedicle screw loosening (Ambati *et al*. 2014, Kim *et al.* 2020). The dimension of both types of screws was 50 mm in length, 5 mm in shaft diameter, and 3 mm pitch having triangular threads (with angles $90^0$, $36.7^0$ and $53.3^0$) placed inward in the mid-sagittal plane. Earlier studies suggested improved screw stability by using enlarged screw diameters to fit the pedicle properly (Viezens *et al.* 2021, Otsuki *et al.* 2021). The normal pedicle screw design was derived from the EXPEDIUM 5.5 system (DepuySynthes Spine, Inc, Raynham, MA), while the expandable pedicle screw design was adopted from Tai *et*

*al.* (2015). Following the expansion, the expandable pedicle screw exhibited around 2.0 mm in diameter extension i.e. the newly expanded screw diameter was 7.0 mm (Wu *et al.* 2010). To secure the implants, two rods having 40.0 mm length and 3.0 mm diameter were inserted through screw heads.

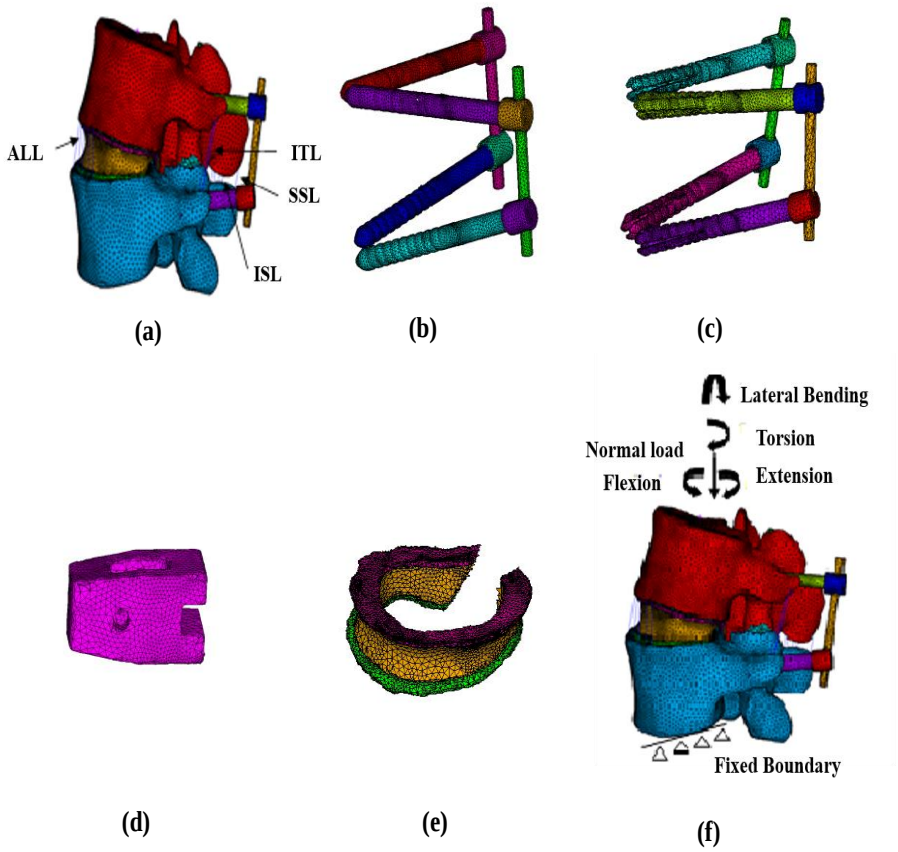


**Fig 3.2:** The curated models of different parts of an implanted L4-L5 FSU-(a) with ligament ALL, ITL, ISL, SSL (b) normal pedicle screw-rod system (c) expandable pedicle screw-rod system (d) cage (e) Intervertebral disc (f) Loading and boundary condition.

### 3.2.2 FE model generation and analysis

Both intact and implanted L4-L5 vertebrae were meshed using HyperMesh 2021.1(Altair Engineering Inc., Troy, Michigan, United States) (Figs 3.1a, 3.2a) and the simulation was carried out in Ansys FE software v 19 (ANSYS Inc., PA, USA). The mesh was generated using 4-noded tetrahedral elements and the average edge length was ~1.0 mm (Figures 3.1, 3.2). To enhance the accuracy, a mesh convergence study of the intact L4-L5 FE model was carried out using varying element sizes. The von Mises stress variation was 5% for the first two models and 2% for the second-third models. Finally, the second model with element size 0.5 mm-1.5 mm was chosen for

further investigation. The intact model comprised 261,425 elements and the implanted models comprised ~7,50,000 elements. In the intact FE model, seven types of ligaments were represented as tension-only node-to-node link elements that mimic soft tissue properties (Talukdar *et al.* 2021). These ligaments were namely anterior longitudinal ligament (ALL), posterior longitudinal ligament (PLL), ligamentum flavum (LF), intertransverse ligament (ITL), interspinous ligament (ISL), facet capsular ligaments (FCL) and supraspinous ligament (SSL), (Figs.3.1a,3.2b). Nevertheless, LF, FCL and PLL were removed following surgical guidelines for the implanted FE models (Figure 3.2a).

### 3.2.3 Material properties

A location-based linear relationship between apparent bone density and CT grey value was used for cancellous bone material properties given by,

$$\rho = 0.022 + 0.001121 \times HU \tag{3.1}$$

In this relationship, the lowest CT value was zero considered as water with a density of 0.022 g/cm$^3$ and the highest CT number 1526 corresponding to be highest cortical bone density 1.73 g/cm$^3$. Cancellous bone was considered as heterogenous, linear, elastic, and isotropic and followed apparent density-elastic modulus power law relation $E = 4730\rho^{1.56}$ (Talukdar *et al.* 2023, Morgan *et al*. 2003). The resulting Young's modulus of cancellous bone varied from 31.1943 to 5521.28 MPa.

**Table 3.1:** Material properties corresponding to various components of the FSU.

| Components | Young's modulus (MPa) | Poisson's ratio | Reference |
|---|---|---|---|
| Cortical bone | 12000 | 0.3 | Talukdar *et al.* 2021 |
| Cancellous bone | Location dependent (from CT scan data) | 0.33 | Talukdar *et al.* 2021 |
| Bony endplates | 12000 | 0.29 | Talukdar *et al*. 2021, Wong *et al.* 2022 |
| Cartilaginous endplates | 23.8 | 0.4 | Xu *et al.* 2016 |
| Nucleus pulposus | 0.1 | 0.49 | Li *et al.* 2014 |
| Annulus fibrosus | 9 | 0.4 | Li *et al.* 2014 |
| Cage | 110000 | 0.3 | Su *et al*. 2021 |
| Pedicle screw | 110000 | 0.3 | Wong *et al.* 2022 |
| Ti Rod | 110000 | 0.3 | Wong *et al*. 2022 |

Cortical bone and endplates were anticipated to be homogenous, linear, elastic and isotropic (Alanay *et al.* 2007, Talukdar *et al.* 2021). The nucleus pulposus was assumed to be an incompressible fluid with a low elastic modulus (Huang *et al.* 2022b). All the implants were considered to be made of Titanium alloy. The material properties are described in tabular form in Table 3.1. The ligament properties used for the study are adopted from earlier literature by Talukdar *et al*. (2021), given in Table 3.2.

**Table 3.2:** Ligament properties taken from Talukdar *et al*. 2021.

| Ligaments | Young's modulus (MPa) | Poisson's ratio | Cross-sectional area ($mm^2$) |
|---|---|---|---|
| Anterior longitudinal | 20 | 0.4 | 63.7 |
| Posterior longitudinal | 20 | 0.4 | 20 |
| Flavum | 19.5 | 0.4 | 40 |
| Intertransverse | 58.7 | 0.4 | 3.6 |
| Interspinous | 11.6 | 0.4 | 40 |
| Supraspinous | 15 | 0.4 | 30 |
| Capsular | 32.9 | 0.4 | 60 |

### 3.2.4 Applied Loading and Boundary Conditions

The applied loading condition for the current study included four physiological load cases flexion, extension, lateral bending and torsion. For both the intact and the implanted FSUs, the nodes situated at the superior surface of L4 were designated as slave nodes and a master node was created on the superior surface of the L4 vertebra. The slave nodes and the master node were rigidly coupled to have similar deformation (Talukdar *et al.* 2023). The rotational degree of freedom was offered to the master node by assigning a massless element MASS21 to it. A follower load technique was used creating point element FOLLOW21 with master node to apply force and moment. The follower load technique realistically simulates in vivo spinal loading by aligning the load vector with the spine's natural curvature, minimizing unnatural forces and preserving stability. This method enhanced the accuracy of SED and bone remodelling predictions, providing a reliable evaluation of pedicle screw performance under physiological conditions (Rohlmann *et al.* 2009, Kim *et al.* 2007). The loading condition was achieved in two subsequent steps, where first, a compressive axial load of 300 N was applied and thereafter 7.5 Nm moment was applied on the master node to simulate various movements (Huang *et al.* 2022b). The nodes located on the inferior

surface of L5 were constrained for all degrees of freedom (Talukdar *et al.* 2022, Huang *et al*. 2022b). (Figs. 3.1d,3.2f).

### 3.2.5 Contact simulation

3D non-linear surface-to-surface contact element was chosen at articulating facet joints for contact simulation. The interface between the cartilages was modelled as Coulomb friction with a friction coefficient of 0.2 (Zhou *et al*. 2020). The contact simulation utilized for the study was the Augmented Lagrange contact algorithm. To converge the non-linear solution, a penalty stiffness of 1 N/mm and penetration tolerance factor of 0.25 were chosen between the facet cartilages. In the cases of intact and implanted bones, bonded contact was considered for all other components (Sanjay *et al.* 2021).

### 3.2.6 Bone remodelling algorithm

The adaptive bone remodelling theory was based on strain energy density and was inspired by earlier works (Huiskes *et al.* 1987, Huiskes and Rietbergan 1995). A site-specific formulation was used (Huiskes and Rietbergan 1995, van Rietbergen *et al.* 1993, Carter *et al.* 1982) for the study. For both intact and implanted FSU, the local (per element) elastic strain energy ($S$) per unit of bone mass averaged over a loading history served as the reference and actual stimulus. To allow some variations into account, an average strain energy density, $U_a$, for some loading cases was used to calculate the remodelling stimulus given by the following

$$S = \frac{1}{n}\sum_{i=1}^{n}\frac{U_i}{\rho} = \frac{U_a}{\rho} \tag{3.2}$$

The dead zone ($s$) was quantified as $\pm 0.75$ of the reference stimulus (Talukdar *et al.* 2022, Huiskes *et al.* 1992, Pal *et al.* 2010, Ghosh and Gupta 2014, Mondal and Ghosh 2019b). The iterative method of computing the bone density changes due to prosthesis implantation was continued until a new equilibrium density pattern was achieved. The specific mathematical expression for the alteration of apparent density was defined as

$$\rho = \begin{cases} a(\rho)\{S - (1 \pm s)S_{ref}\}\tau\Delta & \text{if } S \le (1-s)S_{ref} \text{ or } S \ge (1+s)S_{ref} \\ 0 & \text{if } S_{ref}(1-s) < S < S_{ref}(1+s) \end{cases} \tag{3.3}$$

Where $a(\rho)$ represents free surface area per unit volume for bone ($mm^2/mm^3$) in internal bone structure. In his study, Martin established that bone apposition and resorption can occur at free bone surfaces (Martin 1972). The internal free surface per unit volume for bone was assessed as a function of bone apparent density is given by

(Martin 1991).

$$a(\rho) = -0.0293 + 8.5124\rho - 4.887\rho^2 - 1.568\rho^3 + 3.7182\rho^4 - 1.6352\rho^5 \quad (3.4)$$

The intact FSU served as a reference for the remodelling stimulus of each bone element. This was compared with the remodelling stimulus of the bone element at an analogous position in the implanted FSU. The iterative bone remodelling algorithm was based on earlier investigations (Talukdar *et al.* 2022, Pal *et al.* 2014, Ghosh and Gupta 2014). The integration in steps of 'simulation time scale' $\boldsymbol{\tau}\Delta t$ was executed likewise in previous literature (Talukdar *et al*. 2022, Suarez *et al.* 2012). For the calculation of $\Delta t$, the adaptive rate ($\boldsymbol{\tau}$) was taken as 129.6 g/mm$^2$ (J/g) (Huiskes *et al.* 1987, Ghosh and Gupta 2014). The upper and lower bounds of bone density were considered 1.73 and 0.01 g/cm$^3$ respectively (Huiskes *et al.* 1992, Ghosh and Gupta 2014). The remodelling algorithm continued until the bone density alteration did not exceed more than 0.005 g/cm$^3$ per element and per time increment ($\boldsymbol{\tau}\Delta t$).

For simplification and improved understanding of bone remodelling patterns, both L4 and L5 vertebrae were bisected in the transverse plane and the inferior half was studied. Similarly, the L4-L5 vertebra was bisected along the sagittal plane, and one-half of the vertebra was selected for further analysis. Subregional analyses were performed by dividing the selected region into specific areas of interest, particularly focusing on regions near the cage and screw implantation sites. The remodelling stimulus and density changes in these regions of interest were evaluated to identify localized effects of implant design and loading conditions. This approach allowed for a detailed analysis of bone remodelling behaviour maintaining computational efficiency.

## 3.3 Result

### 3.3.1 Verification and Validation of FE model

The verification of a numerical model is associated with the accuracy along with the efficiency of the model to solve the governing equation by convergence with variation of resolution of the discrete model (Eremina *et al.* 2022). Generally, optimum discrete representation has less than 5% difference. Thus, by mesh convergence study, comparing von Mises stress of L4-L5 vertebra of the intact model with different element sizes, the element size 0.5 mm-1.5 mm was chosen for the investigation.

One-to-one direct experimental validation of living objects was not feasible since the CT scan dataset belongs to a living object, so, the FE model validation was

performed indirectly (Talukdar *et al*. 2021). To achieve that, the ROM of the intact FSU model was subjected to applied loading and the ROM values were compared with earlier literature. The value of ROM of the L4-L5 vertebra was measured as: $8.82^0$ for flexion, $6.36^0$ for extension, $3.7^0$ for torsion and $5.9^0$ for lateral bending respectively. Fig. 3.3 showed the predicted ROM values compared with previous studies for different physiological movements and it was observed that individual ROMs were in the range of earlier literature, followed the same trend and thus validated the model. The ROM of the vertebrae decreases with age, continuous repeated movement of the spine, and injury (Norris 1995). A study conducted on 204 individual FSUs showed the ROM tended to increase down the vertebra and was higher for female spine segments (Cook *et al*. 2015).

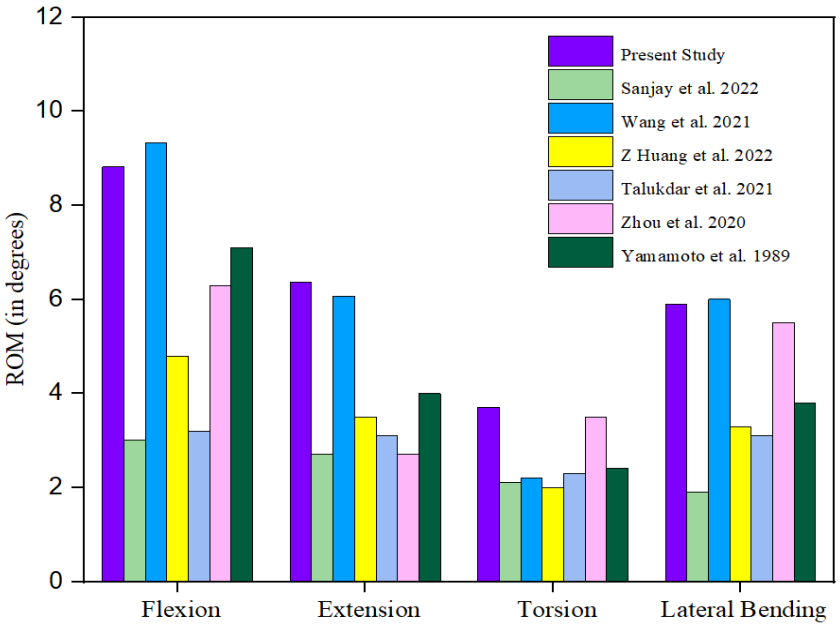


**Fig. 3.3:** Comparison of ROM values of the current intact FE model with those obtained from earlier literature: Flexion, Extension, Torsion, and Lateral bending.

The ROM of the intact model was considered as 100% (Jain and Khan 2022), and thus by considering the intact bone as a reference, the ROM of the implanted models were compared. Implantation resulted in a reduction in ROM for various movements. Earlier experimental studies on cadaveric specimens using L4-L5 vertebra showed implantation reduced ROM for all loading conditions (Montanari *et al*. 2024). It was predicted that 83%, 90%, 80%, and 77% reduction for flexion, extension, torsion, and lateral bending occurred after the implantation of the normal pedicle screws respectively. However, after the implementation of expandable pedicle screws, the predicted reduction in the same order were 75%, 78%, 70%, and 66% respectively.

### 3.3.2 Strain (von Mises) for cancellous bone

The equivalent strain (von Mises) contour for the cancellous bone under various physiological movements is shown in Fig. 3.4. In the case of intact bone, the peak strain was ~0.0025 for cancellous bone under lateral bending. The peak strain was found in lateral bending near the posterior side in the intact FSU. The implantation of screws and cages in the FSU resulted in an increase in peak strain area mostly near the screw and cage insertion area. The highest peak strain achieved after implantation was near ~0.01. The peak strain was predicted to be distributed over a relatively greater area when subjected to torsional load after implantation. It was observed from Fig. 3.4 that the peak strain was estimated to be greater in the case of L5 vertebra than L4 vertebra for intact and implanted FSU. In models with expandable pedicle screws, the peak von Mises strain area near the cage and screw insertion area was considerably higher than that of normal pedicle screws for all loading cases.

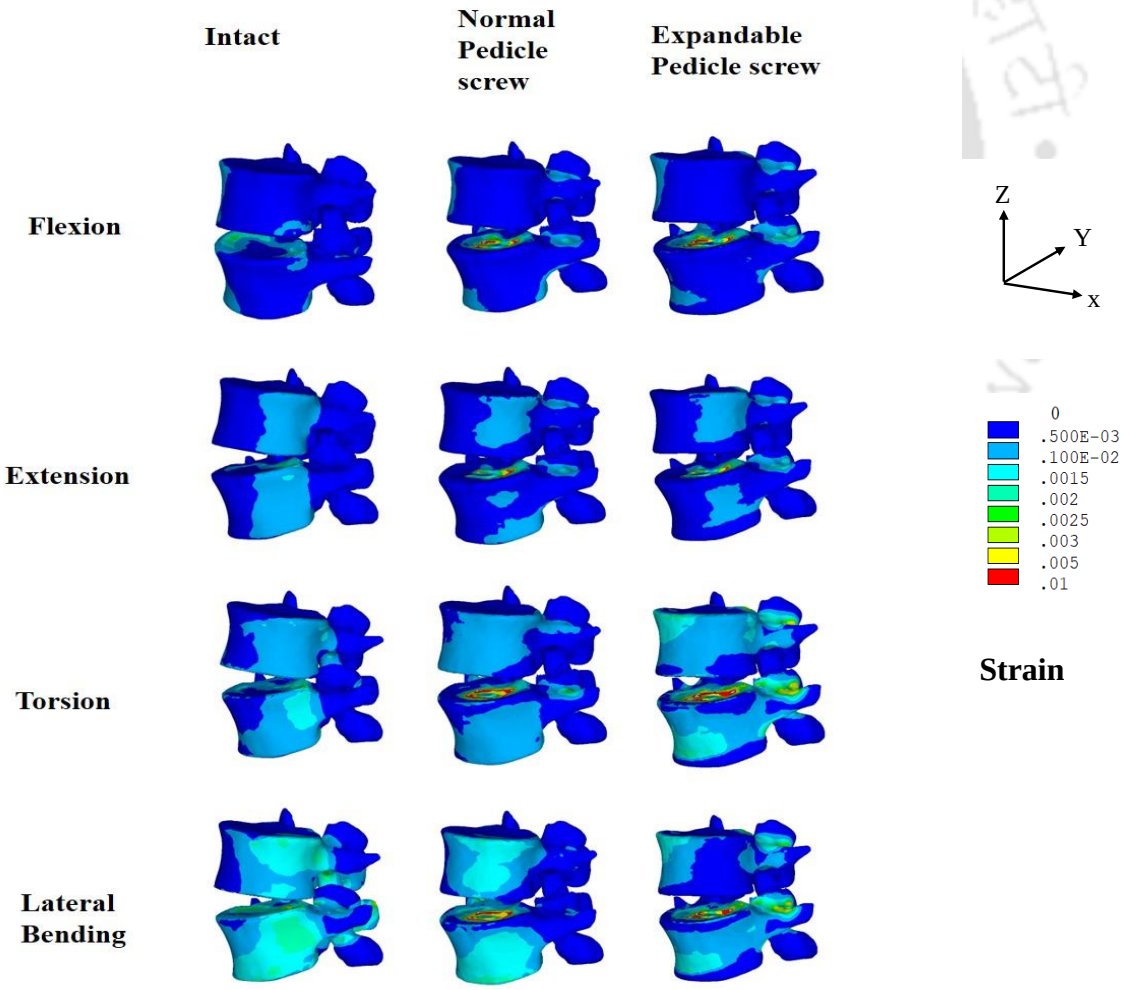


**Fig. 3.4:** Von Misses strain contours in cancellous bone for (a) intact FSU and FSUs corresponding to (b) normal and (c) expandable pedicle screw, respectively.

### 3.3.3 Strain energy density (SED) distribution for cancellous bone

The current study chose the SED plot to predict bone density variations. The L4-L5 vertebra was bisected equally in the sagittal plane and one-half was considered for further study (Fig. 3.5). In the case of intact bone, the least SED area was observed in extension and the highest SED area was seen in lateral bending with a peak value of 0.01 J/g. Implantation of normal pedicle screw resulted in a significant increase of SED for all the movements. An increase of SED of 40-85% was observed for a large area near the cage on L5 for lateral bending. The SED increment for L5 was more than that of L4 for normal pedicle screws. When the L4-L5 vertebra was implanted with expandable pedicle screws, the increase of SED was highest (30-75%) in the case of flexion near the cage area in L5. The SED increase was comparatively greater in the L5 than L4 vertebra for all the cases except lateral bending. In lateral bending, 10-20% SED reduction was seen in L5 vertebra.

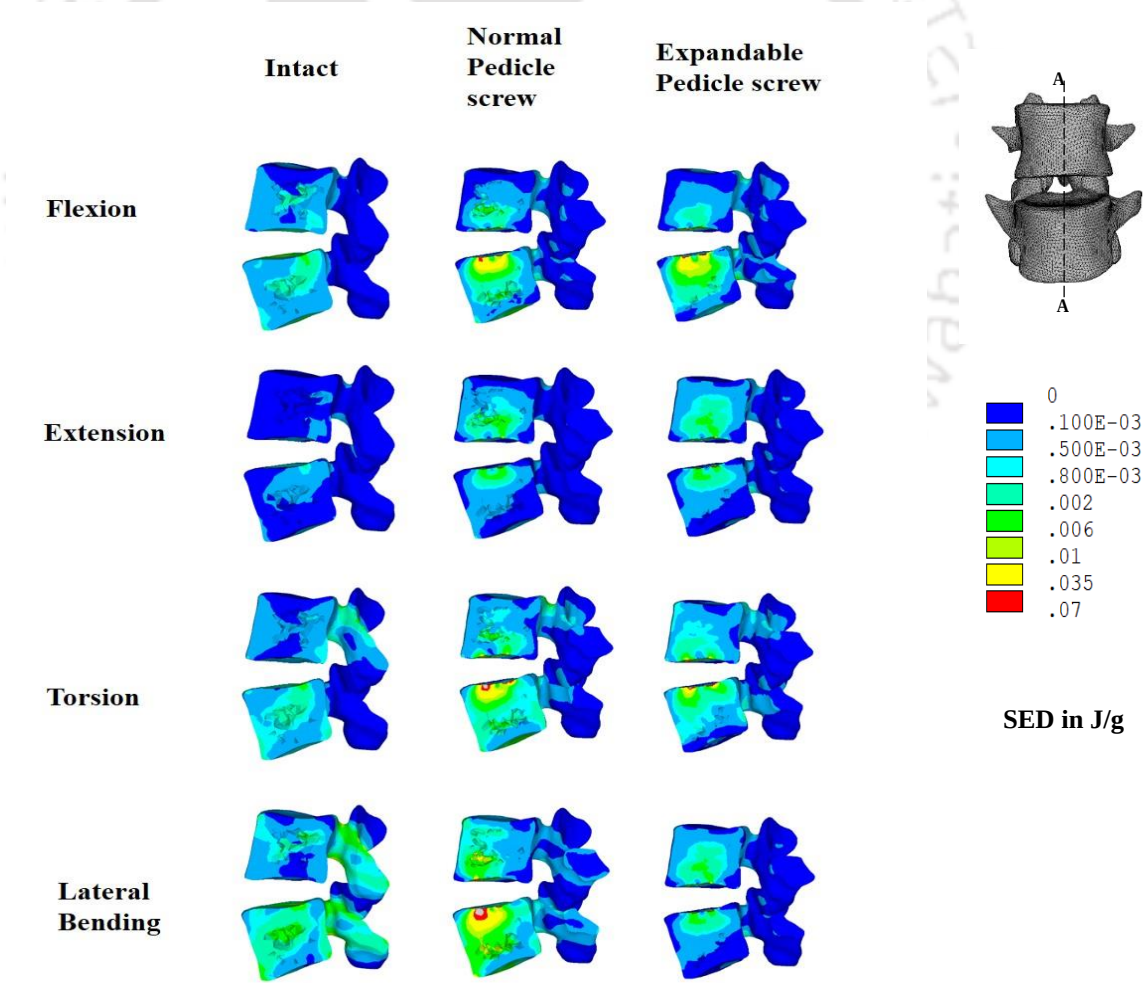


**Fig. 3.5:** Strain Energy Density distribution (J/g) for cancellous bone in (a) intact FSU and FSUs corresponding to (b) normal and (c) expandable pedicle screw, respectively.

### 3.3.4 Bone remodelling for cancellous bone

Both normal and expandable pedicle screws were inserted in the L4-L5 vertebra and after implantation, the alterations in the distribution of bone density following the achievement of equilibrium in bone remodelling are studied here. Two regions of interest (ROI) in the inferior ends of both the L4 and L5 vertebra for both types of implantations are shown in Fig. 3.6. The bone remodelling algorithm was calculated by taking the average of all four loading conditions. For convenience, the study used the reference to the flexion condition.

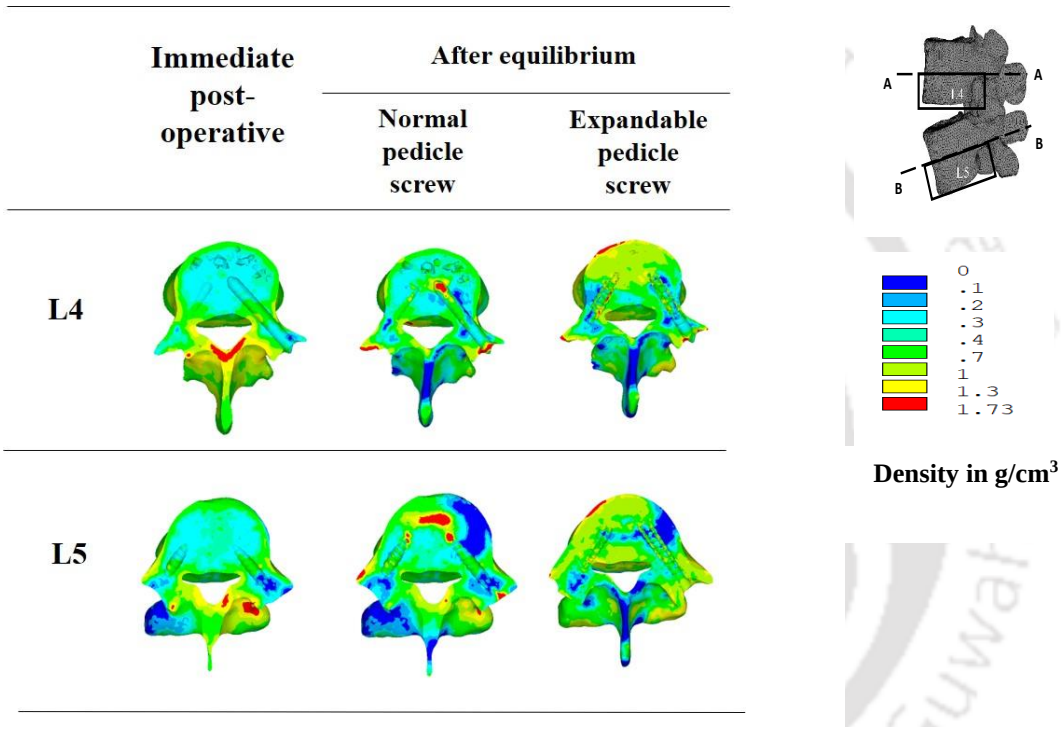


**Fig. 3.6:** Bone density distribution (g/cm$^3$) for cancellous bone (L4-L5 vertebra separately) in implanted FSUs corresponding to (a) normal pedicle screw and (b)expandable pedicle screw, respectively.

In the case of the L4 vertebra, post equilibrium, implantation of the normal pedicle screw resulted in 60-80% bone apposition near the screw tip and screw insertion area but the bone apposition area was comparatively less (Fig. 3.6). Around 10-45% bone resorption was there near the screw length area, middle-posterior region of screw length and posterior side of the cancellous bone. For the expandable pedicle screw, 50-75% bone apposition occurred in the central to anterior region and screw insertion area. Some increase in bone density along the screw length was visible, but bone resorption was present near the screw area and posterior cancellous bone.

For the L5 vertebra, normal screw implantation resulted in a 30-90% bone density increase in the screw tip, central-anterior left region and screw insertion area after attaining equilibrium. Bone resorption of 25-60% occurred in the central-anterior right region of the cancellous bone and central-posterior screw length area. Around 10-20% bone resorption was observed in posterior cancellous bone. In the case of expandable pedicle screw implantation, post equilibrium, around 40-75% bone density increase was evident in the central-left anterior region of cancellous bone and screw insertion area. Bone density of 20-50% was reduced in the central-right anterior region and posterior area of cancellous bone.

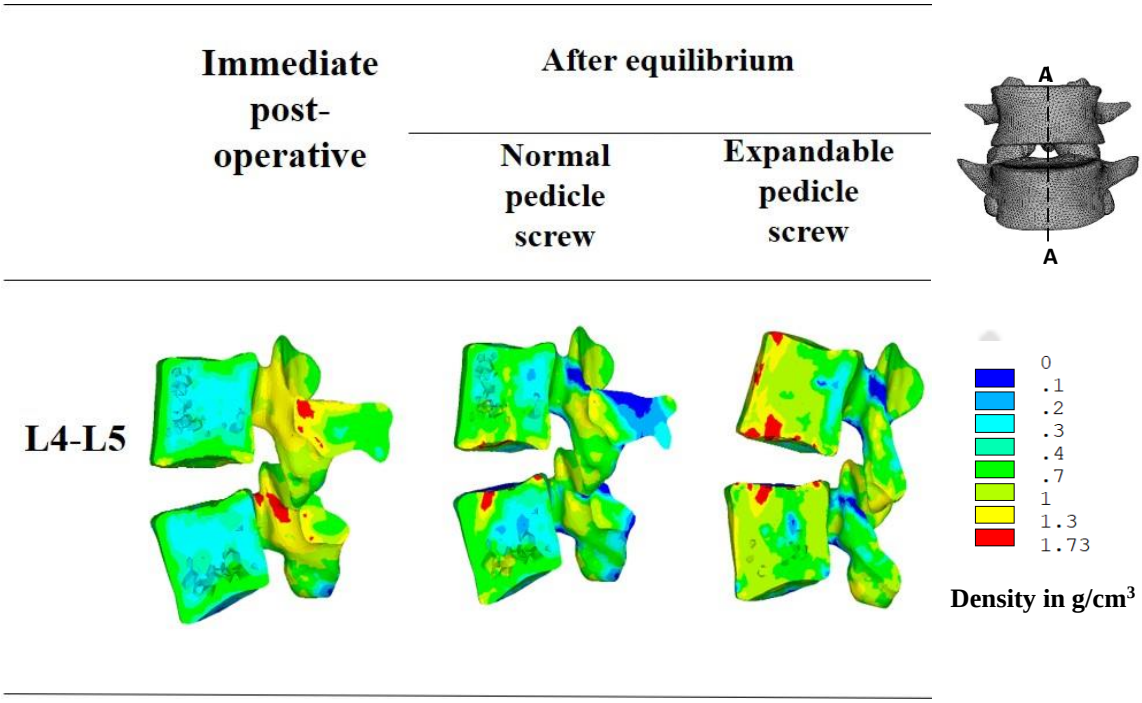


**Fig. 3.7:** Bone density distribution (g/cm$^3$) for cancellous bone (sectional view) in sectional view in AA plane in implanted FSUs corresponding to normal pedicle screw and expandable pedicle screw, respectively.

A sectional view of the L4-L5 vertebra with both the implanted screws with post-implantation as well as after bone remodelling was depicted in Fig. 3.7 for better understanding. In the area of the normal pedicle screw, an increase in bone density was observed in the anterior region of the cancellous bone with a 35-50% increase near the cage insertion area. Bone resorption was seen in the posterior region after remodelling. An increase in bone density post-equilibrium was observed near the cage insertion area. 40-60% bone density reduction mostly in the mid-inferior side of the L5 vertebra as

well as a slight decrease in the posterior region was seen after remodelling. In the case of the expandable pedicle screw implanted model, a 70-90% bone density increase was observed in the anterior-central region of L4 specifically near the cage area 5-15% bone resorption was observed in the posterior side of the L4 vertebra. In the case of the L5 vertebra, post-attainment of equilibrium with an expandable pedicle screw resulted in 60-85% bone apposition in anterior, posterior area, cage insertion area and minute bone resorption near central region. It was evident from the figure that the bone density post-implantation was found to be more in expandable pedicle screws (Fig. 3.7).

### 3.4 Discussion

This study was conducted to estimate the bone density variation and compare the normal pedicle screws and the expandable pedicle screws post-implantation/attainment of equilibrium on lumbar vertebra L4-L5. Initially, from the CT scan dataset, detailed 3D models of L4-L5 intact vertebrae, and implanted L4-L5 vertebrae with normal and expandable pedicle screws were created. Thereafter, those models were studied for four physiological loading conditions to understand their biomechanical behaviour under various loading conditions. SED was plotted to get an initial indication of bone remodelling as SED in intact and implanted bone is considered a reference stimulus for bone remodelling (Sanjay *et al*. 2018, Ghosh and Gupta 2014). To study the long-term bone remodelling pattern for both types of pedicle screws, the L4-L5 vertebra was divided into eight regions of interest. This study was precisely helpful to estimate the bone remodelling in cancellous bone with normal pedicle screw and expandable pedicle screw and compare between the two types with the help of previous computational as well as clinical studies.

**Table 3.3:** Average Bone Density in g/cm$^3$ of L4 vertebra and L5 vertebra: Immediate post-operative and after equilibrium condition.

| Region of Interest | Immediate post-operative | After Equilibrium | |
|---|---|---|---|
| | | Normal Pedicle Screw | Expandable Pedicle Screw |
| L4 vertebra | 0.6198 | 0.6297(+1.59%) | 0.7194(+16.07%) |
| L5 vertebra | 0.5302 | 0.5498 (+3.7%) | 0.6807(+28.38%) |

Differences in geometries would lead to variations in peri-prosthetic strain distribution and bone remodelling around implanted cancellous bone. More strain shielding would result in bone density loss suggesting potential failure that might lead to failure of the implant. A decrease in bone density post-implantation suggested that more load was transferred through the cortical bone than the cancellous bone (Ghosh *et al.* 2013, Saviour *et al.* 2023). Nonetheless, the localised increase in bone density adjacent to the fusion site was attributed to load transfer occurring at the fusion site (Van Rijsbergen *et al.* 2018, Talukdar *et al.* 2022). In the current FE investigation, an axial compressive load of 300 N along with 7.5 Nm moment were applied to the master node of the L4 vertebra. Four physiological loading conditions were achieved by varying the moment application direction (Figs. 3.1d,3.2f).

The trend and the numerical value of variation of ROM of the intact models went along with the findings of earlier literature (Huang *et al.* 2022b, Zhou *et al.* 2020, Wang *et al.* 2021). Implantation resulted in ~70-90% reduction of ROM for both models across all the loading cases. The highest and least reduction of ROM was achieved for extension and lateral bending respectively for both types of screws. As established in the previous study by Sanjay *et al*. (2022) the reduction of ROM of expandable pedicle screw implanted models was lesser than that of normal pedicle screw implanted models.

**Table 3.4:** Average Bone Density in g/cm$^3$ for L4-L5 vertebra in ROI 1-8: Immediate post-operative and after equilibrium condition.

| | **Immediate post-operative** | **After Equilibrium** | |
|---|---|---|---|
| **Region of Interest** | | **Normal Pedicle Screw** | **Expandable Pedicle Screw** |
| ROI1 | 0.5010 | 0.5695 (+13.6%) | 0.6989(+39.5%) |
| ROI2 | 0.5802 | 0.5601 (-3.46%) | 0.6297(+8.53%) |
| ROI3 | 0.6000 | 0.7190(+19.83%) | 0.8088(+34.8%) |
| ROI4 | 0.6150 | 0.6695(+8.86%) | 0.7589(+23.39%) |
| ROI5 | 0.4800 | 0.6288(+31%) | 0.7186(+49.7%) |
| ROI6 | 0.5020 | 0.5794(+15.4%) | 0.6443(+28.34%) |
| ROI7 | 0.5198 | 0.6192(+19.12%) | 0.6890(+32.55%) |
| ROI8 | 0.5150 | 0.5030(-2.33%) | 0.6691(+29.92%) |

It was observed that the implantation of a screw-rod system along with a TLIF cage significantly showed a variation in the strain contour during different loading conditions (Talukdar *et al.* 2021, Polokeit *et al.* 2003). The von Mises strain values were in accord with previous studies (Talukdar *et al*. 2022, Cristofolini *et al.* 2013). The strain concentration in cancellous bone increased significantly underneath the cages post-implantation (Polokeit *et al.* 2003). The peak strain for all the models was higher in the L5 vertebra than in the L4 vertebra (Talukdar *et al.* 2022, Talukdar *et al.* 2021). However, the peak strain area varied with the application of load direction for intact and implanted cases (Fig. 3.4). The peak strain was found to be greatest in torsional loading cases with expandable pedicle screw instrumentation. SED acts as a stimulus for bone density variation (Huiskes *et al.* 1987, Jang *et al.* 2009). A decrease in SED post-implantation indicated bone density loss in that area after bone remodelling (Sanjay *et al.* 2018). It was estimated that cage implantation would result in bone apposition after equilibrium (Fig. 3.5).

The implantation of both types of screws along with the cages led to the bone remodelling in the cancellous bone. It was estimated that after equilibrium, bone was densified near the cage insertion area, screw tip and screw insertion area (Figs. 3.6, 3.7). The implantation of both types of pedicle screws resulted in increased bone density, and as a result, the adverse effect of strain shielding was prevented (Talukdar *et al.* 2022). It was observed that the average density increase in the L5 vertebra was found to be more than the L4 vertebra after equilibrium (Table 3.3). The study clearly showed that implantation of expandable pedicle screws (~16%-28%) along with the cage resulted in more bone apposition than the case of normal pedicle screws (~1.5%-4%) with cage implantation. The average bone density variation with time for normal pedicle screw and expandable pedicle screw for the lower halves of the L4 vertebra and L5 vertebra were shown in Fig. 3.8. For both vertebrae, the slope of expandable pedicle screws implanted models was steeper than the normal pedicle screws implanted models indicating bone apposition with different numerical values. Considering both types of screws the L4-L5 cancellous bone was divided into eight ROIs (ROI 1- ROI 8) to analyse the bone remodelling in a detailed manner (Fig. 3.9). ROI 1-ROI 4 were used to demonstrate the L4 vertebra and ROI 5-ROI 8 was to describe the L5 vertebra. Bone apposition was seen for both types of screws for all the ROIs except ROI 2 and ROI 8. In ROI 2 and ROI 8, in the case of a normal pedicle screw some bone resorption was seen (Figs. 3.9b, 3.9h). It was observed that bone density in L4 was more than L5 in

immediate post-operative conditions. However, the increase in bone density after bone remodelling was greater in the L5 vertebra than in the L4 vertebra (Table 3.3, Table 3.4). In rest ROIs, a ~9-30% increase in bone density was found after remodelling when implanted with normal pedicle screws. However, an increase of ~8-50% in bone density was observed for all the ROIs with expandable pedicle screws (Fig. 3.9). The bone density increases for both cases was more around the cage. This was justified by an earlier numerical study where bone apposition was seen in endplates, area above and below the bony bridge after remodelling (Calvo-Echineque *et al.* 2019). The study by Talukdar *et al.* (2022) showed an increase of 9-14% in bone density in the L4-L5 vertebra and our study was in good agreement with the results in the case of normal pedicle screw implantation.

The interaction between expandable pedicle screws and cancellous bone is supposed to increase the screw-bone fixation strength by allowing more contact area (Cook *et al.* 2001, Wan *et al*. 2010). Earlier studies suggested that the pedicle screw fixation strength was highly correlated with bone mineral density (Reinhold *et al*. 2006, Chen *et al.* 2014). Clinically, it was established that bone density decreases as the distance from the fusion site increases indicating localised bone remodelling (Singh *et al*. 2005). The study by Chen *et al.* (2014) suggested bone density increased around the fins of expandable pedicle screws and it was established in the current study. The cancellous bone that surrounded the expanded portion of the expandable pedicle screw was compressed to some extent post-expansion and thus became denser (Wan *et al.* 2010). In the animal study by Wan *et al*. (2010), they established that newly formed bone tissues grew in the fins of expandable pedicle screws indicating greater screw-bone contact and improved pullout strength. Bone mass change during bone remodelling could be achieved by varying geometry, and expanded fins regulate bone remodelling by increasing bone density. The conventional pedicle screws generate higher localized SED values, the expandable screws create a more effective remodelling stimulus by engaging a larger bone volume and redistributing the mechanical loads during the remodelling phase. This explains the greater observed density changes for expandable screws, despite lower peak SED values

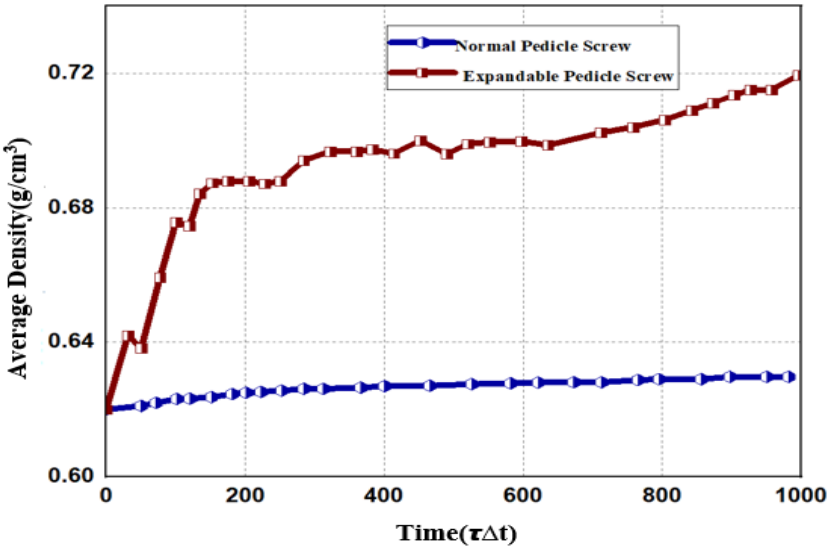


(a)

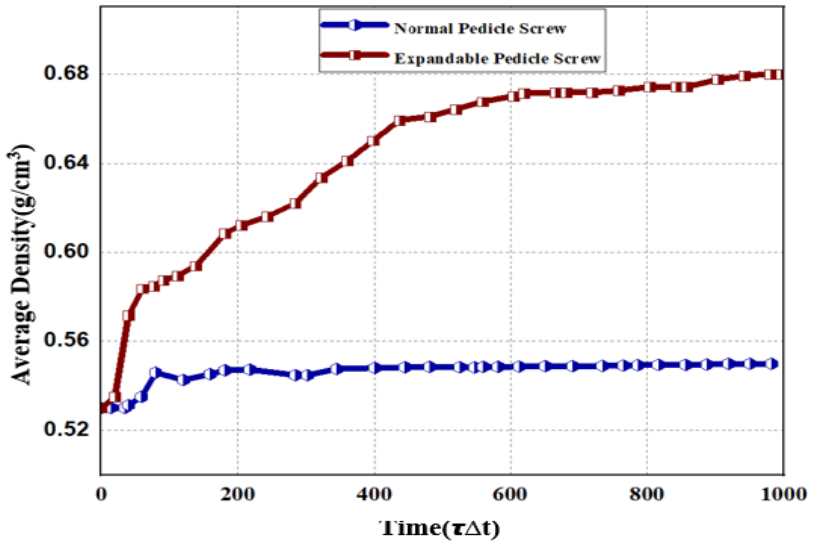


(b)

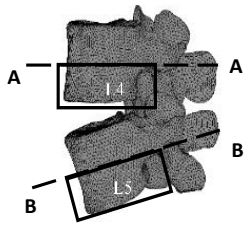


**Fig. 3.8:** Average bone density variation with time increments for cancellous bone ROI of (a) L4 vertebra, (b) L5 vertebra after implantation.

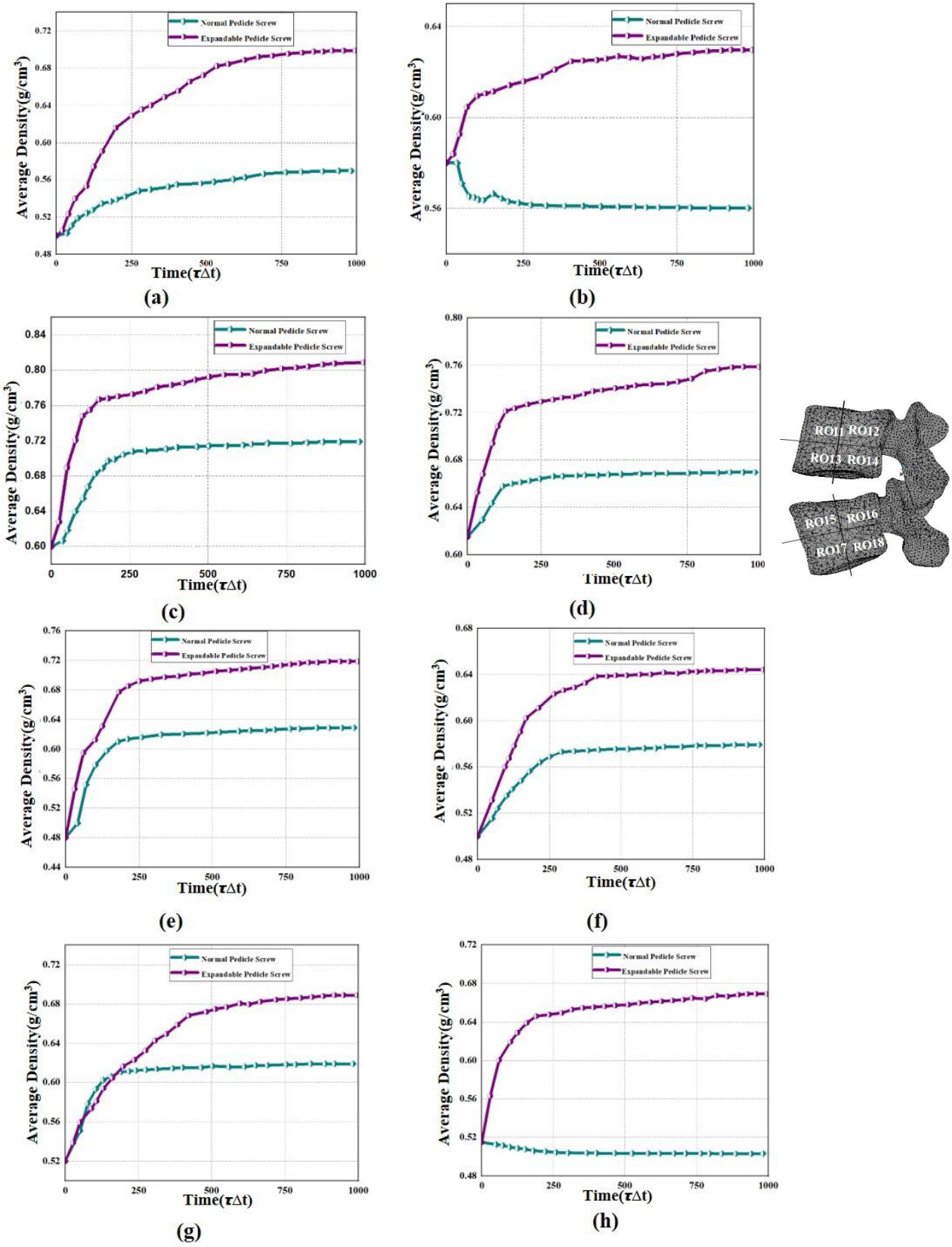


**Fig. 3.9:** Average bone density variation with time increments for cancellous bone for L4-L5 vertebra in (a)ROI1, (b)ROI2, (c)ROI3, (d)ROI4, (e)ROI5, (f)ROI6, (g)ROI7, (h)ROI8.

Thus, by following Wolff's law, the mechanical stability of expanded pedicle screws was maintained lowering the risk of loosening (Wan *et al.* 2010, Jovanoic *et al.* 2004). In the clinical study by Wu *et al.* (2010), it was observed, six months post-surgery with cemented expandable pedicle screws, spinal fusion was achieved without screw loosening. Earlier studies suggested the use of expandable pedicle screws as an alternative to normal and cannulated pedicle screws due to their good performance owing to higher pullout value after fusion (Aycan *et al.* 2017). Gazzeri *et al.* (2020) ensured in their clinical study the advantages of expandable pedicle screws for the elderly population with osteoporosis. In earlier clinical studies, there was a report of adjacent disc degeneration with an increase in bone density due to variation in loading condition at the disc because of increased stiffness (van Rijsbergen *et al.* 2018, Pye *et al.* 2006). The bone density decreases in the trabecular core and increases in the vertebral wall due to degenerated discs resulting from load shifting (Homminga *et al.* 2012). In the large-scale microstructural load-based adaptive loading study, the rotation of axial load results in bone density resorption and adaptation to a new structure (Badilatti *et al.* 2016). However, to maintain good bone health, it is essential to pursue a demanding physical activity as moderate-intensity activities alone tend to cause bone degradation at all lumbar levels (Favier *et al.* 2021). Based on a review article by Maimoun *et al.* (2011) it was concluded that bone loss following spinal cord injury initiates after injury and reaches its peak within 1 to 4 months. Subsequently, after 6 months, the bone loss decreases gradually. Interestingly, the review suggested that the intensity of bone loss is not correlated with the level of injury and health-related complications.

Some limitations and assumptions made in the current study, nonetheless, are listed below. Firstly, the cancellous bone isotropic nature was justified by previous literature (Talukdar *et al.* 2022). Secondly, an adaptive rate ($\tau$) 129.6 g/mm$^2$ (J/g) months was considered for bone remodelling like the pelvis and femur (Chanda *et al.* 2020, Ghosh and Gupta 2014). Due to unawareness of the exact adaptation rate, the results were presented using a simulation timescale that was $\tau\Delta t$, and the total time was around 8 months (Talukdar *et al.* 2022). The adaptive rate was site-specific and could potentially vary from one patient to another. This study was grounded on patient-specific CT scan data. Conduction of multiple spine-based studies based on age, and sex would be advantageous in terms of deriving a broader conclusion based on vertebral load transfer (Weinans *et al.* 1993). In the case of a young healthy spine, cage insertion

is not recommended clinically (Polokeit *et al*. 2003). Additionally, it needs to be mentioned that muscles were not included in the study even though they play a substantial role in maintaining lumbar spine stability (Newell and Driscoll 2021, Zhang *et al.* 2018, Biswas *et al.* 2019). One limitation of this study is the lack of modelling trabecular damage around the standard and expandable pedicle screws. Differences in damage, influenced by load distribution and screw expansion, could significantly affect remodelling patterns. Future studies should include cancellous bone damage modelling to better understand implant-bone interactions Moreover, the ligaments were treated to be tension-only elements for static load transfer (Zhang *et al.* 2018, Talukdar *et al.* 2021). Further, the combination of the bone remodelling algorithm with bone ingrowth would be beneficial in terms of generalised conclusions.

### 3.5 Summary of the findings

In conclusion, this study, based on patient-specific CT- scan data, compared the bone density variation of normal pedicle screw and expandable pedicle screw instrumented FSUs. Both types of screws, along with TLIF cages, significantly increased bone density post-implantation, indicating no stress shielding after bone remodelling. However, quantitatively expandable pedicle screws demonstrated superior performance, with a more uniform and substantial bone apposition (16-28% increase) across the ROIs in the L4-L5 vertebra compared to normal pedicle screws (1.5-4% increase). This increase was particularly noticeable in the cancellous bone near the cage and screw insertion areas. Expandable pedicle screws promoted improved load distribution, enhanced anchorage, and more effective remodelling while reducing localized strain shielding. Despite their advantages, the increase in bone density may pose a potential risk of disc degeneration over time. Nevertheless, due to their ability to provide greater stability, mitigate strain shielding, and facilitate long-term remodelling, expandable pedicle screws are preferred over conventional normal pedicle screws for spinal fusion processes.

# Chapter 4

## Pullout strength comparison among three novel expandable pedicle screws

### 4.1 Introduction

Lower back pain is a leading cause of chronic disability and affects a significant proportion of the global population at any point in their life (Adams 2004, Hartvigsen *et al*. 2018). Spinal instability is a key contributor to LBP and, the pedicle screw is used globally as a spinal fixation device for stabilisation of the posterior spine, and ensuring proper alignment (Cetin and Bircan 2021a, Bianco *et al.* 2017). However, achieving stable fixation, particularly in patients with weaker bone remains challenging (Varghese *et al.* 2018).

Osteoporotic patients encounter significant complications with spinal fixation because of the low BMD, which weakens the bone-screw interface (Arslan *et al.* 2013, Sanjay *et al.* 2022). The interface strength is reliant on factors, like BMD, screw design, core diameter of the screw, and the tendency of osseointegration (Arslan *et al.* 2013). Screw pullout, loosening, breakage, misalignment, and pedicle fracture are common complications during or post-surgery (Cetin and Bircan 2021a), with screw loosening delaying recovery in 0.6-11% of spinal fusion cases (Hsu *et al*. 2005, Amaritsakul *et al.* 2014, Varghese *et al.* 2017).

In severe osteoporosis, most pedicle screws are embedded within the weakened bone (Arslan *et al.* 2013). Expandable pedicle screws, which feature design enhancements like fins, improve pullout force (POF) and fixation stability (Kiyak *et al.* 2018). These screws increase bone contact area without significantly enhancing the diameter, reducing the risk of pedicle fractures (Lei *et al.* 2006, Esenkaya *et al*. 2006). Biomechanical studies including FEA, are cost-effective and provide detailed insights into screw performance (Sanjay *et al.* 2022, Sanjay *et al*. 2018, Driescharf *et al.* 2014, Kim *et al*. 2010). Bone (foam) was modelled using the Johnson-Cook material model in numerical studies to simulate its behaviour (Cetin and Bircan 2021b).

Pullout strength is a key metric for assessing the stability of spinal implants under various conditions (Shen *et al*. 2019). The maximum POF can be defined as the load at which the pedicle screw dislodges its anchorage with the bone (Jendoubi *et al.* 2018). Numerous studies have conducted pullout experiments of bone screws either using synthetic bones (Hashemi *et al.* 2009, Seng *et al*. 2018, Cetin and Bircan 2021a, Weildling *et al.* 2022) or human cadavers (Zhang *et al*. 2006, Tai *et al.* 2022, Krishnan *et al.* 2020), or animal samples (Inceoglu *et al.* 2004, Cann *et al.* 2015). Synthetic bone foam is widely preferred due to its homogeneity, reproducibility and similarity to human cancellous bone (Hsieh *et al.* 2019). However, its friction coefficients with screws differ from natural bone due to variations in composition, porosity, and moisture content (Cristofolini *et al.* 1996). While natural bone's hydration and trabecular structure enhance screw fixation, synthetic models often misestimate friction and pullout strength (Heiner 2008). Advances like adding porosity and hydrophilic coatings improve synthetic bone models, but validation with natural bone remains essential. Foam with a density of 240 kg/m$^3$ (grade 15) is commonly used in studies targeting osteoporotic conditions (Cetin and Bircan 2021a, Damisih *et al*. 2023). While physical pullout tests provide direct measurements of screw performance, FEA complements these experiments by enabling the evaluation of additional virtual designs and simulating realistic bone properties beyond synthetic foam. FEA provides detailed insights into stress distribution, deformation, and other biomechanical factors that might be difficult or impossible to measure experimentally. This dual approach delivers deeper insights into screw behaviour under various conditions, allowing for more informed design optimization.

The pedicle screw design plays a vital role in the success rate of surgery specifically for osteoporotic patients (Aycan *et al.* 2017). Studies showed standard screws often lack sufficient stability in osteoporotic bones (Christodoulou *et al.* 2015), leading to the development of expandable pedicle screws. These screws offer greater pullout strength and load-bearing capacity than standard designs (Rassi-Neto *et al.* 2002, Lei *et al.* 2006, Vishnubotla *et al.* 2011). Fins in expandable screws further enhance performance, with 4-fin outperforming 2-fin configuration (Kiyak *et al.* 2018).

Clinically, expandable pedicle screws combined with cement augmentation have shown effective results in osteoporotic patients and revision surgeries, delivering outcomes comparable to surgeries in healthy bone (Wu *et al.* 2012, Cook *et al.* 2001).

The ability to increase contact area while minimising the risk of pedicle fractures makes expandable screws a promising solution for challenging cases (Esenkaya *et al.* 2006).

This study investigates the pullout performance of 4-fin expandable pedicle screws using ASTM F 543-13 standards on synthetic foam mimicking osteoporotic bone. The objectives of the study have been further subdivided as: (a) performing a pullout test for three types of expandable pedicle screws with various threads, and (b) estimating pullout performance numerically considering the elastoplastic behaviour of foam.

## 4.2 Material and Methods

### 4.2.1 Expandable Pedicle screw designs

The expandable pedicle screws for testing were fabricated following the specifications of the American Society of Testing and Materials (ASTM) F136-02a. They were designed to have cylindrical cores having poly-axial screw heads. The screws were

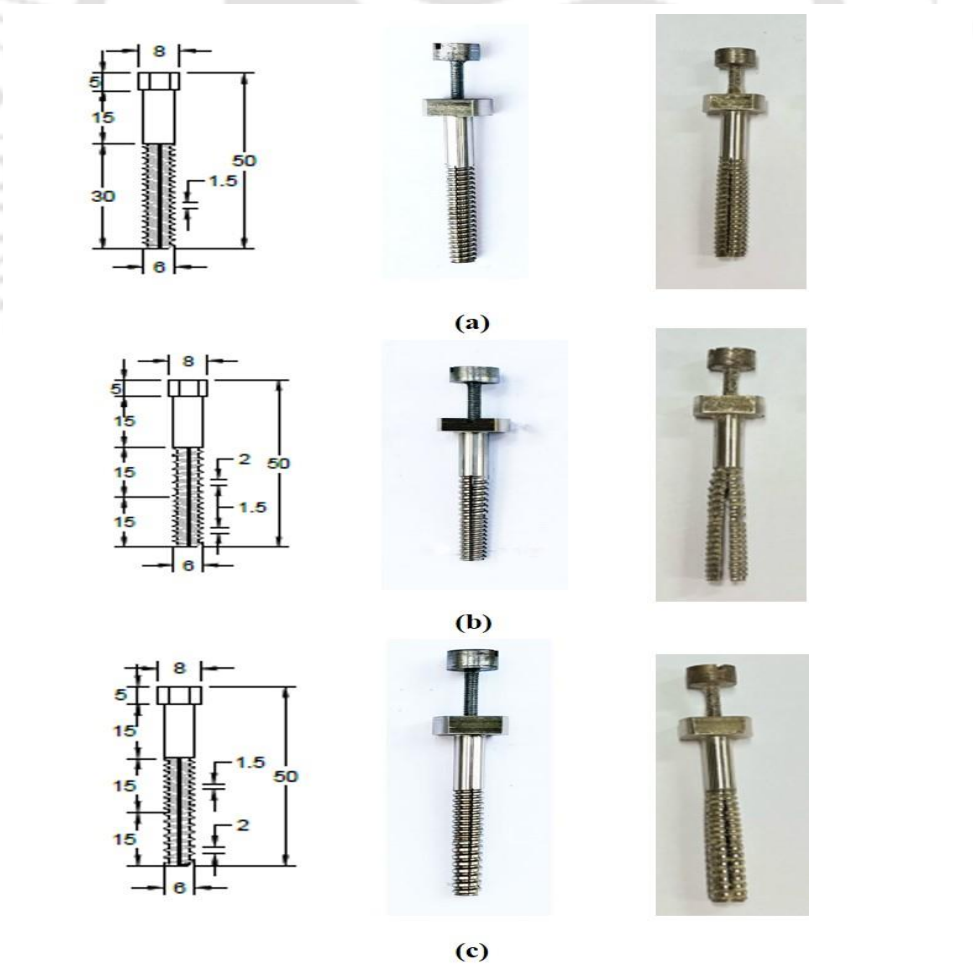


**Fig. 4.1:** Non-expanded (2D and 3D) and expanded pedicle screws (L-R) of (a) type 1 (b) type 2 (c) type 3.

designated as type 1, type 2 and type 3 for simplification based on thread patterns using the software Autodesk Fusion 360 as shown in Fig 4.1. The overall thread portion is 30 mm in length. The type 1 are single thread screws having a constant core and thread diameter and uniform pitch of 1.5 mm (Fig. 4.1a). However, Type 2 (Fig. 4.1b) features a dual-thread design, with a 1.5 mm pitch in the proximal region and a 2 mm pitch in the distal region, both of equal length. In contrast, Type 3 (Fig. 4.1c) has a dual-thread design where the pitch is 2 mm in the proximal region and 1.5 mm in the distal region. The concept of using a dual-thread design was based on a previous study that explored the combination of different pitch lengths in the proximal, middle, and distal regions (Shen *et al.* 2019). All dimensions of the screws are provided in Table 4.1. For expansion of the tips of the screws, pins are inserted at the screw head. Stainless steel implants have comparable or superior biomechanical properties to titanium. Stainless steel is often preferred for spinal implants, including screws, due to its higher strength, fatigue resistance, and cost-effectiveness, especially when large quantities of screws are needed. Moreover, in applications where bending or torsional load is present, titanium may not be an ideal choice owing to its subpar shear resistance. The screws were made of stainless steel (SS 304L) using CNC turning and wear-cut machining using a CAD model, a technique commonly used for implant fixation (Zhang *et al.* 2006). The expandable pedicle screws were fabricated locally (Tool Room and Training Centre, North Guwahati, Assam, India).

**Table 4.1:** Design specifications of expandable pedicle screw.

| **Screw type** | **Design** | **Thread shape** | **Outer diameter (mm)** | **Inner diameter (mm)** | **Thread width (mm)** | **Pitch(mm)** | |
|---|---|---|---|---|---|---|---|
| | | | | | | **Proximal (1/2)** | **Distal (1/2)** |
| Type 1 | Cylindrical | V | 6 | 4.6 | 1 | 1.5 | 1.5 |
| Type 2 | Cylindrical | V | 6 | 4.6 | 1 | 1.5 | 2 |
| Type 3 | Cylindrical | V | 6 | 4.6 | 1 | 2 | 1.5 |

### 4.2.2 Synthetic Bone

Rigid polyurethane (PU) foam acts as an alternative to cadaveric bone due to its comparable mechanical behaviour, uniform structural properties and extensive availability (Seng *et al*. 2018). To generalise findings despite PU foam's differences

from real bone, the study relies on consistent comparisons between screw designs. FEA models real bone properties, and trends are validated with prior cadaveric or clinical data. PU foam is a reliable tool for initial testing, with further validation needed for real bone applications. In our study, we used cellular PU foam block samples of size 40 mm× 40 mm× 40 mm following ASTM F1839-08 protocols from Sawbones Europe AB, Malmo, Sweden. The selected foam was of Grade 15 (compressive strength of 4.9 MPa, compressive modulus of 123 MPa) designated specifically for low osteoporotic trabecular bone (compressive strength of 3.9MPa) (Cetin and Bianco 2021a, Giesen *et al.* 2001). Each of the test samples was drilled without pre-tapping (30 mm deep) in the centre of the surface (40 mm × 40 mm) along the longitudinal axis of the pedicle screws perpendicular to the foam. The drilling and screw insertion into the foams (up to full length without pre-tapping) was performed by an experienced surgeon (Fig. 4.2a).

### 4.2.3 Pullout Test

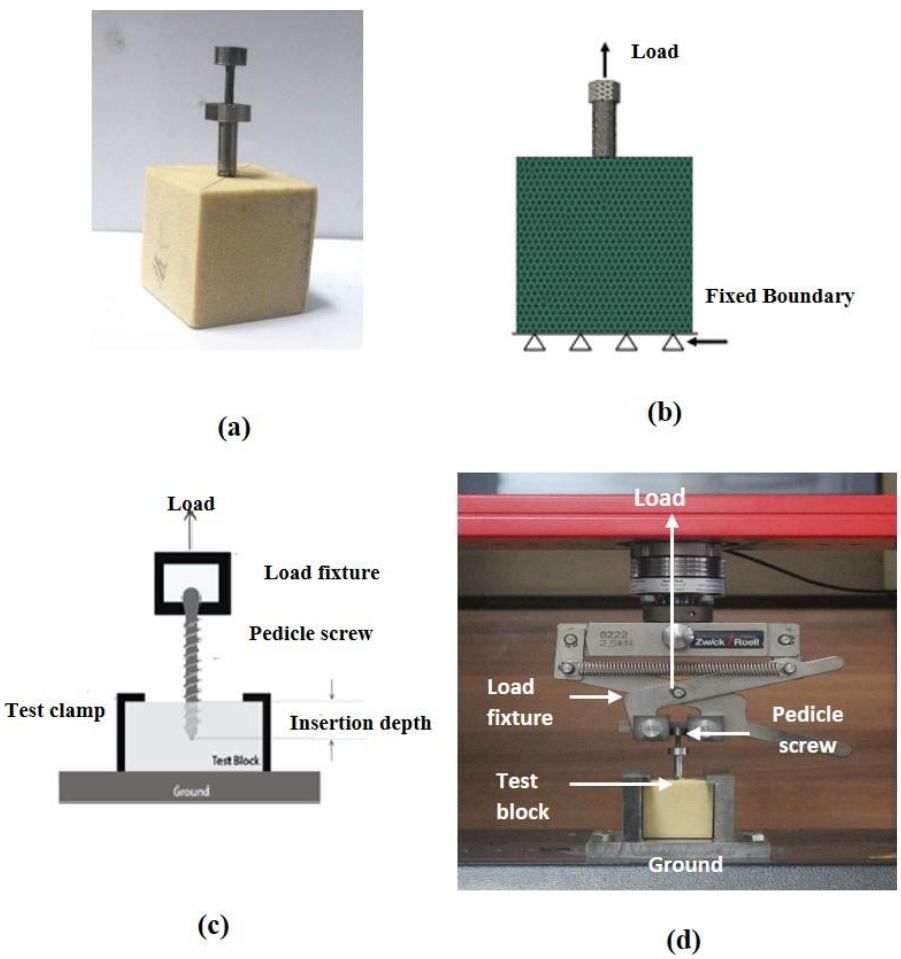


**Fig. 4.2**: Pre-pullout set up: (a) screw inserted on foam (b) Loading and boundary condition of the meshed model (c) Schematic diagram of test set up (d) test set up.

The screw-inserted foam block was placed into a custom-made fixture that had the provision to hold the screw head on the top surface (Fig. 4.2). The fixture was made of mild steel to ensure minimum deflection during testing. The screw pullout was performed following ASTM F543-13 standards using a 5 kN electromechanical universal testing machine (Zwick Roell, Z005TN) (Fig. 4.2d) following displacement control mode at a rate of 5 mm/min (Weildling *et al.* 2022). The termination of the tests was designed at the point of screw failure or detachment from the block.

During the screw extraction process, the load initially increased sharply, followed by a rapid drop. A data acquisition system was used to record the load-displacement curve. The ultimate POF was defined as the maximum load (pullout strength) sustained by the screw before the failure. Failure was distinct at the point at which the load reached its peak and then experienced a sudden decrease (Aycan *et al*. 2017). Samples of each screw type were tested thrice for reproducibility.

### 4.2.4 Statistical analysis

Parametric tests like ANOVA assume the data is normally distributed and with 3 sets of screws, the normality assumptions cannot be confidently checked. For the three sets of screws, non-parametric methods are more robust and do not rely on assumptions about the underlying data distribution. Non-parametric tests like the Kruskal-Wallis test is more appropriate for small sample sizes. The biomechanical performance of the three groups of expandable pedicle screws was assessed by statistically comparing the ultimate POF. For the three sets of screws (580 N, 567 N, and 596 N for first screw, 683 N, 703 N, 691 N for the second screw, and 841 N, 825 N, 810N for the third screw), non-parametric analysis using Kruskal-Wallis test was conducted using manual calculation. For this, first, the data are ranked, calculated the rank sum of each group. This followed by the calculation of Krushkal Wallis H statistics, p-value calculation and finally Dunn's test to compare significant differences among groups.

### 4.2.5 FE modelling and model geometry

Three-dimensional (3D) FE models were employed to analyze the stress distribution during the pullout test using ABAQUS/explicit software (ABAQUS/explicit version 2022). The foam blocks were created using 3-matic software 11.0 with dimensions of 40 mm × 40 mm × 40 mm, and the screws were inserted at the centre up to a depth of 30 mm from the top surface. The mesh element type selected for the study for both screw and foam was C3D4 (4-noded tetrahedral). Meshing was carried out in

Hypermesh 2021, and the meshed geometry was subsequently imported to ABAQUS for simulation. A mesh refinement study was performed to ensure the accuracy and reliability of the FE models. The mesh density was systematically varied, and numerical convergence was confirmed when successive analyses showed less than a 3% variation in results across three different mesh sizes. The optimal mesh, with element sizes ranging from 0.25 mm to 1.5 mm, was selected for the numerical analysis of screw pullout performance. The foam model contains approximately 80,000 volume elements, while the screw model comprises around 15,000 elements each. The material properties of both foam blocks and screws were assumed as homogenous, elastic and isotropic based on the literature (Varghese *et al*. 2016b, Zhang *et al.* 2006). The simulated material properties of the foam and screw are given in Table 4.2. Previous studies have indicated that interface modelling significantly affects the local stress-strain distribution in the bone surrounding the screws (Macleod *et al.* 2012). Therefore, a finer mesh density was applied at the screw-bone interface to capture these localized effects more accurately.

**Table 4.2:** Material properties of foam and screws.

| | **Density, ρ (kg/m$^3$)** | **Young's modulus (MPa)** | **Poisson's ratio** | **Reference** |
|---|---|---|---|---|
| Foam | 240 | 173 | 0.3 | Varghese *et al*. 2016a |
| Screw | 7850 | 193,000 | 0.3 | Zhang *et al*. 2006 |

Foam is often modelled considering the Johnson-Cook material model to predict the elastoplastic behaviour of cancellous bone (Cetin and Bircan 2021b, Remache *et al*. 2020, Prasannavenkadesan and Pandithevan 2021, O'Neill and Vaughan 2021). The Johnson-Cook material model is given by the following equation (Demirbas *et al.* 2022).

$$\sigma = (A + B(\mathcal{E}P)^n(1 + Cln\frac{\dot{\varepsilon}}{\dot{\varepsilon}0}) \times (1 - (\frac{T - T_{room}}{T_{melt} - T_{room}})^m) \quad (4.1)$$

where A, B, n, C, $\mathcal{E}_p$, $\dot{\varepsilon}$, $\dot{\varepsilon}_0$ and m are yield stress, the hardening modulus, the hardening exponent, the strain rate coefficient, the equivalent plastic strain, the reference strain rate and thermal softening respectively. $T_{room}$ and $T_{melt}$ are room and melt temperature respectively. The values are tabulated in Table 4.3.

**Table 4.3:** Johnson-Cook plasticity model constants for cancellous bone adapted from Demirbas *et al*. 2022.

| Yield stress, A(MPa) | Hardening modulus,B (MPa) | hardening exponent, n | thermal softening coefficient(m) | strain rate coefficient,C | reference strain rate, $\dot{\varepsilon}_0$ | $T_{melt}$ (K) | $T_{room}$ (K) |
|---|---|---|---|---|---|---|---|
| 28 | 0.1 | 0.1 | 0.02 | 0.015 | 0.001 | 1573 | 293 |

Previous studies (Xu *et al.* 2019, Cetin and Bircan 2021b) established that screw-bone contact conditions have a substantial influence on the loading at the screw-bone interface compared to the bonded condition. The screw-bone interface had a general contact algorithm (contact action-all with self) with a penalty coefficient of friction of 0.61 (Cetin and Bircan 2021b). The base nodes of the foam were inhibited from moving in any direction. In the pullout loading condition, an axial force of 5.0 mm/min was applied to the screw head (Lee *et al*. 2019) (Fig. 4.2b).

## 4.3 Result

### 4.3.1 Experimental Validation of Pullout Test

The ultimate loads sustained before the failure of the expandable pedicle screws were identified. The experimentally calculated POFs for three sample sets of type 1, type 2, and type 3 were 580±15N (1A, 1B, 1C), 690±15N (2A, 2B, 2C) and 825±15N (3A, 3B, 3C) respectively. The highest value of the separation force signifies the screw's pullout force and the corresponding displacement is known as the pullout displacement. The abrupt decrease in pullout force with continuous axial movements through the test was considered inadequate (Esenkaya *et al.* 2006). The Krushkal Hallis H statistics value was 7.2 and the p-value using Chi-squared distribution was found to be 0.0273. Dunn's

**Table 4.4:** Comparison of pullout results for three types of expandable pedicle screws.

| Screw set | z value | z vs $z_{critical}$ | Significance ($z>z_{critical}$) |
|---|---|---|---|
| Type 1 vs Type2 | 1.34 | 1.34<2.39 | Not significant |
| Type 1 vs Type 3 | 2.68 | 2.68>2.39 | Significant |
| Type 2 vs Type 3 | 1.34 | 1.34<2.39 | Not significant |

test was manually performed to determine the significant difference. The $z_{critical}$ value was found to be 2.39 and comparing it for each pair, the statistical significance was achieved.

Numerically calculated maximum POF for the three screw types were 602.31 N, 705.77 N and 838.27 N, respectively and found to be in the range of experimental maximum POF. The characteristic POF vs displacement curves for both experimental and FEA for the three types of expandable pedicle screws were shown in Fig. 4.3, and they showed similar trends. Thus, the corroboration of the numerical results with the experimental findings gave sufficient confidence to the results of the pullout tests performed in the present study.

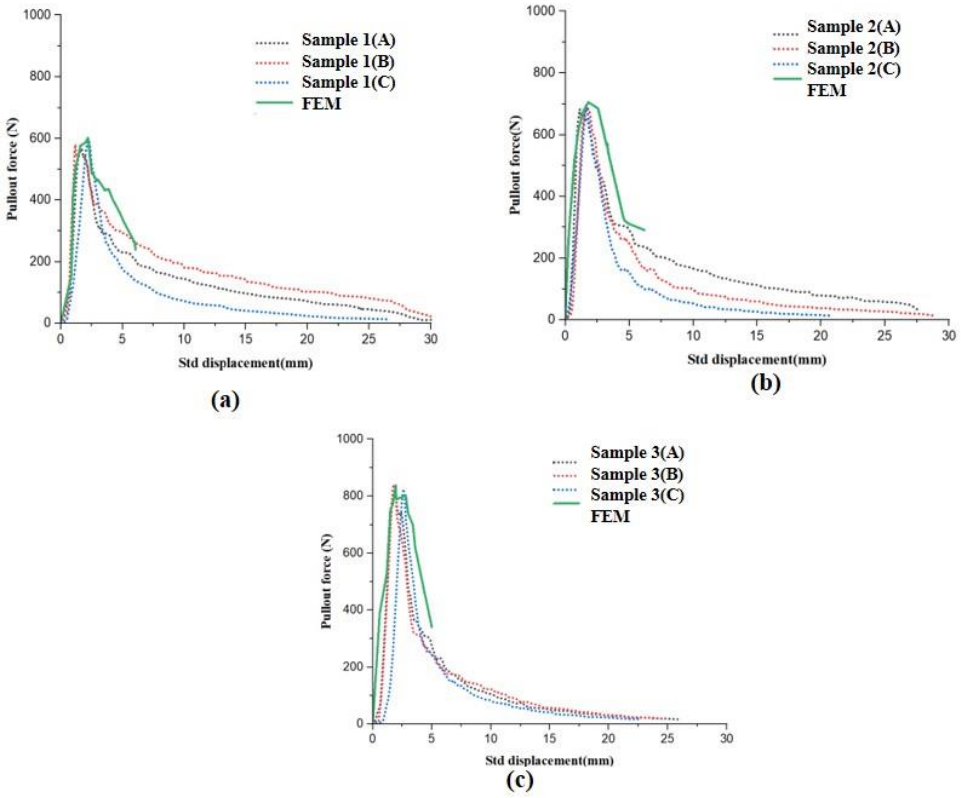


**Fig. 4.3**: Axial pullout test validated with FE studies for (a) type 1(b) type2 (c) type 3 screws.

### 4.3.2 Pullout FE simulation of foam

Fig. 4.4 depicts a clear outline of the pullout simulation process. The cross-sectional view of the bone and pedicle screw interface was shown and the progress of the pullout simulation was presented in three steps for better understanding. Initially (Fig. 4.4a), high stress was visible at the bottom portion of the screw thread region (marked in the dotted circle in Fig.4.4a). Further, the bone fracture was initiated after reaching maximum POF, thus shifting the high-stress region upwards throughout the screw-foam

interface (Fig. 4.4b). Thereafter, (Fig. 4.4c), the complete separation of the expandable pedicle screws from the foam occurred by debonding of neighboring elements. From the stress contour, it was visible that the region of peak stress was highest in type 3, followed by type 2 and type 1 respectively. The average von Mises stress distribution of the foam was calculated for the three types of screws and was found to be 17.85 MPa, 21.11 MPa and 25.83 MPa, respectively.

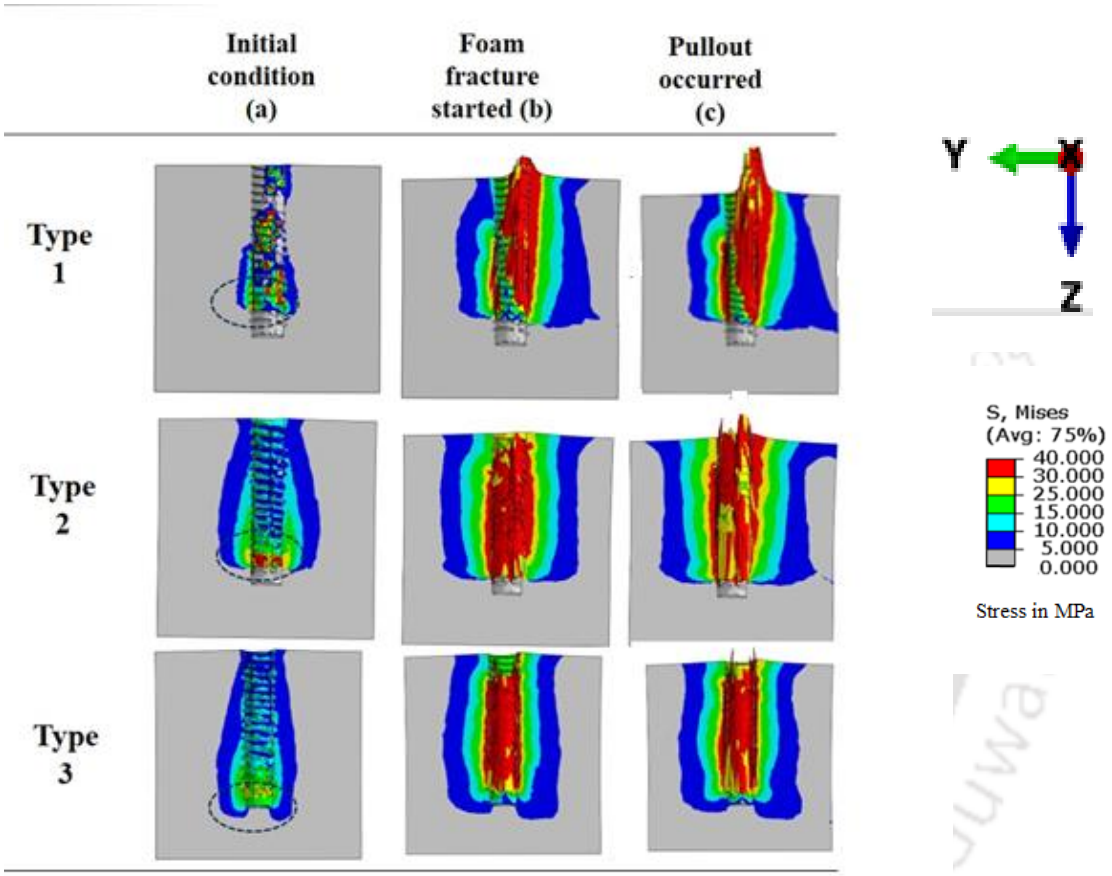


**Fig. 4.4:** Axial pullout simulation results for type 1, type 2, and type 3 screws (a)starting of the simulation, (b) Foam fracture started (c)pullout completed.

## 4.4 Discussion

This study compared the pullout strength of three types of expandable pedicle screws with various thread patterns to optimize the distribution of forces along the screw and improve its anchorage within the bone. By incorporating different pitch lengths, the designs aimed to enhance stability, reduce the risk of screw loosening, and minimize stress concentrations, particularly in osteoporotic bone, where weakened density poses significant challenges. The pedicle screw fixation technique is a globally accepted surgical technique (Gao *et al.* 2011). However, challenges persist in patients with

osteoporosis due to screw loosening and failure, which compromises stability and clinical outcomes (Wu *et al.* 2012, Chen *et al*. 2009). Enhancing the biomechanical performance of pedicle screws is, therefore, essential for achieving improved clinical results (Kubaik *et al.* 2019).

Experimental pullout tests revealed significant differences among the three screw designs. Type 1 screws exhibited the lowest maximum pullout force (580±15 N), while type 3 screws achieved the highest (825±15 N). Stress distribution analysis indicated that stress concentration varied by screw type: near the shank for type 1, the mid-shank for type 2, and the threaded tip for type 3 screws. Dual-threaded screws (i.e. screws with two pitches) showed superior pullout strength than the conventional pedicle screws (Yaman *et al*. 2015, Wu *et al.* 2023). The improvement in dual-threaded screws is likely due to increased surface contact at the bone-screw interface, which enhances anchorage (Wu *et al.* 2023, Seng *et al.* 2018). Contrarily Guftason *et al*. (2019) showed that constant-pitch threads possess more pullout strength than the screws with variable pitch.

Notably, type 3 screws outperformed type 2 screws, possibly due to their coarse-pitch threads at the proximal end providing better primary stability by increasing contact area and distributing the load more effectively (Daud *et al.* 2021). Post-pullout observations showed foam debris covering the screw threads, although the screws themselves remained intact (Cetin and Bircan 2021b, Wu *et al*. 2023). Pullout failure typically occurred within a displacement of 2 mm (Guftason *et al.* 2019), and statistical analysis confirmed significant differences ($z < z_{critical}$) for group 2 (type 1 screw vs type 3 screw). On average, type 3 screws demonstrated 42.05% greater pullout strength than type 1, while type 3 screws showed a 19.16% more pullout than type 2.

FEA provided additional insights into pullout mechanics. The foam was modelled using the Johnson-Cook material model to capture its elastoplastic behaviour. Simulations showed high initial stress at the proximal threads of the screw-foam interface (Bianco *et al.* 2017, Cetin and Bircan 2021b), where failure first occurred, followed by fracture near the screw tip (Chatzitergos *et al*. 2010). Stress redistribution and debonding near the proximal threads were consistent with experimental findings as well as previous studies (Chatzistergos *et al*. 2014) (Fig 4.4).

The observed variation in pullout forces reported in the literature (200–3000 N) (Cetin and Bircan 2021a) can be attributed to differences in bone density, screw design,

diameter, and insertion depth (Cetin and Bircan 2021b, Hsu *et al.* 2005). In this study, the use of low-density foam (grade 15) to simulate osteoporotic bone resulted in a maximum pullout force of approximately 1000 N, aligning with previous research (Gao *et al.* 2011, Kim *et al.* 2012a, Damisih *et al*. 2023). The average von Mises stress around the screw thread for the study (l9-57 MPa) was consistent with prior studies (Cetin and Bircan 2021b). The force-displacement curve profiles obtained from the FE simulation closely matched the experimental results and trends reported in the literature. Dual-threaded screws showed higher pullout resistance due to increased bone volume between threads, enhancing mechanical interlocking (Wu *et al*. 2023, Seng *et al.* 2018). The finding highlights the potential of optimized thread designs for improved screw fixation strength, predominantly in osteoporotic patients.

Despite these findings, the study has several limitations. The use of synthetic foam blocks does not replicate the morphological and material heterogeneity of human bone. Moreover, the Johnson-Cook material model parameter was not varied, and only low-density osteoporotic foam was tested. Similar tests on high-density synthetic foams would be beneficial (Kiyak *et al.* 2018). Future studies should consider mechanical forces, such as bending, cyclic loading, and shear stress, to better simulate in vivo conditions (Seng *et al*. 2018). Human errors during screw insertion, such as torque variability, should also be investigated (Lee *et al.* 2019). Further, the potential risk of pedicle fracture during insertion and the probable benefits of cement augmentation, which significantly improves fixation strength for severely osteoporotic patients, warrant additional exploration (Wu *et al.* 2012, Amaritsakul *et al*. 2014).

### 4.5 Summary of the findings

This study demonstrates the biomechanical advantages of dual-threaded expandable pedicle screws, particularly type 3, in enhancing pullout strength. Using synthetic PU foam mimicking osteoporotic bone, experimental and numerical analyses were conducted to evaluate the screw designs. The Johnson-Cook material model was applied in finite element simulations to predict pullout performance. Dual-threaded screws outperformed constant-pitch screws due to increased surface contact at the bone-screw interface, with type 3 showing the highest pullout strength. While promising, these findings require further validation through cadaveric or clinical studies. This research provides a foundation for improving pedicle screw designs, especially for patients with poor bone quality.

# Chapter 5

## Influence of three novel expandable pedicle screws on osseointegration: An FE study based on mechanoregulation algorithms

### 5.1 Introduction

The spine, a complex load-bearing structure, endures significant stress during daily activities and eventually degrades with age. The degeneration reduces the mineral content of cancellous bone, leading to osteoporosis (Krishnan *et al.* 2020) and a diminished load-sharing capacity, ultimately results in spinal instability. Surgeons have employed several fusion and non-fusion techniques for the lumbar spine (Pradeep and Pal 2024). The long-term success of such procedures depends on achieving stable bone-implant integration with surrounding tissues and ensuring the longevity of the orthopaedic implants (Causay *et al*. 2021).

The uncemented implants attain stability through osseointegration, where bone grows into or onto the implant's surface, providing mechanical stability by interlocking. Osseointegration is the percentage of the surface of the implant in direct contact with bone (D'lima *et al.* 1998). Besides, successful integration requires proper biological fixation of bone with intermediate soft tissues surrounding the implant (Ghosh *et al.* 2020). Though pedicle screws have become a popular choice for spinal fixation, complications like screw bending, breakage, and aseptic loosening often lead to revision surgery (Okuda *et al*. 2006, Chatzigtergos *et al.* 2010). The primary reason for aseptic loosening is insufficient initial fixation associated with mid and longstanding instability (Sun *et al.* 2024).

The expandable pedicle screws offer superior anchorage capacity and have shown advantages over conventional pedicle screws (Cook *et al*. 2001, Sanjay *et al.* 2022). Design innovations, such as dual-thread cylindrical configurations, aim to improve the implant success rate by enhancing mechanical stability and osseointegration (Amaritsakul *et al.* 2014, Ghosh *et al*. 2020, Sun *et al*. 2024). Osseointegration occurs through two processes: bone ingrowth, where bone penetrates the implant's porous

surface, and bone on-growth, where bone attaches through a textured surface (Kim *et al.* 2016, Ghosh *et al.* 2020). The surface modification techniques at macroscopic (length scale in order of millimetres or higher) and microscopic (dimension from submicron to microns) scales are employed to enhance these processes, improving the mechanical interlocking between the implant and the bone (Andrekiv *et al.* 2008b, Ghosh *et al.* 2020).

The mechanical loading significantly influences the peri-implant bone adaptation (Duyck *et al.* 2007, Mathieu *et al.* 2014). Force or displacement-controlled mechanical loading enhances bone formation around rough implant surfaces (Mathieu *et al.* 2014, Tarlochan *et al.* 2018). Previous studies have extensively analysed bone growth under force-controlled (Mukherjee and Gupta 2015, Mathai and Gupta 2021b, Ghosh *et al.* 2022a) and displacement-controlled (Andrekiv *et al.* 2008b, Mukherjee and Gupta 2014, Ghosh *et al.* 2020) conditions. The process of bone growth around the implants resembles bone fracture healing (Davies 1996, Isaksson 2012, Ghosh *et al.* 2020, Mohendas *et al.* 2021). Here MSC differentiate into fibrous tissue, cartilage and bone under favorable loading conditions (Mathai and Gupta 2021b). The MSCs are derived from bone marrow stroma and differentiate into cells of mesodermal lineages (Barry 2003).

Several mechanoregulation theories have been extensively employed to simulate FE models to predict bone formation (Lacroix and Prendergast 2002a, Viceconti *et al.* 2004, Tarlochan *et al.* 2018, Mehboob *et al.* 2020), particularly in indirect fracture healing (Isaksson *et al.* 2006a). However, no single mechanoregulation algorithm has proven universally superior for predicting osteogenesis (Ghosh *et al.* 2022b). Boccaccio *et al.* (2011) and Postigo *et al.* (2014) had investigated bone regeneration and tissue differentiation in spinal fusion, primarily focusing on cages and intervertebral discs. An earlier study by van Rijsbergan *et al.* (2018) and Calvo Echenique *et al.* (2019) combined tissue differentiation with bone remodelling to understand bone growth post-disc degeneration and nucleotomy. A recent study was performed considering various types of lumbar interbody fusion to estimate the best technique for the favourable biomechanical environment for osteogenesis by developing a mechanoregulation algorithm iteratively evaluating MSC and their differentiated cells (Lu *et al.* 2024). These studies considered mechanoregulation-based studies on lumbar fusion considering cages and intervertebral discs. Integrating high-resolution micro-computed

tomography (micro-CT) datasets into FE models improves accuracy. Micro-CT provides detailed bone microstructure, including trabecular architecture, damage mechanisms and bone-implant heterogeneity (Wu *et al.* 2015, Guha *et al*. 2022).

Despite the advancements, no prior studies have evaluated tissue differentiation around distinct expandable pedicle screws. The study aims to address this gap by (1) developing and comparing two FE-based mechanoregulation algorithms for three types of expandable pedicle screws with various thread designs (single, dual-thread) under two force-controlled loading conditions and (2) observing the influence of the local mechanical conditions on peri-prosthetic osseointegration. Since the study is a preliminary study on the various designs of homogenised expandable pedicle screws, bone structure in a simplified cube is used for further investigation with physiological loading conditions (axial compression load combined with extension moment).

## 5.2 Materials and Methods

To assess how design variations in three types of expandable pedicle screws affect their osseointegration capabilities, we simulated two independent mechanoregulation-based adaptive tissue differentiation algorithms using a FE model of the bone-implant interface. The bone-implant interfaces were developed mimicking the experimental set-up that measured the pullout strengths of the expandable pedicle screws inserted in a cubical foam specimen (40 mm x 40 mm x 40mm) in the previous chapter. However, recognizing that the mechanical properties of foam do not accurately represent the mechanical properties of an actual human bone, we modelled a similar cubic structure (40 mm x 40 mm x 40mm) representing the homogenized cancellous bone of a vertebral body. This simplified representation of the vertebra was conceptualized from studies representing foam as a vertebra for pullout tests (Cetin and Bircan 2021a) (Fig. 5.1a). By employing two independent mechanoregulation algorithms, it is aimed to assess the sensitivity of each mechanical stimulus and their magnitude in predicting tissue growth at the bone-implant interface, aligning the simulations with the clinical results.

### 5.2.1 Development of expandable pedicle screw implanted 3D FE model

Three bone-implant interface models with distinct expandable pedicle screws (type 1, type 2, type 3) were developed. Autodesk Fusion 360 software was used to create the expandable pedicle screws with cylindrical cores and poly-axial screw heads, following the American Society of Testing and Materials (ASTM) F136-02a specifications. Fig. 5.1b represents the longitudinal section of the expandable pedicle screw implanted bone

with the granulation tissue in between them. The type 1 expandable pedicle screw has a uniform pitch of 1.5 mm. However, type 2 has a dual thread (1.5 mm in proximal and 2.0 mm in distal) pitch in equal length. The type 3 expandable pedicle screws were designed just the opposite of type 2 in the order of pitch (2.0 mm in proximal and 1.5

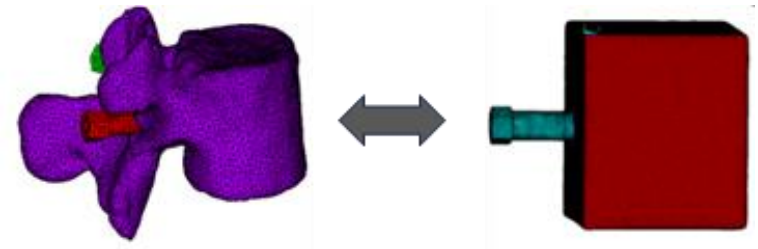

**(a)**

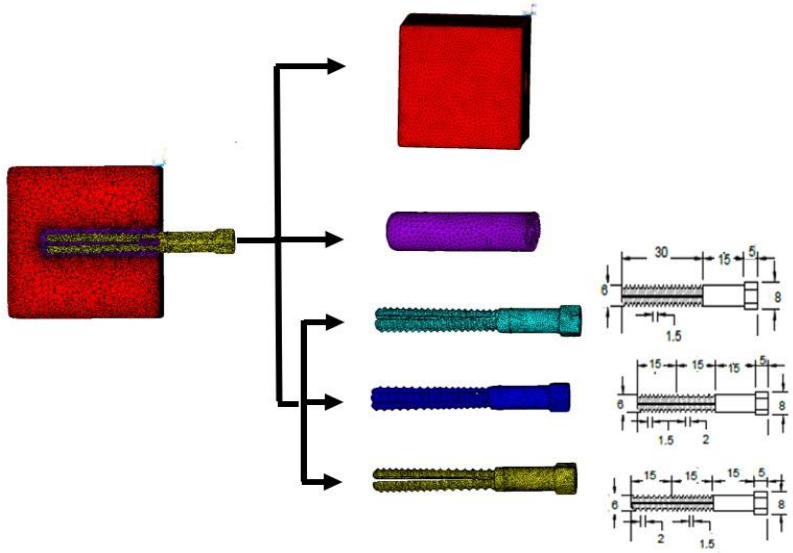


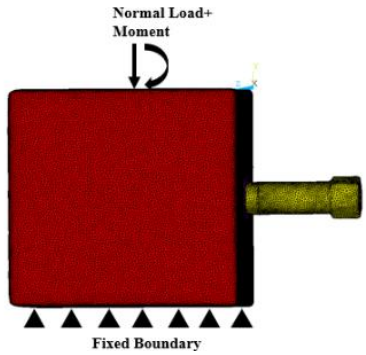


**(c)**

**Fig. 5.1:** (a) Implanted vertebra equivalence to screw-foam system (b) Representative CAD model of the bone-implant system with (top to bottom) foam, tissue, and implant (Type 1, Type 2, Type 3) (c) Loading and Boundary Condition.

mm in distal). In the current study, the implants (expandable pedicle screws) were inserted up to 30.0 mm (depth of threaded portion) into the bone. The gap of 1.0 mm between the bone-implant throughout was assumed to be the layer of granulation tissue.

The bone and the granulation tissue were developed using 3-matic software 11.0. The meshing was created using 4-noded tetrahedral elements in Hypermesh 2021.1 (Altair Engineering Inc., Troy, Michigan, United States) and finally, simulation was conducted using Ansys FE software v 19.0(ANSYS Inc., PA, USA). A mesh convergence study was conducted for the FE models to achieve consistent mesh results based on peak von Mises stress developed when subjected to force-controlled loading (150N load, 10 Nm moment) with variations of edge length. The convergence was achieved with the second model, which had an edge length of 0.5 mm and a variation of less than 3% with the other two models. However, the tissue and the bone element size ranged from 0.5 mm to 1.5 mm. The bone was considered linear, elastic, and transversely isotropic (Kim *et al*. 2015) whereas, the granulation tissue and the implants were assumed to be linear, elastic, and isotropic. The material properties are provided in Table 5.1. The implant-tissue and tissue-bone interfaces for all three models were considered perfectly bonded (Ghosh *et al.* 2021b, Mukherjee and Gupta 2016).

**Table 5.1:** Material properties of bone, tissue and screw

| | **Young's modulus(MPa)** | **Poisson's ratio** | **Reference** |
|---|---|---|---|
| **Bone** | $E_x$=200,$E_y$=140,$E_z$=140<br>$G_{xy}$=$G_{xz}$=$G_{yz}$=48.3 | $\upsilon_{xy}$=0.45, $\upsilon_{xz}$=0.315, $\upsilon_{yz}$=0.315 | Kim *et al.* 2015, Zhou *et al.* 2019 |
| **Tissue** | 1 | 0.3 | Ghosh *et al.* 2020 |
| **Screw** | 1100000 | 0.3 | Sanjay *et al.* 2022, Kim *et al.* 2010 |

### 5.2.2 Applied loading and boundary conditions

In the FE model, the top surface nodes of the bone were considered slave nodes, with a master node positioned centrally above the surface. The slave nodes and master nodes were rigidly coupled to maintain uniform deformation, as suggested by Talukdar *et al.* (2021). A massless element, MASS 21 was assigned to the master node to facilitate rotational degree of freedom. To assess loading effects, two scenarios were applied at

the master node. Load case 1 comprises 150 N axial load (negative Z direction) combined with 10 Nm extension moment (negative Y direction) while load case 2 of 150 N axial load with 5 Nm extension respectively. These loading conditions aligned with earlier studies on vertebrae (Chen *et al.* 2005, Liao *et al.* 2017, Wang *et al.* 2020). The loading was applied at the master node (Talukdar *et al.* 2021). All the nodes in the bottom surface were constrained for movements following earlier studies (Talukdar *et al.* 2021, Sanjay *et al.* 2022). Fig. 5.1c illustrates this setup.

### 5.2.3 Mechanobiological Tissue Differentiation Algorithm

The numerical framework of the mechanoregulation-based tissue differentiation algorithm utilized in the current study incorporates two principal features namely mechanical and biological presented in Fig. 5.2. The mechanical aspect of the algorithm integrates the mechanical stimulus. Osteocytes detect the mechanical stimuli and respond by releasing biochemical signals that promote MSC to differentiate into bone-forming cells and enhance bone formation. In contrast, the biological aspect deliberates the MSC migration, proliferation, tissue deposition, differentiation and replacement from the host bone interface to the implant interface (Andreykiv *et al.* 2008b, Ghosh *et al.* 2022a). In the beginning, only granulation tissue was present between the bone and the implant indicating other cells' concentration to be zero (Andreykiv *et al.* 2008b). The regularised concentration of the MSCs at the bone-granulation tissue interface was estimated to be unity (Andreykiv *et al.* 2008b, Ghosh *et al.* 2020). A transient-diffusion model was used to evaluate the migration of MSCs within the interfacial tissue region (Lacroix and Prendergast 2002a, Lacroix and Prendergast 2002b, Lacroix *et al.* 2002, Ghosh *et al.* 2020) given by the equation

$$k \nabla^2 c = \frac{dc}{dt} \tag{5.1}$$

where $k$ is the diffusion constant (0.1 $mm^3$/day) (Ghosh *et al.* 2021a) and $c$ represents the element-specific concentration of undifferentiated stem cells (Lacroix and Prendergast 2002a, Mukherjee and Gupta 2015). The diffusion constant selection was based on the assumption that the MSC migration inside the granulation tissue would be complete within 42 days (6 weeks) equivalent to 42 iterations i.e., one iteration would signify one day of healing. The logic behind considering 42 iterations was that bone healing/growth usually takes place within 6-8 weeks (Mukherjee and Gupta 2016, Ghosh *et al.* 2022a, Mathai and Gupta 2021b). On the incidental edges of the granulation tissue, a zero-diffusion boundary condition was implemented considering

no cell loss from the granulation tissue towards the impermeable implant. To repair the bone defects, the antecedent cells from the bone-granulation tissue interface migrate towards the healing region and differentiate into various cellular phenotypes depending on local mechanical stimuli (Barry 2003, Isaksson *et al*. 2006a, Ghosh *et al*. 2020).

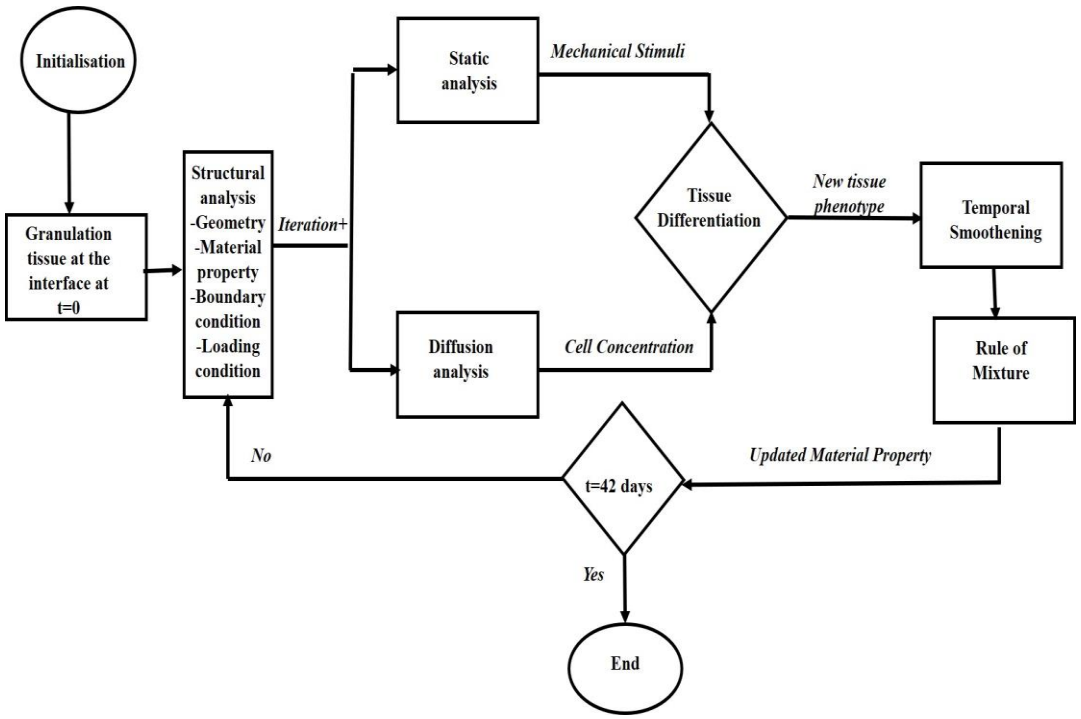


**Fig. 5.2:** Schematic overview of mechanoregulation based tissue differentiation algorithm.

The spatial estimation of the mechanoregulated tissue phenotype would instigate the existence of granulation tissue along with newly differentiated tissue at any instance in time (Ghosh *et al*. 2020). The effective tissue material properties (Young's modulus, E and Poisson's ratio, ν) were estimated numerically following a rule of mixture given by Eqs. 5.2 and 5.3:

$$E_{n+1}=\left(\frac{C_{max}-C_{min}}{C_{max}}\right)_n E_{granulation}+\left(\frac{C_{tissue}}{C_{max}}\right)_n E_{tissue} \quad (5.2)$$

$$\nu_{n+1}=\left(\frac{C_{max}-C_{min}}{C_{max}}\right)_n \nu_{granulation}+\left(\frac{C_{tissue}}{C_{max}}\right)_n \nu_{tissue} \quad (5.3)$$

where, $E_{n+1}$ and $\nu_{n+1}$ are the resulting Young's modulus and Poisson's ratio of the newly formed tissue after $n^{th}$ iteration; $E_{granulation}$ (also $\nu_{granulation}$) and $E_{tissue}$ (also $\nu_{tissue}$) are the material properties of the granulation tissue and the newly formed tissue phenotype respectively; $c_{max}$ and $c_{tissue}$ are the maximum cell concentration assumed to be unity and the actual element-specific cell concentration. The temporal smoothening method was introduced to reduce numerical uncertainty due to abrupt variation in

material properties following each iteration (Lacroix and Prendergast 2002a, Lacroix and Prendergast 2002b). This method updates the material properties of the newly formed tissue by averaging local material properties over the previous 10 estimated material property values given by Equations. 5.4 and 5.5 (Dickinson *et al.* 2012, Mukherjee and Gupta 2016, Ghosh *et al.* 2020):

$$E_{n+1,\ smoothened}=\frac{1}{10}\sum_{i=n}^{n-9} E_i \quad (5.4)$$

$$\nu_{n+1,\ smoothened}=\frac{1}{10}\sum_{i=n}^{n-9} \nu_i \quad (5.5)$$

**Table 5.2:** Predicted tissue phenotype material properties and the mechanical stimulus based on different mechanoregulation algorithm (Carter *et al*. 1988, Claes and Heigele 1999, Lacroix and Prendergrast 2002a, Isaksson *et al.* 2006, Mehboob *et al*. 2017, Mehboob *et al*. 2020, Ghosh *et al.* 2020, Mohendas *et al.* 2021).

| **Tissue phenotype** | **Young's modulus (MPa)** | **Poisson's ratio** | **Deviatoric strain+ Hydrostatic pressure** | | **Deviatoric strain only** |
|---|---|---|---|---|---|
| | | | **Strain stimulus (in %)** | **Hydrostatic Pressure stimulus (in MPa)** | **Strain stimulus (in %)** |
| Granulation tissue | 1 | 0.167 | - | - | - |
| Fibrous tissue | 2 | 0.167 | - | >0.15 | >0.05 |
| Cartilage | 10 | 0.167 | >5<br><-5<br>>15<br><-15 | >-0.15<br>>-0.15<br><-0.15<br><-0.15 | 0.025 to 0.05 |
| Immature bone | 1000 | 0.3 | -15 to +15 | <-0.15 | 0.0005 to 0.025 |
| Mature bone | 6000 | 0.3 | -5 to +5 | -0.15 to +0.15 | 0 to 0.00005 |

Claes and Heigele (1999) reported that local mechanical signals at the granulation tissue computed as hydrostatic pressure and deviatoric strain are responsible for the differentiation of MSCs into fibroblasts, chondrocytes, osteoblasts (Barry 2003, Isaksson *et al*. 2006a, Ghosh *et al.* 2022a). On reaching maturity, the new phenotypes would convert into fibrous tissue, cartilage and bone (Claes and Heigele 1999, Ghosh *et al*. 2020). This study investigated two mechanoregulation theories (Table 5.2). The first category was the theory used in earlier literature incorporating deviatoric strain and

hydrostatic pressure (Claes and Heigele 1999, Dickinson *et al.* 2012, Mukherjee and Gupta 2016, Ghosh *et al.* 2020), hereafter named hydrostatic pressure-deviatoric strain theory (HPDST). The second category, hereafter named deviatoric strain theory (DST) considered deviatoric strain only (Isaksson *et al*. 2006a, Mehboob *et al*. 2017, Mehboob *et al*. 2020). Previous literature suggested that deviatoric strain alone could be used for predictive modelling of tissue differentiation (Isaksson *et al*. 2006b, Isaksson 2012).

The mechanoregulatory tissue-differentiation algorithm applied in the study was developed using a custom MATLAB script (MATLAB 2017a, The MathWorks Inc., Natrick,MA,USA). A master-batch script (DOS) was developed to consecutively launch ANSYS module (structural analysis) and MATLAB module (tissue differentiation computation) in each iteration. The simulation was set for 42 iterations indicating 6-weeks post operation in a 64-bit Windows 2010 server with Intel® Core™ i7-9700U 8-core CPU, 32GB RAM.

### 5.3 Result

#### 5.3.1 Spatial distribution of tissue phenotype according to mechanoregulation-based algorithm

During the process of mechanoregulation-based tissue differentiation, various types of tissues were formed, ranging from fibrous tissue to bone. The mechanoregulation-based algorithms predicted the tissue phenotypes. The first approach (HPDST) combined hydrostatic pressure and deviatoric strain to predict peri-prosthetic tissue differentiation. The second mechanoregulation theory (DST) employed only deviatoric strain for predicting tissue phenotypes. Figs. 5.3 and 5.4 shows the spatial distribution of tissue phenotype considering the two types of mechanoregulation algorithms with two different loading scenarios for the three types of expandable pedicle screws over 6 weeks.

In the HPDST model (Fig. 5.3), immature bone tissue was formed towards the host bone site within the first week, with some traces of mature cartilage. Over time, immature bone is converted to intermediate bone tissue and some mature bone tissue. After 6 weeks, the mature bone formation was found to be most in type 3 and least in type 1 expandable pedicle screws for both loading cases.

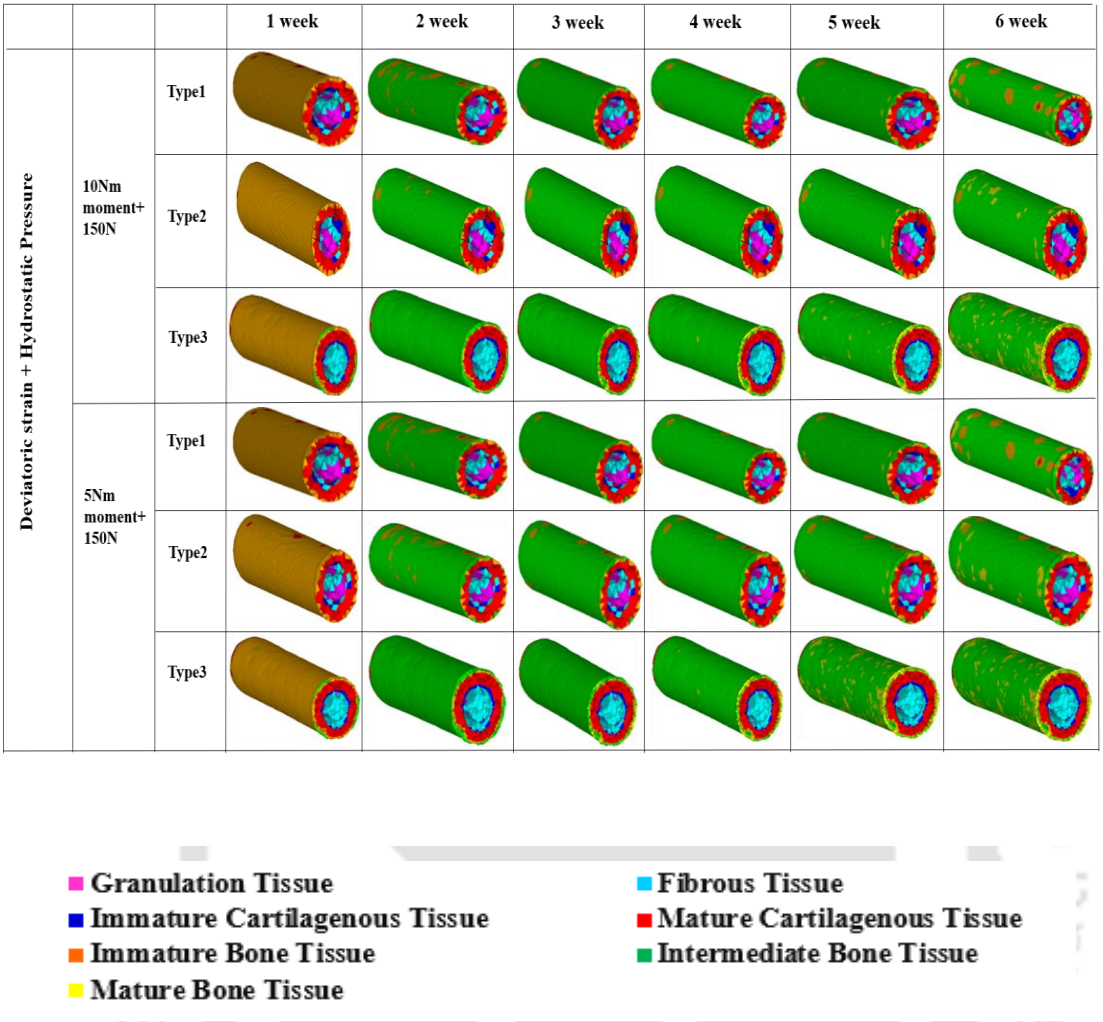


**Fig. 5.3:** Spatial distribution of tissue on-growth for three types of expandable pedicle screws for two loading cases considering deviatoric strain and hydrostatic pressure after 6 weeks of healing.

The spatial plots obtained using DST (Fig. 5.4) showed a similar trend to HPDST, except for type 2 expandable pedicle screws. Unlike other screw designs, type 2 screw showed predominantly mature cartilage at the host bone site after the first week, followed by significant immature bone tissue and some traces of mature bone tissue after $6^{th}$ week. However, in all the cases, predominantly fibrous tissue, undifferentiated stem cells and immature cartilage were observed towards the implant site.

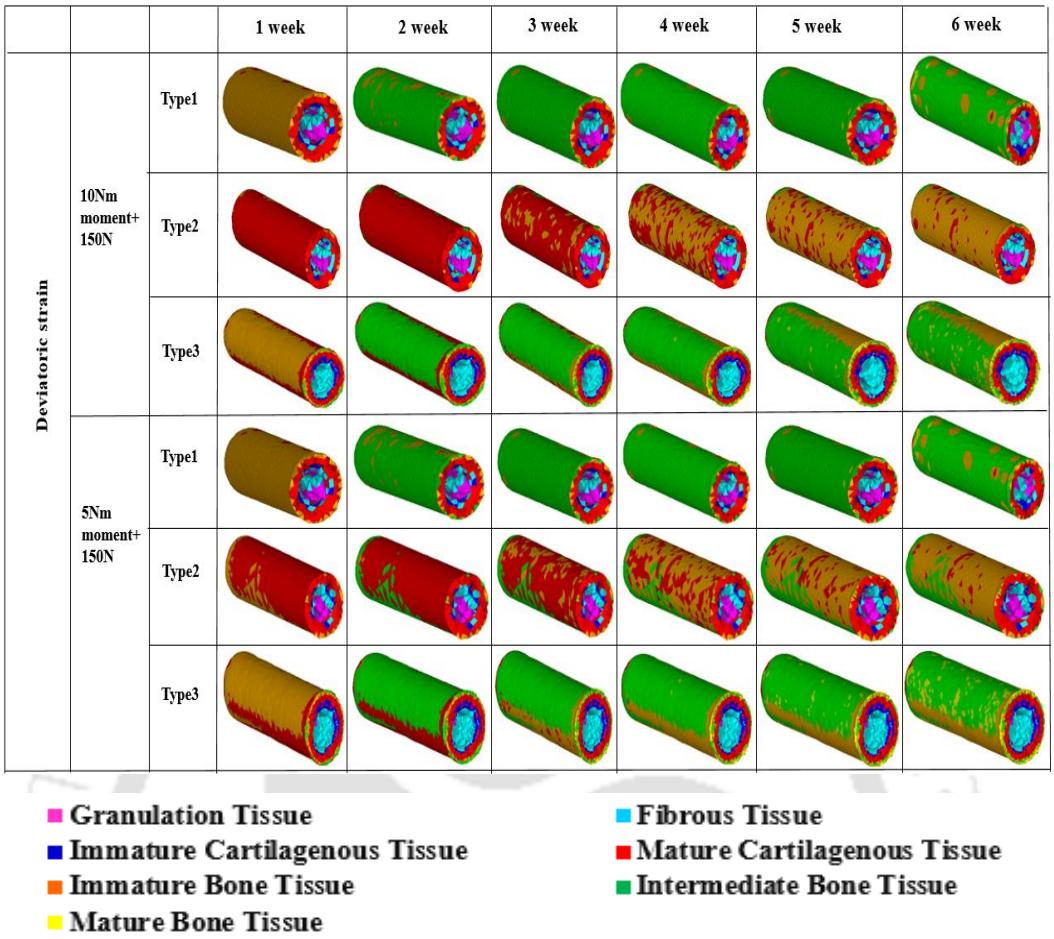


**Fig. 5.4:** Spatial distribution of tissue on-growth for three types of expandable pedicle screws for two loading cases considering deviatoric strain after 6 weeks of healing.

### 5.3.2 Temporal Distribution Around Tissue Phenotype

It is crucial to estimate the tissue phenotype developed in percentage over the time of bone healing. Figs. 5.5 and 5.6 showed the progressive distribution of tissue phenotypes, week by week, starting from the initial day of simulation. Originally, undifferentiated MSCs were present in the granulation tissue.

In Fig. 5.5, bone on growth was highest in type 3 (~28.79 %), followed by type 2 (~19.73 %) and type 1 (~12.84 %) under load case 2. A similar trend in bone growth was observed in Fig. 5.6. When considering deviatoric strain, the maximum bone growth was predicted for type 3 screws (~21.63 %), with type 1 (~12.82%) and type 2 (~12.91%) exhibiting almost identical growth under load case 2. Regarding cartilage formation, type 2 screws showed the highest chondrocyte (cartilage) formation (~57.87%), followed by type 1 (~55.47%) and type 3 (~54.04%) under load case 1(DST). Bone formation percentages for load case 1 (DST) were ~12.82% for type 1,

~11.21% for type 2, and ~21.05% for type 3. For load case 1 (HPDST), the bone formation was ~12.84%, ~18.81%, and ~28.22% for type 1, type 2, and type 3 screws, respectively.

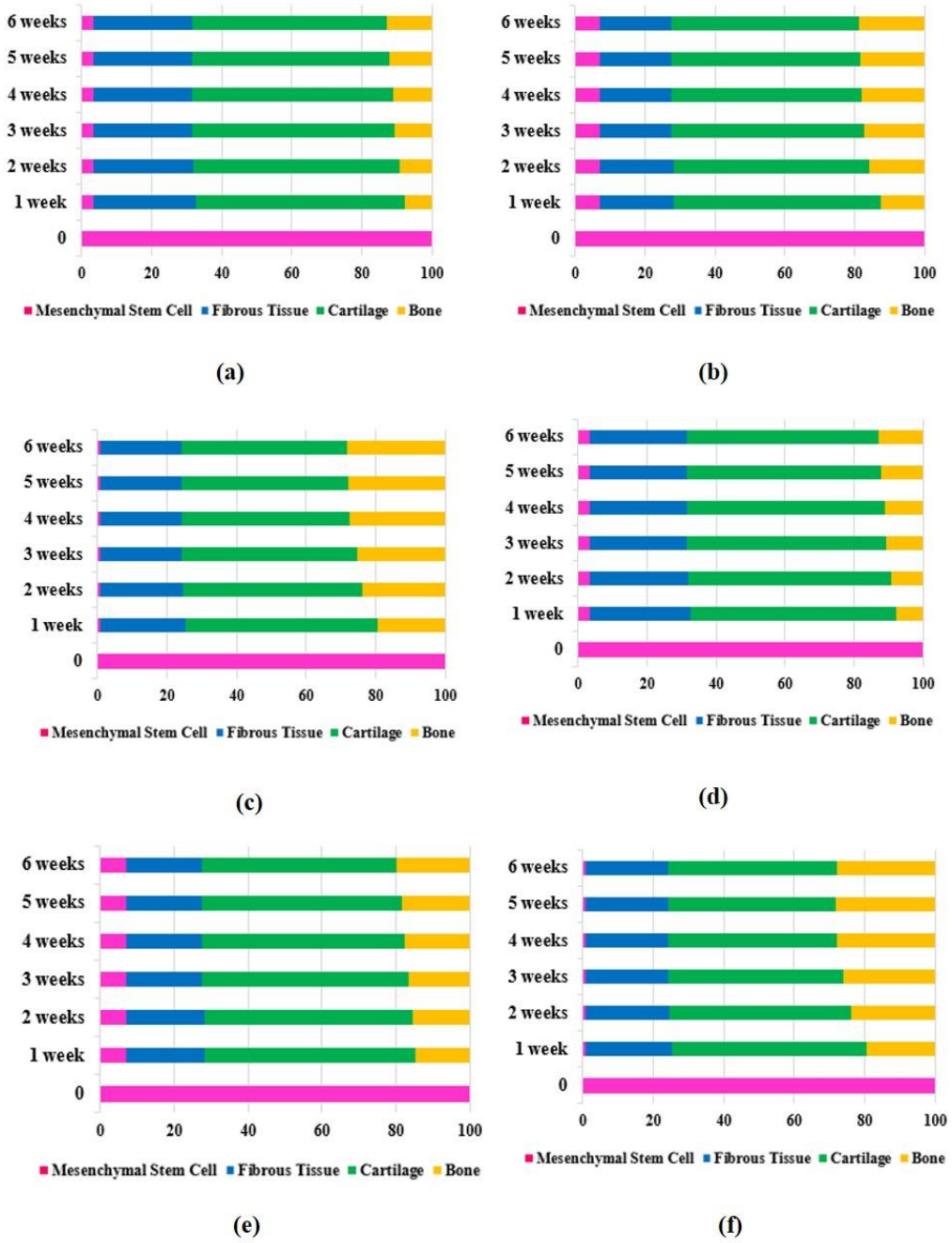


**Fig. 5.5:** Influence of mechanical stimulus (HPDST) on tissue growth for loading-10Nm,150N (a)type 1 (b)type 2 (c) Type 3, 5Nm,150N (d)type 1 (e)type 2 (f) Type 3.

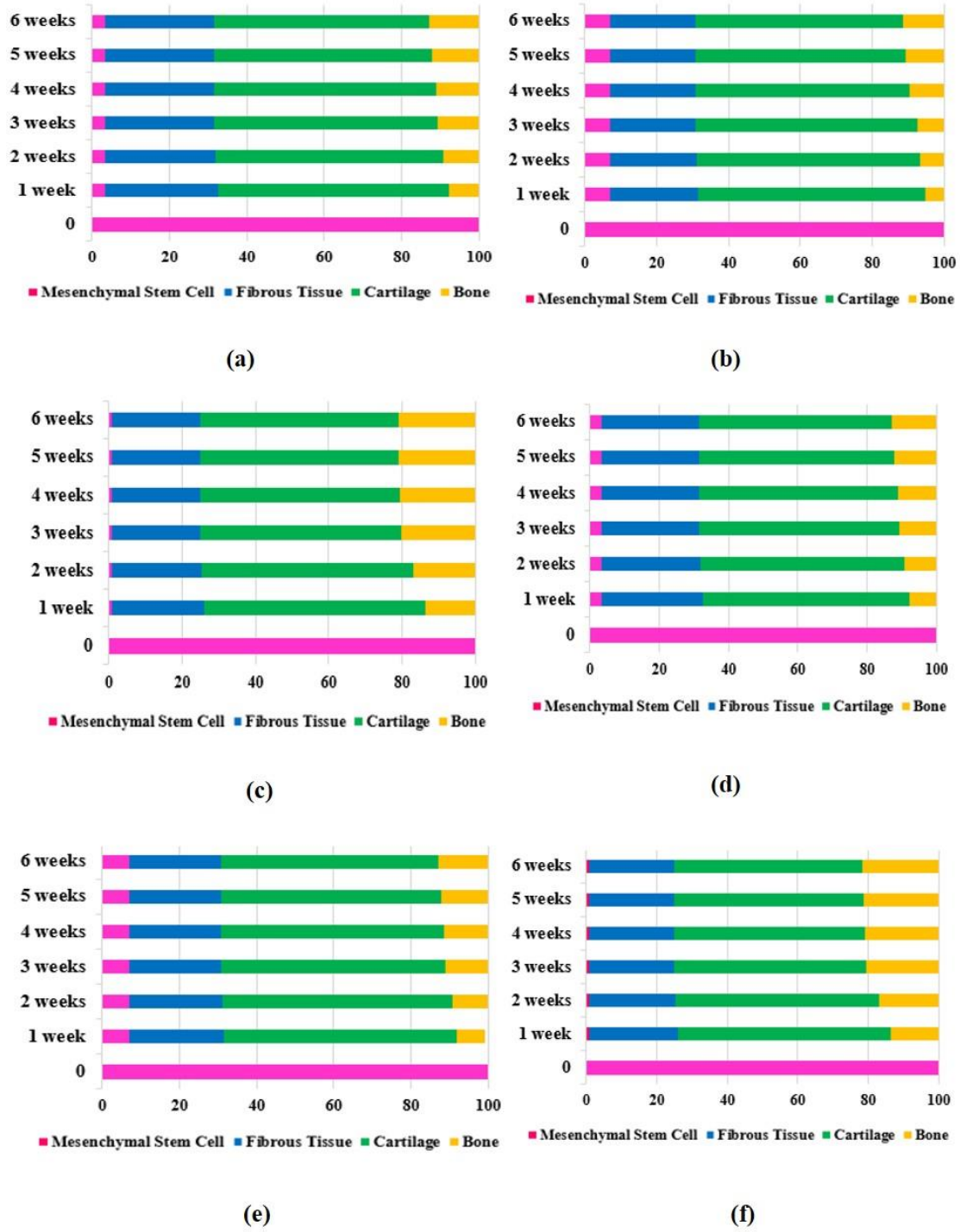


**Fig. 5.6:** Influence of mechanical stimulus (DST) on tissue growth for loading - 10Nm,150N (a)type 1 (b)type 2 (c) Type 3, 5Nm,150N (d)type 1 (e)type 2 (f) Type 3.

For both mechanoregulation algorithms, the formation of bone mesenchymal cells (BMSCs) and fibrous tissue was observed. Type 1 screws showed ~3.46 % BMSCs and ~28.23 % fibrous tissue, type 2 showed ~7.18 % BMSCs and ~23.74% fibrous tissue

and type 3 showed ~0.69 % BMSCs and ~24.22% fibrous tissue under load case 1. The cartilage formation after 6 weeks was highest for all screw types under load case 1(HPDST), with ~55.47% for type 1, ~53.56% for type 2, and ~47.38% for type 3. In load case 2 (HPDST), cartilage formation remained relatively high at ~55.47%, ~52.64%, and ~46.81% for the three screw types, respectively.

This summary of tissue formation highlights the varying responses of the bone-implant interface under different loading conditions, with notable differences in bone and cartilage formation depending on the screw type and the mechanoregulation approach.

### 5.3.3 Average Young's modulus of tissue phenotype

The average Young's modulus of the tissue phenotype over a time of 6 weeks is presented in Fig. 5.7 for the two load cases. The Young's modulus for each tissue phenotype was calculated and then the average value was assessed to estimate the overall stiffness of the interfacial tissue. The tissue stiffness was found to be highest for type 3 expandable pedicle screws using both HPDST (~392 MPa) and DST for both loading cases (~304 MPa). The type 1 expandable pedicle screw had tissue stiffness of ~174 MPa for both loading cases considering the two mechanoregulation-based algorithms. Considering type 2 screws with HPDST showed tissue stiffness of ~264 MPa for the two load cases. The least stiffness was seen for type 2 expandable pedicle screws with deviatoric strain only (~158 MPa) for load case 1.

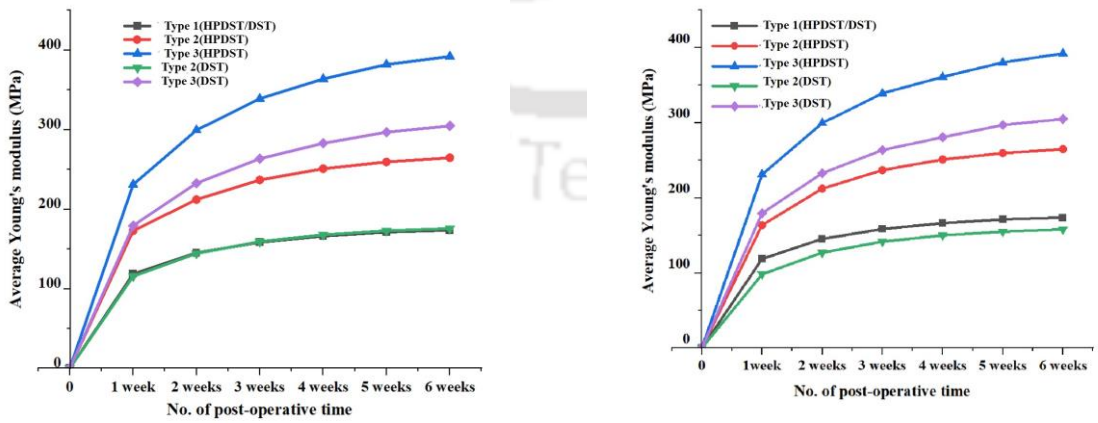


**Fig. 5.7:** Influence of tissue stiffness based on mechanical stimulus at the bone-implant interface for loading- (a)10Nm,150N (b)5Nm,150N.

### 5.4 Discussion

The study aimed to evaluate the osteogenesis around three distinct expandable pedicle screws within a model that mimics the cancellous bone in a single vertebral body. Two mechanoregulation-based tissue differentiation algorithms were employed to predict tissue differentiation around the expandable pedicle screws.

The first algorithm utilised two different mechanical stimuli viz. deviatoric strain and hydrostatic pressure, that dictates the tissue differentiation (Carter *et al.* 1988, Claes and Heigele 1999, Lacroix and Prendergast 2002b, Mukherjee and Gupta 2017, Ghosh *et al.* 2020). The second algorithm was based on deviatoric strain only (Isaksson *et al.* 2006a, Isaksson 2012, Kim *et al*. 2012b, Son *et al.* 2014). The magnitudes of each stimulus are chosen from the earlier models developed (Dickinson *et al.* 2012, Ghosh *et al*. 2020, Isaksson *et al*. 2006a). Both models applied identical loading conditions to the three types of screws to determine the optimal screw design for promoting osteogenesis and to assess the sensitivity of each differentiation algorithm in predicting bone growth.

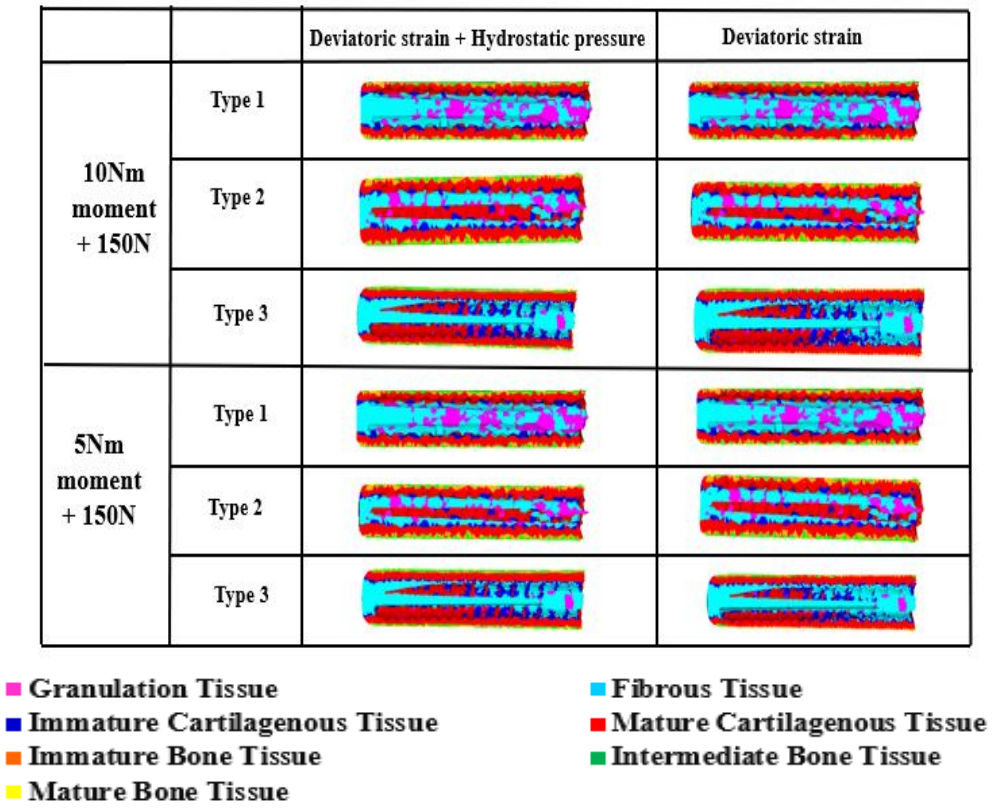


**Fig. 5.8:** Spatial distribution (cross-sectional view) of tissue on-growth for three types of expandable pedicle screws for two loading cases considering deviatoric strain+ hydrostatic pressure (HPDST) and deviatoric strain (DST) after 6 weeks of healing.

Figs. 5.3 and 5.4 illustrated the spatial tissue distribution over six weeks for both loading cases and mechanoregulation algorithms. Considering HPDST, immature bone tissue appeared after the 1st week, along with traces of intermediate bone tissue and mature cartilaginous tissue (Sulaiman *et al.* 2024). Although significant cartilaginous tissue formed over time, immature bone tissues differentiated slowly, eventually maturing as the healing was processed. The DST model also showed immature bone tissue and mature cartilage post-first week. The early formation of immature bone suggests that osteogenesis is governed by intramembranous ossification. However, the presence of substantial cartilaginous tissue indicates inhibition of endochondral ossification due to constant compressive load (150 N) applied at the bone's top surface (Chao and Inoue 2003). Since the peri-prosthetic osteogenesis follows similar phases of bone fracture healing, i.e. both ossification processes endochondral and intramembranous ossification are feasible (Sulaiman *et al*. 2024, Ghosh *et al*. 2023). After 6 weeks, both type 1 and type 3 screws exhibited bone formation (mostly intermediate with some amount of mature and immature bone). However, type 2 screws showed a concentration of immature bone tissue with some intermediate bone under load case 2 and mature cartilage in case of load case 1. This indicated that similar loading scenarios with different magnitudes can lead to different tissue formation in the long-term healing period. Therefore, load-controlled optimally designed screws are essential for better osteogenesis.

Fig. 5.8 presented the spatial distribution surrounding the implant site post 6 weeks. The front end (1.5 mm pitch) of type 2 screws had less fibrous tissue and more cartilaginous tissue than the front end of type 3 screws (2 mm pitch). The granulation tissue in type 2 was more towards the back side (2mm pitch), indicating less differentiation to osteogenic cells due to higher pitch. The central portion of type 2 had more mature cartilage whereas the similar region in type 3 screw showed more fibrous tissue. This suggests that the areas with a 1.5 mm pitch are differentiated more than the area having a 2 mm pitch (Ghosh *et al*. 2020). These findings corroborate with the earlier studies that reported that screws with smaller pitch increase screw surface area and eventually improve bone-implant stability (Orisi *et al*. 2012).

This might explain the reason behind the differentiation of most of the MSCs of type 3 expandable pedicle screws into fibrous tissue, cartilage and bone. However, type 1 screw having a constant 1.5 mm pitch exhibited less differentiation compared to the

dual-threaded screws. Thus, dual-threaded screws might offer better anchorage than single-threaded screws (Wu *et al*. 2023). The increased bone growth around dual-pitch screws indicates a higher probability of cell adhesion (Anselme 2000).

After 6 weeks of bone healing, for the three types of expandable pedicle screws, the predicted bone growth percentage varied from ~13 % to ~29 % and the cartilage percentage ranged from ~47 % to ~55 % considering the HPDST model. However, considering the DST model, the bone formation percentage ranged from ~11 % to ~22 % and cartilage formation from ~53 % to ~58 %. These results corroborate an earlier study by Ghosh *et al.* (2020) where the bone formation variation was 11-25 %. Another study predicted 20-50 % bone formation around an uncemented femoral implant (Mathai and Gupta 2021b). The bone percentage change of 5-15 % was observed for different kinds of loading in the case of normal walking for non-textured femoral stem (NTFS) (Ghosh *et al.* 2022a). The present study also observed that MSCs differentiated into fibrous tissue in the initial two weeks, with no further differentiation of both of these cells/tissues observed thereafter. The amount of MSC and fibrous tissue varied for the three types of expandable pedicle screws. The type 1 screw exhibited the highest volume of fibrous tissue, suggesting a greater probability of aseptic loosening (Ghosh *et al.* 2020). Overall, the percentage of MSCs differentiated to both cartilage and bone for the three types of expandable pedicle screws are ~68 %, ~72 %, ~75 % (with HPDST) and ~68 %, ~70 %, ~75 % (with DST) for type 1, type 2 and type 3 respectively.

Fig. 5.7 showed the change in average tissue stiffness over the post-operative days for both the loading cases and mechanoregulation algorithms. There was a gradual increase in tissue stiffness with time, which indicated enhanced stability of the bone-implant interface (Son *et al.* 2014, Mukherjee and Gupta 2017, Tarlochan *et al.* 2018, Mathai and Gupta 2021b, Sulaiman *et al*. 2024). As bone formation progresses, the load-bearing capacity of the implant increases due to increased stiffness (Mori *et al.* 2024). Although HPDST showed better load-carrying capacity compared to DST for type 3 expandable pedicle screws, both mechanoregulation theories predicted type 3 screw to be the most efficient design for promoting osteogenesis. The mechanoregulation algorithm with deviatoric strain only (DST) showed lower load-bearing capacity.

The results indicated that the loading condition showed a slight impact on osseointegration at the implant surface (Mukherjee and Gupta 2017). Figs. 5.5 and 5.6 demonstrated that increased load reduced osseointegration (Ghosh *et al.* 2022a). This might be because a higher load (moment) increases the probability of aseptic loosening, resulting in a lower rate of osteoblast formation (Ghosh *et al*. 2020). The direct influence of moment application on bone growth was not reported earlier. However, shear and tensile load decreased bone healing thus indicating reduced osseointegration (Ma *et al.* 2023).

The type of osteogenesis indicated the clinical significance. Contact osteogenesis involves bone formation on the implant surface moving towards the host bone, creating bone bridges and distant osteogenesis engrosses new bone formation on the existing bone surface progressing towards the implant surface (Kim *et al.* 2021). The present study showed the evolution towards the longstanding secondary stability of the prosthesis (Kuzyk and Schemitch 2011). A previous study by Choi *et al.* (2017) conveyed that contact and distance osteogenesis might occur concurrently and thus are not mutually exclusive. This was established in a previous study for non-textured femoral stem (NTFS) (Ghosh *et al.* 2022a). This study showed favourable conditions for osteogenesis at the edge of the host bone than in the locality of the implant surface and thus developed distance osteogenesis. The primary cause of the absence of contact osteogenesis was because of the non-existence of a micro-roughened surface over the smooth macro-textures of the expandable pedicle screws (Ghosh *et al*. 2020). Many of the preceding studies observed distant osteogenesis (Sennerby *et al*. 1993, Liu and Niebur 2008, Puthumanapully 2010, Ghosh *et al*. 2020, Causay *et al.* 2021, Ghosh *et al.* 2022a).

There seems to have certain limitations while performing the study. The recent study is a simplified model that did not incorporate the full complexity of a realistic lumbar vertebra model, including elements like cage and ligaments (Postigo *et al.* 2014, Pradeep *et al.* 2024). The lack of a detailed micro-CT dataset would limit its ability to capture the complex interactions between screws and surrounding bones. This study was limited to axial loading and extension movement, without considering other forces like shear stress or cyclic loading (Seng *et al*. 2018). The reason behind this simplification was that the moment direction did not have any influence since it was considered a cube. Nevertheless, the full-scale expandable pedicle screw implanted

vertebra model would assess the mechano-biological algorithm in a better way. Yet, that would involve lots of complexity to run the arduous multi-scale assessment which might need parallel computing and thus would be expensive (Ghosh *et al.* 2020). Patient-specific models were not utilized, which could provide more personalized insights into implant performance (Ghosh *et al.* 2022a, Mathai and Gupta 2021b). The mechanoregulation-based tissue differentiation algorithm has considered a constant diffusion rate for the MSCs whereas, in reality, the diffusion rate varies throughout the bone-implant interface (Ghosh *et al*. 2022a).

This model did not deliberate porous coating of the implant surface, bone density, cellular activities, osteogenic and chondrogenic growth factors (Ghosh *et al*. 2021b, Mathai and Gupta 2021b, Mohendas *et al.* 2021). Further, the combination of bone growth along bone remodelling would give better outcomes of connective tissue growth (Mukherjee and Gupta 2016, Chanda *et al*. 2020). The cell-phenotype-based mechanoregulation algorithm would be beneficial for exhaustive cellular response with subsequent tissue differentiation (Issakson *et al.* 2008a, Mukherjee and Gupta 2016). The use of another constant pitch-based screws would be helpful for comparison with type 1 screws. This study considered two mechanoregulation algorithms and for both the deviatoric strain values are different which might create variation in results.

### 5.5 Summary of the findings

The study provides valuable insights into the influence of pedicle screw design and loading conditions on osteogenesis at the bone-implant interface. The findings emphasize the importance of optimizing screw design, particularly thread pitch, and loading conditions to enhance the implant stability and promote effective bone healing. The results indicated the usefulness of dual-threaded expandable pedicle screws over conventional single-threaded ones under both HPDST and DST mechanoregulation algorithms. The percentage variation of bone growth for HPDST and DST are ~13-29 % and ~11-22 % respectively, for the three types of expandable pedicle screws. The results estimated comparatively higher bone growth for both loading cases considering HPDST. Nonetheless, a clinical assessment would be more beneficial to get more realistic insights. Future research incorporating more complex models using micro-CT data and additional mechanical forces is recommended to build upon these findings. Further, to diminish the failure associated with stress shielding and interfacial stresses,

future design optimization-based studies would be helpful, which might provide a route to minor modifications of the screw redesign for improved osteogenesis.

# Chapter 6

## Conclusions and Future Scope of Work

### 6.1 Introduction

Spinal fusion is considered to be the gold standard and the most effective surgical treatment for various types of spine-related issues such as degenerative disc diseases, spondylolisthesis, spondylolysis, and spondylosis that cause chronic lower back pain. Pedicle screws are most commonly used for posterior spinal fixation, by providing stability, pain reduction, proper anatomical alignment and finally improving life quality. However, complications like failed bony fusion, aseptic loosening, screw pullout, screw breakage, dispositioning of screws, and pedicle fracture post-surgery lead to revision surgery.

To diminish the issues specifically related to loosening, the expandable pedicle screws were introduced with improved anchorage capacity through an increase in screw diameter/length and an enhanced screw-bone interface. Clinical results showed improvement in biomechanical fixation strength in bone of specifically compromised quality with expandable pedicle screws than conventional pedicle screws. The expandable pedicle screws are expected to facilitate bone growth around the fins and develop long-term stability by lowering post-operative complications, mitigating strain shielding and promoting bone remodelling.

The development of a 3D model of a lumbar spine is a crucial step in analysing load transfer under various physiological loading conditions. Earlier, many numerical studies were carried out based on various factors for conventional pedicle screws but studies on expandable pedicle screws were limited. The current study aimed to investigate the immediate post-operative effect of lumbar interbody fusion instrumented with expandable pedicle screws and compared their biomechanical performance with normal pedicle screws without compromising the structural integrity.

The primary goal of the study was to develop novel expandable pedicle screws with design variations for improved pullout resistance, better bone remodelling properties and enhanced osseointegration. In this study, stress-strain failure

mechanisms have been investigated using FE analyses combined with bone remodelling simulation and compared for both normal pedicle screws and expandable pedicle screws. Three types of expandable pedicle screws were developed with various thread designs and pullout tests were performed. The extent of osseointegration on the three types of expandable pedicle screws was investigated preclinically based on mechanorgulation algorithms (HPDST and DST).

### 6.2 Significance and major contribution of the thesis

The study was focused on the design and development of expandable pedicle screws for lumbar vertebra. To achieve the primary goal, an investigation of the load transfer during physiological movements for the intact and implanted models was conducted using FE analysis. The implanted models included both conventional normal pedicle screws and expandable pedicle screws and were compared based on stress-strain data. The applied physiological loading condition included flexion, extension, torsion and lateral bending. The following are the conclusions and major contributions of the thesis.

- The FE models of intact and implanted (normal and expandable pedicle screw) FSUs of anatomically placed manufacturer-supplied CAD model of the L4-L5 vertebra was developed. Cortical and cancellous bones were separated through Boolean operations in a clinically admissible manner. The physiological loads were applied on a central node of (rigid body element RBE3) L4 vertebra and the bottom nodes of L5 were constrained. The intact model was validated by comparing ROM and mesh convergence was achieved using von Mises stress. The results indicated that the loading and boundary conditions has a substantial influence on stress-strain distribution within FSU. The implantation of both types of screws and the cage resulted in a significant (~30-100 %) change in stress distribution. The peak strain was predicted to be greater for expandable pedicle screw implanted models.
- An improved FE model of intact and instrumented with normal and expandable pedicle screw implanted L4-L5 FSU was developed from CT scan data. Heterogeneous material property based on power-law was used for cancellous bone. The influence of ligaments, and physiological loading condition on strain and strain energy density were studied for all the models. A strain energy-based bone remodelling algorithm was employed to investigate the evolutionary alteration in bone density distribution around normal and expandable pedicle

screws. In case of normal pedicle screws, 60-80 % bone apposition was seen in the L4 vertebra and 30-90 % in the L5 vertebra near the screw tip, screw insertion region in a less area and bone resorption in some other regions. Expandable pedicle screw insertion resulted in 50-75 % bone apposition in the L4 vertebra and 40-75 % in the L5 vertebra in the central anterior region, screw insertion site in a huge area. Bone apposition was substantial near the cage insertion area for both types of screws. Quantitatively huge bone apposition was observed for all regions of interest (ROIs) of the L4-L5 vertebra implanted with expandable pedicle screws.

- Three different types of expandable pedicle screws were designed with various threads and a pullout test was performed using ASTM standards on 15-grade PU foam. The results from the pullout test predicted that dual-threaded expandable pedicle screws have higher pullout strength than conventional single-threaded expandable pedicle screws. The statistical calculation using non-parametric tests (Kruskal-Wallis test) indicated significant differences between type 1 and type 3 screw groups only among the three groups of expandable pedicle screws ($z < z_{critical}$). The tests were validated by analysing stress distribution during the pullout test using ABAQUS/ explicit software. The average von Mises stress distribution of the foam for the three types of screws was found to be 17.85 MPa, 21.11 MPa, 25.83 MPa respectively. The numerically projected maximum pullout strengths of three expandable pedicle screws were 602.31 N, 705.77 N and 838.27 N respectively.

- The study further explored the spatial distribution of evolutionary bone growth around the three types of expandable pedicle screws using mechanoregulation algorithms (HPDST and DST). The results indicated that for the three types of expandable pedicle screws, the percentage bone growth prediction was varying from around 13 to 29 % and cartilage percentage change was between 47 to 55 % while considering HPDST. However, considering DST, the percentage deviation of bone and cartilage formation was found to be in the range of around 11 to 22 % and 53 to 58 % respectively. It was observed that the area having 1.5 mm pitch is differentiated more than the area having 2 mm pitch, thus indicating screws with smaller pitch increases screw surface area and eventually improve bone-implant stability.

The loading conditions bore marginal influence on the extent of osseointegration on the implant surface. The results from both the algorithms indicated the usefulness of dual-threaded expandable pedicle screws over conventional single-threaded ones.

### 6.3 Limitations of the study

The study focused on the design and development of expandable pedicle screws as an alternative to conventional pedicle screws using preclinical analysis and some pullout tests. However, some limitations remain during the study.

- The study used FE models of L4-L5 vertebra conducted based on patient-specific data. It's crucial to acknowledge that there is substantial variety in bone morphometric boundaries around diverse ethical groups. A multi-spine analysis could provide better insights into the variation of load transfer.
- The bones and intervertebral disc (IVD) were anticipated to possess linear elastic and isotropic material properties. However, they are both anisotropic and viscoelastic. The time-dependent simulations were absent and could limit the understanding of long-term biomechanical behaviour.
- The study did not consider dynamic loading and muscle forces that would significantly influence spinal biomechanics. Muscle force and dynamic simulation incorporation would have enhanced the accuracy of load transfer predictions.
- The potential cancellous bone damage due to the insertion of pedicle screws specifically expandable pedicle screws were not analysed. However, investigation of damage impact on bone mechanical properties and fracture risk are essential.
- During pullout tests, high-density synthetic foam blocks were not analysed. The synthetic foam blocks do not replicate the morphological and material heterogeneity of human bone.
- The lack of a detailed micro-CT dataset would limit the ability to capture the complex interactions between expandable pedicle screws and surrounding bones.

### 6.4 Scope for Future Research

Refinement of future design and clinical applicability of expandable pedicle screws should be incorporated in multiple directions.

- Future studies should incorporate complex loading cases like cyclic loading, stair climbing, running and jogging to get better insights.
- The future scope of the study includes integrating local bone property variation due to insertion-induced damage for a more comprehensive investigation. The long-term effects of expandable pedicle screws on bone integrity and implant stability under different physiological loading conditions can be explored.
- Including external bone remodelling might offer an additional impression of implant-induced bone adaptation. To gain an idea of the degree of osseointegration with the implant-bone interface and its subsequent outcome on load transfer and bone remodelling around the implant, a separate study on evolutionary bone ingrowth simulation would be essential.
- Future research should expand to include models with varying bone densities, particularly osteoporotic conditions and validate the findings with data from older or trauma patients. Personalised, patient-specific models and simulations of fractured vertebrae could improve clinical applicability.
- The inclusion of insertion techniques of the pedicle screws would help in assessing the risks associated with pedicle fracture during insertion. Using different grades of PU foam for pullout tests can enhance understanding of pullout resistance under varying bone densities.
- Integrating mechanoregulation models (HPDST and DST) with bone microstructural characteristics, such as porosity and trabecular thickness can enhance predictive accuracy. Advancements in computational power and imaging techniques, such as high-resolution three-dimensional imaging modalities, can facilitate the inclusion of these complex microstructural features into the models leading to improved orthopaedic implant design.
- Machine learning (ML) in combination with FEA can facilitate a data-driven optimization of expandable pedicle screw design. ML models

trained on FE results can predict biomechanical performance better, aiding in the development of optimized screw design,

- Finally, in vivo evaluations and clinical trials would validate the safety and effectiveness of the proposed expandable pedicle screw designs before commercial implementations.

# References


Adams MA (2004). Biomechanics of back pain. Acupunct Med. 22(4):178-88

Aghajanloo M, Abdoli A, Poorolajaj J, Abdolmaleki S (2023). Comparison of clinical outcome of lumbar spinal stenosis surgery in patients with and without osteoporosis: a prospective cohort study. J. Orthop. Surg. Res. 18:443.

Aguirre JI, Castillo EJ, Kimmel DB (2021). Biologic and pathologic aspects of osteocytes in the setting of medication-related osteonecrosis of the jaw (MRONJ). Bone153:116168.

Alanay A, Vyas R, Shamie AN, Sciocia T, Randolph G, Wang JC (2007). Safety and efficacy of implant removal for patients with recurrent back pain after a failed degenerative lumbar spine surgery. J Spinal Disord Tech 20(4):271–277.

Alexandru D and So W (2012). Evaluation and Management of Vertebral Compression Fractures. Perm J 16(4):46-51.

Alizadeh M, Kadir MRA, Fadhli MM, Fallahiarezoodar A, Azmi B, Murali MR, Kamarul T (2013). The use of X-shaped cross-link in posterior spinal constructs improves stability in thoracolumbar burst fracture: A finite element analysis. J. Orthop. Res. 31(9):1447–1454.

Altman GH, Horan RL, Martin I, Farhadi J, Stark PR, Volloch V, Richmond JC, Vaunjak-Novakovic G, Kaplan DL (2002). Cell differentiation by mechanical stress. FASEB journal,16(2):270-2.



Alexandru D and So W (2012). Evaluation and Management of Vertebral Compression Fractures. Perm J 16(4):46-51.

Alizadeh M, Kadir MRA, Fadhli MM, Fallahiarezoodar A, Azmi B, Murali MR, Kamarul T (2013). The use of X-shaped cross-link in posterior spinal constructs improves stability in thoracolumbar burst fracture: A finite element analysis. J. Orthop. Res. 31(9):1447–1454.

Altman GH, Horan RL, Martin I, Farhadi J, Stark PR, Volloch V, Richmond JC, Vaunjak-Novakovic G, Kaplan DL (2002). Cell differentiation by mechanical stress. FASEB journal,16(2):270-2.



Amaritsakul Y, Chao C.K, Lin J (2014). Comparison study of the pullout strength of conventional spinal pedicle screws and a novel design in full and backed-out insertion using mechanical tests. Proc. IMeche Part H: J Engineering in medicine 228(3): 250-257.

Ambati DV, Wright EK, Lehman RA, Kang DG, Wagner SC, Dmitriev AE (2014). Bilateral pedicle screw fixation provides superior biomechanical stability in transforaminal lumbar interbody fusion: A finite element study. Spine 15(8): 1812–1822.

Andreev D, Liu M, Weidner D, Kachler K, Faas M, Grüneboom A, Schlötzer-Schrehardt U, Muñoz LE, Steffen U, Grötsch B, Killy B, Krönke G, Luebke AM, Niemeier A, Wehrhan F, Lang R, Schett G, Bozec A (2020). Osteocyte necrosis

triggers osteoclast-mediated bone loss through macrophage-inducible C-type lectin. J Clin Invest. 130(9):4811-4830.

Andreykiv A, van Keulen E, Prendergast PJ (2008a). Simulation of fracture healing incorporating mechanoregulation of tissue differentiationand dispersal/proliferation of cells. Biomech Model Mechanobiol. 7:443-461.

Andreykiv A, Keulen Fv, Prendergast P (2008b). Computational Mechanobiology to Study the Effect of Surface Geometry on Peri-Implant Tissue Differentiation. J. Biomech. Eng. 130:051015-1.

Angele P, Yoo JU, Smith C, Mansour J, Jepsen KJ, Nerlich M, Johnstone B (2003). Cyclic hydrostatic pressure enhances the chondrogenic phenotype of human mesenchymal progenitor cells differentiated in vivo. J. Orthop. Res. 21(3):451-7.

Anselme K (2000). Osteoblast adhesion on biomaterials. Biomater. 21:667-681.

Arslan AK, Demir T, Ormeci MF, Camuscu N, Tureyen K (2013). Postfusion pullout strength comparison of a novel pedicle screw with classical pedicle screws on synthetic foams. Proc. IMeche Part H: J Engineering in medicine. 227(2):114-119.

Ashman RB, Cowin SC, Van Buskirk WC, Rice JC. A continuous wave technique for the measurement of the elastic properties of cortical bone. J Biomech. 17(5):349-61.

Atlas SJ, Deyo RA (2001). Evaluating and Managing Acute Low Back Pain in the Primary Care Setting. J. Glob. Inf. Manag 16:120–131.

Aycan MF, Tolunay T, Demir T, Yaman ME, Usta Y (2017). Pullout performance comparison of novel expandable pedicle screw with expandable poly-ether-ether-ketone shells and cement augmented pedicle screws. ProcIMechEPart H: J Engineering in Medicine. 231(2):169–175.

Ayturk UM, Puttlitz CM (2011) Parametric convergence sensitivity and validation of a finite element model of the human lumbar spine. Comput. Methods Biomech. Biomed. Eng14(8): 695–705.

Badilatti SD, Chridten P, Levchuk A, Marangalou JH, Rietbergen Bv, Parkinson I, Muller R (2016). Large-scale microstructural simulation of load-adaptive bone remodeling in whole human vertebrae. BiomechModel Mechanobiol. 15:83-95.

Bagge M (2000). A model of bone adaptation as an optimization process. J Biomech. 33:1349-1357.

Barry FP (2003). Biology and clinical applications of Mesenchymal Stem Cells. Birth Defects Res (Part C). 69:250-256.

Bashkuev M, Reitmaier S, Schmidt H (2018). Effect of disc degeneration on the mechanical behavior of the human lumbar spine: a probabilistic finite element study. Spine J. 18(10):1910-1920.

Beaupre GS, Orr TR, Carter DR (1990a). An approach for time-dependent bone modeling and remodeling application: a preliminary remodeling simulation. J Orthop res. 8(5):662-70.

Beaupre GS, Orr TR, Carter DR (1990b). An approach for time-dependent bone modeling and remodeling application-Theoretical Development. J Orthop Res. 8(5):651-61.

Beatty, S. (2018). We need to talk about lumbar total disc replacement. International Journal of Spine Surgery, 12(2), 201–240

Belytschko T, Kulak RF, Schultz AB (1974). Finite element stress analysis of an intervertebral disc. J. Bopmech, 7(3): 277-85.

Bereczki F, Turbucz M, Kiss R, Eltes PE, & Lazary A (2021). Stability Evaluation of Different Oblique Lumbar Interbody Fusion Constructs in Normal and Osteoporotic Condition – A Finite Element Based Study. Frontiers in Bioengineering and Biotechnology, 9: 749914.

Bianco RJ, Arnoux PJ, Wagnac E, Eng P, Thiong JMM, Aubin CE (2017). Minimizing Pedicle Screw Pullout Risks A Detailed Biomechanical Analysis of Screw Design and Placement. Clin Spine Surg. 30: E226-E232.

Biswas JK, Rana M, Roy S, Majumder S, Roychoudhury A (2018). Effect of range of motion (ROM) for pedicle screw fixation on lumbar spine with rigid and semi-rigid rod materials: A finite element study. IOP Conf Ser. Mater. Sci Eng 402:012146.

Biswas JK, Sahu TP, Rana M, Roy S, Karmakar SK, Mazumder S, Roychowdhury A (2019). Design factors of lumbar pedicle screws unde bending load: A finite element analysis. Biocybern Biomed Eng 39(1):52–62.

Biswas JK, Malas A, Majumdar S, Majumdar S, Rana M (2022). A comparative finite element analysis of artificial intervertebral disc replacement and pedicle screw fixation of the lumbar spine. Comput Methods Biomech. Biomed. Eng. 12:1-9.

Boccaccio A, Kelly DJ, Pappalettere C (2011). A mechano-regulation model of fracture repair in vertebral bodies. J Orthop Res.29(3):433-43.

Boccaccio A, Vena P, Gastaldi D, Franzoso G, Pietrabissa R, Pappalettere C (2008). Finite element analysis of cancellous bone failure in the vertebral body of healthy and osteoporotic subjects. Proc IMechE Part H: J Engineering in Medicine 222:1023-1036.

Boccaccio A, Pappalettere C, Kelly D (2007). The influence of Expansion Rates on Mandibular Distraction Osteogenesis: A computational analysis. Ann. Biomed. Eng. 35(11):1940-1960.

Bokov A, Aleynik A, Dydykin A, Bulkin A, Mlyavykh S (2018). Implant related complications in patients operated on with expandable pedicle screws and technical solutions for revision surgery. AMJ ;11(8):443–447.

Bowden AE, Guerin HL, Villarraga ML, Patwardhan AG, Ochoa JA (2008). Quality of motion considerations in numerical analysis of motion restoring implants of the spine. Clinical Biomechanics, 23(5), 536–544.

Burval DJ, McLain RF, Milks R, Inceoglu S (2007). Primary pedicle screw augmentation in osteoporotic lumbar vertebrae: Biomechanical analysis of pedicle fixation strength. Spine, *32*(10), 1077–1083.

Calvo-Echenique A, Bashkuev M, Reitmaier S, Palomar AP, Schmidt H (2019). Numerical simulations of bone remodelling and formation following nucleotomy. J. Biomech. 88:138-147.

Cann SL, Cachon T, Viguier E, Miladi L, Odent T, Rossi JM, Chabrand P (2015). Pedicle screw fixation study in immature porcine spines to improve pullout resistance during animal testing. Plos one. 10(10): e0127463.

Carter DR (1978). Anisotropic analysis of strain rosette information from cortical bone. J biomech, 11(4):199-202.

Carter DR, Vasu R, Harris WH (1982). Stress distributions in the acetabular region-II. Effects of cement thickness and metal backing of the total hip acetabular component. J Biomech. 15(3):165-170.

Carter DR (1984). Mechanical loading histories and cortical bone remodelling. Calcif Tissue Int 36: S19-S24.

Carter DR and Wong M (1988). The role of mechanical loading histories in the development of Diarthrodial joints. J. Orthop Res. 6:804-816.

Carter DR, Blenman PR, Beauprè GS (1988). Correlation between mechanical stress history and tissue differentiation in initial fracture healing. J. Orthop. Res. 6(5):736-48.

Carter DR, Orr TE, Fyhrie DP (1989). Relationships between loading history and femoral cancellous bone architecture. J Biomechanics, 22(3):231-244.

Castro WH, Halm H, Jerosch J, Malms J, Steinbeck J, Blasius S (1996). Accuracy of pedicle screw placement in lumbar vertebrae. Spine (Phila Pa 1976).21(11):1320-4.

Causay GC, Picha GJ, Price J, Pelletier MH, Wang T, Walsh WR (2021). The effect of novel pillar surface morphology and material composition demonstrates uniform osseointegration. J. Mech. Behav. Biomed. Mater, 123:104775.

Cegoñino J, Calvo-Echenique A, Pérez-Del Palomar A. (2015). Influence of different fusion techniques in lumbar spine over the adjacent segments: A 3D finite element study. Journal of Orthopaedic Research, 33(7), 993–1000.

Cetin A, Bircan DA (2021a). Experimental investigation of pull-out performance of pedicle screws at different polyurethane (PU) foam densities. Proc. IMeche Part H: J Engineering in medicine. 235(6): 709-716.

Chanda S, Gupta S, Pratidhar DK (2016) Effect of interfacial conditions on shape optimization of cementless hip stem: an investigation based on a hybrid framework. Struct Multidisc Optim 53: 1143-1155.

Chanda S, Mukherjee K, Gupta S, Pratidhar DK (2020). A comparative assessment of two designs of hip stem using rule-based simulation of combined osseointegration and remodelling. Proc ImechE Part H. 234(1):118-128.

Chapman JR, Harrington RM, Lee KM, Anderson PA, Tencer AF, Kowalski D (1996). Factors affecting the pullout strength of cancellous bone screws. J. Biomech. Eng118:391-398.

Chatzistergos PE, Sapkas G, Kourkoulis SK (2010). The influence of the insertion technique on the pullout force on pedicle scres. Spine 35: E332-E337.

Chatzistergos PE, Magnissalis EA, Kourkoulis SK (2014). Numerical simulation of bone screw induced pretension: The cases of under-tapping and conical profile. Med Eng Phys 36:378-386.

Chen CS, Cheng CK, Liu CL, Lo WH (2001). Stress analysis of the disc adjacent to interbody fusion in lumbar spine. Med Eng Phys 23(7):483-491.

Chen CS, Chen WJ, Cheng CK, Jao SHE, Chueh SC, & Wang CC (2005). Failure analysis of broken pedicle screws on spinal instrumentation. Med. Eng & Phys, 27(6), 487–496.

Chen LH, Tai CL, Lai PL, Lee DM, Tsai TT, Fu TS, Niu CC, Chen WJ (2009). Pullout strength for cannulated pedicle screws with bone cement augmentation in severely osteoporotic bone: Influences of radial hole and pilot hole taping. Clin Biomech 24:613-618.

Chen HC, Lai YS, Chen WC, Chen JW, Chang CM, Chen YL, Wang ST, Cheng CK (2015). Effect of different radial hole designs on pullout and structural strength of cannulated pedicle screws. Med. Eng. Phys. 37:746-751.

Chen SH, Lin SC, Tsai WC, Wang CW, Chao SH (2012). Biomechanical comparison of unilateral and bilateral pedicle screws fixation for transforaminal lumbar interbody fusion after decompressive surgery--a finite element analysis. BMC Musculoskelet Disord. 13:72.

Chen SI, Lin RM, Chang CH (2003). Biomechanical investigation of pedicle screw-vertebrae complex: A finite element approach using bonded and contact interface conditions. MedEng Phys 25(4):275–282.

Chen YL, Chen WC, Chou CW, Chen JW, Chang CM, Lai YS, Cheng CK, Wang ST (2014). Biomechanical study of expandable pedicle screw fixation in severe osteoporotic bone comparing with conventional and cement-augmented pedicle screws. Med Eng Phys. 36:1416-1420.

Chao EY, Inoue N (2003). Biophysical stimulation of bone fracture repair, regeneration and remodelling. Eur Cell Mater. 6:72-84.

Chiang MF, Zhong ZC, Chen CS, Cheng CK, Shih SL (2006). Biomechanical Comparison of Instrumented Posterior Lumbar Interbody Fusion With One or Two Cages by Finite Element Analysis. SPINE 31(19):E682-E689.

Cho W, Cho SK, Wu C (2010) The biomechanics of pedicle screw-based instrumentation. J Bone Joint Surg 92B:1061-5.

Choi JY, Sim JH, Yeo ISL (2017). Characteristics of contact and distance osteogenesis around modified implant surfaces in rabbit tibiae. J Periodontal Implant Sci. 47(3):182-192.

Chou HY and Müftü S (2013). Simulation of peri0implant bone healing due to immediate loading in dental implants. J. Biomech. 46(14):871-878.

Christodoulou E, Chinthakunta S, Reddy D, Khalil S, Apostolou T, Dress P, Kafchitas K (2015). Axial pullout strength comparison of different screw designs: fenestrated screw, dual outer diameter screw and standard pedicle screw. Scoliosis 10:15.

Chu YL, Chen CH, Tsuang FY, Chiang CJ, Wu Y, Kuo YJ (2019). Incomplete insertion of pedicle screws in a standard construct reduces the fatigue life: A biomechanical analysis. PLoS ONE, 14(11), 1–11.

Claes LE and Heigele CA (1999). Magnitudes of local stress and strain along bony surfaces predict the course and type of fracture healing. J. Biomech. 32:255-266.

Cristofolini L, Brandolini N, Danesi V, Juszczyk MM, Erani P, Viceconti M (2013). Strain distribution in the vertebrae under different loading configurations. Spine. 13:1281-1292.

Cristofolini L, Viceconti M, Cappello A, Toni A (1996). Mechanical Composition of whole bone composite femur models. J. Biomechanics, 29(4):525-535.

Cook DJ, Yeager MS, Cheng BC (2015). Range of motion of the intact lumbar segment: a multivariate study of 42 lumbar spines. Int J Spine Surg. 5; 9:5.

Cook SD, Barbara J, Rubi M, Salkeld SL, Whitecloud TS (2001). Lumbosacral fixation using expandable pedicle screws: an alternative in reoperation and osteoporosis.Spine J 1:109-114. https://doi.org/ 10.1016/s1529-9430(01)00020-1.

Cook SD, Salkeld SL, Whitecloud TS, Barbera J (2000). Biomechanical evaluation and preliminary clinical experience with an expansive pedicle screw design, J. Spinal Disord 13:230-6. https://doi.org/ 10.1097/00002517-200006000-00006.

Coombs MT, Glos DL, Wall EJ, Kim J, Bylski-Austrow DI (2013). Biomechanics of Spinal Hemiepiphysiodesis for Fusionless Scoliosis Treatment Using Titanium Implant. Spine, 38(23), E1454–E1460.

Cowin SC and Hegedus DH (1976). Bone remodelling I: theory of adaptive elasticity. J. Elast. 6(3):313-326.

Cowin SC (1986). Wolff's law of trabecular architecture at remodelling equilibrium. J. Biomech Eng. 108(1):83-8.

Damisih D, Hanafi R, Gumelar MD, Sah J, Rahmania AW, Gustiono D, Nurlina N, Arrifqi MH, Setyadi I, Triwibowo B, Kozin M, Jujur IN (2023). Pullout strength evaluation of titanium pedicle screw in different grades of polyurethane. AIP Conf. Proc. 2719,030020.

Danesi V, Zani L, Scheele A, Berra F, Cristofolini L (2014). Reproducible reference frame for in vitro testing of the human verterbrae. J Biomech. 47:313-318.

Daniell JR, Osti OL (2018). Failed back surgery syndrome: A review article. Asian Spine J 12(2):372-379.

Daud R, Kae WY, Ayu HM, Shah A (2021). Effect of thread profile variation on pullout and bending strength of a pedicle screw. IOP Conf Series: Materials Science and Engineering 1078:012025.

Davies JE (1996). In Vitro Modeling of the Bone/Implant Interface. The Anat Rec. 245(2):426-445.

Davies JE (2003). Understanding peri-implant endosseous healing. J. Dent. Edu 67(8):932-949.

Demirbas A E, Ekici R, Mustafa K, Alkan A (2022). Bone stress and damage distributions during dental implant insertion: a novel dynamic FEM analysis. Comput Methods Biomech Biomed Engin. 1381-1392.

De Kater EP, Sakes A, Edsrom E, Elmi-Terander A, Kraan G (2022). Beyond the pedicle screw-a patent review. Eur Spine J, 31:1553-1565.

Demir T, Camuscu N, Tureyan K (2012). Design and biomechanical testing of pedicle screw for osteoporotic incidents. Proc. IMeche Part H: J Engineering in medicine. 226(3):256-262.

Demir E, Eltes P, Castro APG, Lacroix D, Toktaş İ (2020). Finite element modelling of hybrid stabilization systems for the human lumbar spine. Proceedings of the Institution of Mechanical Engineers, Part H: Journal of Engineering in Medicine, 234(12), 1409–1420.

Dickinson A, Taylor A, Browne M (2012). Implant-bone interface healing and adaptation in resurfacing hip replacement. Comput. Methods. Biomech. Biomed. Engin. 15(9):935-947.

D'Lima D, Lemperle SM, Chen PC, Holmes RE, Colwell C (1998). Bone Response to Implant Surface Morphology. J Arthoplasty, 13(8),928-934.

Doblaré M and García JM (2002). Anisotropic bone remodelling model based on a continuum damage-repair theory. J Biomech, 35:1-17.

Dong XN, Guo XE (2004). The dependence of transeversely isotropic elasticity of human femoral cortical bone on porosity. J Biomech. 37:1281-1287.

Dreischarf M, Zander T, Shirazi-Adl A, Puttlitz CM, Adam CJ, Chen CS, Goel VK, Kiapour A, Kim YH, Labus KM, Little JP, Park WM, Wang YH, Wilke HJ, Rohlmann A, Schmidt H (2014). Comparison of eight published static finite element models of the intact lumbar spine: Predictive power of models improves when combined together. J. Biomech 47(8):1757–1766.

Duyck J, Slaets E, Sasaguri K, Vandamme K, Naert I (2007). Effect of intermittent loading and surface roughness on peri-implant bone formation in a bone chamber model. J Clin Periodontrol. 34:998-1006.

Edidin AA, Ong KL, Lau E, Kurtz SM (2015). Morbidity and mortality after vertebral fractures: Comparison of vertebral augmentation and nonoperative management in the medicare population. Spine, 40(15), 1228–1241.

Eremina G, Smolin A, Xie J, Syrkashev V (2022). Development of a computational model of the mechanical behavior of the L4-L5 lumbar spine: application to disc degeneration. Materials. 15:6684.

Esenkaya I, Denizhan Y, Kaygusuz M A, Yetmez M, Kelestemur MH (2006). Comparison of the pull-out strengths of three different screws in pedicular screw revisions: a biomechanical study. Acta Orthop Traumatol Turc. 40(1):72-81.

Espinha LC, Fernandes PR, Folgado J (2010). Computational analysis of bone remodeling during an anterior cervical fusion. J. Biomech. 43:2875-2880.

Fan W, Guo L X (2019). A comparison of the influence of three different lumbar interbody fusion approaches on stress in the pedicle screw fixation system: Finite element static and vibration analyses. International Journal for Numerical Methods in Biomedical Engineering, *35*(3).

Favier CD, McGregor A, Phillips ATM (2021). Maintaining bone health in the lumbar spine: Routine activities alone are not enough. Front Bioeng. Biotecnol. 9:661837.

Fermandes P, Rodrigues HC, Jacobs CR (1999). A model of bone adaptation using a global optimisation criterion based on the trajectorial theory of Wolff. Comput. Methods. Biomech. Biomed. Eng.2:125-138.

Fisher C, Harty J, Yee A, Li CL, Komolibus K, Grygoryev K, Lu H, Burke R, Wilson BC, Andersson-Engles S (2022). Perspective on the integration of optical sensing into orthopedic surgical devices. J. Biomed. Opt. 27(1):010601.

Frost HM (1964). The laws of bone structure. Springfield Illionis USA Charles C Thomas Publisher.

Frost HM (1987). Bone "mass" and the "mechanostat": a proposal. Anat. Rec. 219(1):1-9.

Fu J, Yao ZM, Wang Z, Cui G, Ni M, Li X, Chen JY (2017). Surgical treatment of osteoporotic degenerative spinal deformity with expandable pedicle screw fixation: 2-year follow-up clinical study (2018). Orthop Traumatol Surg Res104(3):411-415.

Fu CJ, Chen WC, Lu ML, Cheng, C. H., & Niu, C. C. (2020). Comparison of paraspinal muscle degeneration and decompression effect between conventional open and minimal invasive approaches for posterior lumbar spine surgery. Scientific Reports, *10*(1).

Farshad M, Aichmair A, Gerber C, Bauer DE (2020). Classification of perioperative complications in spine surgery. Spine J. 20:730-736.

Fuster, V. (2017). Changing Demographics: A New Approach to Global Health Care Due to the Aging Population. Journal of the American College of Cardiology, 69(24), 3002–3005.

Fyhrie DP, Carter DR (1986). A unifying principle relating stress to trabecular bone morphology. J. Orthop. Res. 4:304-317.

Galbusera F, Volkheimer D, Reitmaier S, Berger-Roscher N, Kienle A, Wilke HJ (2015). Pedicle screw loosening: a clinically relevant complication? Eur Spine J, 24:1005-1016.

Gao M, Lei W, Wu Z, Liu D, Shi L (2011). Biomechanical evaluation of fixation strength of conventional and expansive pedicle screws with or without calcium-based cement augmentation. Clin Biomech. 26:238-244.

Garcia JM, Doblare M, Cegonino J (2002). Bone remodelling simulation: a tool for implant design. Comput. Mater. Sci. 25:110-114.

Gardener TN, Mishra S, Marks L (2004). The role of osteogenic index, octahedral shear stress and dilatational stress in the ossification of a fracture callus. Med Eng Phys. 26(6):493-501.

Gautschi OP, Schatlo B, Schaller K, Tessitore E (2011). Clinically relevant complications related to pedicle screw placement in thoracolumbar surgery and their management: a literature review of 35,630 pedicle screws. Neurosurg Focus, 31(4): E8.

Gazzeri R, Roperto R., Fiore C (2016). Surgical treatment of degenerative and traumatic spinal diseases with expandable screws in patients with osteoporosis: 2-Year follow-up clinical study. J. Neurosurg. Spine 25(5):610–619.

Gazzeri R, Panagiotopoulos K, Galarza M, Bolognini M, Callovini G (2020). Minimally invasive spinal fixation in an aging population with osteoporosis: clinical and radiological outcomes and safety to expandable screws versus fenestrated screws augmented with polymethylmethacrylate. Neurosurg. Focus. 49(2):E14.

Gharaei H (2018). Clinical anatomy of the spine for pain interventionist. J of Anes & Criti Care Open Access. 10(4):140-145.

Ghiselli G, Wang JC, Bhatia NN, Hsu WK, Dawson EG (2004). Adjacent segment degeneration in the lumbar spine. J Bone Joint Surg Am. 86(7):1497-503.

Ghosh R, Mukherjee K, Gupta S (2013). Bone remodelling around uncemented metallic and ceramic acetabular components. Proc IMeche Part H: J Engineering in Medicine. 227(5):490-502.

Ghosh R and Gupta S (2014). Bone remodelling around cementless composite acetabular components: The effects of implant geometry andimplant-bone interfacial conditions. J Mech Behav Biomed Mater. 32:257-269.

Ghosh R, Chanda S, Chakraborty D (2020). The influence of macro-textural designs over implant surface on bone on-growth: A computational mechanobiology based study. COMPUT BIOL MED, 124:103937.

Ghosh R, Hazra A, Chanda S, Chakraborty D (2022a). Computational assessment of growth of connective tissues around textured hip stem subjected to daily activities after THA. Med Biol Eng Comput. 61:525-540.

Ghosh R, Chanda S, Chakraborty D (2022b). Application of finite element analysis to tissue differentiation and bone remodelling approaches and their use in design optimization of orthopaedic implants: A review. Int J Numer.38: e3637.

Ghosh R, Chanda S, Chakraborty D (2021b). Qualitative predictions of bone growth over optimally designed macro-textured implant surfaces obtained using NN-GA based machine learning framework. Med Eng Phys. 95:64-75.

Ghosh R, Chanda S, Chakraborty D (2023). "Combined Influence of Material Properties of Bone and Implant on Bone Growth Over Macro-Textured Implant Surface." North-East Research Conclave. Singapore: Springer Nature Singapore. 243-254.

Gibson LJ (1985). The mechanical behaviour of cancellous bone. J. Biomechanics,18(5):317-328.

Giacaglia, GEO, & Lamas W de Q (2015). Pedicle screw rupture: A case study. Case Studies in Engineering Failure Analysis, *4*, 64–75.

Giesen EBW, Ding M, Dalstra M, van Eijden TMGJ (2001). Mechanical properties of cancellous bone in the human mandibular condyle are anisotropic. J. Biomech. 34:799-803.

Girardo M, Cinnella P, Gargiulo G, Viglierchio P, Rava A, Aleotti S (2017). Surgical treatment of osteoporotic thoraco-lumbar compressive fractures: the use of pedicle screw with augmentation PMMA. European Spine Journal, *26*, 546–551.

Giori NJ, Ryd L, Carter DR (1995). Mechanical Influences on Tissue Differentiation at bone-cement interfaces. J Arthoplasty.11(4):581-91.

Girardi FP, Cammisa FP Jr, Sandhu HS, Alvarez L (1999). The placement of lumbar pedicle screws using computerised stereotactic guidance. J Bone Joint Surg Br. 81(5):825-9.

Glaser J, Starley M, Sayre H, Sayre H, Woody J, Found E, Spratt K (2003). A 10-year follow up Evaluation of Lumbar Soine Fusion with Pedicle Screw Fixation. SPINE 28(13):1390-1395.

Godinho M.I, Carvalho V, Matos MT, Fernandes P R, Castro APG (2021). Computational modeling of lumbar disc degeneration before and after spinal fusion. Clinical Biomechanics, 90.

Goel VK and Seenivasan G (1994). Applying bone-adaptive remodelling theory to ligamentous spine. IEEE Eng. Med. Biol. Mag 1994; 13(4):508-516.

Goel VK, Ramirez SA, Rietbergen Bv, Sumner DR, Turner TM, Galante JO (1995). Cancellous bone Young's modulus variation within the vertebral body of a ligamentous lumbar spine-Application of bone adaptive remodelling concepts. ASME J. Biomech. Eng. 117(3): 266-272.

Goel VK, Kiapour A, Faizan A, Krishna M, Friesen T (2007). Finite Element Study of Matched Paired Posterior Disc Implant and Dynamic Stabilizer (360° Motion Preservation System). SAS Journal 1(1):55–62.

Goldstein S, Christina L.,Choma TJ (2015). Surgical Management of Spinal Conditions in the Elderly Osteoporotic Spine. Neurosurgery. 77: S98-S107.

Gokhale NS, Deshpande SS, Bedekar SV, Thite AN (2008). Book- practical finite element analysis. 445.

Granhead H, Jonson R, Hansson T (1987). The loads on the lumbar spine during extreme weight lifting. Spine. 12(2):146-9.

Guftason P A, Veenstra J M, Jastifier J R (2019). The effect of pitch variation and diameter variation on screw pullout. Foot & Ankle Specialist 12(3):258-263.

Guo HZ, Tang YC, Guo DQ, Luo PJ, Li YX, Mo GY, Ma YH, Peng JC, Liang D, Zhang SC (2020). Stability Evaluation of Oblique Lumbar Interbody Fusion Constructs with Various Fixation Options: A Finite Element Analysis Based on Three-Dimensional Scanning Models. World Neurosurgery, 138, e530–e538.

Guha I, Zhang X, Rajapakse CS, Chang G, Saha PK (2022). Finite element analysis of trabecular bone microstructure using CT imaging and continuum mechanical modeling. Med Phys. Jun;49(6):3886-3899.

Guvenc Y, Akyoldas G, Senturk S, Erbulut D, Yaman O, Ozer AF (2019). How to reduce stress on the pedicle screws in thoracic spine? Importance of Screw Trajectory: A finite element analysis. Turk Neurosurg. 29(1):20-25.

Haddas, R., Xu, M., Lieberman, I., & Yang, J. (2019). Finite Element Based-Analysis for Pre and Post Lumbar Fusion of Adult Degenerative Scoliosis Patients. Spine Deformity, *7*(4), 543–552.

Halm H, Niemeyer T, Link T, Liljenqvist U (2000). Segmental pedicle screw instrumentation in idiopathic thoracolumbar and lumbar scoliosis. Eur Spine J. 9(3):191-7.

Halvorson TL, Kelley LA, Thomas KA, Thomas KA, Whitecloud TS III, Cook SD (1994). Effect of Bone Mineral Density on Pedicle Screw Fixation. Spine 19(21):2415-2420.

Han Z, Ren B, Zhang L, Ma C, Liu J, Li J, Liu X, Liu Q, Mao K, Tang P (2022). Finite Element Analysis of a Novel Fusion Strategy in Minimally Invasive Transforaminal Lumbar Interbody Fusion. Biomed Res Int. 11;2022: 4266564.

Hart RT, Davy DT, Heiple KG (1984). Mathematical modeling and Numerical Solutions for Functionally dependent bone remodeling. Calcif Tissue Int, 36:S104-S109.

Hart RT, Davy DT (1989). Theories of bone modelling and remodelling, In bone mechanics (Ed Cowin, S.C.) Boca Reton, FL, CRC Press,449-454.

Hartvigsen J, Hancock M J, Kongsted A, Louw Q, Ferreira M L, Genevay S, Hoy D, Karppinen J, Pransky G, Sieper J, Smeets RJ, Underwood M (2018). What low back pain is and why we need to pay attention. The Lancet, 391(10137), 2356–2367.

Hashemi A, Bednar D, Ziada S (2009). Pullout strength of pedicle screws augmented with particulate calcium phosphate: An experimental study. J. Spine. 9:404-410.

Heinar AD (2008). Structural properties of fourth-generation composite femurs and tibias. J Biomech. 2008 Nov 14;41(15):3282-4.

Heo M, Yun J, Park SH, Choi YS, Lee SS, Park S (2020). Design of a Lumbar Interspinous Fixation Device for Minimally Invasive Surgery and Spine Motion Stabilization. Journal of Medical and Biological Engineering, 40(1), 1–10.

Heo M, Yun J, Kim H, Lee SS, Park S (2022). Optimization of a lumbar interspinous fixation device for the lumbar spine with degenerative disc disease. PLoS One. 17(4): e0265926.

Holister SL, Brennan JM and Kikuchi N (1994). A homogenization sampling procedure for calculating trabecular bone effective stiffness and tissue level stress. J Biomech, 27(4):433-444.

Homminga J, Aquarius R, Bulsink VE, Jansen CTJ, Verdonschot N (2012). Can vertebral density changes be explained by intervertebral disc degeneration? Med. Eng. Phys. 34:453-458,

Hsieh M K, Liu M Y, Chen J K, Tsai TT, Lai PL, Niu CC, Tai CL (2019). Biomechanical study of the fixation stability of broken pedicle screws and subsequent strategies. Plos one. 14(6): e0219189.

Hsieh PC, Koski TR, O'Shaughnessy, BA, Sugrue P, Salehi S, Ondra S, Liu JC (2007). Anterior lumbar interbody fusion in comparison with transforaminal lumbar interbody fusion: Implications for the restoration of foraminal height, local disc angle, lumbar lordosis, and sagittal balance. Journal of Neurosurgery: Spine, *7*(4), 379–386.

Hsu CC, Chao CK, Wang JL, Hou SM, Tsai YT, Lin J (2005). Increase of pullout strength of spinal pedicle screws with conical core: bioechanical tests and finite element analyses. J. Orthop 23:788-794.

Huang S, Min S, Wang S, Jin A (2022). Biomechanical effects of an oblique lumbar interbody fusion combined with posterior augmentation: a finite element analysis. BMC Musculoskelet Disord. 23(1):611.

Huang Z bin, Nie MD Zhang NZ, Liu S, Yuan J bin, Lin X M, Cheng CK, Shi ZC, Mao N F (2022). Biomechanical evaluation of a short-rod technique for lumbar fixation surgery. Frontiers in Bioengineering and Biotechnology, *10*.

Huiskes R, Weinans H, Grootenboer HJ, Dalstra M, Fudula B, Sloff TJ(1987). Adaptive Bone-Remodelling theory applied to prosthetic design analysis. J Biomech; 20(11-12):1135-1150.

Huiskes R, Weinans H, van Rietbergen B (1992). The relationship between stress shielding and bone resorption around total hip stems and the effects of flexible materials. Clin. Orthop. Relat. Res. 274:124-34.

Huiskes R and van Rietbergen B (1995) . Preclinical testing of total hip stems: The effects of coating placement. Clin Orthop Relat Res. 319:64-76. PMID:7554651.

Inceoglu S, Ferrara L, McLain RF (2004). Pedicle screw fixation strength: pullout versus insertion torque. J. Spine. 4:513-518.

Inoue G, Saito W, Miyagi M, Imura T, Shirasawa E, Ikeda S, Mimura Y, Kuroda A, Yokozeki Y, Inoue S, Akazawa T, Nakazawa T, Uchida K, Takaso M (2021). Prevalence and location of endplate fracture and subsidence after oblique lumbar interbody fusion for adult spinal deformity. BMC Musculoskeletal Disorders, 22(1).

Isaksson H, Wilson W, van Donkelaar CC, Huiskes R, Ito K (2006a). Comparison of biophysical stimuli for mechano-regulation of tissue differentiation during fracture healing. J Biomech. 39:1507-1516.

Isaksson H, van Donkelaar CC, Huiskes R, Ito K (2006b). Corroboration of Mechanoregulation Algorithms for Tissue Differentiation during Fracture Healing: Comparison with In Vivo Results. J. Orthop Res. 24(5):898-907.

Isaksson H, van Donkelaar CC, Huiskes R, Ito K (2008a). A mechano-regulatory bone-healing model incorporating cell-phenotype specific activity. J. Theor. Biol. 255(2):230-246.

Isaksson H, van Donkelaar CC, Huiskes R, Yao J, Ito K (2008b). Determining the most important cellular characteristics for fracture healing using design of experiments methods. J. Theor. Biol. 255(1):26-39.

Isaksson H (2012). Recent advances in mechanobiological modelling of bone regeneration. Mech. Res. Commun. 42:22-3.

Jacobs CR, Levenston MC, Beauprè GS, Simo JC, Carter DR (1995a). Numerical instabilities in bone remodelling simulations: the advantages of a node-based finite element approach. J. Biomech. 28(4):449-459.

Jacobs CR, Simo JC, Beauprè GS, Carter DR (1997). Adaptive bone remodelling incorporating simultaneous density and anisotropy considerations. J. Biomech. 30(6):603-613.

Jain P, Khan MR (2022). Comparison of novel stabilisation device with various stabilisation approaches: A finite element based biomechanical analysis. Int J Artif Organs.

Jang IG, Kim IY (2008). Computational study of Wolff's law with trabecular architecture in the proximal human femur using topology optimization. J. Biomech. 41:2353-2361.

Jang IG, Kim II Y, Kwak BM (2009). Analogy of strain energy density based bone remodelling algorithm and structural topology optimization. J. Biomech. Eng. 131:011012-(1-7).

Jee WSS (2008). Integrated bone tissue physiology: anatomy and physiology. In: Bone Mechanics Handbook Ed: Cowin SC New YorkInforma Healthcare.

Jendoubi K, Khadri Y, Bendjaballah M, Slimane N (2018). Effect of insertion type and depth on the pedicle screw pullout strength: a finite element study. Appl Bionics Biomech 26:1460195.

Jovanoic JD and Jovanoic ML (2004). Biomechanical model of vertebra based on bone remodelling. *Facta Universitatis* series Medicine and Biology. 11(1):35-39.

Kabins MB, Weinstein JN (1991) The History of Vertebral and Pedicle Screw Fixation. The lowa orthop j 11127-136.

Kang S, Park C H, Jung H, Lee S, Min YS, Kim CH, Cho M, Jung GH, Kim DH, Kim KT, Hwang JM (2022). Analysis of the physiological load on lumbar vertebrae in patients with osteoporosis: a finite-element study. Scientific Reports, 12(1), 1–15.

Kanno H, Onoda Y, Hashimoto K, Aizawa T, Ozawa H (2022). Innovation of surgical techniques for screw fixation in patients with osteoporotic spine. J. Clin. Med. 11,257.

Kelly DJ and Prendergast PJ (2005). Mechano-regulation of stem cell differentiation and tissue regeneration in osteochondral defects. J Biomech.38:1413-1422.

Keramat A, Larigani B, Adibi H (2012). Risk factors for spinal osteoporosis as compared with femoral osteoporosis in Urban Iranian women. Iranian Journal of Public Health41(10):52–59.

Kiapour A, Anderson DG, Spenciner DB, Spenciner DB, Ferrara L, Goel VK (2012). Kinematic effects of a pedicle-lengthening osteotomy for the treatment of lumbar spinal stenosis Laboratory investigation. J. Neurosurg. Spine 17(4):314–320.

Kim DH, Hwang RW, Lee GH, Joshi R, Baker KC, Arnold P, Sasso R, Park D, Fischgrund J (2020). Comparing rates of early pedicle screw loosening in posterolateral lumbar fusion with and without transforaminal lumbar interbody fusion. Spine J. 20: 1438-1445.

Kim K, Park WM, Kim YH, Lee S (2010). Stress analysis in a pedicle screw fixation system with flexible rods in the lumbar spine. Proc IMechE Part H: J Engineering in Medicine 224(3):477–485.

Kim K, Kim YH Lee S. (2007). Increase of load-carrying capacity under follower load generated by trunk muscles in lumbar spine. Proc IMechE Part H: J Engineering in Medicine 221(3), 229–235.

Kim HJ, Kang KT, Chun HJ, Lee CK, Chang BS, Yeom JS (2015). The influence of intrinsic disc degeneration of the adjacent segments on its stress distribution after one-level lumbar fusion. Eur Spine J. 24: 827–837.

Kim JT, Yoo JJ (2016). Implant Design in Cementless Hip Arthoplasty. Hip Pelvis. 28(2):65-75.

Kim YY, Choi WS, Rhyu KW (2012a). Assessment of pedicle screw pullout strength based on various screw designs and bone densities-an ex vivo biomechanical study. Spine J. Feb;12(2):164-8.

Kim HJ, Chang SH, Jung HJ (2012b). The simulation of tissue differentiation at a fracture gap using a mechano-regulation theory dealing with deviatoric strains in the presence of a composite bone plate. Compos. B Eng. 43:978-987.

Kim UG, Choi JY, Lee J, Yeo IS (2021). Existing Bone-Derived Bone Morphogenic Protein-2 Initiates Contact Osteogenesis on the Surface of a Titanium Implant. Research Square.

Kiyak G, Balikci T, Heydar AM, Bezer M (2018). Comparison of the Pullout Strength of different pedicle screw designs and augmentation techniques in osteoporotic bone model. Asian Spine J. 12(1):3-11.

Krishnan V, Varghese V, Kumar G S, Yoganandan N (2020). Identification of pedicle screw pullout load paths for osteoporotic vertebrae. Asian Spine J. 14(3):273-279.

Kubaik A J, Jonas K L, Dearn K D, Shepherd DET (2019). Comparison of the mechanical properties of two designs of polyaxial pedicle screw. Eng. Fail. Anal. 95:96-106.

Kumaran Y, Shah A, Katragadda A, Padgaonkar A, Zavatsky J, McGuire R, Serhan H, Elgafy H, Goel VK (2021). Iatrogenic muscle damage in transforaminal lumbar interbody fusion and adjacent segment degeneration: a comparative finite element analysis of open and minimally invasive surgeries. European Spine Journal, 30(9), 2622–2630.

Kurtz M (2010). Finite element modeling of the Human Lumbar Spine.

Kuzyk PRT, Schemitsch EH (2011). The basic science of peri-implant bone healing. Indian J. Orthop. 45(2):108-115.

Kwon J, Ha M. & Lee MG. (2020). Alternative pedicle screw design via biomechanical evaluation. Applied Sciences (Switzerland), *10*(14).

la Barbera L, Galbusera F, Villa T, Costa F, & Wilke H J (2014). ASTM F1717 standard for the preclinical evaluation of posterior spinal fixators: Can we improve it? Proceedings of the Institution of Mechanical Engineers, Part H: Journal of Engineering in Medicine, *228*(10), 1014–1026.

La Barbera L, Cianfoni A, Ferrari A, Distefano D, Bonaldi G, & Villa T. (2019). Stent-screw assisted internal fixation of osteoporotic vertebrae: A comparative finite element analysis on SAIF technique. Frontiers in Bioengineering and Biotechnology, *7*(OCT).

Lacroix D, Prendergast PJ, Li G, Marsh D (2002). Biomechanical model to simulate tissue differentiation and bone regeneration: application to fracture healing. Med. Biol. Eng. Comput. 40(1):14-21.

Lacroix D and Prendergast PJ (2002a). Three dimensional Simulation of Fracture Repair in the Human Tibia. Comput. Methods Biomech. Biomed. Engin. 5:5,369-376.

Lacroix D and Prendergast PJ (2002b). A mechano-regulation model for tissue differentiation during fracture healing: analysis of gap size and loading. J Biomech. 35:1163-1171.

Lange N, Stadtmuller T, Scheibel S, Reischer G, Wagner A, Meyer B, Gempt J (2022). Analysis of risk factors for perioperative complications in spine surgery. Nature portfolio. 12:14350.

Laugesen LA, Paulsen RT, Carreon L, Ernst C, Andersen MØ (2017). Patient-reported Outcomes and Revision Rates at a Mean Follow-up of 10 Years After Lumbar Total Disc Replacement. Spine (Phila Pa 1976). 42(21):1657-1663.

Lee E S, Gok T S, Heo J Y, Kim YJ, Lee SE, Kim YH, Lee CS (2019). Experimental evaluation of screw pullout force and adjacent bone damage according to pedicle screw design parameters in normal and osteoporotic bones. Appl. Sci. 9:586.

Lei W, Wu Zixiang. (2006). Biomechanical evaluation of an expansive pedicle screw in calf vertebrae. Eur Spine J 15:321-326.

Li C, Zhou Y, Wang H, Wang H, Liu J, Xiang L (2014). Treatment of unstable thoracolumbar fractures through short segment pedicle screw fixation techniques using pedicle fixation at the level of the fracture: A finite element analysis. PLoS One9(6):1–9.

Li J, Shang J, Zhou Y, Li C, Liu H (2015). Finite element analysis of a new pedicle screw-plate system for minimally invasive transforaminal lumbar interbody fusion. PLoS ONE, 10(12):1–16.

Li Y, Cheng H, Liu ZC, Wu JW, Yu L, Zang Y, He Q, Lei W, Wu ZX (2013). In vivo study of pedicle screw augmentation using bioactive glass in osteoporosis sheep. J Spinal Disord Tech 26(4):118–123.

Liao JC, Chen WP, Wang H (2017). Treatment of thoracolumbar burst fractures by short-segment pedicle screw fixation using a combination of two additional pedicle screws and vertebroplasty at the level of the fracture: A finite element analysis. BMC Musculoskelet. Disord.18(1):1–8.

Ling Q, He E, Zhang H, Lin H, Huang W. (2019). A novel narrow surface cage for full endoscopic oblique lateral lumbar interbody fusion: A finite element study. Journal of Orthopaedic Science, 24(6), 991–998.

Liu X and Niebur GL (2008). Bone ingrowth into a porous coated implant predicted by a mechano-regulatory tissue differentiation engineering. Biomech Model Mechanobiol. 7:335-344.

Liu CL, Zhong ZC, Hsu HW, Shih SL, Wang ST, Hung C, Chen CS (2011). Effect of the cord pretension of the Dynesys dynamic stabilisation system on the biomechanics of the lumbar spine: A finite element analysis. European Spine Journal, 20(11), 1850–1858.

Liu MY, Tsai TT, Lai PL, Hsieh MK, Chen LH, Tai CL (2020). Biomechanical comparison of pedicle screw fixation strength in synthetic bones: Effects of screw shape, core/thread profile and cement augmentation. Plos One 15(2): e0229328.

Liu ZX, Gao ZW, Chen C, Liu ZY, Cai XY, Ren YN, Sun X, Ma XL, Du CF, Yang Q (2022). Effects of osteoporosis on the biomechanics of various supplemental fixations co-applied with oblique lumbar interbody fusion (OLIF): a finite element analysis. BMC Musculoskelet Disord. 23(1):794.

Louois R (1984). Fusion of the lumbar and sacral spine by internal fixation with screw plates. Clin Orthop Res. 203:18-33.

Lu YM, Hutton WC, Gharpuray VM (1996). Do bending, twisting, and diurnal fluid changes in the disc affect the propensity to prolapse? A viscoelastic finite element model. Spine (Phila Pa 1976). 21(22):2570-9.

Lu T, Sun Z, Xia H, Qing J, Rashad A, Lu Y, He X (2024). Comparing the osteogenesis outcomes of different lumbar interbody fusion (A/O/X/T/PLIF) by evaluating their mechano-driven fusion processes. Comput. Biol. Med. 171:108215.

Lv QB, Gao X, Pan XX, Jin HM, Lou XT, Li SM, Yan YZ, Wu CC, Lin Y, Ni WF, Wang XY, Wu AM (2018). Biomechanical properties of novel transpedicular transdiscal screw fixation with interbody arthrodesis technique in lumbar spine: A finite element study. J Orthop Translat. 10;15: 50-58.

Ma Q, Miri Z, Haugen HJ, Moghanian A, Loca D (2023). Significance of mechanical loading in bone fracture healing, bone regeneration, and vascularization. J. Tissue Eng. 14:1-34.

Macleod AR, Pankaj P, Simpson HRW (2012). Does screw-bone interface modelling matter in finite element analyses? J. Biomech. 45:1712-1716.

Maimoun L, Fattal C, Sultan C (2011). Bone remodelling and calcium homeostasis in patients with spinal cord injury: a review. Metab Clin Exp. 60:1655-1663.

Markolf KL (1972). Deformation of the thoracolumbar intervertebral joints in response to external loads: a biomechanical study using autopsy material. J Bone Joint Surg 54(3):511-33. PMID: 5055150.

Martin RB (1991). Determinants of the mechanical properties of bones. J Biomech. 24 Suppl 1:79-88.

Martin RB (1972). Effects of geometric feedback in development of osteoporosis. J. Biomech. 5(5):447-455.

Martin BI, Mirza SK, Comstock BA, Gray DT, Kreuter W, Deyo RA (2007). Reoperation rates following lumbar spine surgery and the influence of spinal fusion procedures. Spine, *32*(3), 382–387.

Más Y, Gracia L, Ibarz E, Gabarre S, Peña D, Herrera A (2017). Finite element simulation and clinical followup of lumbar spine biomechanics with dynamic fixations. PLoS ONE, 12(11).

Mathai B, Dhara S, Gupta S (2021a). Orthotropic bone remodelling around uncemented femoral implant: A comparison with isotropic formulation. Biomech. Model. Mechanobiol. 20(3):1115-1134.

Mathai B, Gupta S (2021b). Bone Ingrowth Around an Uncemented Femoral Implant Using Mechanoregulatory Algorithm: A Multiscale Finite Element Analysis. J. Biomech. Eng. 144/021004-(1-10).

Mathieu V, Vayron R, Richard G, Lambert G, Naili S, Meningaud JP, Haiat G (2014). Biomechanical determinants of the stability of dental implants: Influence of the bone-implant interface properties. J Biomech. 47:3-13.

Matsuda N, Morita N, Matsuda K, Wanatabe M (1998). Proliferation and Differentiation of Human Osteoblastic Cells associated with differential activation of MAP Kinases in response to Epidermal growth factor, Hypoxia, and Mechanical stress in vitro. Biochem. And Biophys. Research Communications. 249:350-354.

Matsukawa K, Yato Y, Hynes RA, Imabayashi H, Hosogane N, Yoshihara Y, Asazuma T, Nemoto K (2017). Comparison of Pedicle Screw Fixation Strength Among Different Transpedicular Trajectories: A Finite Element Study. Clin Spine Surg. 30(7):301-307.

Matsukawa K, Yato Y, Imabyakshi H, Hosogane N, Asazuma T, Nemoto K (2015). Biomechanical Evaluation of Cross Trajectory Technique for Pedicle Screw

Insertion: Combined Use of Traditional Trajectory and Cortical Bone Trajectory. Orthop Surg. 2015 Nov;7(4):317-23.

McNamara LM, Prendergast PJ (2007). Bone remodelling algorithms incorporating both strain and microdamage stimuli. J. Biomech. 40:1381-1391.

Mehboob A, Mehboob H, Kim J, Chang SH, Tarlocahan F (2017). Influence of initial biomechanical environment provided by fibrous composite intermedullary nails on bone fracture healing. Compos. Struct. 175:123-134.

Mehboob H, Ahmed F, Tarlochan F, Mehboob A, Chang SH (2020). A comprehensive analysis of bio-inspired design of femoral stem of primary and secondary stabilities using mechanoregulatory algorithm. Biomech. Model. Mechanobiol.19(6):2213-2226.

Merimi M, El-Majzoub R, Lagneaux L, Agha DM, Bouhtit F, Meuleman N, Fahmi H, Lewalle P, Fayyad-Kazan M, Najar M (2021). The therapeutic potential of Mesenchymal Stromal Cells for Regenerative Medicine: Current Knowledge and Future Understandings. Front. Cell Dev. Biol. 9:661532.

Miyashita T, Ataka H, Kato K, Tanno T (2019). Pedicle screw shift without loosening following instrumented posterior fusion. Neurosurg. Rev. 42:691-698.

Mohendas Y, Tahani M, Rouhi G, Tahami M (2021). A mechanobiological approach to find the optimal thickness for the locking compression plate: Finite element investigations. Proc IMechE Part H: J Engineering in Medicine. 235(4):408-418.

Mohi Eldin MM, Ali AM (2014). Lumbar transpedicular implant failure:a clinical and surgical challenge and its radiological assessment. Asian Spine J. 8(3):281-97.

Mondal S, Ghosh R (2019a). Effects of implant orientation and implant material on tibia bone strain, implant-bone micromotion, contact pressure, and wear depth due to total ankle replacement. Proc IMechE Part H: J Engineering in Medicine 233(3):318-333.

Mondal S and Ghosh R (2019b). Bone remodelling around the tibia due to total ankle replacements: effects of implant material and implant-bone interfacial conditions. Comput Methods Biomech Biomed. 22(16):1247-1257.

Mondal S and Ghosh R (2021). Bone remodelling around the tibia due to total ankle replacement: effects of implant material and implant-bone interfacial conditions. Comput. Methods Biomech. Biomed. Eng. 22:16: 1247-1257.

Moore DC, Maitra RS, Farjo LA, Graziano GP, Goldstein SA (1997). Goldstein Restoration of Pedicle Screw Fixation With an in Situ Setting Calcium Phosphate Cement. SPINE , 22(15):1696-1705.

Moran JM, Berg WS, Berry JL, Geiger JM, Steffee A (1989). Transpedicular screw fixation. J. Orthop. Res. 107-114.

Morgan EF, Bayraktar HH, Keaveny TM (2003). Trabecular bone modulus-density relationships depend on anatomic site. J Biomech 36(7): 897-904.

Montanari S, Barbanti Bròdano G, Serchi, E, Stagni R, Gasbarrini A, Conti A,Cristofolini L (2024). Experimental ex vivo characterization of the biomechanical effects of laminectomy and posterior fixation of the lumbo-sacral spine. *Sci Rep* **14**, 30001.

Mori Y, Kamimura M, Ito K, Koguchi M, Tanaka H, Kurishima H, Koyama T, Mori N, Mashashi N, Aizawa T (2024). A Review of the Impacts of Implant Stiffness on Fracture Healing. Appl. Sci. 14:2259.

Mukherjee K and Gupta S (2014). Simulation of tissue differentiation around acetabular cups: the effects of implant-bone relative displacement and polar gap. Advances in Biomechanics and Applications. 1(2):95-109.

Mukherjee K, Gupta S (2015). Bone ingrowth around porous-coated acetabular implant: a three-dimensional finite element study usingmechanoregulatory algorithm. Biomech Model Mechanobiol. 15(2):389-403.

Mukherjee K and Gupta S (2016). Influence of Implant Surface Texture Design on Peri-Acetabular Bone Ingrowth: A Mechanobiology Based Finite Element Analysis. J. Biomech. Eng. 139:031006-(1-8).

Mukherjee K, Gupta S (2017). Influence of Implant Surface Texture Design on Peri-Acetabular Bone Ingrowth: A Mechanobiology Based Finite Element Analysis. J Biomech Eng. 1;139(3).

Nachemson A (1966). The load on Lumbar Disks in different positions of the body. Clin. Orthop. Relat. Res. 45: 107-122.

Nakahashi M, Uei H, Tokuhashi Y, Maseda M, Sawada H, Soma H, Miyakata H (2019). Vertebral fracture in elderly female patients after posterior fusion with pedicle screw fixation for degenerative lumbar pathology: A retrospective cohort study. BMC Musculoskeletal Disorders, *20*(1), 1–6.

Natarajan RN, Watanabe K, Hasegawa K (2018). Biomechanical Analysis of a Long-Segment Fusion in a Lumbar Spine-A Finite Element Model Study. J Biomech Eng. 140(9).

Newcomb AG, Baek S, Kelly BP, Crawford NR (2017). Effect of screw position on load transfer in lumbar pedicle screws: a non-idealized finite element analysis. Comput Methods Biomech Biomed Engin. 20(2):182-192.

Newell E and Driscoll M (2021). The examination of stress shielding in a finite element lumbar spine inclusive of the thoracolumbar fascia. Med Biol Eng Comput. 59:1621-1628.

Nikkhoo, M., Lu, M. L., Chen, W. C., Fu, C. J., Niu, C. C., Lin, Y. H., & Cheng, C. H. (2021). Biomechanical Investigation Between Rigid and Semirigid Posterolateral Fixation During Daily Activities: Geometrically Parametric Poroelastic Finite Element Analyses. Frontiers in Bioengineering and Biotechnology, *9*:646079.

Norris CM (1995). Spinal Stabilisation: 2. Limiting Factors to End-range Motion in the Lumbar Spine, Physiotherapy, Volume 81, Issue 2,64-72.

Okuda S, Miyauch A, Oda T, Haku T, Yamamoto T, Iwasaki M (2006). Surgical complications of posterior lumbar interbody fusion with total facetectomy in 251 patients. J Neurosurg Spine, 4:304-309.

Okuyama K, Abe E, Suzuki T, Tamura Y, Chiba M, Sato K (2001). Influence of bone mineral density on pedicle screw fixation: a study of pedicle screw fixation augmenting posterior lumbar interbody fusion in elderly patients. Spine J. 1(6):402-7.

O'Neill M, Vaughan TJ (2021). High-speed cutting of synthetic trabecular bone-A combined Experimental –Computational Invesstigation. Appl. Mech. 2(3):650-665.

Orisi E, Giavaresi G, Trire A, Ottani V, Salgaretto S (2012). Dental Implant Thread Pitch and Its Influence on the Osseointegration Process: An In Vivo Comparison Study. Int J Oral Maxillofac Implants. 27:383-392.

Otsuki B, Fujibayashi S, Tanida S, Shimizu T, Murata K, Matsuda K (2021). Possible Association of Pedicle Screw Diameter on Pseudoarthrosis Rate After Transforaminal Lumbar Interbody Fusion. World Neurosurg 150: e155-e161.

Pal B, Gupta S, New AMR (2010). Influence of the change in stem length on the load transfer and bone remodelling for a cemented resurfaced femur. J Biomech. 43:2908-2014.

Panjabi MM, Duranceau J, Goel V, Oxland T, Takata K (1991). Cervical human vertebrae. Quantitative three-dimensional anatomy of the middle and lower regions. Spine (Phila Pa 1976). 16(8): 861-9.

Park P, Garton HJ, Gala VC, Hoff JT, & McGillicuddy JE (2004). Adjacent segment disease after lumbar or lumbosacral fusion: Review of the literature. *Spine, 29*(17), 1938–1944.

Pauwel F (1960). A new theory on the influence of mechanical stimuli on the differentiation of supporting tissue. The tenth contribution to the functional anatomy and causal morphology of the supporting structure. Z Anat Entwicklungsgesch. 121:478-515.

Paxinos O, Tsitsopoulos P, Zindrick MR, Voronov LI, Lorenz MA, Havey RM, Patwardhan AG (2010). Patwardhan.Evaluation of pulloutstrength and failure mechanism of posterior instrumentation in normal and osteopenic thoracic vertebrae. J.Neeurosurg.13(4):469-476.

Pearson HB, Dobbs CJ, Grantham E, Niebur GL, Chappuis JL, Boerckel JD (2017). Intraoperative biomechanics of lumbar pedicle screw loosening following successful arthrodesis. J. Orthop. Res. 35(12):2673–2681.

Polokeit A, Ferguson SJ, Nolte LP, Orr TE (2003). Factors influencing stresses in the lumbar spine after the insertion of intervertebral cages: finite element analysis/ Eur Spine J. 12:413-420.

Ponnusamy K E, Iyer S, Gupta G, Khanna A J (2011). Instrumentation of the osteoporotic spine: Biomechanical and clinical considerations. Spine Journal, 11(1), 54–63.

Postacchini F, Postacchini R, Menchetti PPM, Sessa P, Paolino M, & Cinotti G (2016). Lumbar interspinous process fixation and fusion with stand-alone interlaminar lumbar instrumented fusion implant in patients with degenerative spondylolisthesis undergoing decompression for spinal stenosis. Asian Spine Journal, *10*(1), 27–37.

Postigo S, Schmidt H, Rohlmann A, Putzier M, Simon A, Duda G, Checa S (2014). Investigation of different cage designs and mechano-regulation algorithms in the lumbar interbody fusion process-A finite element analysis. J Biomech. 47:1514-1519.

Pradeep K, Mahapatra B, Pal B (2024). Effects of open and minimally invasive Transforaminal Lumbar Interbody Fusion (TLIF) surgical techniques on mechanical behaviour of fused L3-L4 FSU: A comparative finite element study. Med. Eng. Phys, 123:104084.

Prasannavenkadesan V, Pandithevan P (2021). Bone drilling simulation using Johnson-Cook model combined with Cowper-Symonds model validated with in-vitro experiments. Mechanics of Advanced Materials and Structures. 29(25):4546-4556.

Prendergast PJ and Taylor D (1994). Prediction of bone adaptation using damage accumulation. J. Biomechanics. 27(4):1067-1076.

Prendergast PJ, Huiskes HWJ (1995). Mathematical modelling of microdamage in bone remodelling and adaptation. Eds: Odgaard A, Weinans H. Singapore, World Scientific Publishers,213-224.

Prendergast PJ, Huiskes R, Soballe K (1997). Biophysical stimuli on cells during tissue differentiation at implant interfaces. J Biomech. 30(5):539-48.

Prendergast PJ and Huiskes R (1996). Finite element analysis of fibrous tissue morphogenesis- A study of the osteogenic index with a biphasic approach. Mech. Compos. Mater. 32:144-150.

Puthumanapully PK (2010). Simulation of tissue differentiation in uncemented hip implants based on a mechanoregulatory hypothesis. Dissertation, University of Southampton.

Pye SR, Reid DM , Adams JE, Silman AJ, O'Neill TW (2006). Radiographic features of lumbar disc degeneration and bone mineral density in men and women. Ann Rheum Dis. 65:234-238.

Qi W,Yan Y bo, Zhang Y, Lei W, Wang PJ, Hou J (2011). Study of stress distribution in pedicle screws along a continuum of diameters: a three-dimensional finite element analysis. Orthop. Surg 3(1):57–63.

Rahyussalim AJ, Kurniawati T, Besri NN, Hukmi K (December) (2019). Osteoporotic pedicle screw: Review of various types of pedicle screw and cement augmentation. AIP Conf Proc2193.

Rajaee SS, Kanim LEA, Bae HW (2014). National trends in revision spinal fusion in USA. Bone Joint J, 96-B:807-16.

Rassi-Neto A, Shimano A (2002). Biomechanical properties of expander compared with conventional screws. J Neurosurg 97:346-349.

Reinhold M, Schwieger K, Goldahn J, Linke B, Knop C, Blauth M (2006). Influence of screw positioning in a new anterior spine fixator on implant loosening on osteoporotic vertebrae. Spine. 31(4):406-413.

Relly B, Han F, Parker LE, Zhang H (2018). Skeleton-based bio-inspired human activity prediction for real-time human-robor interaction. Auton. Robots. 42:1281-1298.

Remache D, Semaan M, Rossi JM, Pithioux M, Milan JL (2020). Application of the Johnson-Cook plasticity model in the Finite Element simulation of the nanoindenation of the cortical bone. 101, 10346.

REPORT 2021. Norwegian National Advisory Unit on Arthoplasty and Hip Fractures. ISBN: 978-82-91847-26-7. http://nrlweb.ihelse.net.

Rohlmann A, Bauer L, Zander T, Bergmann G, Wilke HJ (2006). Determination of trunk muscle forces for flexion and extension by using a validated finite element model of the lumbar spine and measured in vivo data. J. Biomech. 39(6):981-989.

Rohlmann A, Burra NK, Zander T, Bergmann G (2007). Comparison of the effects of bilateral posterior dynamic and rigid fixation devices on the loads in the lumbar spine: A finite element analysis. Eur. Spine J. 16(8):1223–1231.

Rohlmann A, Zander T, Rao M, Bergmann G(2009). Applying a follower load delivers realistic results for simulating standing. J Biomech. 22;42(10):1520-1526.

Rohlmann A, Lauterborn S, Dreischarf M, Schmidt H, Putzier M, Strube P, Zander T (2013). Parameters influencing the outcome after total disc replacement at the lumbosacral junction. Part 1: Misalignment of the vertebrae adjacent to a total disc replacement affects the facet joint and facet capsule forces in a probabilistic finite element analysis. Eur. Spine J. 22(10):2271–2278.

Roux W (1981). Der ziichtende kampf der teile, oder die 'tei/auslese' imorganismus (therie der 'finktionellen unpassung'), Leipzig, Wilhelm Engelmann.

Saghaei Z, Hashemi A. Homogeneous material models can overestimate stresses in high tibial osteotomy: A finite element analysis (2023). Proc IMechE Part H: J Engineering in Medicine. 237(2):224-232.

Sahu NK, Kaviti AK (2016) A review of use of FEM techniques in Modeling of Human Knee Joint. J. Biomimetics, Biomater. Biomed.Eng 28:1-11.

Sanjay D, Bhardwaj JS, Kumar N, Chanda S (2022). Expandable pedicle screw may have better fixation than normal pedicle screw: preclinical investigation on instrumented L4-L5 vertebrae based on various physiological movements. Med Biol Eng Comput. 60:2509-2515.

Sanjay D, Kumar N, Chanda S (2021) Stress-strain distribution in intact L4-L5 vertebrae under the influence of physiological movements: A finite element (FE) investigation. IOP Conf Ser. Mater. Sci Eng 1206:012024.

Sanjay D, Mondal S, Bhutani R, Ghosh R (2018). The effect of cement mantle thickness on strain energy density distribution and prediction of bone density changes around cemented acetabular component. Proc IMechE Part H: J Engineering in Medicine 232(9):912–921.

Saviour CM, Choudhury JB and Gupta S (2023). Numerical evaluations of an uncemented acetabular component in total hip arthroplasty: effects of loading and interface conditions. J. Biomech. Eng. 145:021009-1-12.

Scannell PT (2006). Mechanoregulation Algorithms Predicting Peri-prosthetic Bone Adaptations. A PhD Thesis, Trinity College, Dublin.

Scannell PT, Prendergast PJ (2009). Cortical and interfacial bone changes around a non-cemented hip implant: simulations using a combined strain/damage remodelling algorithm. Med Eng Phys. 31(4):477-88.

Scemama C, Magrino B, Gillet P, Guigui P (2016). Risk of adjacent-segment disease requiring surgery after short lumbar fusion: results of the French Spine Surgery Society Series. J Neurosurg Spine. 25(1):46-51.

Schafer R, Trompeter K, Fett D, Heinrich K, Funken J, Willwacher S, Bruggermann GP, Platen P. The mechanical loading of the spine in physical activities. Eur Spine J. 32:2991-3001.

Serhan H, Mhatre D, Defossez H, Bono CM (2011). Motion-preserving technologies for degenerative lumbar spine: The past, present, and future horizons. SAS Journal, *5*(3), 75–89.

Schaeren S, Broger I, Jeanneret B (2008). Minimum four-year follow-up of spinal stenosis with degenerative spondylolisthesis treated with decompression and dynamic stabilization. Spine (Phila Pa 1976). 33(18): E636-42.

Seng WRD, Chou SM, Siddiqui SS, Oh JYL (2018). Pedicle Screw Designs in Spinal Surgeon. Spine. 44(3): E144-E149.

Sennerby L, Thomsen P, Ericson LE (1993). Early tissue response to titanium implants inserted in rabbit cortical bone. J. Mater. Sci. Mater.Med. 4:240-250.

Shamji MF, Goldstein, CL, Wang, M, Uribe, JS, Fehlings M G (2015). Minimally invasive spinal surgery in the elderly: Does it make sense? Neurosurgery, *77*(4), S108–S115.

Shen F, Kim HJ, Kang KT, Yeom JS (2019). Comparison of the pullout strength of pedicle screws according to the thread design for various degrees of bone quality. Appl. Sci. 9:1525.

Shen H, Chen Y, Liao Z, Liu W (2021). Biomechanical evaluation of anterior lumbar interbody fusion with various fixation options: Finite element analysis of static and vibration conditions. Clin Biomech (Bristol, Avon). 84:105339.

Shiraji-Adl A, Shrivastava SC, Ahmed AM (1984). Stress analysis of the Lumbar Disc-Body unit in compression. A three-dimensional nonlinear finite element study. Spine 9(2): 120-134.

Singh K, Howard SA, Samartzis D, Nassr A, Provus J, Hickey M, Andersson GBJ (2005). A prospective cohort analysis of adjacent vertebral body bone mineral density in lumbar surgery patients with or without instrumented posterolateral fusion. Spine. 30(15): 1750-1755.

Sivasubramaniam V, Patel HC, Ozdemir BA, Papadopoulos MC (2015). Trends in hospital admissions and surgical procedures for degenerative lumbar spine disease in England: a 15-year time-series study. BMJ Open 5:e009011.

Snell RS. Clinical anatomy by regions. Lippincott Williams & Wilkins. 2011 Oct 28.

Somovilla-Gomez F, Lostado-Lorza R, Corral-Bobadilla M, Escribano-Garcia R (2020). Improvement in determining the risk of damage to the human lumbar functional spinal unit considering age, height, weight and sex using a combination of FEM and RSM. Biomech. Model. Mechanobiol. 19:351-387.

Son DS, Mehboob H, Jung HJ, Chang SH (2014). The finite element analysis for endochondral ossification process of a fractured tibia applied with a composite IM-rod based on a mechano-regulation theory using a deviatoric strain. Compos. B Eng. 56:189-196.

Song M, Sun K, Li Z, Zong J, Tian X, Ma K, Wang S (2021). Stress distribution of different lumbar posterior pedicle screw insertion techniques: a combination study of finite element analysis and biomechanical test. Sci Rep 11,12968 (2021).

Speirs AD, Slomczykowski MA, Orr TE, Siebenrock K, Nolte LP (2000). Three-dimensional measurement of cemented femoral stem stability: an in vivo cadaver study. Clin. Biomech. 15(4): 248-55.

Spilker RL (1980). Mechanical behavior of a simple model of an intervertebral disk under compressive loading. J. Biomech. 13(10):895-901.

Stoltz JF, Magadalou J, George D, Chen Y, Li Y, Isha ND, He X, Remond V (2018). Influence of mechanical forces on bone: Introducton to mechanobiology and mechanical adaptation concept. Journal of cellular Immunotherapy. 4:10-12.

Su KC, Chen KH, Pan CC, Pan CC, Lee CH (2021). Biomechanical Evaluation of Cortical Bone Trajectory Fixation with Traditional Pedicle Screw in the Lumbar Spine: A Finite Element Study. Appl Sci 11(22):10583.

Suarez DR, Weimens H, van Keulen F (2012). Bone Remodelling around a cementless glenoid component. Biomech Model Mechanobiol. 11(6):903-913.

Sulaiman MY, Wicaksono S, Dirgantara T, Mahyuddin AI, Sadputranto SA, Oli'l EM (2024). In Silico Investigation of Mandibular Reconstruction: Tissue Differentiation Dynamics with Particulate-Cancellous Bone Marrow Grafts under Varied Bite Forces and Implant Elastic Moduli. Research Square.

Sun X, Curreli C, Viceconti M (2024). Finite Element Models to Predict the Risk of Aseptic Loosening in Cementless Femoral Stems: A Literature Review. Appl. Sci, 14:3200.

Tai CL, Tsai TT, Lai PL, Chen YL, Chen LH (2015). A Biomechanical Comparison of Expansive Pedicle Screws for Severe Osteoporosis: The Effects of Screw Degisn and Cement Augmentation. PLoS ONE. 10(12):e0146294.

Tai CL, Chen WP, Liu MY, Li YD, Tsai TT, Lai PL, Hsieh MK (2022). Biomechanical comparison of pedicle screw fixation strength among three different screw trajectories using single vertebrae and one-level functional spinal unit. Front. Bioeng. Biotechnol. 10:1054738.

Talukdar RG, Mukhopadhyay KK, Dhara S, Gupta S (2021). Numerical analysis of the mechanical behaviour of intact and implanted lumbar functional spinal units: Effects of loading and boundary conditions. Proc IMechE Part H: J Engineering in Medicine. 235(7):792-804.

Talukdar RG, Saviour, Tiwarekar K, Dhara S, Gupta S (2022). Bone remodeling around solid and porous interbody cages in the lumbar spine. J. Biomech. Eng. 144:101011(1-12).

Talukdar RG, Saviour CM, Dhara S, Gupta S (2023). Biomechanical analysis of functionally graded porous interbody cage for lumbar spinal fusion. Comput. Biol. Med. 164:107281.

Tandon V, Franke J, Kalidindi KKV (2020). Advancements in osteoporotic spine fixation. JCOT. 11(5):778-785.

Tarlochan F, Mehboob H, Mehboob A, Chang SH (2018). Influence of functionally graded pores on bone ingrowth in cementless hip prosthesis: a finite element study using mechano-regulatory algorithm. Biomech. Model. Mechanobiol. 17:701-716.

Tsubota KI, Adachi T, Tomita Y (2003). Effects of a fixation screw on trabecular structural changes in a vertebral body predicted by remodeling simulation. Ann. Biomed 2003;31:733-740.

van Rietbergen B, Huiskes R, Weinans H, Summer DR, Turner TM, Galante JO (1993). The mechanism of bone remodeling and resorption around press-fitted THA stems. J. Biomechanics. 26((4-5):369-382.

van Rijsbergen M, van Rietbergen B, Barthelemy V, Eltes P, Lazary A, Lacroix D, Noailly J, Ho Ba Th MC, Wilson W, Ito K (2018). Comparison of patient-specific computational models vs. clinical follow-up, for adjacent segment disc degeneration and bone remodelling after spinal fusion. Plos One.13(8):e0200899.

Vardiman AB, Wallace DJ, Crawford NR, Riggleman JR, AhrendtsenLA, Ledonio CG (2020). Pedicle screw accuracy in clinical utilization of minimally invasive navigated robot-assisted spine surgery. J Robot Surg.14(3):409-413.

Varghese V, Krishnan V, Kumar GS (2018). Testing pullout strength of pedicle screw using synthetic bone models: Is a bilayer foam model a better representation of vertebra? Asian Spine J. 12(3):398-406.

Varghese V, Kumar G.S, Krishnan V (2017). Effect of various factors on pull out strength of pedicle screw in normal and osteoporotic cancellous bone models. Med. Eng. Phys. 40:28-38.

Varghese V, Venkatesh K, Kumar G S (2016a). Simulation of axial pullout of pedicle screw in synthetic bone models. 2nd International conference on Biomedical systems, signals and images.

Vena P, Franzoso G, Gastaldi D, Contro R, Dallolio V (2005). A finite element model of the L4-L5 spinal motion segment: biomechanical compatability of an interspinous device. Comput Methods Biomech. Biomed. Eng. 8:1:7-16.

Veresciagina K, Mehrkens A, Schären S, Jeanneret B (2018). Minimum ten-year follow-up of spinal stenosis with degenerative spondylolisthesis treated with decompression and dynamic stabilization. J Spine Surg. 4(1):93-101.

Viezens L, Sellenschloh, Puschel K, Morlock MM, Lehmann W, Huber G, Weiser L (2021). Impact of Screw Diameter on Pedicle Screw Fatigue Strength- A Biomechanical Evaluation. World Neurosurg 152: e369-e376.

Viceconti M, Ricci S, Pancanti A, Cappello A (2004). Numerical model to predict the long-term mechanical stability of cementless orthopaedic implants. Med Biol Eng Comput. 42(6):747-753.

Vishnubhotla, S., McGarry, W. B., Mahar, A. T., & Gelb, D. E. (2011). A titanium expandable pedicle screw improves initial pullout strength as compared with standard pedicle screws. The Spine Journal, 11(8), 777–781.

Wan S, Lei W, Wu Z, Liu D, Gao M, Fu S (2010). Biomechanical and histological evaluation of an expandable pedicle screw in osteoporotic spine in sheep. Eur Spine J. 19:2122-2129.

Wang T, Wu B, Duan R, Yuan Y, Qu M, Zhang S, Huang W, Liu T, Yu X (2020). Treatment of Thoracolumbar Fractures Through Different Short Segment Pedicle Screw Fixation Techniques: A Finite Element Analysis. Orthop. Surg. 12:601-608.

Wang Y, Wang J, Tu S, Li S, Yi S, Zhao H, Qiao H, Yan K, Liao B(2021). Biomechanical Evaluation of Oblique lateral locking plate system for oblique interbody fusion: A finite element analysis. Res Sq. 160:e126-e141.

Weildling M, Heilemann M, Schoenfelder S, Heyde CE (2022). Influence of thread design on anchorage of pedicle screws in cancellous bone: an experimental and analytical analysis. Nature 12:805.

Weinans H (1991). Mechanically induced bone adaptations around orthopaedic implants.

Weinans H, Huiskes R, Rietbergen Bv, Sumner DR, Turner TM, Galante JO(1993). Adaptive bone remodelling around bonded noncemented total hip arthoplasty: A coparison between animal experiments and computer simulation. J Orthop Res. 11(4):500-513.

Weinbaum S, Cowin SC, Zeng Y (1994). A model for the excitation of osteocytes by mechanical loading-induced bone fluid shear stresses. J. Biomechanics, 27(3):339-360.

Weinstein JN, Rydevik BL, Rauschning W (1992). Anatomic and technical considerations of pedicle screw fixation. Clin Orthop Relat Res. 284:34-46.

Weng F, Wang J, Yang L, Zeng J, Chu Y, Tian Z (2018). Application value of expansive pedicle screw in the lumbar short-segment fixation and fusion for osteoporosis patients. Exp Ther Med 16(2):665-670.

Wilke HJ, Neef P, Caimi M, Hoogland T, Claes LE (1999). New in vivo measurements of pressures in the intervertebral disc in daily life. Spine, 24(8):755-762.

Witek L, ParentePEL, Torroni A, Greenberg M, Nayak VV, Hacquebord JH, Coelho PG (2023). Evaluation of instrumentation and pedicle screw design for posterior lumbar fixation: A pre-clinical in vivo/ex vivo ovine model. JOR Spine, 6(2), e1245.

White III AA, Panjabi MM (1978). Book-Clinical Biomechanics of the Spine.

Wolff J (1982). Das Gesetz der Transformation der Knochen. Berlin, Herchwikd. Translated as the law of bone remodelling. Springer-Verlag, Berlin.

Wolfram U, Wilke HJ, Zysset PK (2010). Valid μ finite element models of vertebral trabecular bone can be obtained using tissue properties measured with nanoindentation under wet conditions. J. Biomech. 43(9):1731-1737.

Wong CE, Hu HT, Kao LH, Liu CJ, Chen KC, Huang KY (2022). Biomechanical feasibility of semi-rigid stabilization and semi-rigid lumbar interbody fusion: a finite element study. BMC Musculoskelet. Disord. 23:10.

Wu LC, Hsieh YY, Tsuang FY, Kuo YJ, Chen CH, Chiang CJ (2023). Pullout strength of pedicle screws inserted using three different techniques: a biomechanical study on polyurethane foam block. Bioengineering 10:660.

Wu Y, Adeeb S, Doschak MR (2015). Using Micro-CT Derived Bone Microarchitecture to Analyze Bone Stiffness - A Case Study on Osteoporosis Rat Bone. Front Endocrinol (Lausanne). 20;6: 80.

Wu ZS, Cui G, Lei W, Fan Y, Wan S, Ma Z, Sang H (2010). Application of an expandable pedicle screw in the severe osteoporotic spine: A preliminary study. The J. Clinic. Investig.33(6):E368-E374.

Wu ZX, Gao MX, Sang HX, Ma ZS, Cui G, Zhang Y, Lei W (2012). Surgical treatment of osteoporotic thoracolumbar compressive fractures with open vertebral cement augmentation of expandable pedicle screw fixation: A biomechanical study and a 2-year follow up of 20 patients. J. Surg. Res. 173:91-98.

Xiao Z, Wang L, Gong H, Zhu D, Zhang X (2011). A non-linear finite element model of human L4-L5 lumbar spinal segment with three- dimensional solid element ligaments. Theor. App. Mech. Lett.1(6):064001 (1-6).

Xiong GX, Fisher MWA, Schwab JH, Simpson AK, Nguyen L, Tobert DG, Balboni TA, Shin JH, Ferrone ML, Schoenfeld AJ (2022). A natural history of patients treated operatively and nonoperatively for spinal metastases over 2 years following treatment. Spine. 47(7):515-522.

Xu M, Yang J, Lieberman IH, Haddas R (2019). Finite element method-based study of pedicle screw–bone connection in pullout test and physiological spinal loads. Med Eng Phys 67:11–21.

Xu M, Yang J, Lieberman IH, Haddas R(2016). Lumbar spine finite element model for healthy subjects: development and validation. Comput. Methods Biomech. Biomed. Eng. 20(1):1–15.

Yagi M, Ogiri M, Holy CE, Bourcet A (2021). Comparison of clinical effectiveness of fenestrated and conventional pedicle screws in patients undergoing spinal surgery: a systematic review and meta-analysis. Expert Rev Med Devices. 18(10):995-1022.

Yamamoto I, Panjabi MM, Crisco T, Oxland T (1989) Three-dimensional movements of the whole lumbar spine and lumbosacral joint. SPINE 14(11):1256-1260.

Yaman O, Demir T, Arslan KA, Iyidiker MA, Tolunay T, Camuscu N, (2015). The comparison of pullout strengths of various pedicle screw designs on synthetic foams and ovine vertebrae. Turk Neurosurg 25(4):532-538.

Yan JZ, Qiu GX, Wu ZH, Wang XS, Xing ZJ (2011). Finite element analysis in adjacent segment degeneration after lumbar fusion. Int J Med Robot. 201(1):96-100.

Yoganandan N, Kumaresan S, Pintar FA December (2000). "Geometric and Mechanical Properties of Human Cervical Spine Ligaments." ASME. J. Biomech. Eng. 122(6):623–629.

Zander T, Rohlmann A, Burra NK, Burra NK, Bergmann G (2006). Effect of a posterior dynamic implant adjacent to a rigid spinal fixator. ClinBiomech 21(1):767-774.

Zander T, Rohlmann A, Bergmann G (2009). Influence of different artificial disc kinematics on spine biomechanics. Clin Biomech (Bristol, Avon). 24(2):135-42.

Zhang L, Li HM, Zhang R, Zhang H, Shen CL (2021). Biomechanical Changes of Adjacent and Fixed Segments Through Cortical Bone Trajectory Screw Fixation

versus Traditional Trajectory Screw Fixation in the Lumbar Spine: A Finite Element Analysis. World Neurosurgery, 151, e447–e456.

Zhang QH, Tan SH, Chou SM (2006). Effects of bone materials on the screw pull-out strength in human spine. Med. Eng. Phys. 8:795-801.

Zhang Z, Li H, Fogel GR, Xiang D, Liao Z, Liu W (2018). Finite element model predicts the biomechanical performance of transforaminal lumbar interbody fusionwith various porous additive manufactured cages. Comput. Biol. Med. 95:167-174.

Zhao X, Du L, Xie Y, Zhao J (2018). Effect of lumbar lordosis on the adjacent segment in transforaminal lumbar interbody fusion: A finite element analysis. World Neurosurg. 114: E114-E120.

Zhong ZC, Wei SH, Wang JP, Feng CK, Chen CS, Yu Ch (2006). Finite element analysis of the lumbar spine with a new cage using a topology optimization method. Med Eng Phys 28:90-98.

Zhong ZC, Chen SH, Hung CH (2009). Load and displacement-controlled finite element analyses on fusion and non-fusion spinal implants. Proc IMechE Part H: J Engineering in Medicine 223(2):143-157.

Zhou C, Cha T, & Li G (2019). An upper bound computational model for investigation of fusion effects on adjacent segment biomechanics of the lumbar spine. Comput. Methods Biomech. Biomed. Engin. *22*(14), 1126-1134.

Zhou Q, Zeng F, Tu J, Do ng Zq, Ding ZH(2020). Influence of cementaugmented pedicle screw instrumentation in an osteoporotic lumbosacral spine over the adjacent segments: a 3d finite element study. j. orthop. Surg. Res. 15(1):132 (1-8).

Zhu D, Gu GS, Wu W, Gong H, Zhu WM, Jiang T, Cao ZL (2008). Micro-structure and mechanical properties of annulus fibrous of the L4-5 and L5-S1 intervertebral discs. Clinical Biomechanics, 23(SUPLL.1).

Zou D, Muheremu A, Sun Z, Zhong W, Jiang S, Li W. (2020) Computed tomography Hounsfield unit-based prediction of pedicle screw loosening after surgery for degenerative lumbar spine disease. J. Neurosurg. Spine 32: 716-721.

भारतीय प्रौद्योगिकी संस्थान गुवाहाटी
Indian Institute of Technology Guwahati

# About the Author

Devismita Sanjay was born on 28th February 1991 in Rangia, Assam, India. In 2008, she passed her Higher Secondary (10+2) examination with first division (82%) from Cotton College, Guwahati, under Assam Higher Secondary Education Council. She completed her Bachelor's in Mechanical Engineering with first class (76%) from Jorhat Engineering College (Dibrugarh University) in the year 2013. Thereafter, she joined the National Institute of Technology Agartala, Tripura, for her Master's degree in Mechanical Engineering with a specialization in Machine Design and passed with CGPA of 9.25 in 2015. Then, she joined as an Assistant Professor in the Mechanical Engineering Department, Assam Down Town University, Guwahati, Assam and continued till November 2016. In December 2016, she joined the Indian Institute of Technology Mandi, Himachal Pradesh, as a JRF and was introduced to Biomechanics. In December 2018, she joined the Ph.D. program under the supervision of Dr. Souptick Chanda in the Department of Biosciences and Bioengineering, Indian Institute of Technology Guwahati, Assam. She received a Junior and Senior research fellowship from the Ministry of Education, Government of India. She completed all the academic courses with a Cumulative Performance Index of 8.25/10. She presented her Ph.D. synopsis in an open seminar on 12th June 2024 and submitted the Ph.D. thesis in August 2024.

**List of publications from the present thesis:**

## Journals

**Sanjay D**, Bhardwaj JS, Kumar N, Chanda S (2022). Expandable pedicle screw may have better fixation than normal pedicle screw: preclinical investigation on instrumented L4-L5 vertebra based on various physiological movements (Medical and Biological Engineering & Computing, DOI: 10.1007/s11517-022-02625-w).

**Sanjay D**, Sarkar S, Chanda S. Bone remodelling comparison between normal pedicle screw and expandable pedicle screw instrumented L4-L5 vertebrae: a numerical study using FE analysis (*Under review*).

**Sanjay D**, Ghosh R, Bhardwaj JS, Sarkar S, Chanda S. Design of expandable pedicle screws for human vertebra based on strength-based pullout tests and mechanoregulation based tissue differentiation algorithms (*Submitted).*

**Sanjay D**, Chanda S. Finite element study on lumbar vertebra: A review of the literature (*To be communicated*).

## Conference

**Sanjay D**, Kumar N, Chanda S. Stress-strain distribution in intact L4-L5 vertebrae under the influence of physiological movements: A finite element (FE) investigation. International Conference on Recent Advances in Mechanical

Engineering and Nanomaterials (ICRAMEN 2021). Pune, India.16-17 October, 2021.

**Sanjay D**, Bhardwaj JS, Kumar N, Chanda S. The effect of insertion of expandable pedicle screw in L4-L5 vertebra: a preclinical assessment based on various physiological movements. World Congress of Biomechanics 2022. Taipei, Taiwan. 10-14 July,2022.

**Sanjay D**, Ghosh R, Chanda S. Full-cortical vs detailed anatomical vertebra for preclinical assessment of spinal implants. 29thCongress of the European Society of Biomechanics. 20June-3July 2024, Edinburg, Scotland.

**Sanjay D**, Chanda S. Preclinical investigation on the influence of various physiological movements on implanted L4-L5 vertebra with expandable pedicle screw (*To be communicated*).